N70 31575

TRW NO. 13463-6001-RO-OO
NASA CR-72647

SPACE STORABLE INTER-REGEN DESIGN STUDY

BY R. M. WILLIAMS

TRW
SYSTEMS GROUP

PREPARED FOR

NATIONAL AERONAUTICS AND SPACE ADMINISTRATION

FACILITY FORM 602

N70-31575 (ACCESSION NUMBER)	(THRU)
176 (PAGES)	(CODE)
CR# 72647 (NASA CR OR TMX OR AD NUMBER)	(CATEGORY)

NASA LEWIS RESEARCH CENTER

CONTRACT NAS 3-12059

P. N. HERR, PROJECT MANAGER

NOTICE

This report was prepared as an account of Government-sponsored work. Neither the United States, nor the National Aeronautics and Space Administration (NASA), nor any person acting on behalf of NASA:

A. Makes any warranty or representation, expressed or implied, with respect to the accuracy, completeness, or usefulness of the information contained in this report, or that the use of any information, apparatus, method, or process disclosed in this report may not infringe privately-owned rights; or

B. Assumes any liabilities with respect to the use of, or for damages resulting from the use of, any information, apparatus, method or process disclosed in this report.

As used above, "person acting on behalf of NASA" includes any employee or contractor of NASA, or employee of such contractor, to the extent that such employee or contractor of NASA or employee of such contractor prepares, disseminates, or provides access to any information pursuant to his employment or contract with NASA, or his employment with such contractor.

Requests for copies of this report should be referred to

National Aeronautics and Space Administration
Scientific and Technical Information Facility
P. O. Box 33
College Park, Md. 20740

NASA CR-72647
TRW No. 13463-6001-R0-00

FINAL REPORT

SPACE STORABLE
INTER-REGEN DESIGN STUDY

by
R. M. Williams

TRW SYSTEMS GROUP
One Space Park
Redondo Beach, California 90278

prepared for
NATIONAL AERONAUTICS AND SPACE ADMINISTRATION

January 30, 1970

Contract NAS3-12059

NASA LEWIS RESEARCH CENTER
Cleveland, Ohio

P. N. Herr, Project Manager
Liquid Rocket Technology Branch

TABLE OF CONTENTS

	Page
1. SUMMARY	1
2. INTRODUCTION	3
3. THRUSTER ANALYSIS AND DESIGN	4
3.1 Inter-Regen Thruster Design Analysis	4
3.1.1 Thruster Performance	4
3.1.2 Propellant Characteristics	7
3.1.3 Film Coolant Analysis	13
3.1.4 Inter-Regen Thermal Analysis	20
3.2 Graphite Thruster Design Analysis	25
3.2.1 Design Selection	25
3.2.2 Thermal Analysis	28
4. HARDWARE DESCRIPTION	29
4.1 Injector Design	30
4.2 Thrust Chamber Designs	37
4.2.1 Inter-Regen Thrust Chambers	37
4.2.2 Graphitic Thrust Chamber	42
5. EXPERIMENTAL RESULTS	45
5.1 Inter-Regen Chamber Testing	45
5.1.1 Task I - Film Cooled Testing	45
5.1.2 Task II - Duct Cooled Testing	58
5.2 Graphitic Chamber Testing	85
5.3 Data Evaluation	85
5.3.1 Film Cooled Tests	89
5.3.2 Duct Cooled Tests	90
5.3.3 Graphitic Chamber Test	99
6. DISCUSSION AND CONCLUDING REMARKS	103
6.1 Experimental Results and Data Evaluation	103
6.1.1 Propellant Effects	103
6.1.2 Coaxial Injector Effects	104
6.1.3 Duct Cooled Chamber Effects	105
6.1.4 Graphite Chamber Effects	106
6.2 Recommendations	106
APPENDIX A - THERMAL DATA COMPILATION	A-1
APPENDIX B - DISTRIBUTION LIST	B-1
SYMBOLS	S-1
REFERENCES	R-1

PRECEDING PAGE BLANK NOT FILMED

ABSTRACT

The Space Storable Inter-Regen Design Study (Contract NAS3-12059) was a six-month analytical and experimental investigation for evaluating selected internally regenerative (inter-regen) cooled RCS thruster design variables using the space storable propellant combination, FLOX/Propane. Several injector and thrust chamber design variables were evaluated at selected coolant flow rates with a basic program goal of demonstrating steady-state thruster operation with minimum performance degradation. Through the use of a ducted-coolant thrust chamber design, steady-state thermal operation was successfully achieved with metallic (copper) chamber designs, during two test firings of 90 and 310 seconds run durations. These tests represent the first unqualified success for the inter-regen RCS thruster cooling concept using the space storable propellants.

PRECEDING PAGE BLANK NOT FILMED.

1. SUMMARY

The Space Storable Inter-Regen Design Study program effort, Contract NAS3-12059, consisted of analysis, design, fabrication and testing for the evaluation of selected internally regeneratively (inter-regen) cooled thrust chamber variables using the space storable propellant combination, FLOX/propane. The program efforts were primarily directed toward obtaining a better insight into the inter-regen design problems associated with RCS thruster designs. The specific program objectives included the evaluation of both injector and thrust chamber variables as well as a change to the higher carbon content LPG fuel, propane. The overall thrust chamber goal was for steady-state operation with minimal performance degradation and zero throat erosion.

The program was divided into two tasks. Task I involved injector modification and inter-regen testing using the conventional film cooling approach. The baseline injector design conditions were to use the propellants 76% FLOX/propane at a nominal mixture ratio of 4.5 with a chamber pressure of 100 psia (6.89×10^5 nt/m^2) and thrust of 100 pounds (444.8 nt). The two basic injectors employed had different resultant momentum vectors which resulted in different interactions between the primary propellants and the film coolant. The thrust chamber used was a thick wall, tapered, grooved copper chamber with thermocouple instrumentation to obtain axial, radial and circumferential thermal profiles. The primary Task I test goals were to obtain a comparison of the propane coolant with the previously used methane/ethane blend (Contract NAS3-11184) and to determine the effect of the primary propellant resultant momentum vector on the resultant local chamber wall environment and film coolant effectiveness. The results obtained indicated

that increased film coolant effectiveness was achieved with the oxidizer stream canted 30° axially indicating less interaction of the primary propellants and film coolant. With the test hardware and conditions used, no significant advantage of propane over methane/ethane as a film coolant fluid was indicated.

Task II comprised the evaluation of a modified inter-regen chamber design using a metallic duct to protect the coolant until its release into the chamber somewhere upstream of the throat. These chambers were employed to evaluate the duct cooling concept and the use of propane as a duct coolant. Several duct configurations resulted in steady-state operation, however, there was no clear indication that propane was superior to methane/ethane as a ducted chamber coolant. It is significant that the ducted chambers with the coolant flow rates employed did not exhibit any performance losses. In addition, a thrust chamber using graphitic materials was fabricated and tested to evaluate the overall erosion and carbon deposition effects. The one chamber tested showed severe erosion in the head end region of the chamber, adjacent to the primary propellants impingement point on the chamber wall.

2. INTRODUCTION

The Space Storable Inter-Regen Design Study, Contract NAS3-12059, was an evaluation of selected internally regeneratively (inter-regen) cooled thrust chamber variables. This program was a continuation of the extensive analytical and experimental research conducted under Contract NAS3-11184, Space Storable Thruster Investigation. The results of this program (Reference 1) indicated certain problem areas associated with inter-regen operation using the space storable propellants; related principally to the high optimum mixture ratio and the propellant physical properties. In order to achieve inter-regen operation, control of the wall thermal and chemical environment is necessary to limit the heat input to the throat and to insure that the coolant can absorb the heat conducted from the throat. The high optimum mixture ratio limits the amount of coolant available if performance losses are to be minimized. In addition, the physical properties of the space storable fuels severely limit their application as liquid film coolants. The present program is directed toward the circumvention of these problems. A major difference between this and the previous program is the use of propane as the fuel and coolant in place of 55% methane/45% ethane fuel blend. The change to propane was primarily made because of its increased liquid range and theoretical carbon deposition. In addition to the fuel comparison, the present program objectives were to evaluate the effect of injector modifications on the conventional film coolant effectiveness and to evaluate a modified chamber design employing a duct to protect the coolant until its release into the chamber at a location somewhere upstream of the throat. As a supplement to the inter-regen testing, a single test employing a graphitic material thrust chamber was conducted to determine chamber erosion and carbon deposition characteristics in a hot wall chamber design.

3. THRUSTER ANALYSIS AND DESIGN

In this section, the basic thruster design analysis efforts are present These include propellant characteristics, film coolant analysis, inter-regen analysis, graphite chamber analysis and material selection.

3.1 INTER-REGEN THRUSTER DESIGN ANALYSIS

Before proceeding to the detailed thrust chamber thermal design analysi it is necessary to determine the basic thrust chamber parameters. These are determined from the operating conditions, the performance goals and the prop lant performance characteristics.

3.1.1 Thruster Performance

This program utilized the space storable propellant combination 76% FLO (by weight)/propane with the following nominal operating parameters.

Thrust (F)	-	100 lbf vacuum (444.8 nt.)
Chamber Pressure (P_o)	-	100 psia (6.89×10^5 nt/m^2)
Nozzle Expansion Ratio (ϵ)	-	Sea-level (ϵ = 1.75)
Mixture Ratio (O/F)	-	4.5

Theoretical performance data used to determine the thruster propellant rates were obtained from Reference 1 and are reproduced in Figures 3-1 throu This yielded the thruster operating flow rates for various "core" mixture ratios and coolant flow rate percentages (Table 3-1). It should be noted th these flow rates maintain fixed "core" flow rates while varying the coolant flow rate for a given "core" mixture ratio. The use of "core" mixture ratio rather than overall mixture ratio as the fixed flow rate parameter was predi on the zonal performance losses associated with radial mixture ratio variati within the combustion chamber. It was a requirement for chamber heat reject

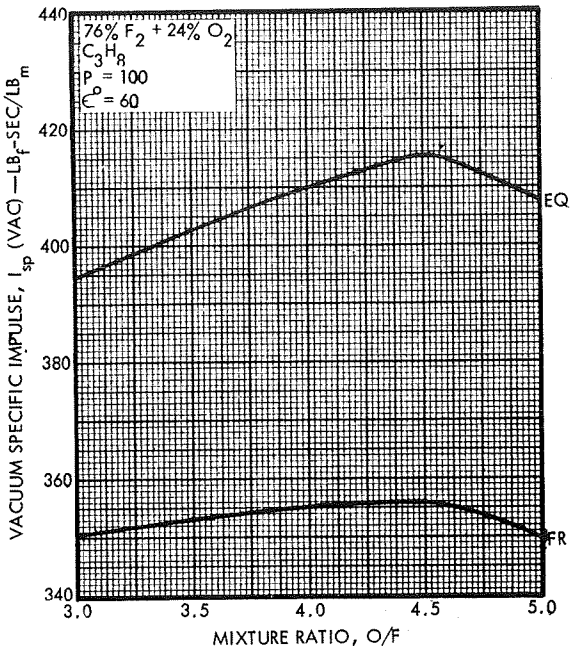

Figure 3-1. Vacuum Specific Impulse (C_3H_8)

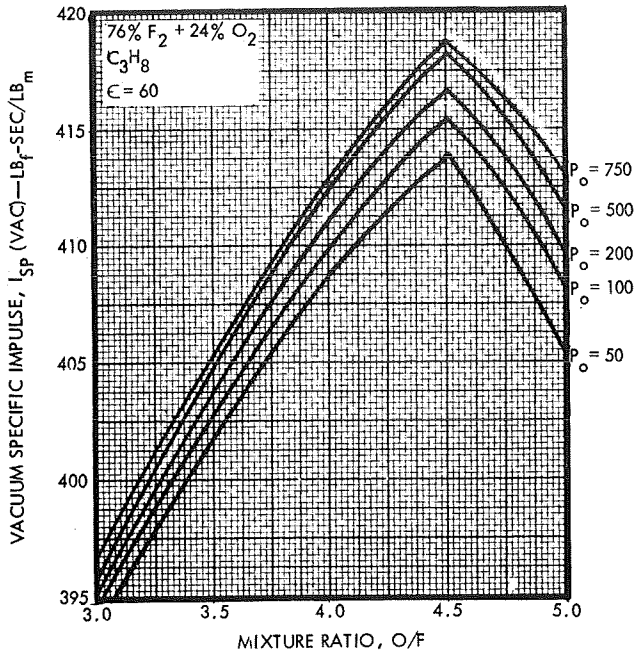

Figure 3-2. Vacuum Specific Impulse (P_c Variation)(C_3H_8)

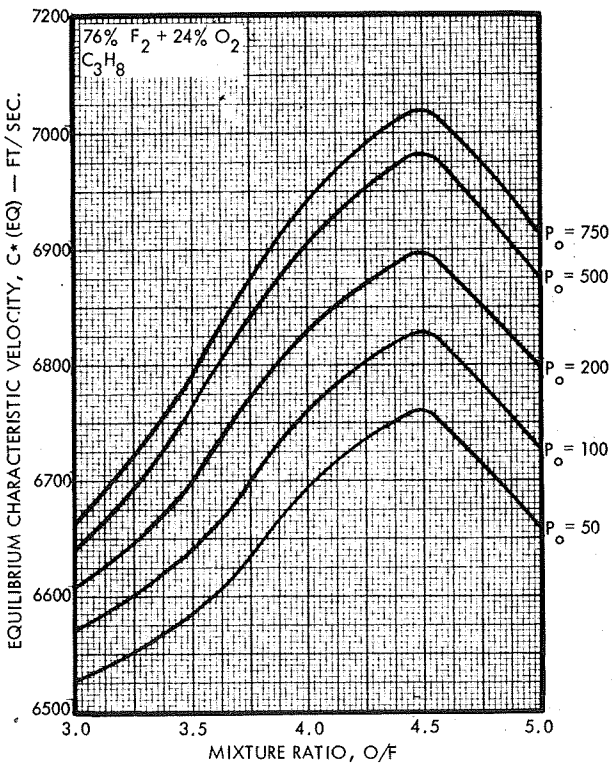

Figure 3-3. Equilibrium Characteristic Velocity (P_c Variation)(C_3H_8)

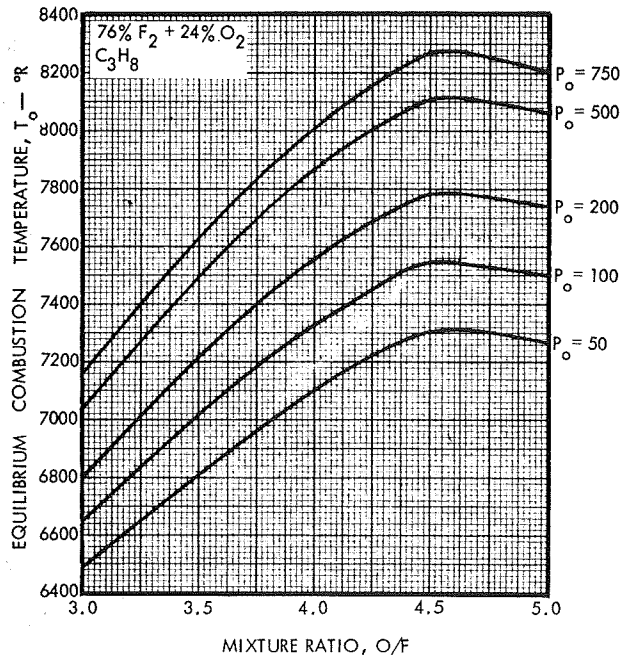

Figure 3-4. Equilibrium Combustion Temperature (P_c Variation)(C_3H_8)

Table 3-1. Thruster Operating Flow Rates

$(O/F)_{core}$	% Cooling	$\dot{\omega}_{ox}$ lbm/sec (Kg/sec)	$\dot{\omega}_{f_{core}}$ lbm/sec (Kg/sec)	$\dot{\omega}_{f_{cool}}$ lbm/sec (Kg/sec)	$\dot{\omega}_{f_{tot}}$ lbm/sec (Kg/sec)	$(O/F)_{overall}$
3.50	0	.2405 (.1091)	.0687 (.0312)	0 (0)	.0687 (.0312)	3.50
	40	.2405 (.1091)	.0687 (.0312)	.0458 (.0208)	.1145 (.0519)	2.10
	60	.2405 (.1091)	.0687 (.0312)	.1029 (.0467)	.1718 (.0779)	1.40
4.50	0	.2530 (.1148)	.0562 (.0255)	0 (0)	.0562 (.0255)	4.50
	40	.2530 (.1148)	.0562 (.0255)	.0375 (.0170)	.0937 (.0425)	2.70
	60	.2530 (.1148)	.0562 (.0255)	.0843 (.0382)	.1405 (.0637)	1.80
5.00	0	.2577 (.1169)	.0515 (.0234)	0 (0)	.0515 (.0234)	5.00
	40	.2577 (.1169)	.0515 (.0234)	.0343 (.0156)	.0858 (.0389)	3.00
	60	.2577 (.1169)	.0515 (.0234)	.0773 (.0351)	.1288 (.0584)	2.00

control that there were mixture ratio radial variations within the combustion chamber. Using a simplified two-zone model (Figure 3-5), the losses associated with zonal operation were estimated. It was found (Reference 1) that the performance losses are very sensitive to the "core" mixture ratio and that reduced losses can be obtained by operating the "core" mixture ratio at or near the optimum value even for large coolant flow rates and hence low overall mixture ratios. Figure 3-6 shows the specific impulse zonal losses for the

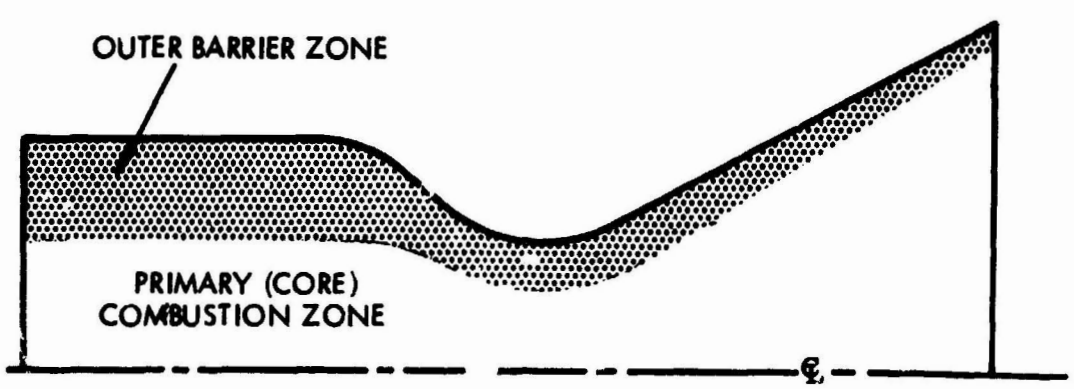

Figure 3-5. Simplified Chamber/Nozzle Zonal Model

FLOX/propane propellants for two operating conditions, one with the "core" mixture ratio fired at the optimum equilibrium value and one with the overall mixture ratio maintained at the optimum value.

3.1.2 Propellant Characteristics

Various propellant characteristics are of primary importance to the successful operation of an inter-regen thrust chamber. These include combustion product species, fuel decomposition and fuel coolant properties.

Figure 3-7 shows the chamber specie concentration for the 76% FLOX/propane propellants as a function of mixture ratio. A knowledge of the combustion species is important because it indicates the need for control of the wall mixture ratio and hence both the wall thermal and chemical environment. Of principal importance is the initiation of the appearance of solid carbon at mixture ratios below 3.0. The thermal analyses and experimental results of the previous program (Reference 1) indicates that carbon deposition in the throat was necessary for inter-regen operation since it acts as a thermal barrier to limit the heat input to the throat. Figure 3-8 shows the carbon mass fraction from each of the LPG fuels. As seen, the higher the carbon to hydrogen ratio the higher the carbon mass fraction. This is one of the primary reasons for selecting propane as the coolant on this program, the other being its physical properties and specifically its higher boiling point.

The propellant physical properties are given in Table 3-2. The physical properties of principal importance to the design of an inter-regen thrust chamber are those associated with the fuel's heat absorption capability, namely, the vapor pressure and heat vaporization (Figures 3-9 through 3-11). From a liquid cooling standpoint, Figure 3-9 shows the maximum temperatures to which

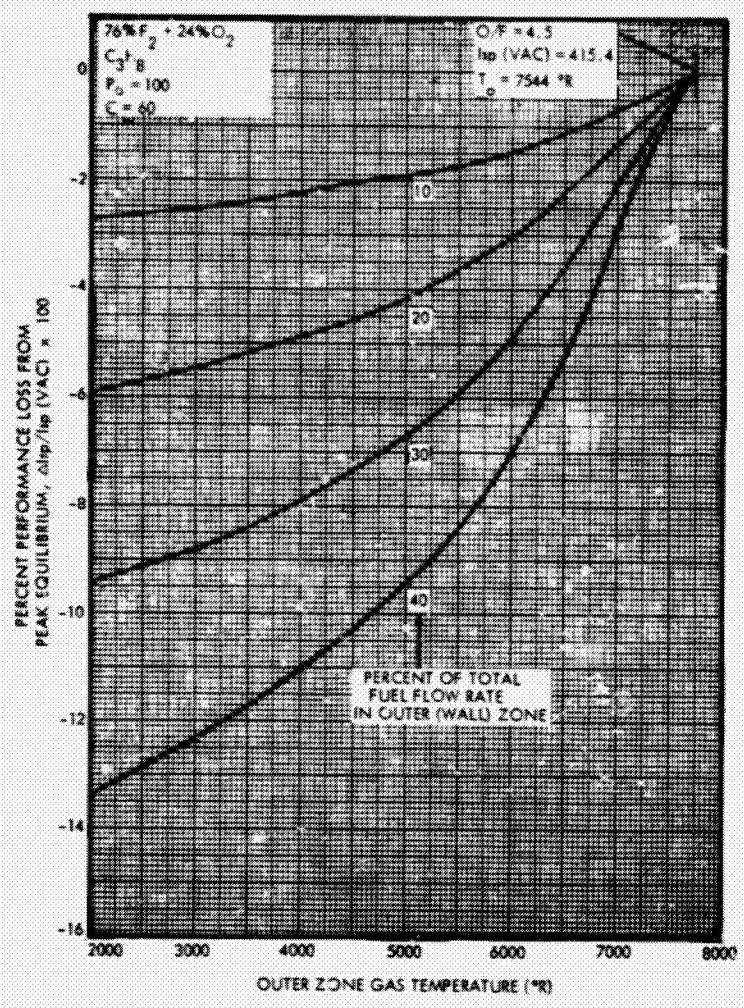

(a) Overall Mixture Ratio Maintained at Peak Equilibrium Value

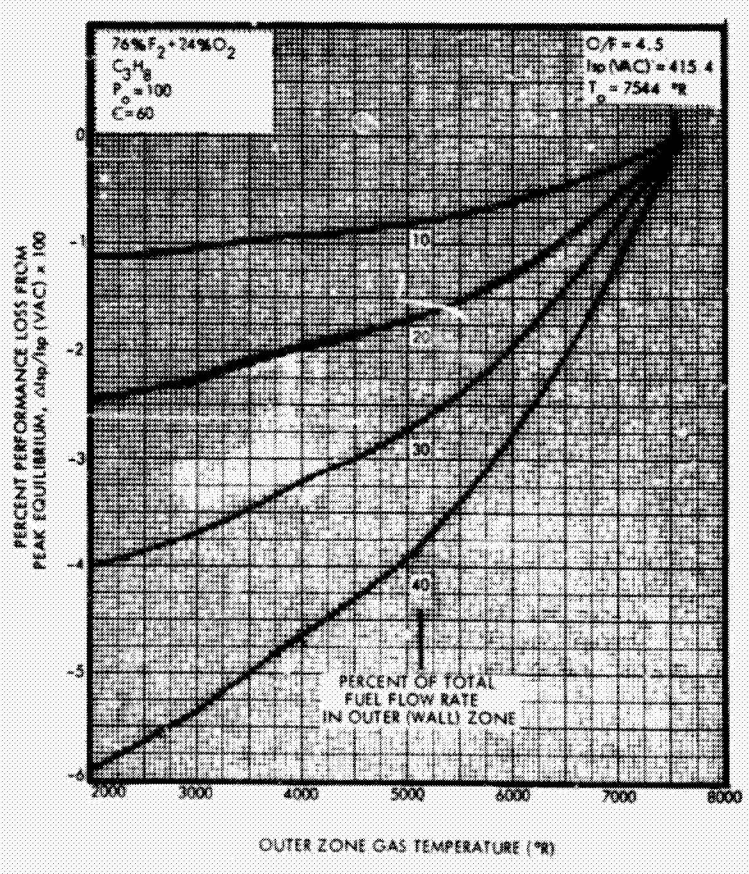

(b) Core Mixture Ratio Maintained at Peak Equilibrium Value

Figure 3-6. Specific Impulse Zonal Losses

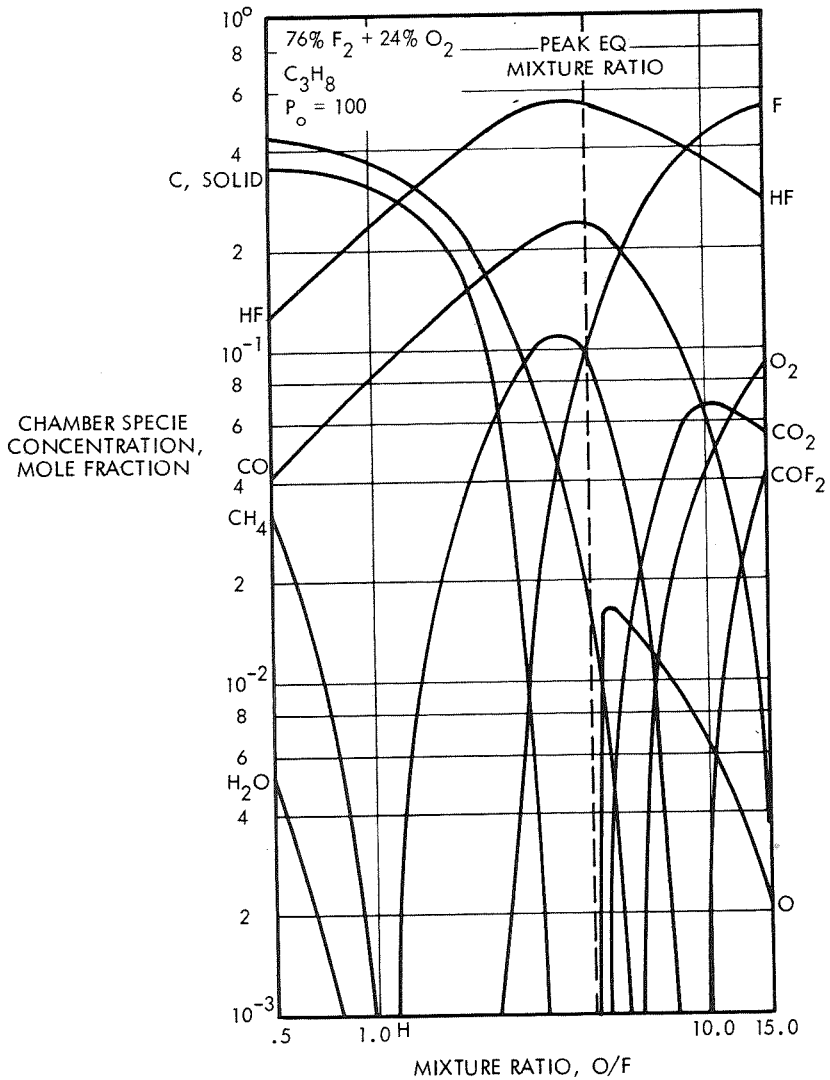

Figure 3-7. Chamber Specie Concentration Mixture Ratio Variation

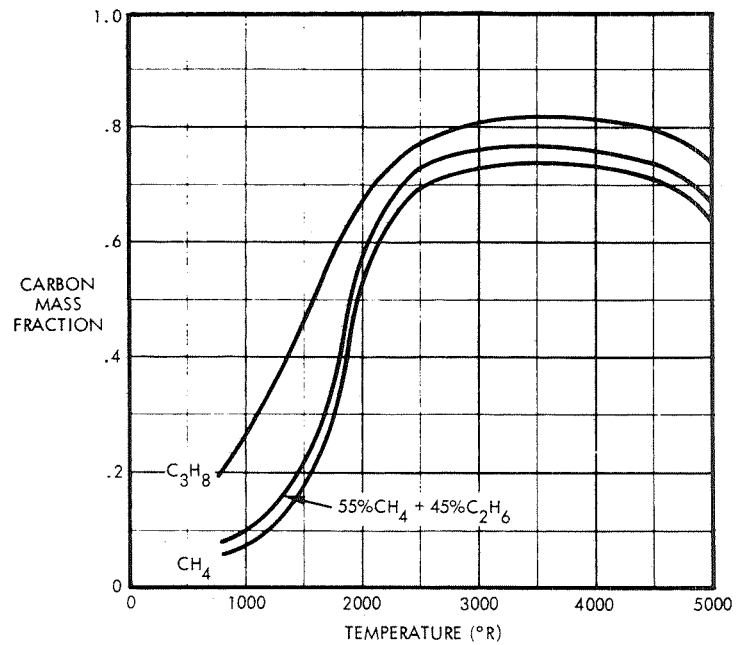

Figure 3-8. Carbon Deposition Mass Fraction (All Fuels)

Table 3-2. Propellant Physical Property Summary

PROPERTY	PROPANE	FLOX
Chemical Formula	C_3H_8	76% F_2 + 24% O_2
Molecular Weight	44.094	36.6
Normal Freezing Point, °R °K	154.0 85.6	--
Normal Boiling Point, °R °K	415.9 231.1	--
Liquid Density at NBP lb/ft^3 Kg/m^3	36.4 583.1	88.51 1417.8
Liquid Density at 140°R, lb/ft^3 Kg/m^3	--	91.49 1465.5
Critical Temperature, °R °K	666.0 370.0	--
Critical Pressure, psia nt/m^2	618.7 4.266×10^6	--
Critical Volume, ft^3/lb m^3/Kg	.0709 .0044	
$\Delta H_{vaporization}$ at NBP, Btu/lb Joules/Kg	183.05 4.26×10^5	--
ΔH_{fusion}, Btu/lb Joules/Kg	34.38 7.99×10^4	--
Viscosity at NBP, lb/ft-sec nt-sec/m^2	1.1×10^{-4} 1.6×10^{-4}	1.4×10^{-4} 2.1×10^{-4}
Thermal Conductivity at NBP, Btu/ft-hr-°R Joules/m-sec-°K	.058 .100	.089 .154
Specific Heat at NBP, Btu/lb-°R Joules/Kg-°K	.532 2.22×10^3	.374 1.57×10^3

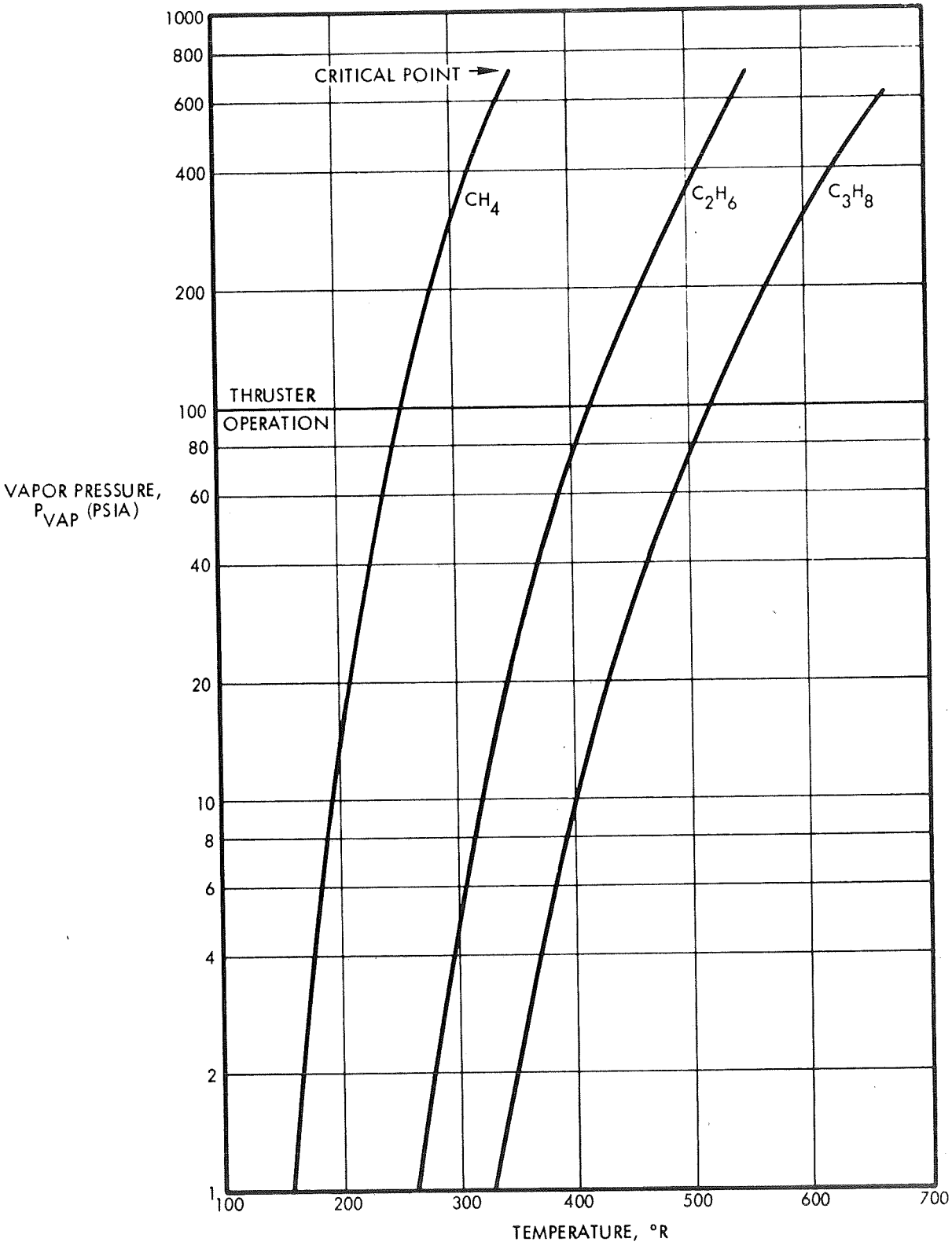

Figure 3-9. LPG Vapor Pressure Variation with Temperature

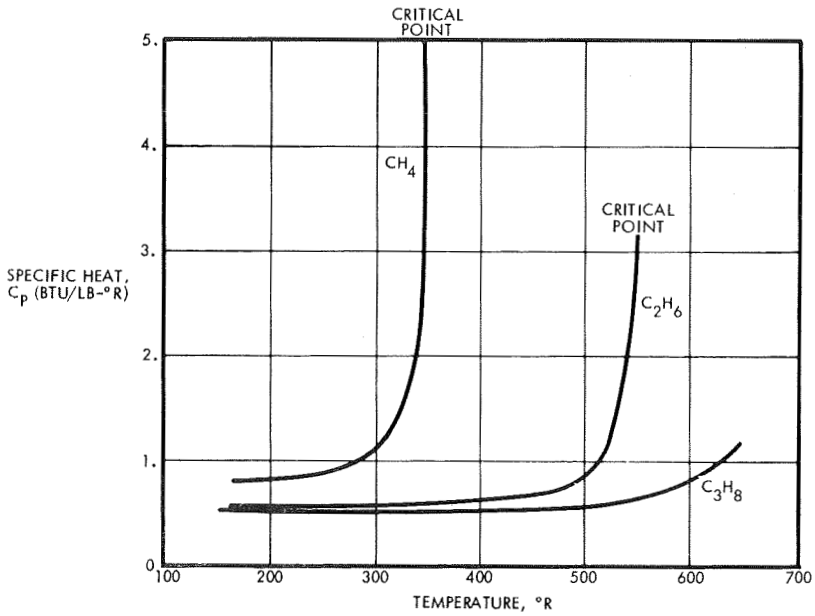

Figure 3-10. LPG Fuel Specific Heat

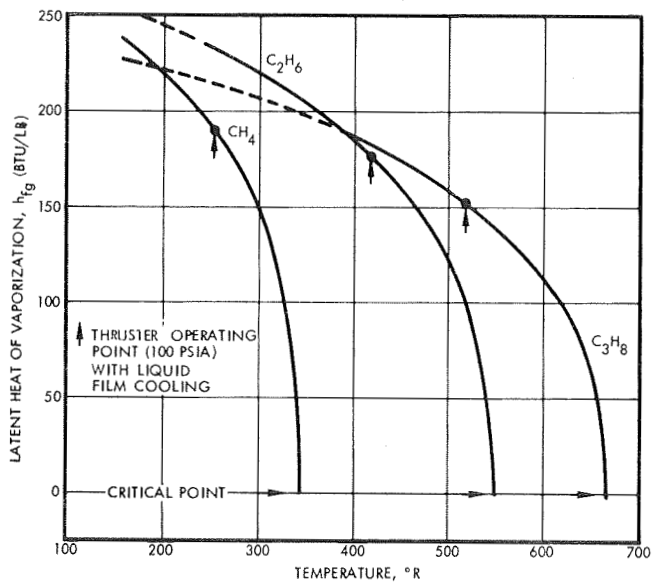

Figure 3-11. LPG Fuel Heat of Vaporization

each of the LPG fuels can absorb heat. As noted, propane can absorb heat as a liquid up to 516°R (287°K) in a 100 psia (6.89×10^5 nt/m^2) environment. However, the fuels can also absorb heat as gases both through sensible heat absorption and by thermal decomposition. Thus, the total heat absorption capability of a given fuel is,

$$H_T = \bar{C}_P \, (T_{sat} - T_{in}) + \Delta H_{fg} + \Delta H_G \qquad (3\text{-}1)$$

where

H_T = total heat absorption capability

T_{sat} = saturation temperature (based on P_o)

T_{in} = inlet temperature

ΔH_{fg} = heat of vaporization at the saturation temperature

ΔH_G = heat absorption of gaseous fuel including decomposition

Figure 3-12 presents the total heat absorption capabilities of three LPG fuels and MMH for comparison. As seen in the figure, propane has nearly the same liquid heat absorption capability of the methane/ethane but has a significantly higher liquid range. For this reason and because of its better theoretical carbon deposition characteristics, propane was selected as the fuel for this program. Another property of importance to inter-regen analysis is the fuel nucleate boiling characteristics. These were evaluated in Reference 1. Figure 3-13 gives the experimental results for propane at two different bulk temperatures.

3.1.3 Film Coolant Analysis

The experimental results of Reference 1 indicated that the film coolant was not remaining as a liquid on the chamber walls. Previous work with earth storable propellants as film coolants indicated cooling efficiencies of 30 to 40 percent. With the use of methane/ethane, a coolant efficiency of less than

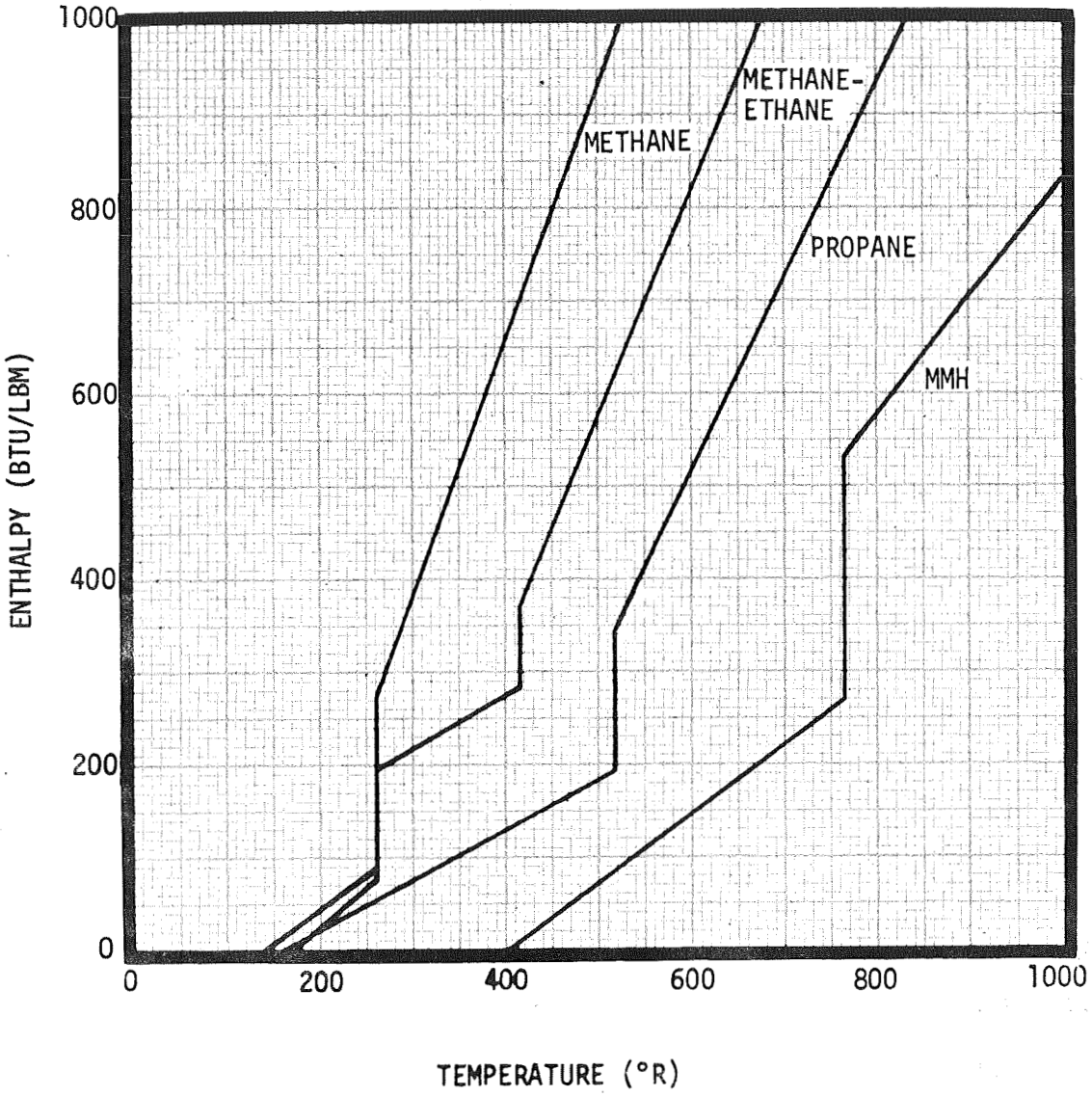

Figure 3-12. Fuel Heat-Absorption Capability

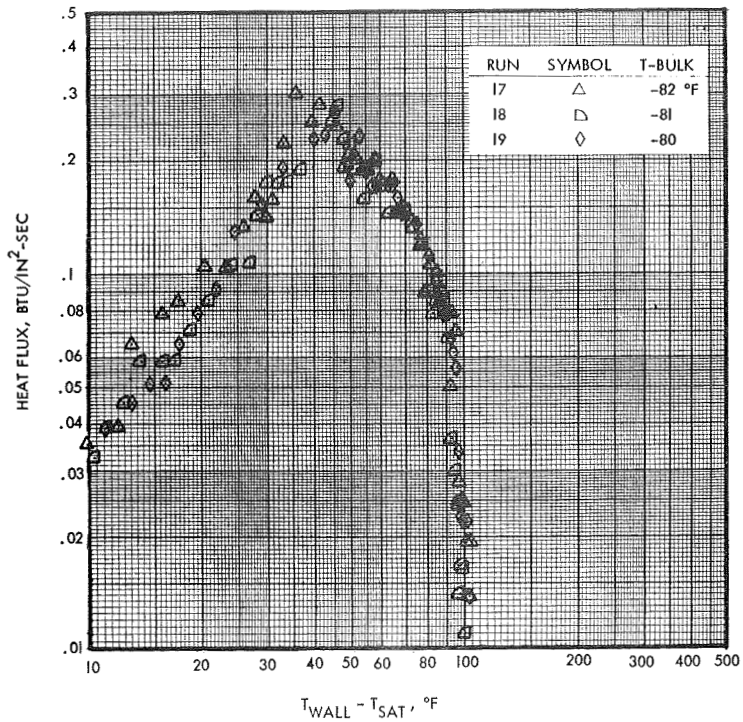

3-13a. Subcooled Pool Boiling of Propane (T_{bulk} = -80°F = 211°K)

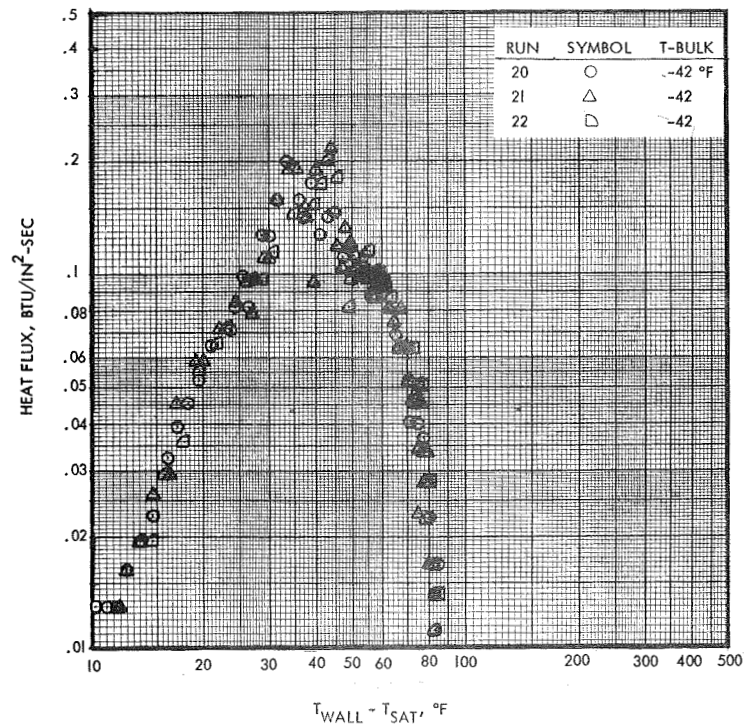

3-13b. Saturated Pool Boiling of Propane (T_{bulk} = -42°F = 232°K)

Figure 3-13. Nucleate Boiling Characteristics of Propane

10 percent were measured. An analysis of the mechanisms involved in the loss of coolant effectiveness is based on a system which considers a cresting wave of coolant which is stripped from the wall by shear with the primary combustion gases. In Reference 2, an approximate energy balance on a gas driven wave of amplitude, h, is given by

$$\frac{dh}{dt} = \left\{ \frac{\beta \rho_g (V_g - c)^2 k}{2\rho_\ell c} - \frac{2\mu_\ell k^2}{\rho_\ell} \right\} h \tag{3-2}$$

where

β = a sheltering parameter $\sim 1/3$

c = wave velocity

k = wave number

ρ = density

μ = viscosity

The wave velocity for capillary type waves is given by

$$c = \sqrt{\frac{\sigma k g}{\rho_\ell}} \tag{3-3}$$

Substitution of this result into the Equation (3-2) for $V_g >> c$ gives

$$\frac{dh}{dt} = \frac{h}{\tau}$$

or

$$\frac{1}{\tau} = \sqrt{\frac{\pi}{2}} \frac{\beta \rho_g V_g^2}{\sqrt{\sigma \rho_\ell g \lambda}} - \frac{8\pi^2 \mu_\ell}{\rho_\ell \lambda^2} \tag{3-4}$$

Now, the amplitude growth-rate is zero for the reciprocal time modulus of

$$\frac{1}{\tau} = 0.0$$

This also defined a minimum wavelength for maintained waves,

$$\lambda_{min} = 2\pi \sqrt[3]{16} \left(\frac{\mu_\ell \sqrt{\frac{\sigma g}{\rho_\ell}}}{\beta \rho_g V_g^2} \right)^{2/3} \qquad (3\text{-}5)$$

At this point we now assume the following ideal wave structure at the point of crest-stripping

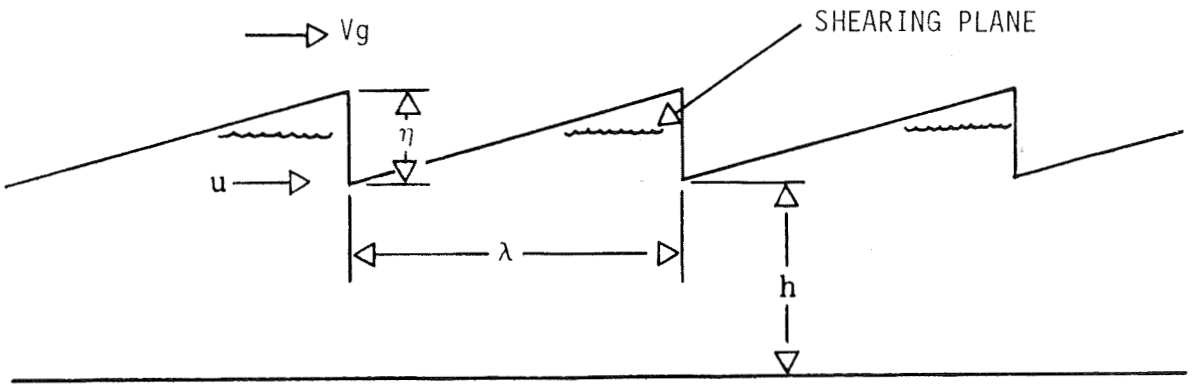

It is necessary to have a value of the parameter, η, in terms of the wavelength, λ, to progress further. Such a relation is available from theoretical hydrodynamics (Reference 3) which gives

$$\frac{u}{c} = \frac{\eta}{h} \qquad (3\text{-}6)$$

where

$$c = \sqrt{gh}$$

$$\eta = u\sqrt{\frac{h}{g}}$$

Performing a force balance between the dynamic force, F_D, and a shearing force, F_μ, on the base of the wave establishes the equilibrium height, η, without requiring knowledge of the h/g ratio (assuming negligible surface-tension). This gives

$$\eta = \left[\frac{2g\mu_\ell \lambda u}{C_D \rho_g V_g^2} \right]^{1/2} = K \left[\mu_\ell \lambda u \right]^{1/2} \tag{3-7}$$

The actual shearing-plane occurs at $b\eta$ and a rigorous dynamic force balance can now be written

$$C_D \frac{\rho g (V_g C)^2}{2g} - \frac{2\sigma}{b\eta} - \frac{\mu_\ell \lambda u}{\eta^2} = \frac{\lambda \rho_\ell}{2} \frac{du}{dt} \tag{3-8}$$

From this relation the time, t_{og}, for the shared element to totally displace can be determined. The mass-rate per wave is then

$$\dot{w}_{s,\lambda} = \frac{b^2 \lambda \eta \rho_\ell}{2gt_{og}} \tag{3-9}$$

The number of waves per unit of length is $1/\lambda$. The total stripping-rate per unit area is then

$$\dot{w}_s = \frac{b^2 \eta \rho_\ell}{2gt_{og}} \tag{3-10}$$

Now b^2 is unknown, as are some of the other interactions; however, the physical property significance can be determined to be

$$\dot{w}_s \sim \frac{1}{\mu} \left(\frac{\rho_\ell}{\sigma}\right)^{1/4} \tag{3-11}$$

It is immediately seen that the stabilizing properties to minimize wave-stripping are viscosity and surface tension. With this result the stripping loss-ratio for selected fluids can be made.

In the previous program (Reference 1), it was found to be impossible to liquid film cool the combustion section of the thruster with the 55-45 methane/

ethane blend coolant. When MMH was substituted at the same percentage flow rate as a film coolant, the combustion section could be liquid-film-cooled a distance of 1.75 inches, and the thruster could be operated in a film/conduction mode.* It is of interest to compare the LPG and MMH with the above theory to determine expected behavior. The loss ratio is

$$\frac{\dot{w}_{C_3H_8,\ s}}{\dot{w}_{MMH,\ s}} = \left(\frac{\mu_{MMH}}{\mu_{C_3H_8}}\right)\left(\frac{\rho_{C_3H_8}}{\rho_{MMH}} \cdot \frac{\sigma_{MMH}}{\sigma_{C_3H_8}}\right)^{1/4} = 3.35 \qquad (3\text{-}12)$$

If the MMH could cool 1.75 inches in the 100 lb_f LPG thruster propane should be expected to cool 0.5 inch, which was in close agreement with the experimental result obtained. The stripping loss is

$$\dot{w}_s = \int_0^A \left(\frac{B}{\mu}\left(\frac{\rho}{\sigma}\right)^{1/4}\right) dA \qquad (3\text{-}13)$$

The loss caused by heat input is given by

$$\dot{w}_Q = \sum_{i=1}^{i} \frac{(Q/A)_i A_i}{\Delta H} \qquad (3\text{-}14)$$

The total loss is

$$\dot{w}_T = \frac{B}{\mu}\left(\frac{\rho}{\sigma}\right)^{1/4} A + \sum_{i=1}^{i} \frac{(Q/A)_i A_i}{\Delta H} \qquad (3\text{-}15)$$

This simplified analysis yields some of the reasons the LPG fuels can not be expected to operate in the conventional film-cooled manner and gives some insight into the problems to be encountered. Of course, factors other than those considered in the above analysis also contribute to the effectiveness of a film coolant. These include not only the coolant properties but also the chamber and injector geometries, the film coolant injection process and the degree of turbulence in the combustion zone.

---

* With a fixed FLOX/LPG primary (core) operating condition. Based on one 8-second test.

3.1.4 Inter-Regen Thermal Analysis

The basic inter-regen thermal analysis takes the basic chamber inner contour and integrates to determine the accumulated heat load into the chamber walls. For steady operation this heat must be removed by the coolant. The chamber heat load can be separated into two components: 1) the nozzle heat load - this must be conducted from the nozzle to the coolant, and 2) the chamber heat load - this is absorbed directly by the coolant. Knowledge of these heat loads and the coolant's heat absorption capability allows an estimation of the coolant flow rate required as given by:

$$\dot{w}_{fcool} = \frac{1}{\eta_{fc}} \left[\frac{\dot{Q}_N}{\Delta HL} + \frac{\dot{Q}_C}{\Delta HT} \right] \qquad (3\text{-}16)$$

where η_{fc} is the film coolant efficiency. As previously stated the results of Reference 1 indicated film coolant efficiencies of about 10% for the methane/ethane fuel in the conventional film cooling application. The Task I effort was partially directed toward comparing the propane and methane/ethane. These results are reported in Section 5.3.1.

3.1.4.1 Duct Analysis and Design

Task II evaluated the use of a ducted coolant design to modify the conventional film cooled inter-regen approach. Such a chamber uses a wall to protect the coolant until its injection into the chamber at a position upstream of the throat. The basic purpose of the duct is to increase the effectiveness of the film coolant into the throat region by isolating it from the primary zone interactions/shear effects. The sketch below illustrates the duct concept and the various heat input regions.

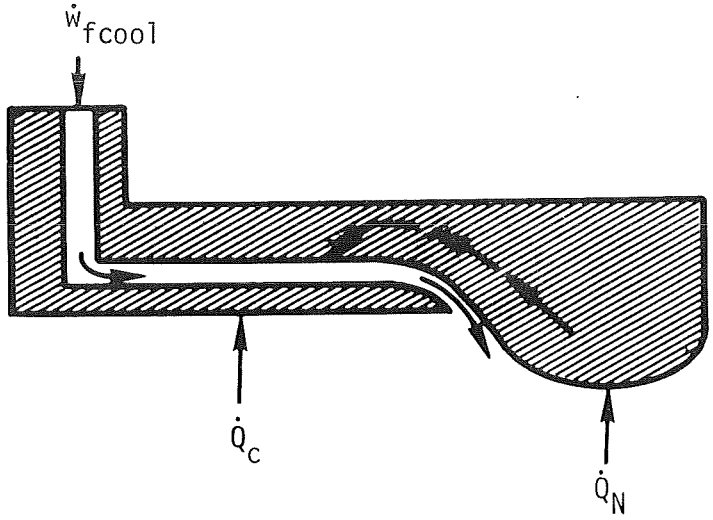

For the duct analysis, data from Reference 1 was used to estimate the operating conditions which the duct would experience. This information is tabulated in Table 3-3. The use of this experimental methane/ethane heat load data and the propane heat absorption capability curve (Figure 3-12) results

Table 3-3. Duct Cooling Chamber Heat Loads

Case	$\dot{w}_{fcool}$ (lbm/sec) (Kg/sec)	$\dot{Q}_C$ (Btu/sec) (Joules/sec)	$\dot{Q}_N$ (Btu/sec) (Joules/sec)	$\dot{Q}_T$ (Btu/sec) (Joules/sec)	$\dot{Q}_T/\dot{w}_{fcool}$ (Btu/lbm) (Joules/Kg)	T_e (°R) (°K)
30% duct 30% film	.0422 (.0191)	20 (21087)	8 (8435)	28 (29522)	664 (1.5×10^6)	660 (367)
60% duct 0% film	.0843 (.0382)	30 (31635)	4 (4217)	34 (35848)	403 (9.4×10^5)	550 (306)
40% dist. duct	.0375 (.0170)	25 (26359)	10 (10544)	35 (36902)	933 (2.2×10^6)	775 (431)
60% dist. duct	.0843 (.0382)	15 (15815)	6 (6326)	21 (22141)	249 (5.8×10^5)	516 (287)

in an estimation of the coolant effluent temperature, (T_e) for each case, also listed in Table 3-3. Only in the 60% coolant cases are the effluent temperatures near the saturation level. For the lower coolant flow rates, the coolant must absorb a significant portion of the heat input as a gas for successful operation to occur.

The next step in the design is to determine the shape of the duct passages, which is determined by the coolant flow rate and heat input. The duct must be sized so that the coolant velocity is high enough to accept the heat input and yet keep the chamber material from exceeding its temperature limit. For most cases the required coolant-side film coefficients are so high as to preclude the use of annular ducts due to the very small gaps which would be required. For rectangular channels the film coefficient for turbulent flow is given by

$$h_g = .023 \frac{k}{d_e} (Pr)^{.4} (Re)^{.8} \tag{3-17}$$

which can be expressed as a function of the flow rate, area per channel and the number of channels.

$$h_g = .023 \frac{k}{d_e} (Pr)^{.4} \left(\frac{\dot{W}_{fcool}}{\mu n}\right)^{.8} \left(\frac{d_e}{A}\right)^{.8} \tag{3-18}$$

In order to achieve reasonable channel sizes, it becomes necessary to use helical channels rather than axial channels. Thermal analyses of the best case of Table 3-3 results in the predicted temperature distribuiton seen in Figure 3-14 In addition to providing the required coolant velocity (i.e., film coefficient) the helical channels also provide increased heat transfer area. An additional advantage of the helical channels is the swirling motion of the coolant following its injection into the chamber will tend to keep it attached to the nozzle wall.

Two duct design approaches were evaluated during the program. One dumps all of the duct coolant at the end of the duct (total duct), while the other has holes drilled radially through the duct wall to admit part of the coolant into the chamber in a distributed manner. This second duct should be less effective from the standpoint of nozzle cooling, but should have smaller performance losses.

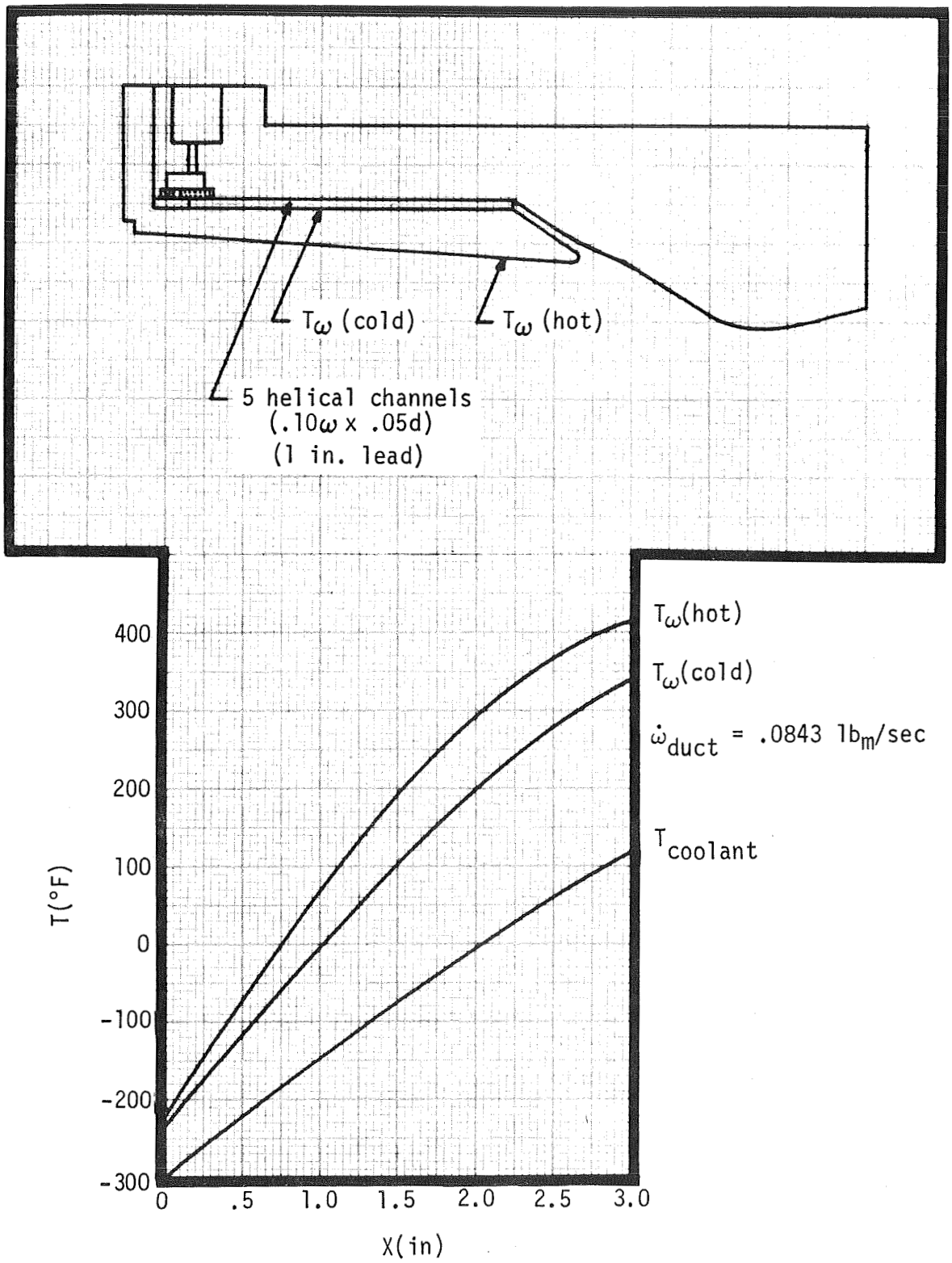

Figure 3-14. Ducted Chamber Design with Best Case Temperature Distribution

3.1.4.2 Duct Channel Geometry

The best duct channel design not only supplies the area required for the desired coolant velocity, but also acts to inhance the heat transfer area in a manner similar to the case of fins in a heat exchanger. The sketch below shows a section of a duct wall with one pair of coolant channels.

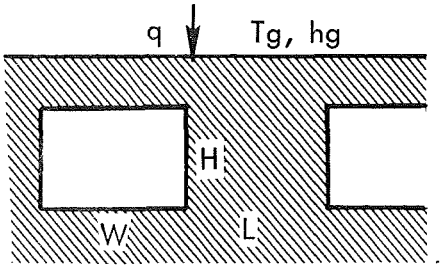

For an infinite conductivity material, the sides of the channels are equally as effective as the face.

The hot gas heat transfer area is given by

$$A_g = W/2 + L/2 \tag{3-19}$$

While the coolant heat transfer area is

$$A_c = W/2 + H \tag{3-20}$$

For the best channel configuration, the coolant area, A_c, should be greater than the gas side (heated) area, A_g.

$$A_c > A_g \quad \therefore \quad H/L > 0.5$$

For a given channel height to width ratio, H/w = C

$$\frac{A_c}{A_g} = \frac{W/2 + H}{W/2 + L/2} \tag{3-21}$$

and

$$\frac{A_c}{A_g} = \frac{W + 2H}{W + 2nH} = \frac{1 + 2C}{1 + 2nC} \tag{3-22}$$

where

$$L/2 = nH \ , \quad n < 1$$

Figure 3-15 shows the area enhancement factor, A_c/A_g, as a function of the channel height to width ratio for selected values of the channel spacing to height parameter. As can be seen, deep channels with small inter-channel spacing give the greatest heat transfer area enhancement. This effect would be somewhat lessened for finite conductivity materials.

3.1.4.3 Duct Thermal Model

A thermal model was generated for use in the experimental data analysis and is shown in Figure 3-16. Certain nodes of the model were made to correspond to the thermocouple locations on the experimental thrust chamber hardware. This model was used with the Thermal Analyzer Program (TAP) with input data coming from the experimental thermocouple data. The TAP program then calculated the temperature at all the nodes and the heat loads for each node. This data was then converted into accumulated heat load and heat flux plots for the tests analyzed (Section 5.3.2).

3.2 GRAPHITE THRUSTER DESIGN ANALYSIS

As a supplement to the major emphasis of this program, one graphite material thrust chamber was designed, fabricated and tested to determine the effects of throat erosion and carbon deposition.

3.2.1 Design Selection

The cooling mode selection for the graphitic material thrust chamber was primarily based on simplicity of design, ease of attachment to the injector and cost. This resulted in the selection of an insulated design where the inner wall operates at very near the local recovery temperature. Following this decision, the selection of material was based on material properties availability and previous test experience. From the previous program, stainless steel cans and ablative material (MX 2625) liners were available. However, the ablative material could not be used as the total insulator due to its relatively low operating temperature. This meant the use of a composite insulator. The material selected as the inner insulator was PYROLAREX 300,* a graphite composite structure with high compressive strength and

* A product of HITCO.

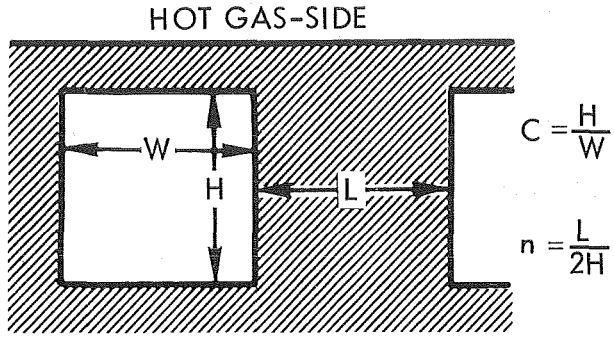

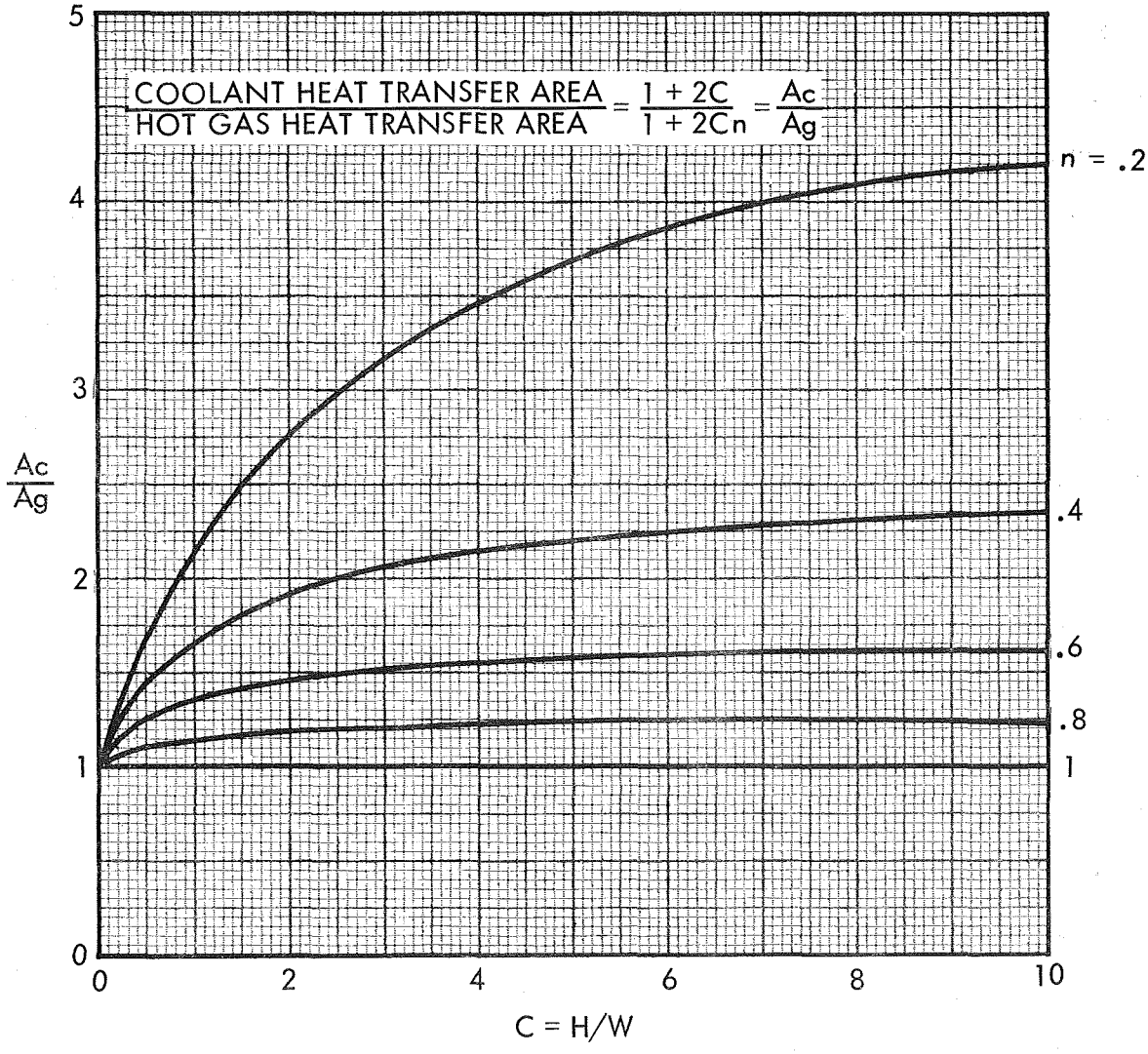

Figure 3-15. Coolant Channel Heat Transfer Area Enhancement

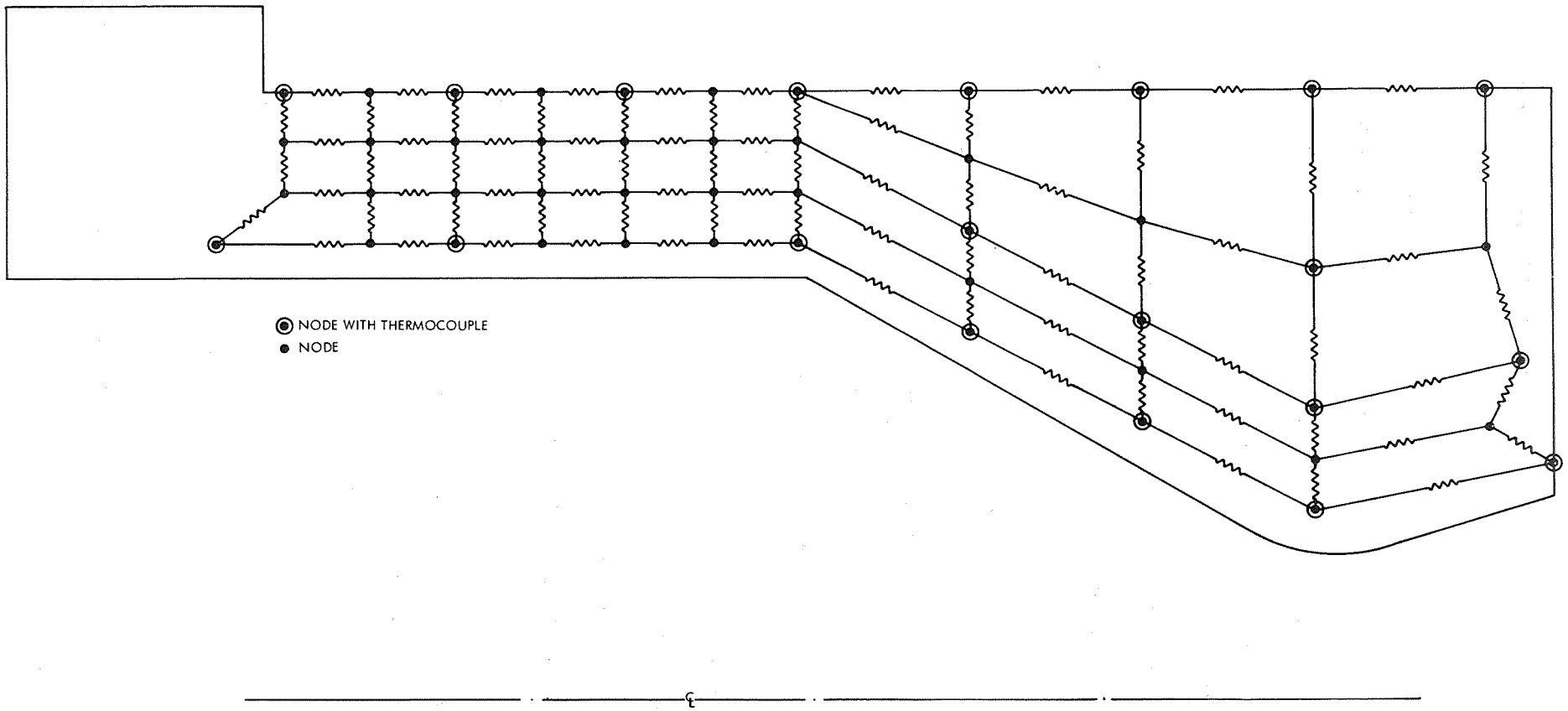

Figure 3-16. Inter-Regen Ducted Chamber Thermal Model

low thermal conductivity. An infiltration process would have permitted the u of this material as the inner liner of the chamber; however, it was decided t insufficient data was available on this product. The final material selectec as the inner chamber walls were CARB-I-TEX* 700 and 700N. These were laminat composite graphite structures. The chamber liner was CARB-I-TEX 700 with the laminate perpendicular to the centerline, while the throat insert was CARB-I-700N with the laminates also perpendicular to the centerline. CARB-I-TEX 700I the asme as 700 but has additional fibers perpendicular to the laminates to the chances of delamination. This basic chamber design is hsown in Figure 3

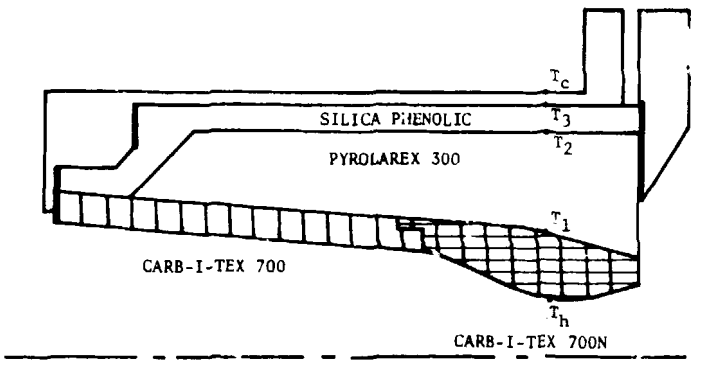

Figure 3-17. Insulated Graphite Thrust Chamber Design

3.2.2 Thermal Analysis

Analysis of the above composite design (Figure 3-17) was used to determ the radial temperature distribution in the throat under steady-state condit for various throat recovery temperatures. These results are shown in Table and indicate that all interface temperatures are compatible with the selecte materials. Previous experimental results (Reference 1) indicates the throa recovery temperature (T_h) to be about 4200°F.

Table 3-4. Insulated Graphitic Thrust Chamber Thermal Analysis Results

T (hot) (°F) (°K)	T_1 (°F) (°K)	T_2 (°F) (°K)	T_3 (°F) (°K)	T (cold) (°F) (°K)
5500 (3311)	5480 (3300)	3720 (2322)	1850 (1283)	1820 (1267)
4500 (2756)	4482 (2746)	3400 (2144)	1720 (1211)	1700 (1200)
3500 (2200)	3484 (2191)	3100 (1978)	1520 (1100)	1500 (1089)

*Carborundum Company

4. HARDWARE DESCRIPTION

The nominal engine design conditions for the test hardware were 100 lb_f (444.8 nt.) vacuum thrust for a nozzle expansion ratio of $\epsilon = 60$ and chamber pressure of 100 psia (6.89×10^5 nt/m^2). The hardware was designed for operation with the 76% fluorine/24% oxygen oxidizer and propane fuel; with propellants delivered to the injector at -300°F (88.7°K).

The basic injector utilized during the program was fabricated during the previous contract (Reference 1). Modifications were made to the pintle assembly for this program.

4.1 INJECTOR DESIGN

The basic injector was that developed under Contract NAS3-11184 (Reference 1) and is shown in Figure 4-1. This injector allowed the use of various pintles to allow different interactions between the primary fuel and oxidizer streams. The fuel gap could be varied with the use of shims placed under the oxidizer pintle. Integrated within the injector was the film coolant with 20 holes of .020 inch (.000508 m) diameter directed 15° from the centerline. Figure 4-2 shows a disassembled view of the injector parts; injector body, pintle, shims, and feed adapter.

Assembly of the injector is accomplished by insertion of the pintle into the injector body with the required shim. The backup shown is then placed over the pintle and the feed adapter is bolted down to seat the pintle with the desired fuel gap. All seals with the injector are solid aluminum in the type "O" condition.

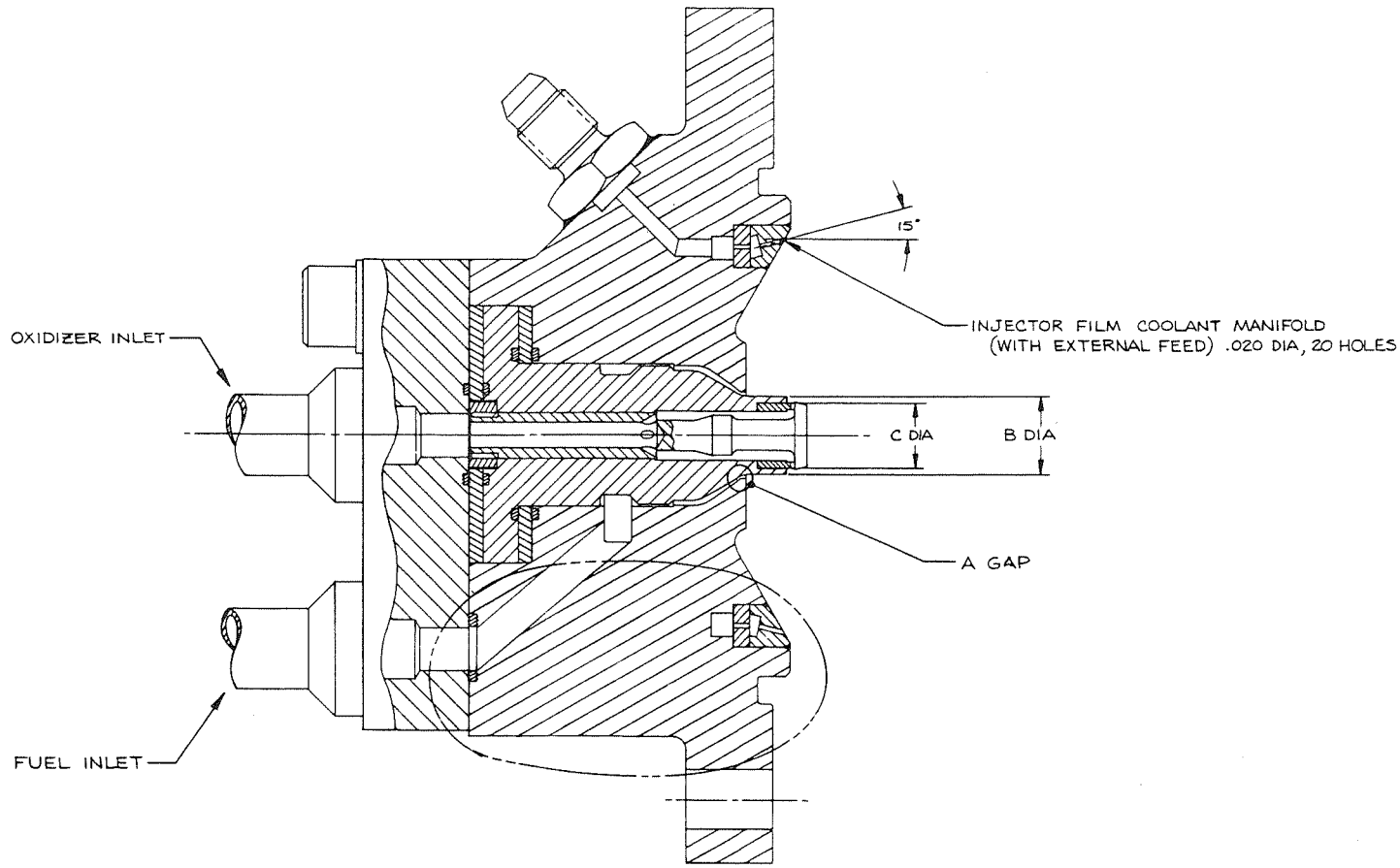

Figure 4-1. 100 lb_f FLOX/LPG Injector Assembly with Integrated Film Coolant

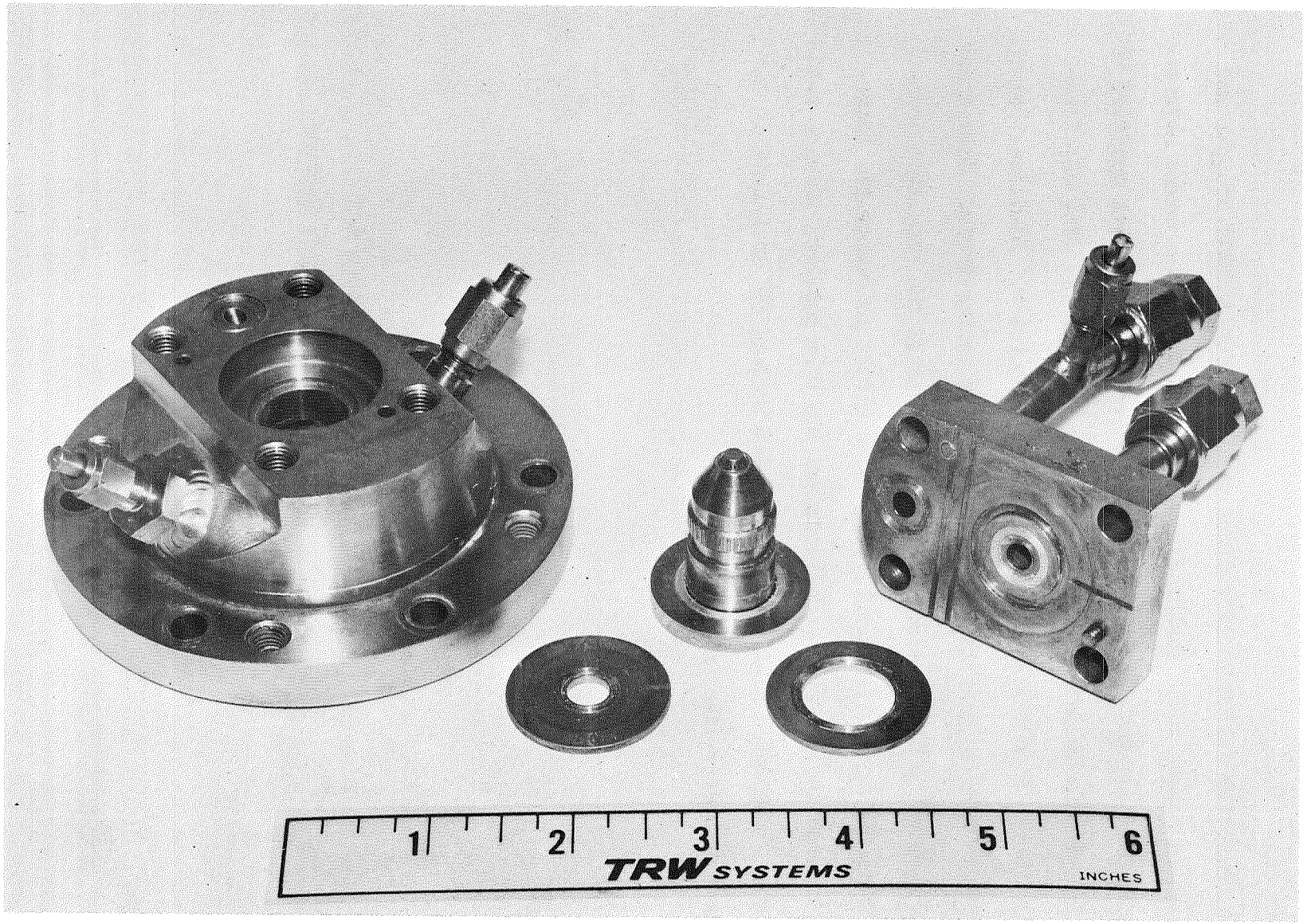

Figure 4-2. Coaxial Injector with Disassembled Parts

Three pintle design modifications were made during this program and are shown in Figure 4-3. The baseline design uses totally radial oxidizer streams. This was the design used in the previous effort, but modified to maintain the same momentum ratio for the new propellants. The resultant momentum vector from this pintle is about 8° downstream. Additional pintle designs were made to cant the resultant momentum vector further downstream. These are shown in Figure 4-3a and 3b. These canted the resultant propellant stream 30° and 60°, respectively, in an effort to reduce the interaction between the primary propellants and the film coolant. Figure 4-4 shows a picture of the three pintles. Figures 4-5 through 4-7 show each of the pintles assembled in the injector body.

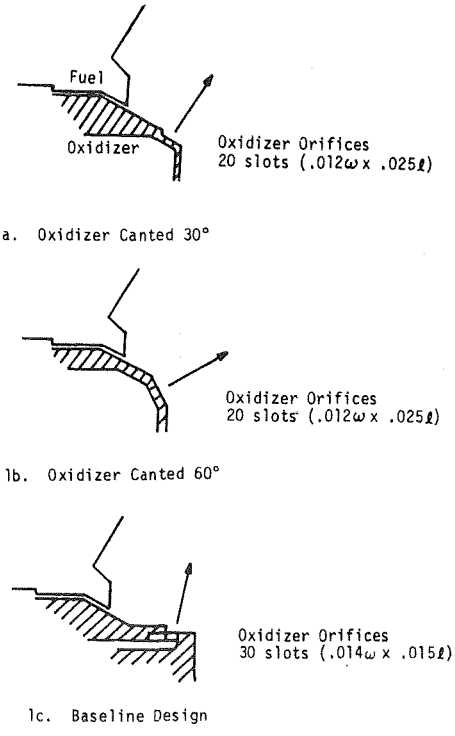

Figure 4-3
Injector Pintle Designs

Figure 4-4. Coaxial Injector Pintle Designs

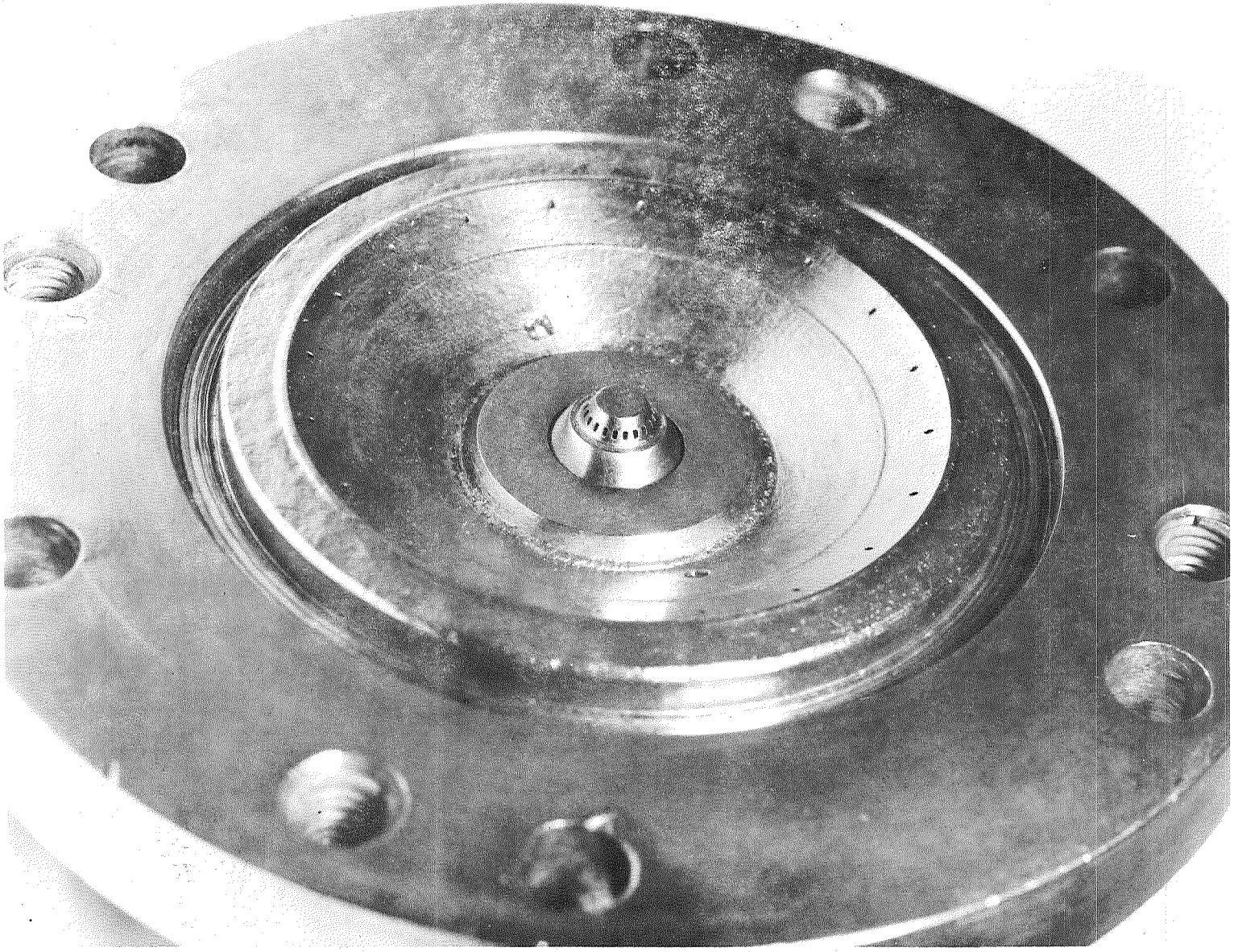

Figure 4-5. Film Cooled Coaxial Injector with 30° Canted Pintle Element

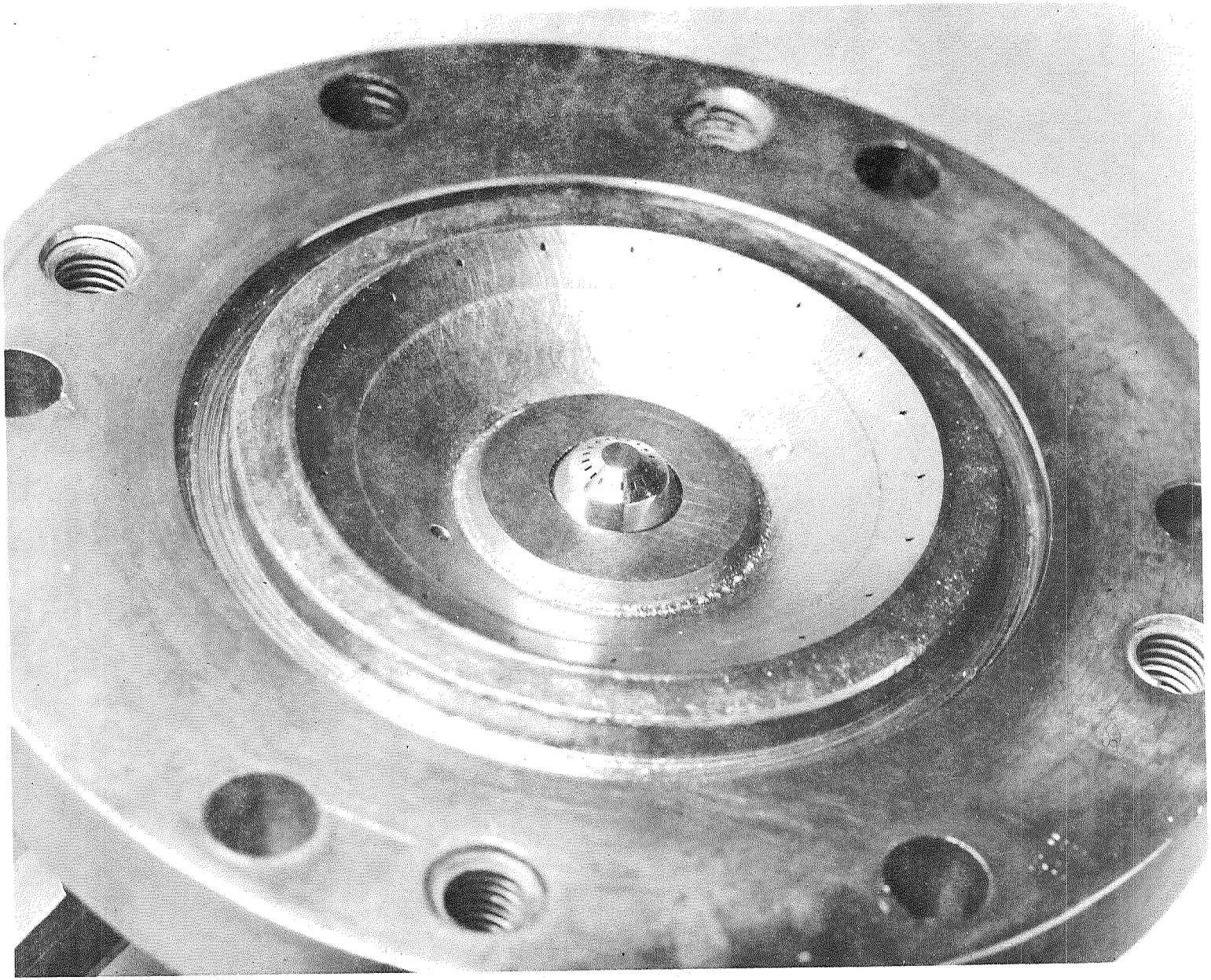

Figure 4-6. Film Cooled Coaxial Injector with 60° Canted Pintle Element

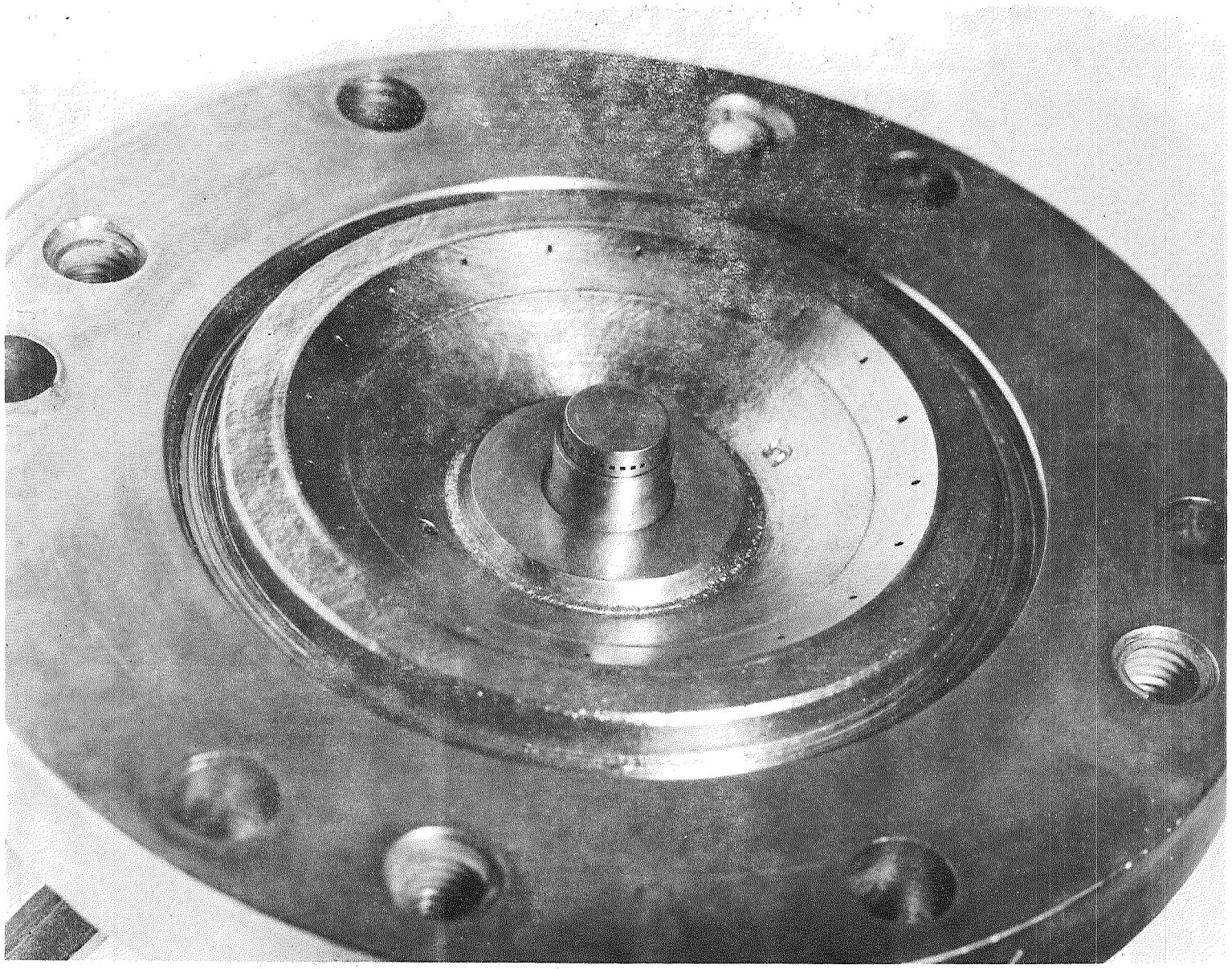

Figure 4-7. Film Cooled Coaxial Injector with Baseline Pintle Element

Prior to testing, each of the injector configurations were water flowed to obtain their hydraulic characteristics. To obtain the various coolant flow rates, an adjustable metering valve was used to split some of the fuel away from the primary injector core. This was also hydraulically characterized. Data from these hydraulic calibrations are shown in Figure 4-8.

4.2 THRUST CHAMBER DESIGNS

The basic thrust chamber design was a thick walled copper chamber with thermocouples located axially, circumferentially and radially to obtain the heat transfer information necessary for the evaluation of the chamber design concepts.

4.2.1 Inter-Regen Thrust Chambers

Two basic inter-regen thrust chambers were used during this program. Both were thick walled copper chambers with one using conventional film cooling while the other employed the previously discussed ducted design approaches.

Figure 4-9 is a sketch of the film cooled inter-regen thruster design with detailed thermal instrumentation. Also indicated in the figure are the resultant momentum vectors from the three pintles previously described. The chamber has tapered walls with axial grooves aligned with the film coolant streams. These acted to protect the film coolant from the primary combustion gases.

The major chamber design effort associated with this program was in the design of ducted chambers. Figure 4-10 shows the original duct chamber design. This design had a modification whereby holes were drilled radially through the duct wall to allow distributed injection of the coolant. Pictures of the

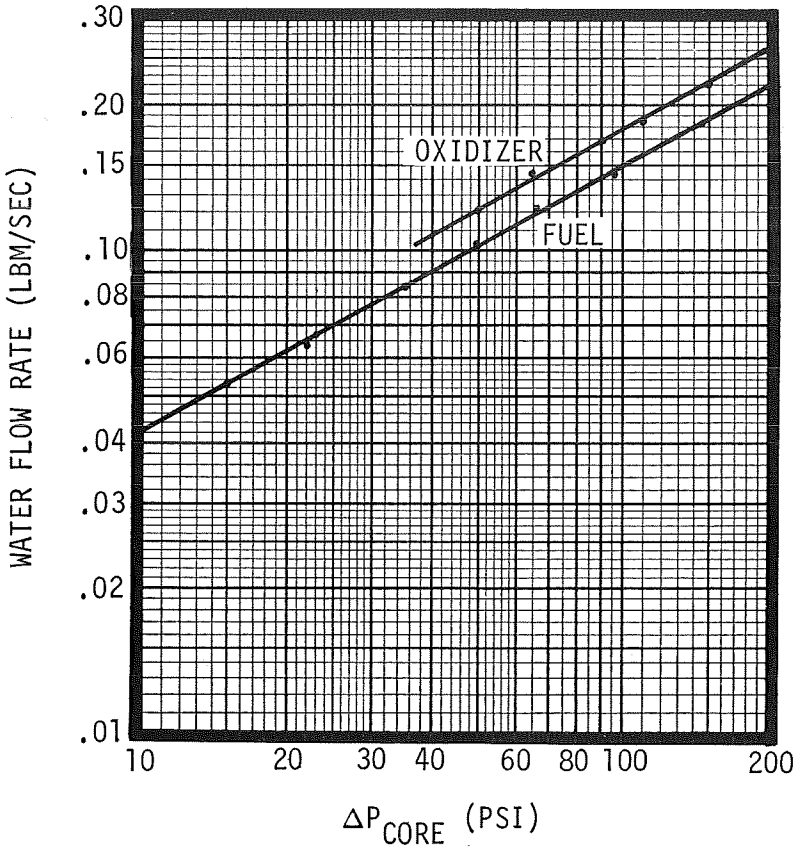

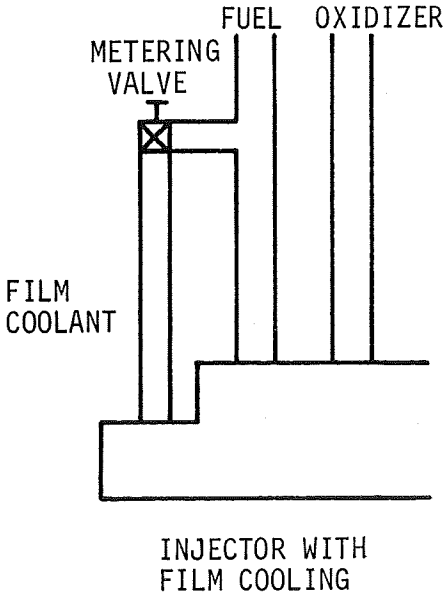

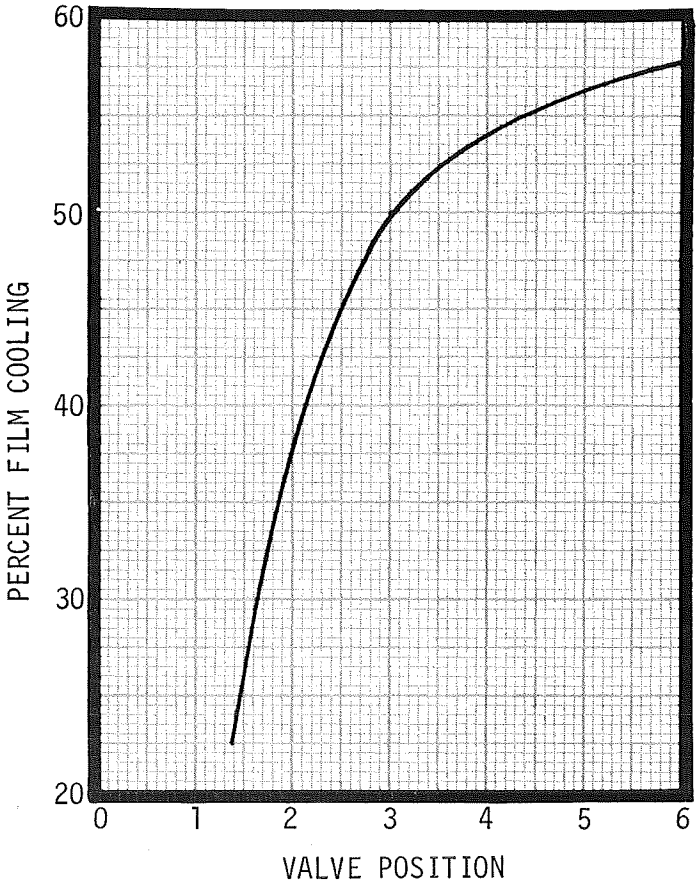

Figure 4-8. Injector Hydraulic Characterization

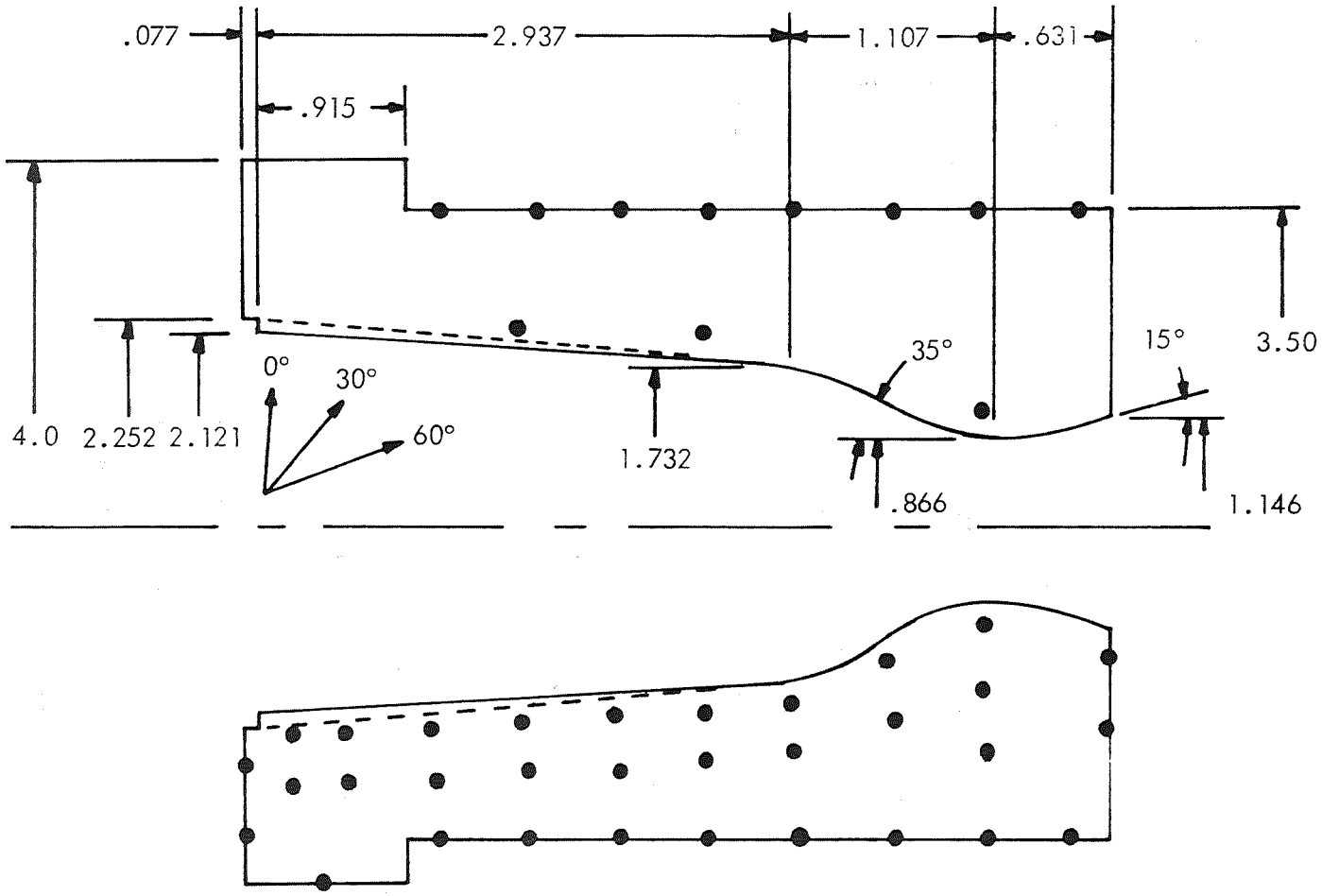

Figure 4-9. Copper Film Cooled Inter-Regen Thrust Chamber with Detailed Thermal Instrumentation (L* = 15)

distributed duct cooled thrust chamber are shown in Figure 4-11. Detailed thermocouple instrumentation similar to that on the film cooled thruster was incorporated in the duct cooled chambers as indicated in Figure 4-10.

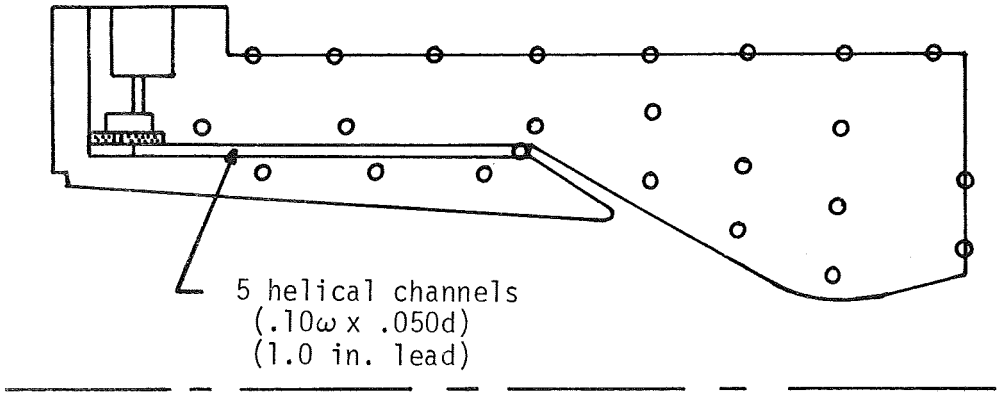

Figure 4-10. Ducted Thrust Chamber Design

Following tests on the original duct design, a modified duct cooled chamber was designed and fabricated. This design appears in Figure 4-12. This design uses a slightly different duct channel geometry configuration to increase the coolant velocity. Incorporated in this design (which consisted of a two-piece duct) was the provision to extend the duct almost to the throat. Again, both the total and distributed ducts were fabricated and the chamber contained thermocouples for detailed thermal information. A photograph of the modified duct chamber ports appears in Figure 4-13.

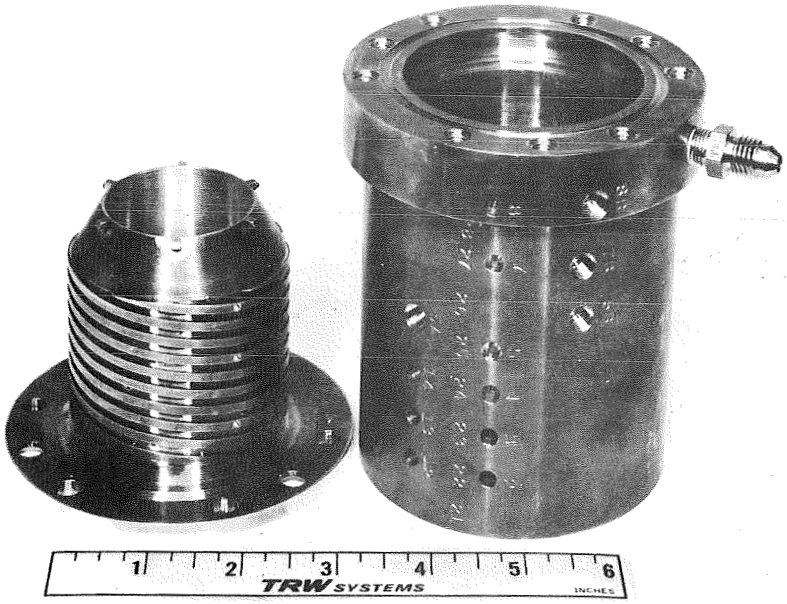

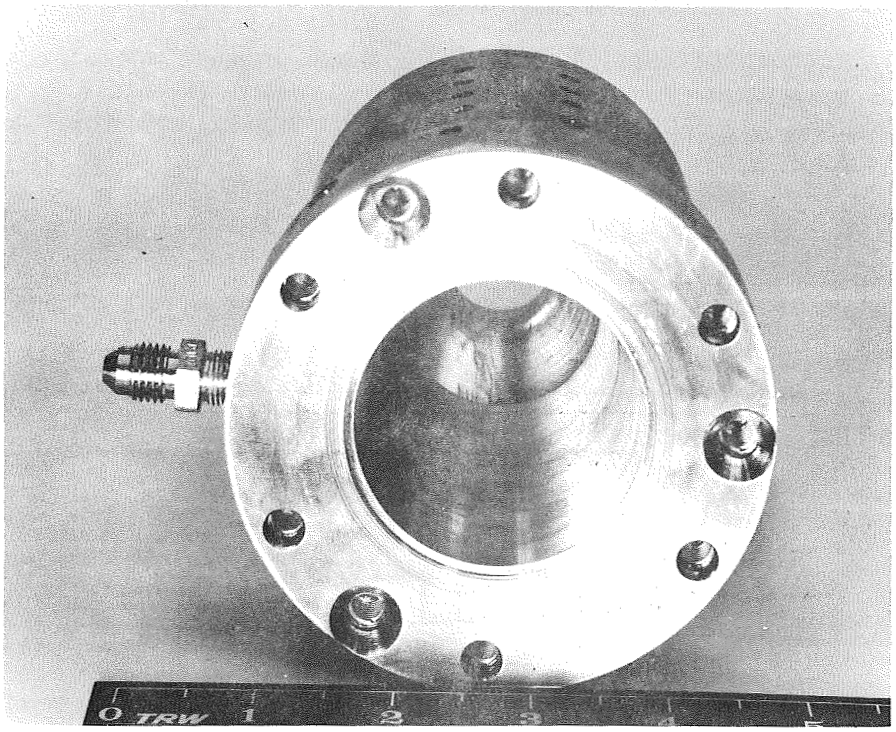

Figure 4-11. Ducted Thrust Chamber (With Distributed Flow Duct)

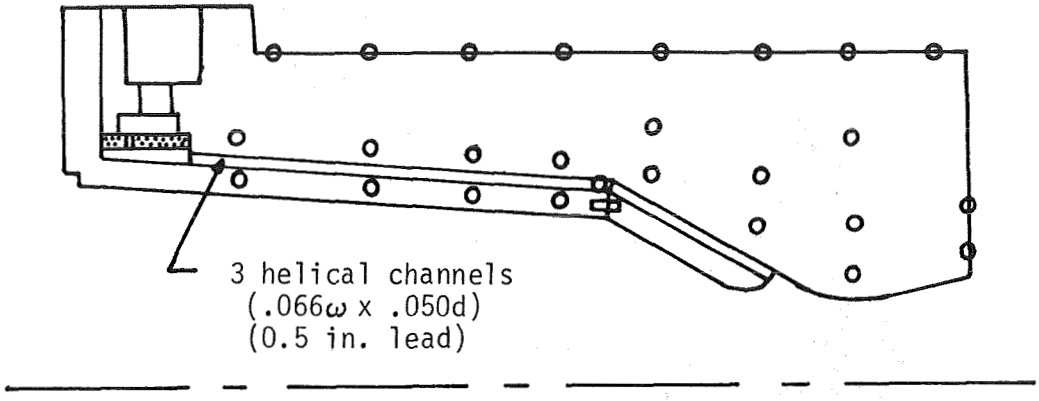

Figure 4-12. Modified Duct Cooled Chamber Design with Instrumentation

4.2.2 Graphitic Thrust Chamber

The graphitic thrust chamber design described in Section 3.2 and shown in Figure 4-14 reveals the composite nature of the design and the detailed thermal instrumentation. Figure 4-15 shows pretest photographs of the thrust chamber.

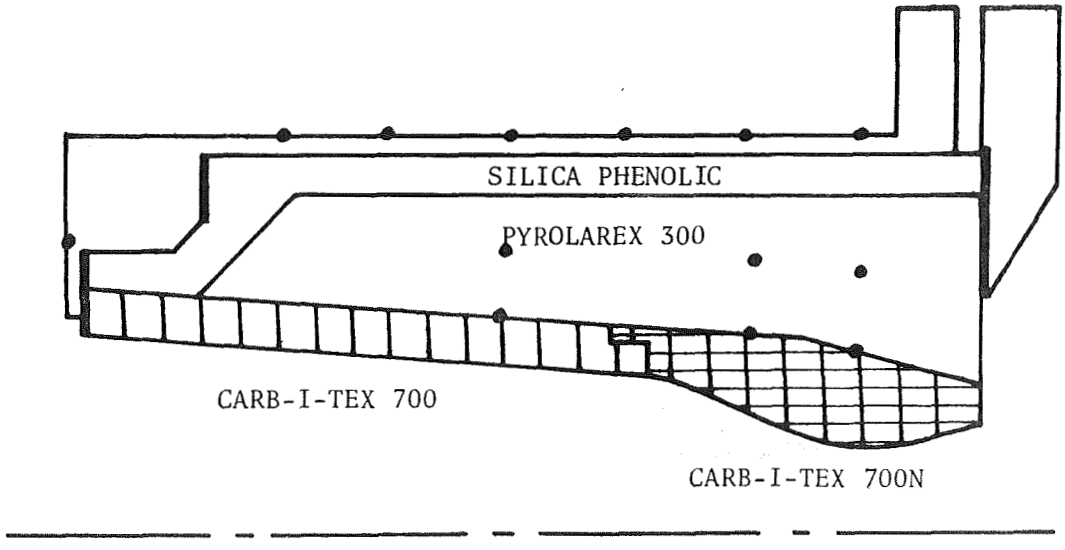

Figure 4-14. Insulated Graphite Thrust Chamber Design With Thermal Instrumentation

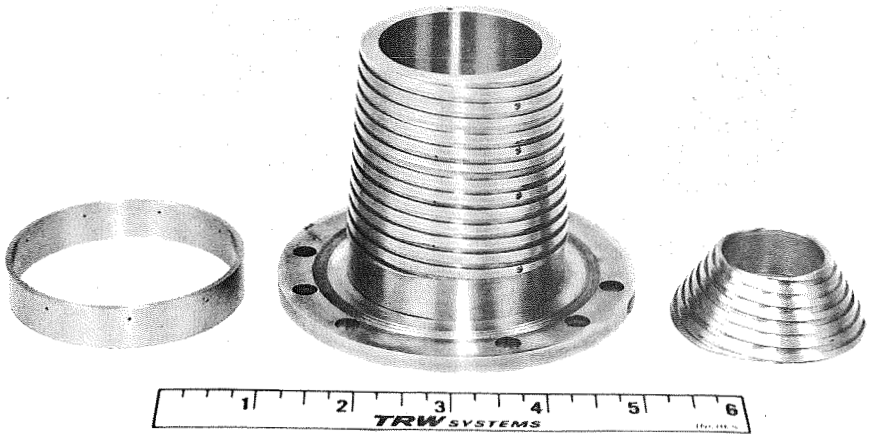

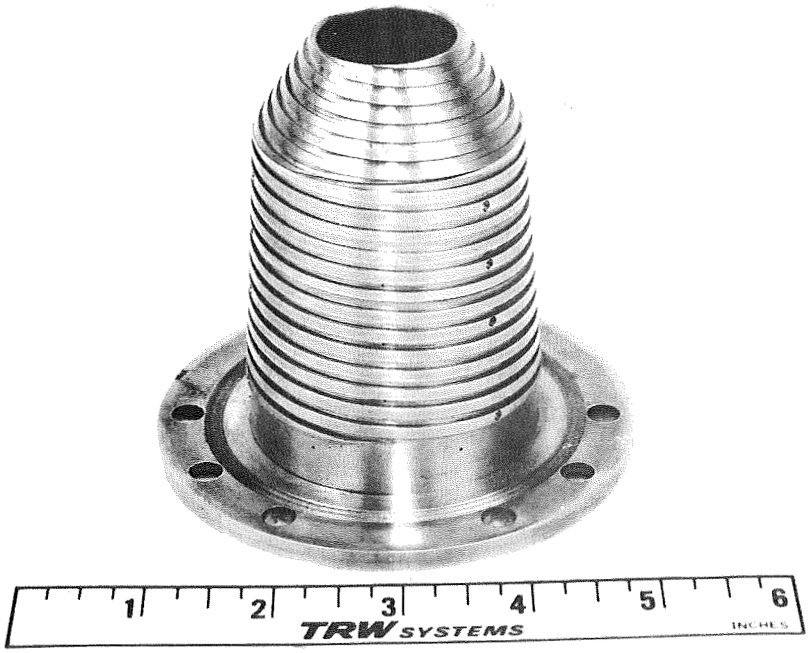

Figure 4-13. Duct Design Parts and Assembly

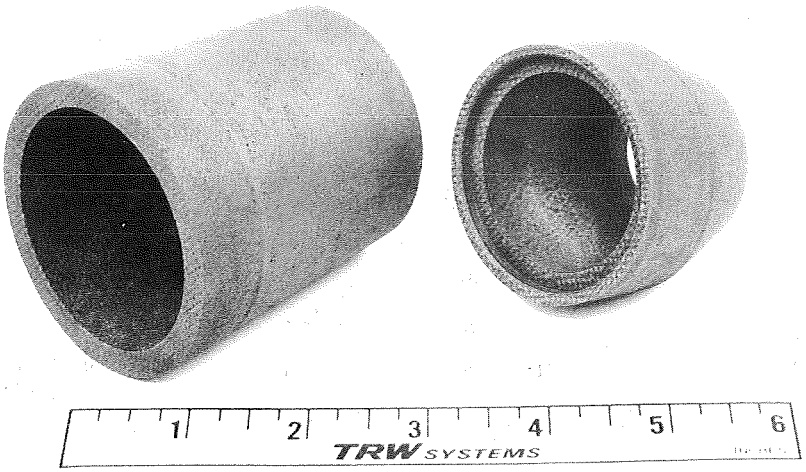

(a) CARB-I-TEX Chamber Walls

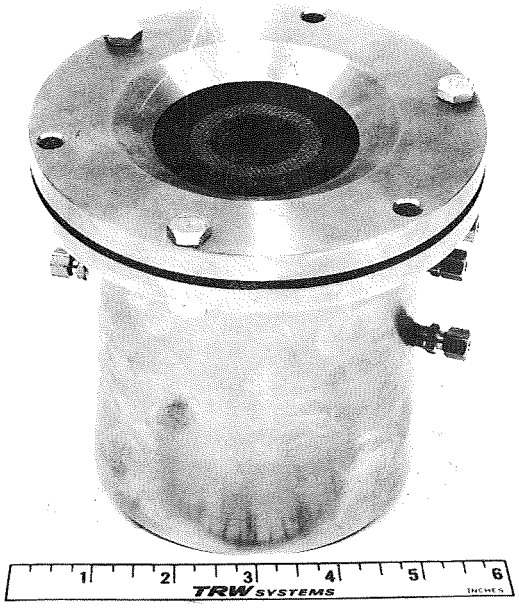

(b) Thrust Chamber Assembly

Figure 4-15. Insulated Graphitic Thrust Chamber

5. EXPERIMENTAL RESULTS

Upon completion of the design and fabrication effort, the experimental test program was begun. This was organized into two (2) principal tasks, film cooled and duct cooled testing, followed by the one graphite chamber test. These tests were conducted in the TRW FLOX/LPG test facility at the Capistrano Test Site. A schematic of the test facility is shown in Figure 5-1 and pictorially in Figure 5-2. Propellant conditioning was accomplished with liquid nitrogen such that the FLOX was delivered to the engine at about -310°F (83.2°K) while the propane was at about -290°F (94.3°K). Flow control was maintained through the use of cavitating venturi elements. Figure 5-3 shows the thrust stand with the copper film cooled inter-regen thrust chamber mounted for testing.

5.1 INTER-REGEN CHAMBER TESTING

All but one test of this program involved inter-regen thrust chambers. These tests were run in two basic series, film cooled tests and duct cooled tests. Following the initial duct cooled tests, an additional set of tests were performed to better define the duct operation. A brief explanation of each test or test sequence is given below. All tests were conducted with a chamber L* of 15 inches, an ϵ_c of 4.0 to 6.0 tapered, an α_c of 35° and an ϵ_e of 1.75. Tests were run until steady-state thermal operation was achieved or until excessive inner wall temperatures were reached.

5.1.1 Task I - Film Cooled Testing

This test series was designed to obtain two basic results. These were a comparison of the propane fuel with the methane/ethane fuel and an evaluation of the effects of changing the injector resultant momentum vector. Table 5-1 summarizes the results obtained in Task I.

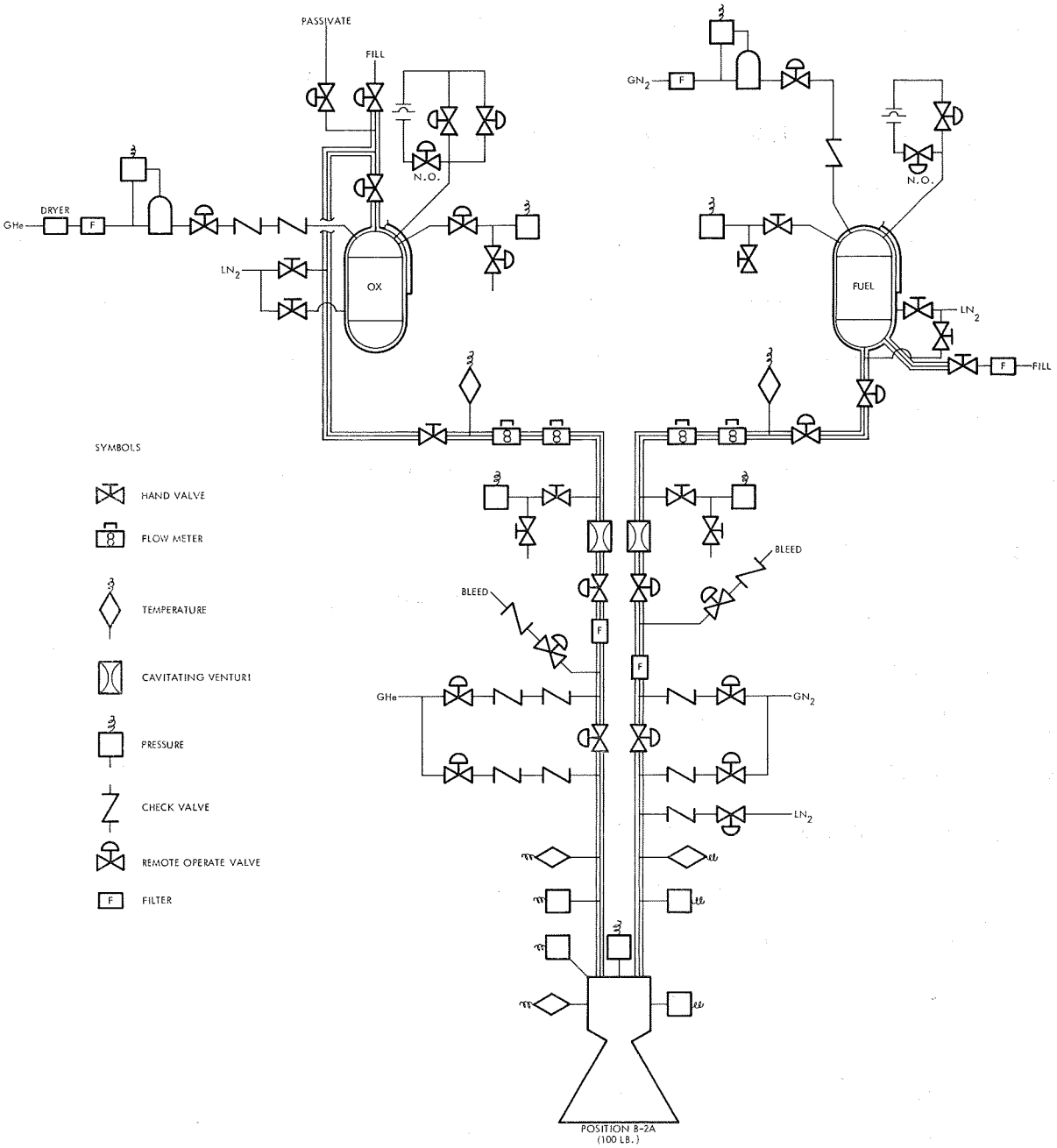

Figure 5-1. Schematic of FLOX/LPG Facility

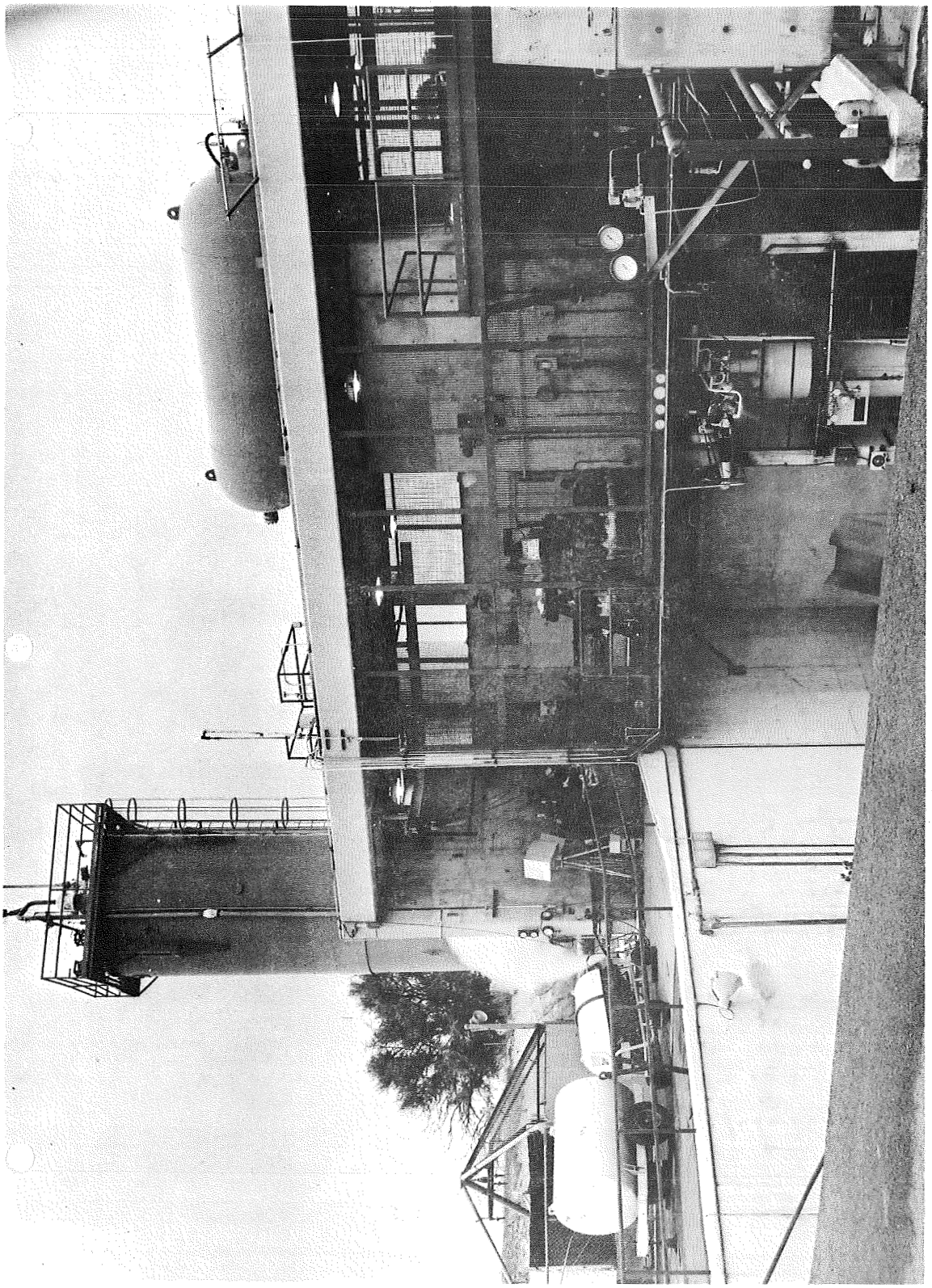

Figure 5-2. Overall View of FLOX/LPG Facility

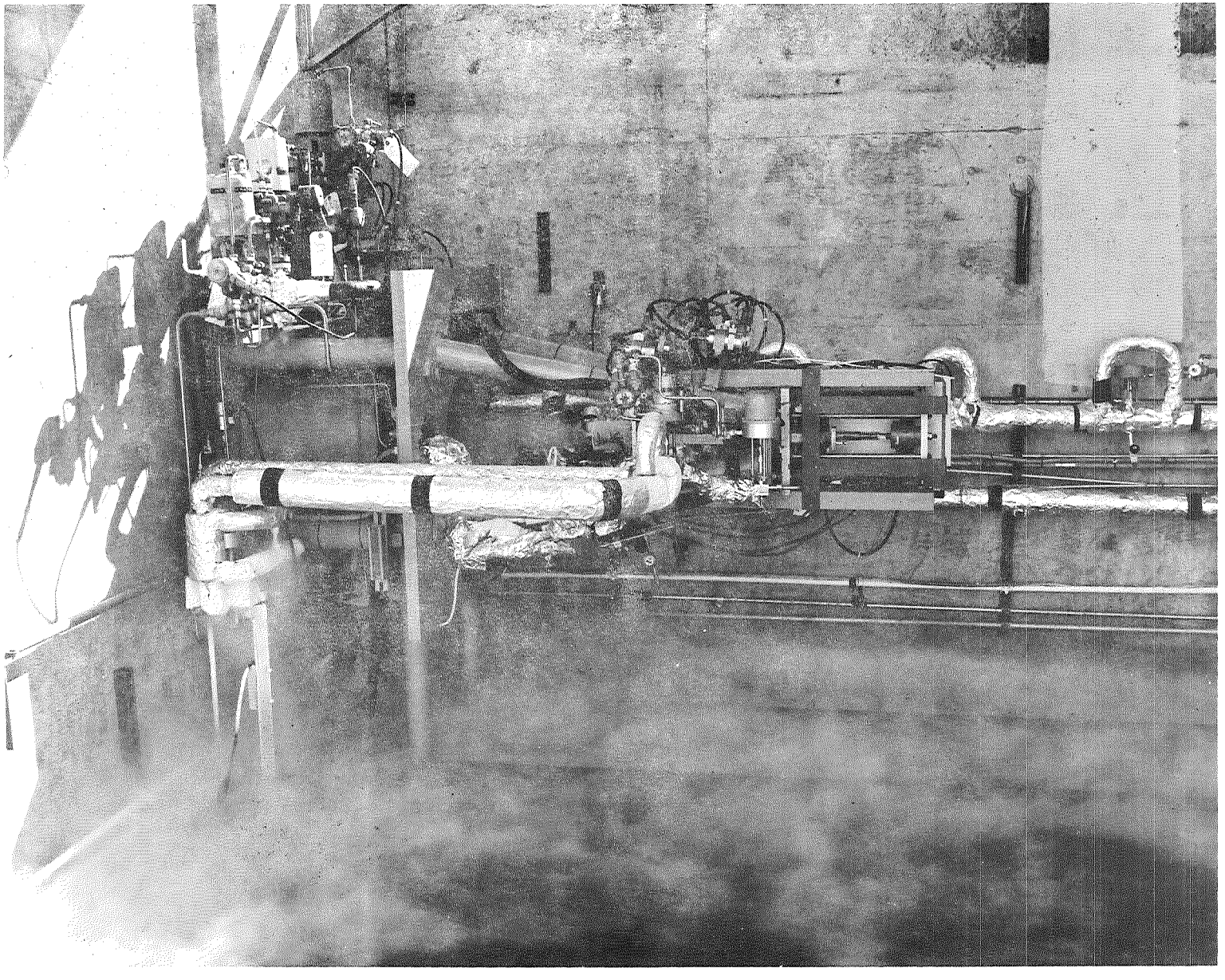

Figure 5-3. View of Thrust Stand With Hardware During Chilldown

Table 5-1. Task I Test Data Summary

Test No.	Duration (sec)	$(O/F)_{overall}$	$(O/F)_{core}$	$\dot{\omega}_T$ (lbm/sec)	$\dot{\omega}_T$ (Kg/sec)	% Cool	P_o (lbf/in^2)	P_o (nt/m^2) x10^{-5}	C^*_p (ft/sec)	C^*_p (m/sec)	ηC^*_p (uncorr)	$F_{(corr)}$ (lbf)	$F_{(corr)}$ (nt)	C^*_F (ft/sec)	C^*_F (m/sec)	ηC^*_F (uncorr.)	Remarks
Task I																	
1	9.5			DIGITAL DATA NOT AVAILABLE													
2	10.75	4.44	5.89	.3096	.1404	24.6	92.6	6.4	5627	1715	82.6	94.1	418.6	5584	1702	82.0	
3	14	4.45	5.93	.3147	.1427	25.0	93.3	6.4	5577	1700	81.9	78.4	348.7	5565	1696	81.7	
4	26	3.28	3.79	.3386	.1536	13.5	96.1	6.6	5342	1628	80.9	86.7	385.7	5703	1738	86.4	
5	20	2.57	4.12	.3308	.1500	37.6	99.8	6.9	5679	1731	88.2	85.0	378.1	5701	1738	88.6	
6	32	2.33	4.52	.3720	.1687	48.4	102.4	7.1	5181	1579	81.5	92.4	411.0	5552	1692	87.4	Baseline Injector
7	43			DIGITAL DATA NOT AVAILABLE													
8	46	1.99	4.77	.3942	.1788	58.3	103.4	7.1	4939	1505	79.2	86.4	384.3	4955	1510	79.4	
9	48	1.82	4.30	.4042	.1833	57.6	102.9	7.1	4792	1461	78.4	85.9	382.1	4777	1456	78.1	Chamber-Injector Leak
10	84	1.42	3.32	.4180	.1896	57.3	95.7	6.6	4308	1313	74.4	76.7	341.2	4227	1288	73.0	
11	26	3.24	3.51	.3378	.1532	7.5	101.7	7.0	5667	1727	85.8	79.5	353.6	5483	1671	83.0	
12	24	2.76	3.28	.3482	.1579	16.2	105.6	7.3	5710	1740	87.8	86.3	383.9	5675	1730	87.3	
13	28	3.87	5.78	.3272	.1484	33.0	99.1	6.8	5700	1737	84.7	81.3	361.6	5695	1736	84.6	
14	24	3.45	4.85	.3290	.1492	28.9	100.2	6.9	5734	1748	86.5	92.1	409.7	6278	1914	94.9	
15	22	2.89	5.02	.3465	.1572	42.5	106.6	7.4	5789	1764	88.4	87.2	387.9	5650	1722	86.3	30° Canted Injector
16	21	2.37	4.76	.3661	.1661	50.2	111.5	7.7	5732	1747	89.8	96.2	427.9	5888	1795	92.2	
17	40	1.34	4.38	.4344	.1970	69.4	114.0	7.9	5080	1548	88.8	95.1	423.0	5256	1692	91.9	
18	40	2.10	5.81	.3782	.1715	63.9	115.0	7.9	5884	1793	93.5	97.7	434.6	5800	1768	92.2	
19	24	1.84	5.25	.3882	.1761	65.0	112.2	7.7	5597	1706	91.2	96.1	427.5	5560	1695	90.6	
20	42	1.38	3.82	.4070	.1846	63.8	104.9	7.2	4990	1521	86.7	91.8	408.3	5061	1543	88.0	

Test 1: This test was a system checkout and did not result in any useful data due to poor flow rate measurement.

Tests (2-6): This test sequence used the baseline pintle element and investigated the effect of the film coolant percentage. Run durations of up to 32 seconds were made, but inter-regen operation was not successful. Typical temperature-time history and axial temperature variation are seen in Figures 5-4 and 5-5.

Tests (7-10): Continuing from the previous tests, a series of tests were run with fixed film coolant percentages, but various "core" mixture ratios. Run duration increased for this test series, however, following the tests a leak was found between the chamber and injector resulting in lower chamber pressure and hence lower heat loads. However, these tests did not indicate any increase in the film coolant effectiveness with propane as the coolant. Typical thermal data are seen in Figures 5-6 and 5-7. Figure 5-8 gives the performance summary for these tests.

Tests (11-16): Using the 30° canted pintle element with the purpose of increasing the chances for a stable film to form on the chamber walls a test series was run with various film coolant percentages. Run durations were shorter than before, but thermal gradients were better indicating some decrease in the interaction between the primary combustion gases and the film coolant. Figures 5-9 and 5-10 show typical thermal data from these tests.

Tests (17-20): Still using the 30° canted pintle element, a test series with fixed film coolant percentages and various "core" mixture ratios was made. These resulted in somewhat increased run duration, but still no steady-state inter-regen operation.

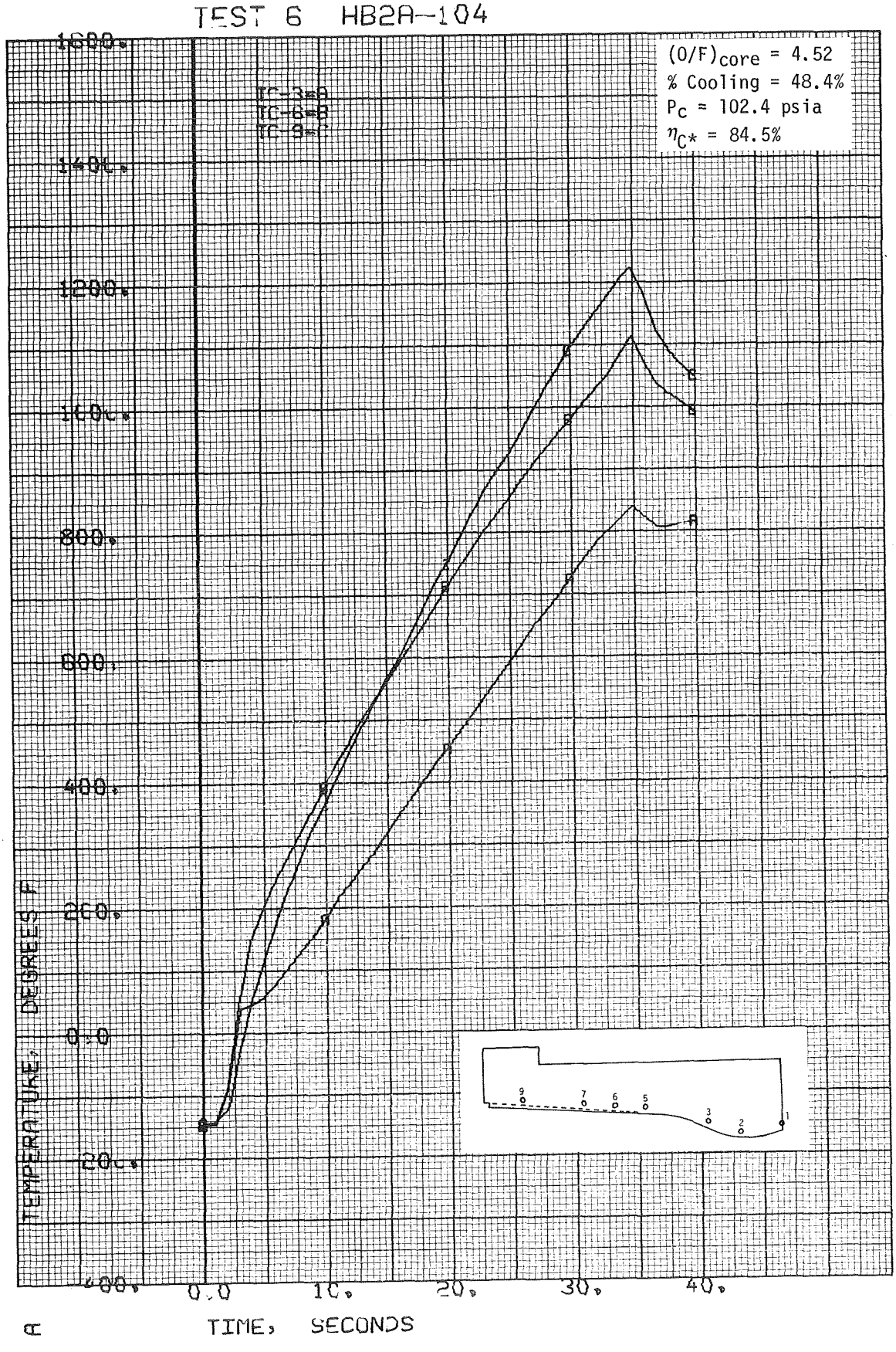

Figure 5-4. Transient Thermal Data for the Baseline Injector (Test 6)

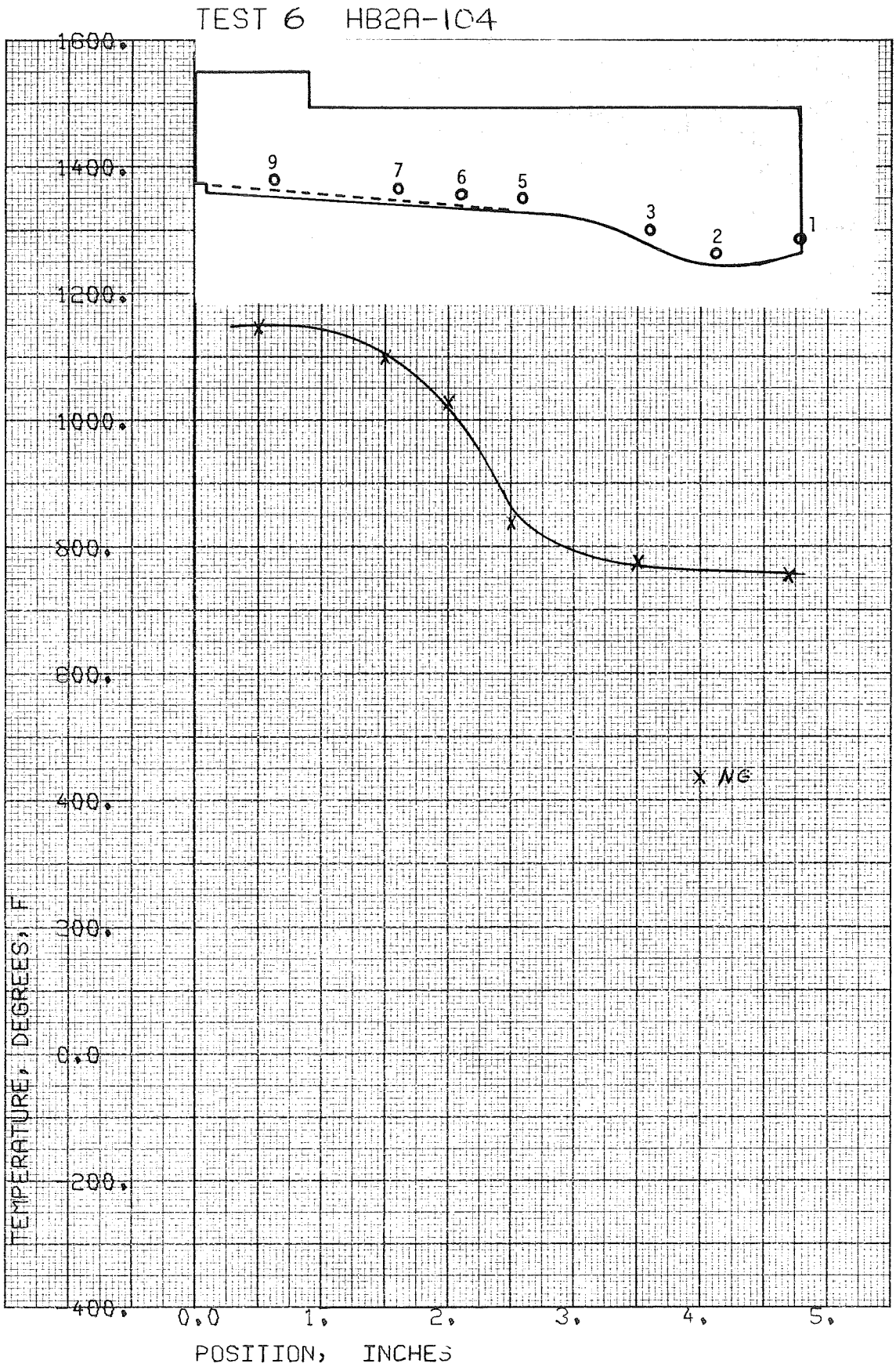

Figure 5-5. Axial Temperature Distribution for the Baseline Injector (Test 6)

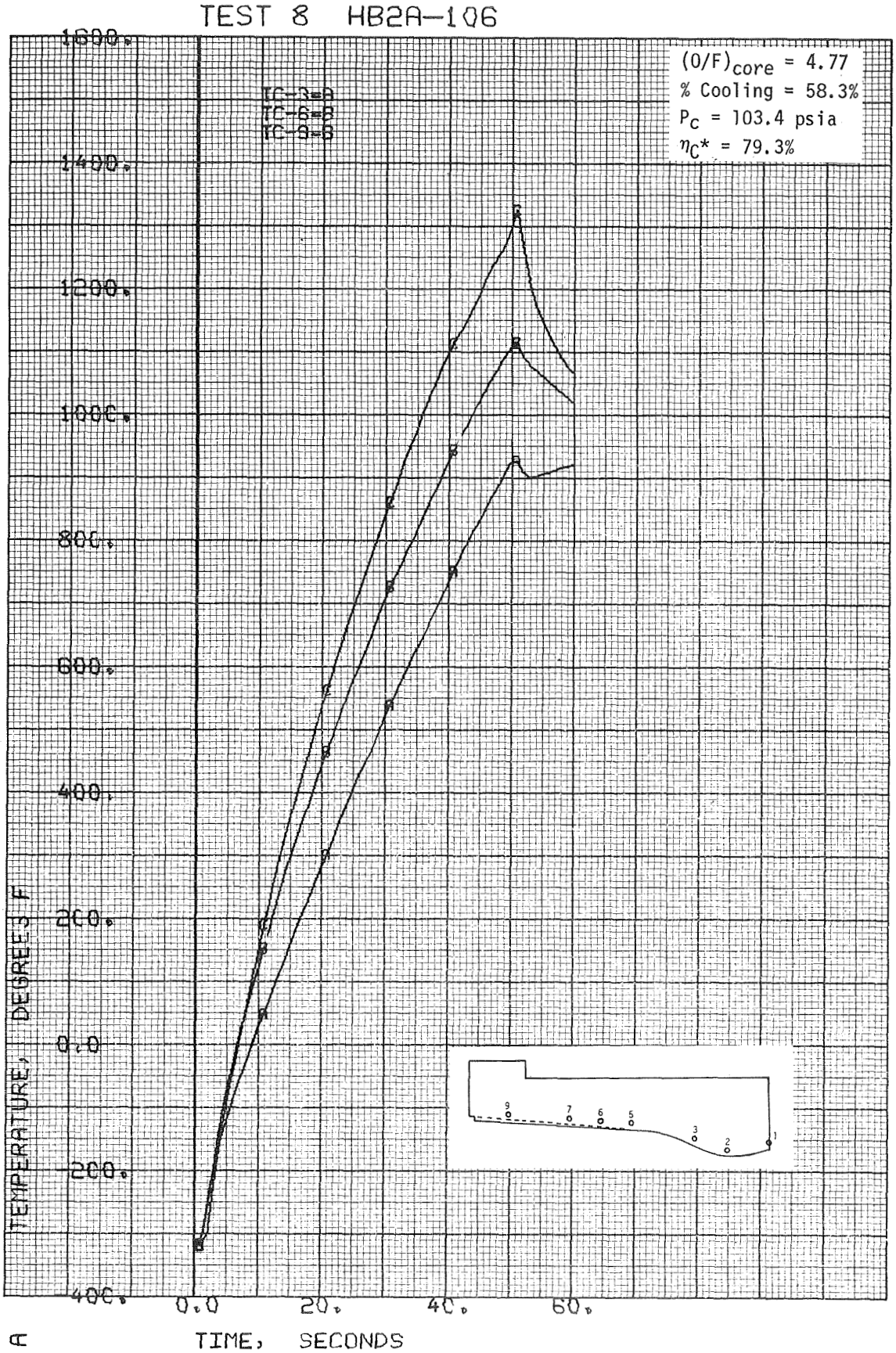

Figure 5-6. Transient Thermal Data for the Baseline Injector (Test 8)

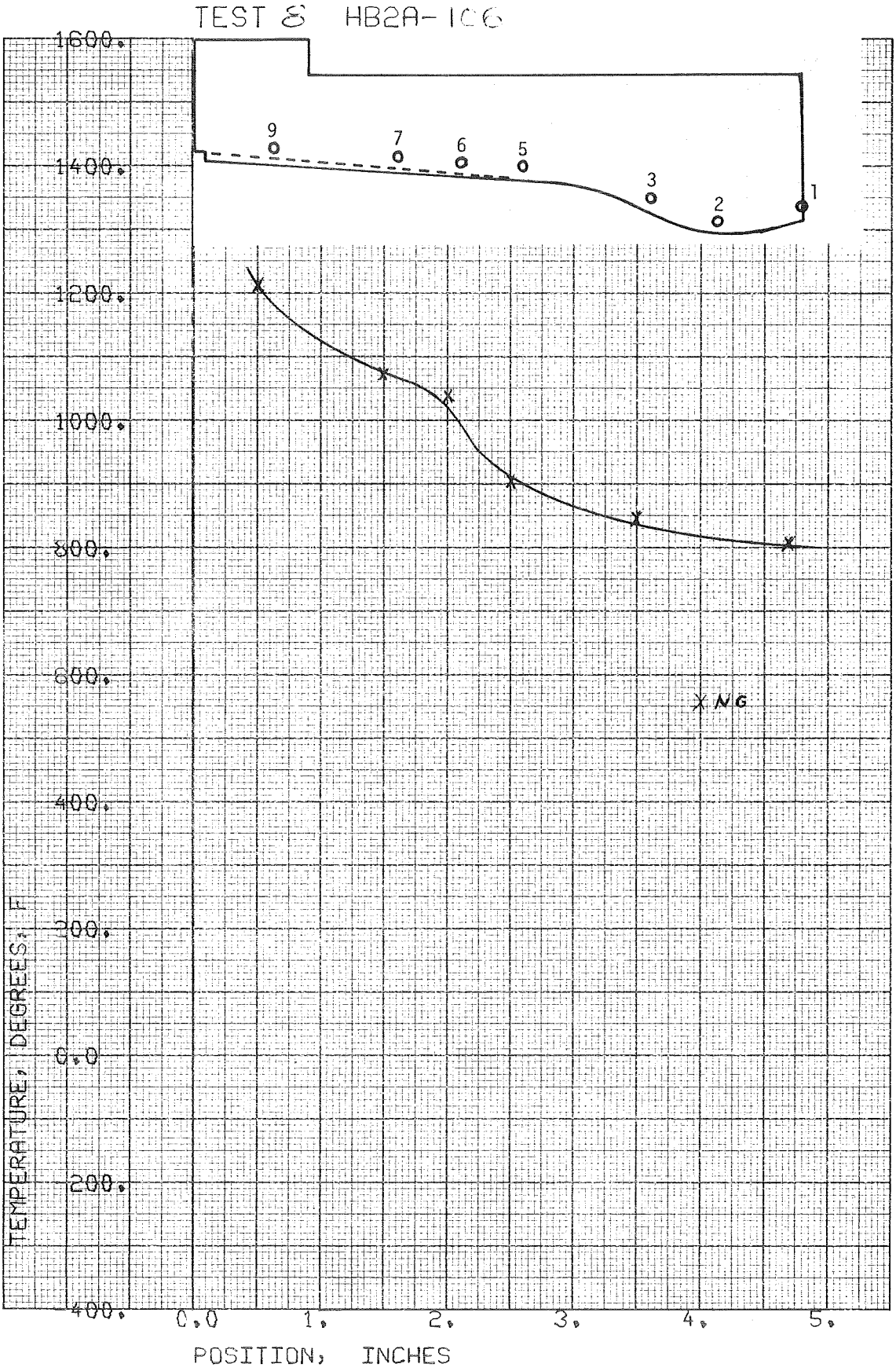

Figure 5-7. Axial Temperature Distribution for the Baseline Injector (Test 8)

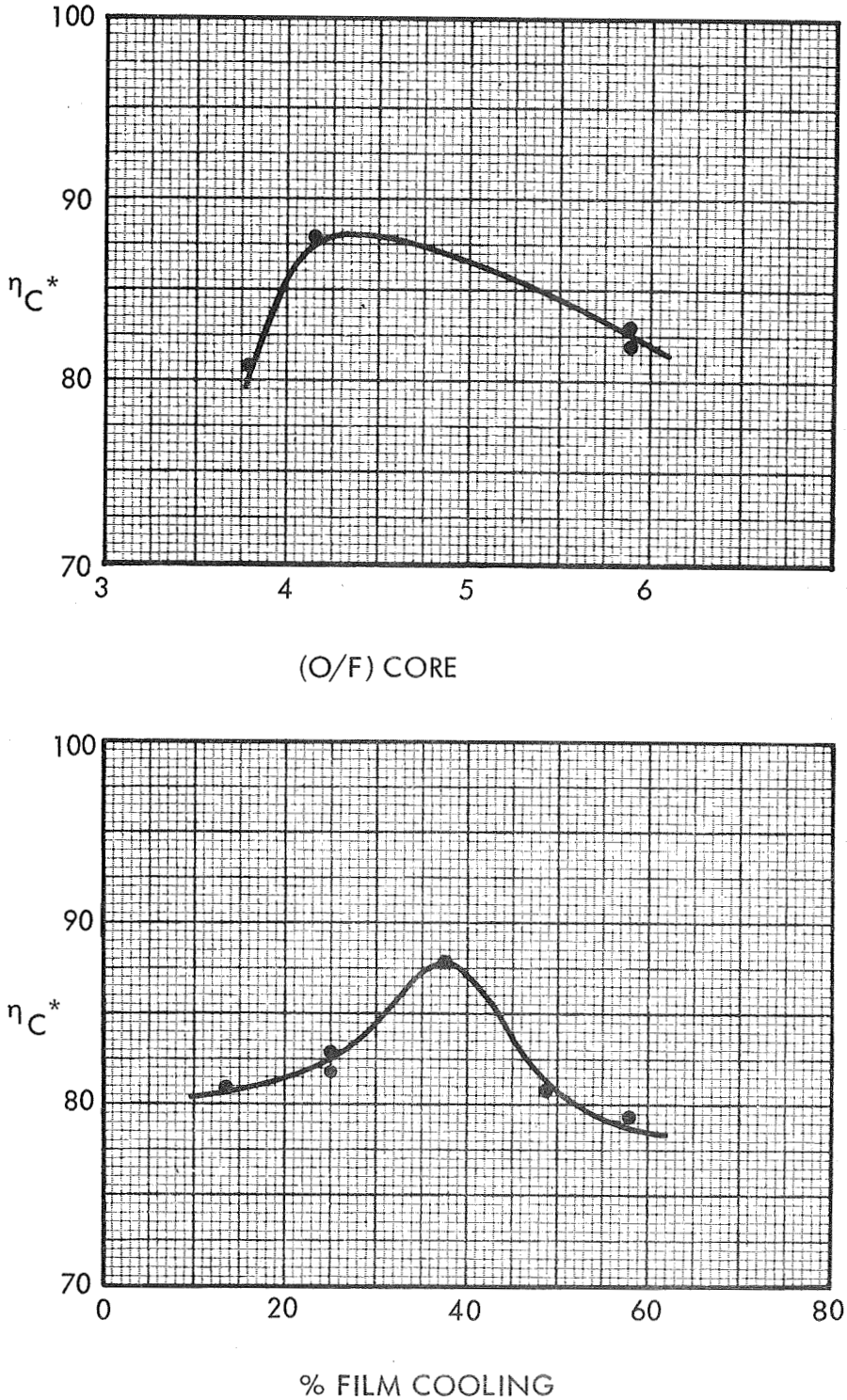

Figure 5-8. Baseline Pintle Performance Efficiency

2

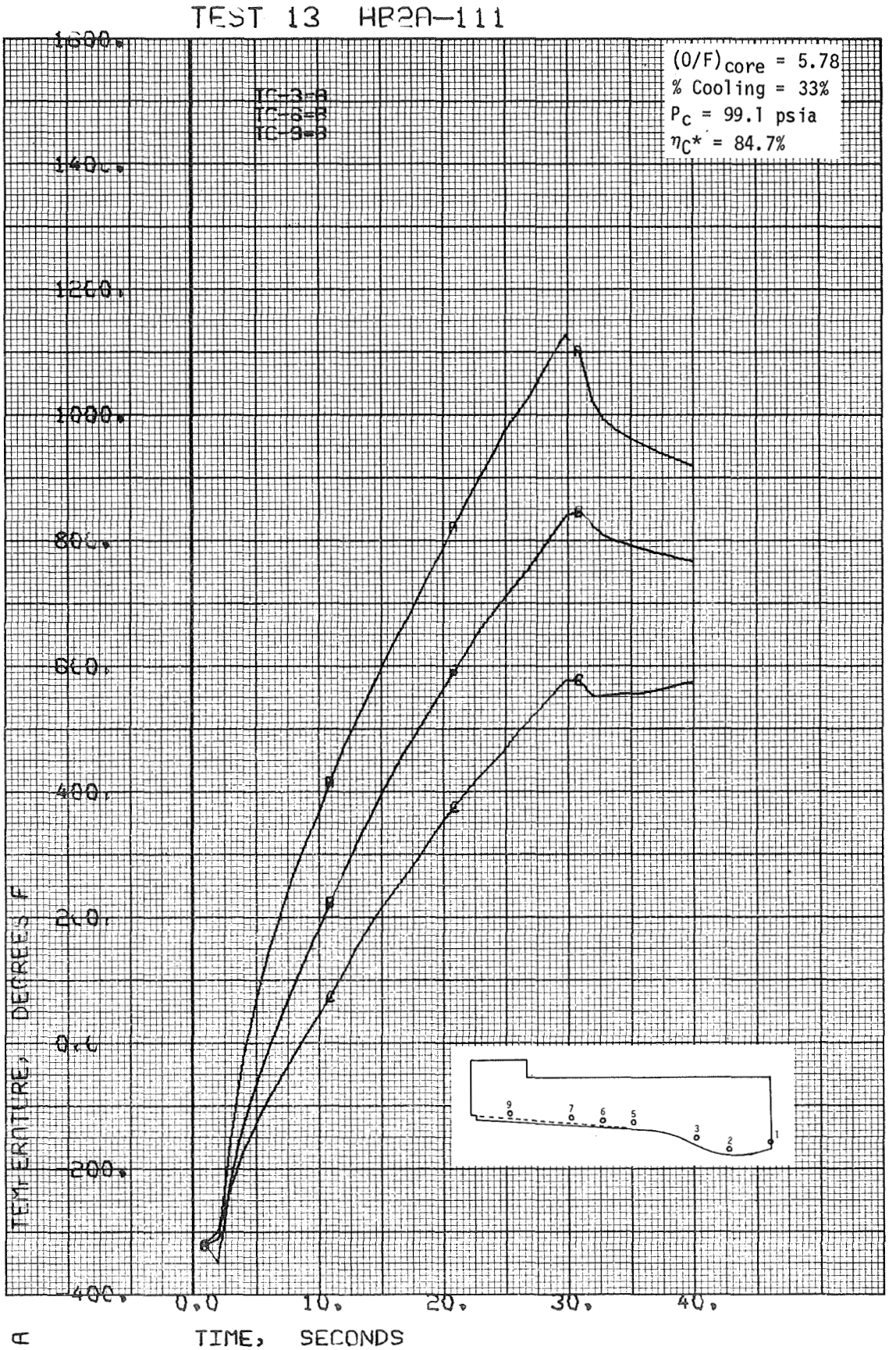

Figure 5-9. Transient Thermal Data for the 30° Canted Injector (Test 13)

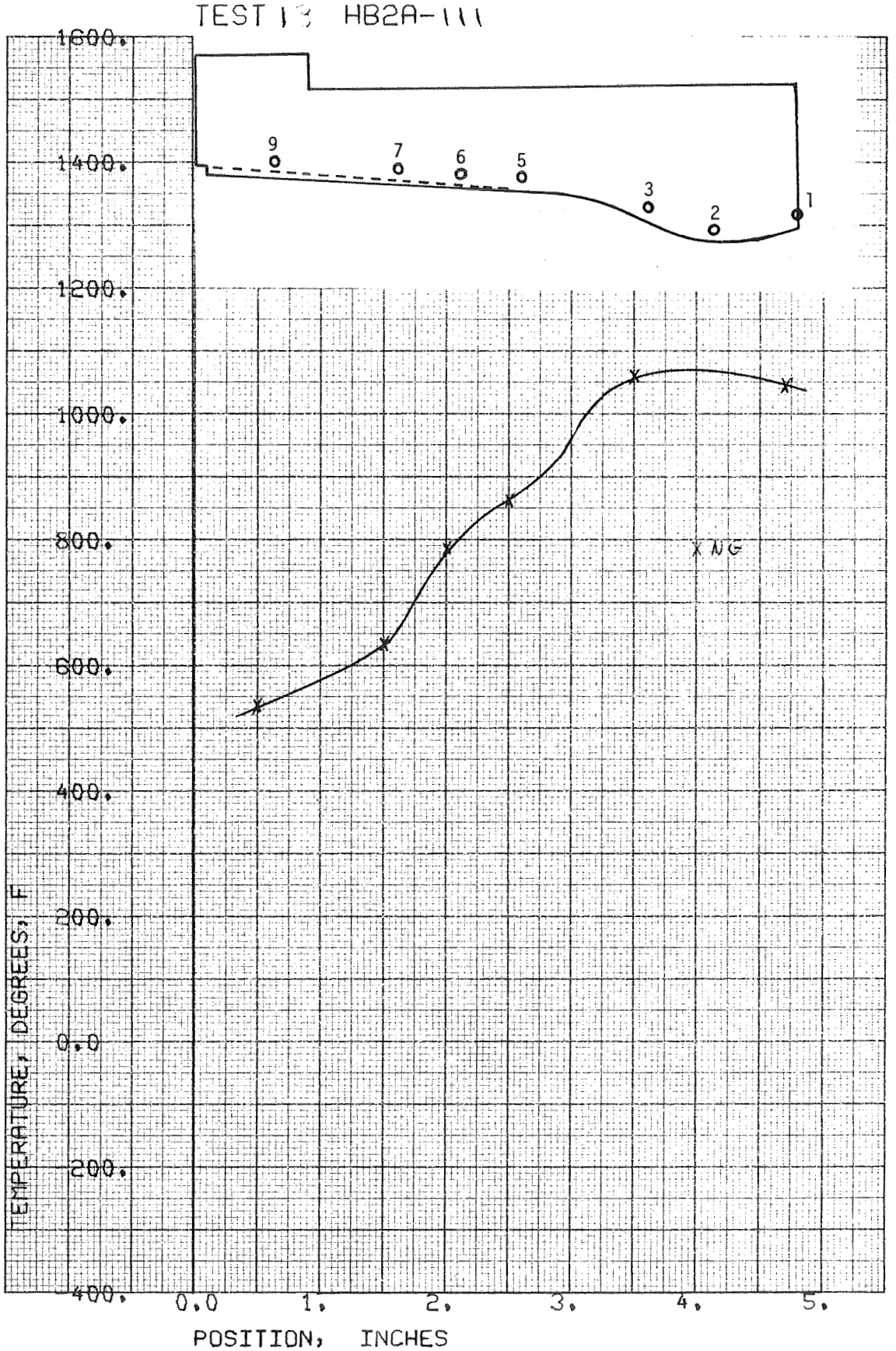

Figure 5-10. Axial Temperature Distribution for the 30° Canted Injector (Test 13)

Figures 5-11 and 5-12 give typical thermal data for these runs. Performance data from these tests is shown plotted in Figure 5-13.

These tests met the requirements of Task I and since no appreciable increase in film cooling effectiveness was found the testing proceeded to the Task II effort. Figure 5-14 shows a picture of the film cooled chamber following the Task I testing. The lack of carbon deposition is the major feature to be noted. This was unexpected since good carbon deposition was noted in Reference 1 with the use of methane/ethane coolant.

5.1.2 Task II - Duct Cooled Testing

The objective of this short test series was to determine the effectiveness of propane as a duct coolant and to determine the limits of duct operation. Two ducted chambers were fabricated for use with the 30° canted pintle injector. Table 5-2 summarizes the data obtained in Task II.

Tests (21-22): These tests were invalid due to a hard start and frozen fuel in the duct manifold.

Tests (23-25): Variations in "core" mixture ratio and duct coolant flow rate were investigated in these tests using the distributed duct. Test number 23 resulted in nearly steady operation as seen by the temperature-time history in Figure 5-15. This curve illustrates that the chamber was operating in the inter-regen condition, but that the heat input to the throat was too great and hence required very high throat temperatures to drive the heat back to the coolant. Test number 24 used a lower "core" mixture ratio and higher coolant flow rate to achieve inter-regen operation as seen in Figure 5-16. Unfortunately,

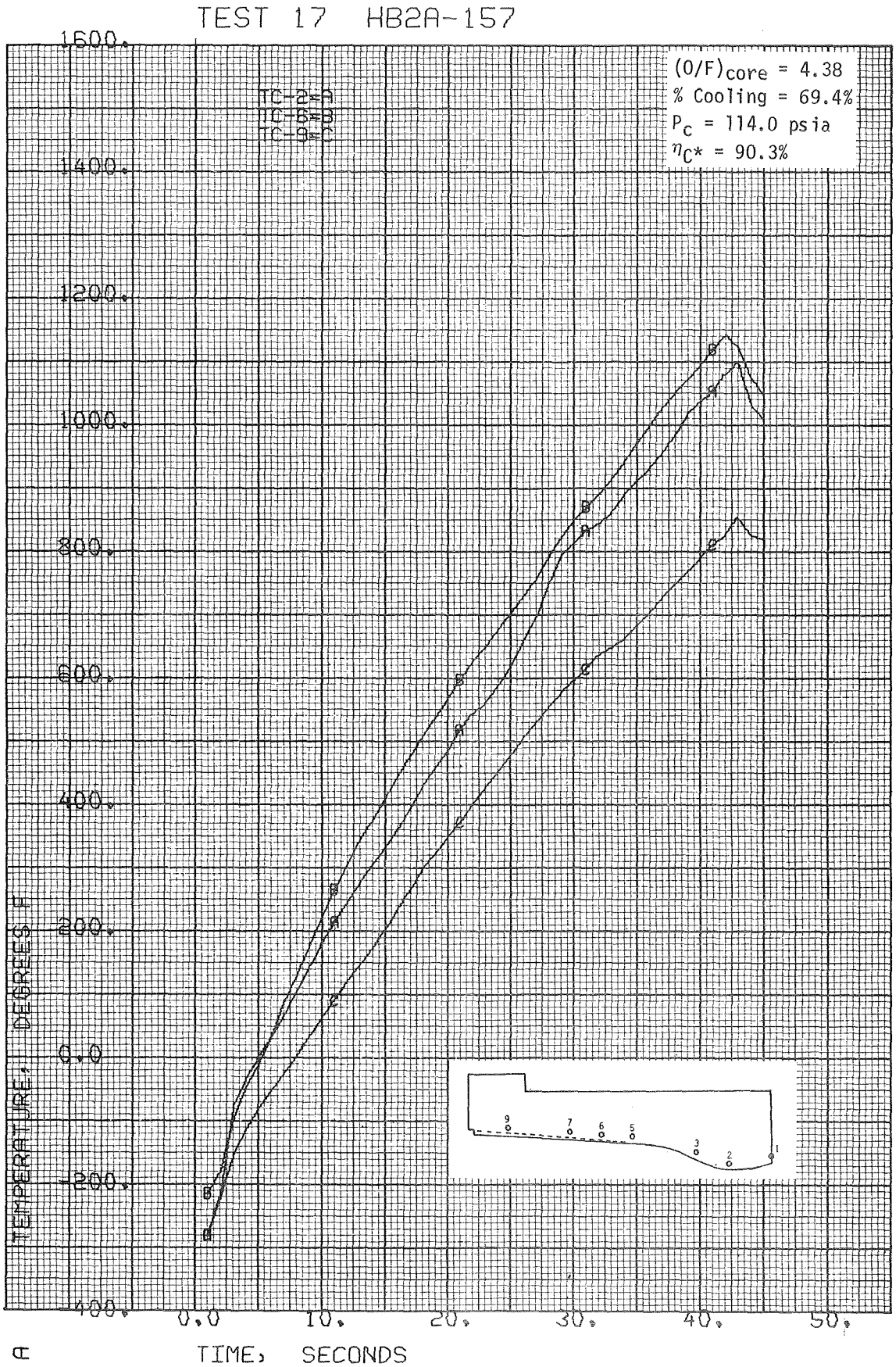

Figure 5-11. Transient Thermal Data for the 30° Canted Injector (Test 17)

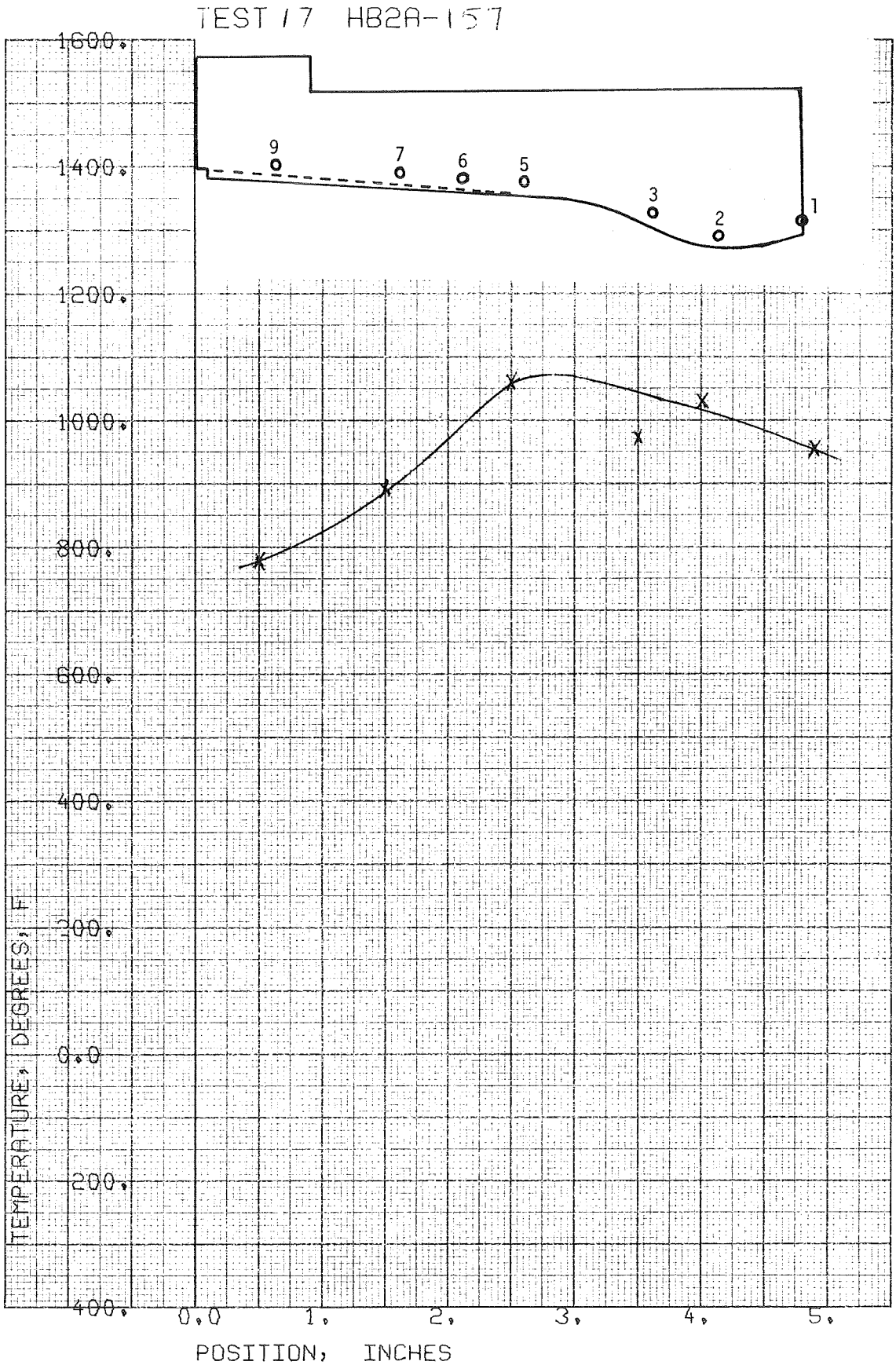

Figure 5-12. Axial Temperature Distribution for the 30° Canted Injector (Test 17)

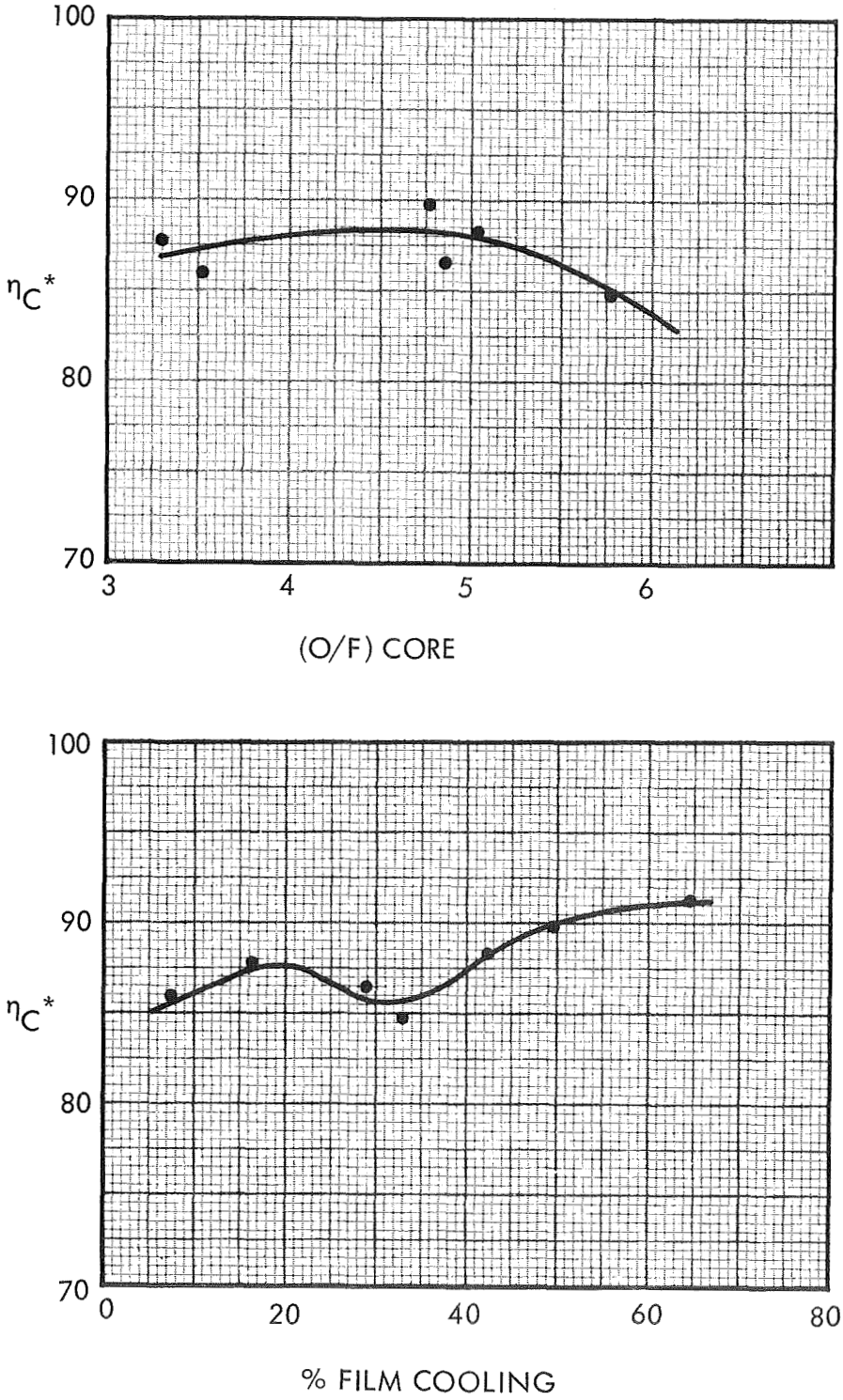

Figure 5-13. Canted Pintle Performance Efficiency

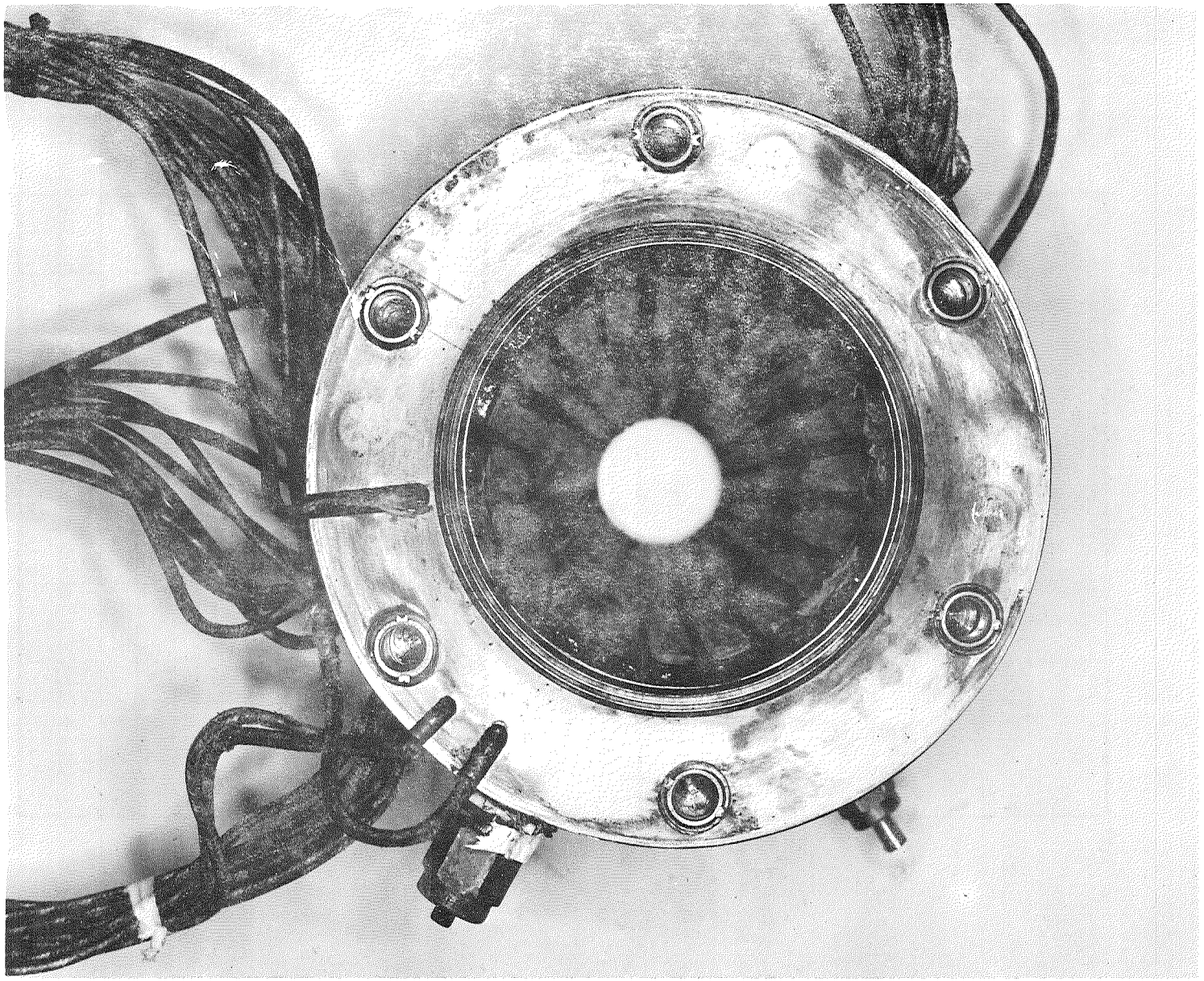

Figure 5-14. Post-Test View of Film Cooled Chamber Showing Lack of Carbon Deposition

Table 5-2. Task II Test Data Summary

Test No.	Duration (sec)	$(O/F)_{overall}$	$(O/F)_{core}$	$\dot{\omega}_T$ (lbm/sec)	$\dot{\omega}_T$ (Kg/sec)	% Cool	P_o (lbf/in^2)	P_o (nt/m^2) x10^{-5}	C^*_P (ft/sec)	C^*_P (m/sec)	ηC^*_P (uncorr)	$F_{(corr)}$ (lbf)	$F_{(corr)}$ (nt)	C^*_F (ft/sec)	C^*_F (m/sec)	ηC^*_F (uncorr.)	Remarks
Task II																	
21	--			HARD START													
22	--			FUEL FROZE													30° Canted Injector
23	58	1.73	4.64	.3884	.1762	62.6	119.4	8.2	5788	1764	95.3	103.4	459.9	5978	1822	98.4	
24	90	1.38	3.66	.4101	.1860	62.3	113.2	7.8	5199	1585	90.2	97.2	432.4	5322	1622	92.3	Distributed Duct Chamber
25	20	2.63	3.59	.3466	.1572	26.7	110.5	7.6	6004	1830	92.9	95.6	425.2	6192	1887	95.8	
26	52	1.76	3.75	.3884	.1762	53.3	116.6	8.0	5653	1723	92.8	96.8	430.6	5596	1706	91.9	
27	30	1.84	4.08	.3970	.1801	55.0	115.5	8.0	5480	1670	89.2	98.2	436.8	5554	1693	90.4	Total Duct Chamber
28	90	1.38	3.11	.4071	.1847	55.5	113.5	7.8	5250	1600	91.0	92.0	409.2	5074	1547	88.0	
29	5			DIGITAL DATA NOT AVAILABLE													
30	--			HARD START													
31	82	1.31	4.51	.4377	.1985	71.1	112.2	7.7	4864	1483	85.6	--	--	--	--	--	Distributed Duct Chamber
32	50	1.49	6.21	.4255	.1930	76.0	105.2	7.3	4752	1448	80.8	--	--	--	--	--	" " "
33	310	1.60	5.16	.4116	.1867	69.4	115.7	8.0	5408	1667	90.5	--	--	--	--	--	Total Duct Chamber
34	40	1.39	4.33	.4392	.1992	68.1	123.6	8.5	5302	1616	91.4	99.0	440.4	5061	1543	87.2	Graphite Chamber

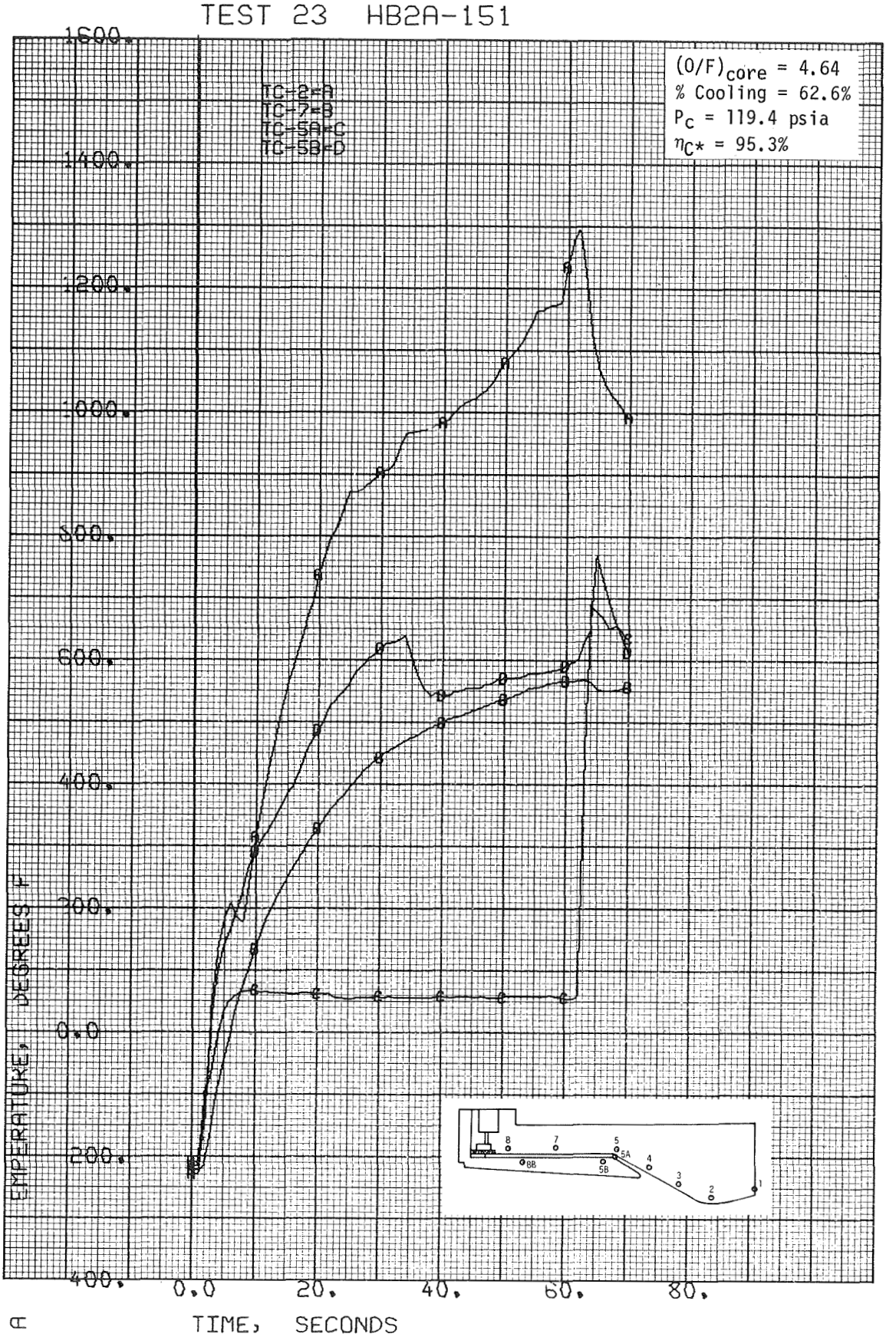

Figure 5-15. Transient Thermal Data for the Distributed Duct Chamber (Test 23)

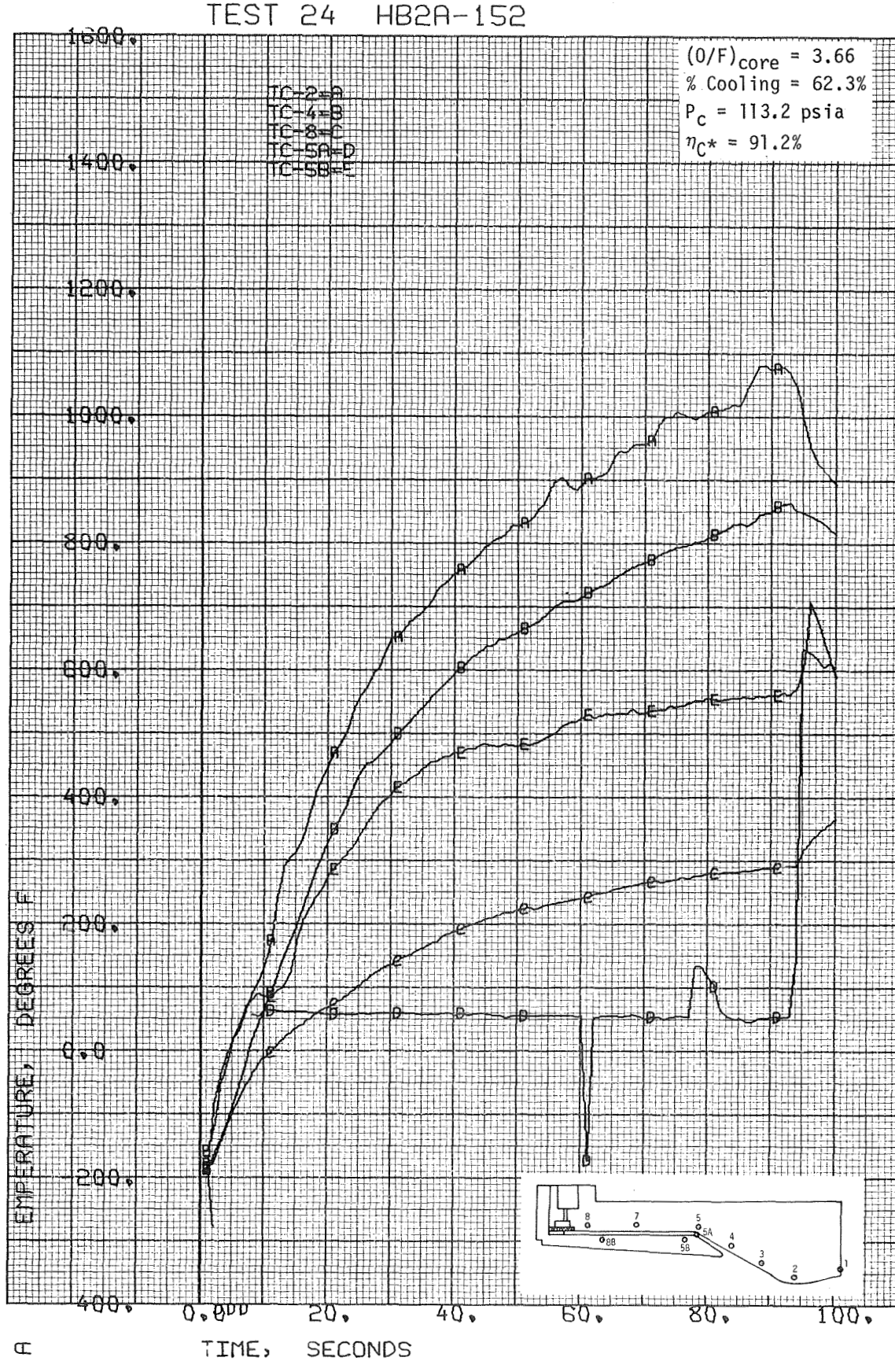

Figure 5-16. Transient Thermal Data for the Distributed Duct Chamber (Test 24)

the test was shut down before steady-state was achieved; however, there is no indication that it would not have been achieved with a throat temperature of about 1200°F. It shall be noted that on each of these tests the duct coolant outlet temperature was at the saturation temperature for propane as was predicted for the best case condition of Section 3.1.4. Figure 5-17 shows the axial temperature distribution for this test. The isotherms are used to determine the conduction paths as noted in Figure 5-35. The effect of decreasing the duct coolant flow rate was dramatically noted in test number 25 (see Figure 5-18) which indicates that the reduced coolant was not able to sufficiently protect the throat region. These tests showed that duct inter-regen cooling with propane was possible and that the distributed duct gave performance increases over the conventional film cooling case. A photograph of the distributed duct chamber appears in Figure 5-19. As can be seen, severe erosion of the duct exit has occurred. This erosion was the result of test number 25 since visual inspection looking up the nozzle after each of the other tests showed no evidence of erosion. It thus appears that the low coolant flow rate of the last test was insufficient to cool the duct. As expected the combustion performance was higher than with the film cooled chamber.

Tests (26-28): The total duct cooled chamber performance and thermal characteristics were determined in these tests under several "core" mixture ratio conditions. Test number 26 used 60% of the fuel as coolant but only one-half of this was directed through the duct with the other half being used for conventional film cooling. As predicted by the inter-regen thermal analysis (Section 3.1.4), the duct coolant was forced into the gaseous phase at high temperatures by the excessive heat loads. The transient thermal data is shown in Figure 5-20. The next test (number 27) used all of the coolant in the duct, but had a higher "core" mixture ratio. The increased duct coolant decreased the

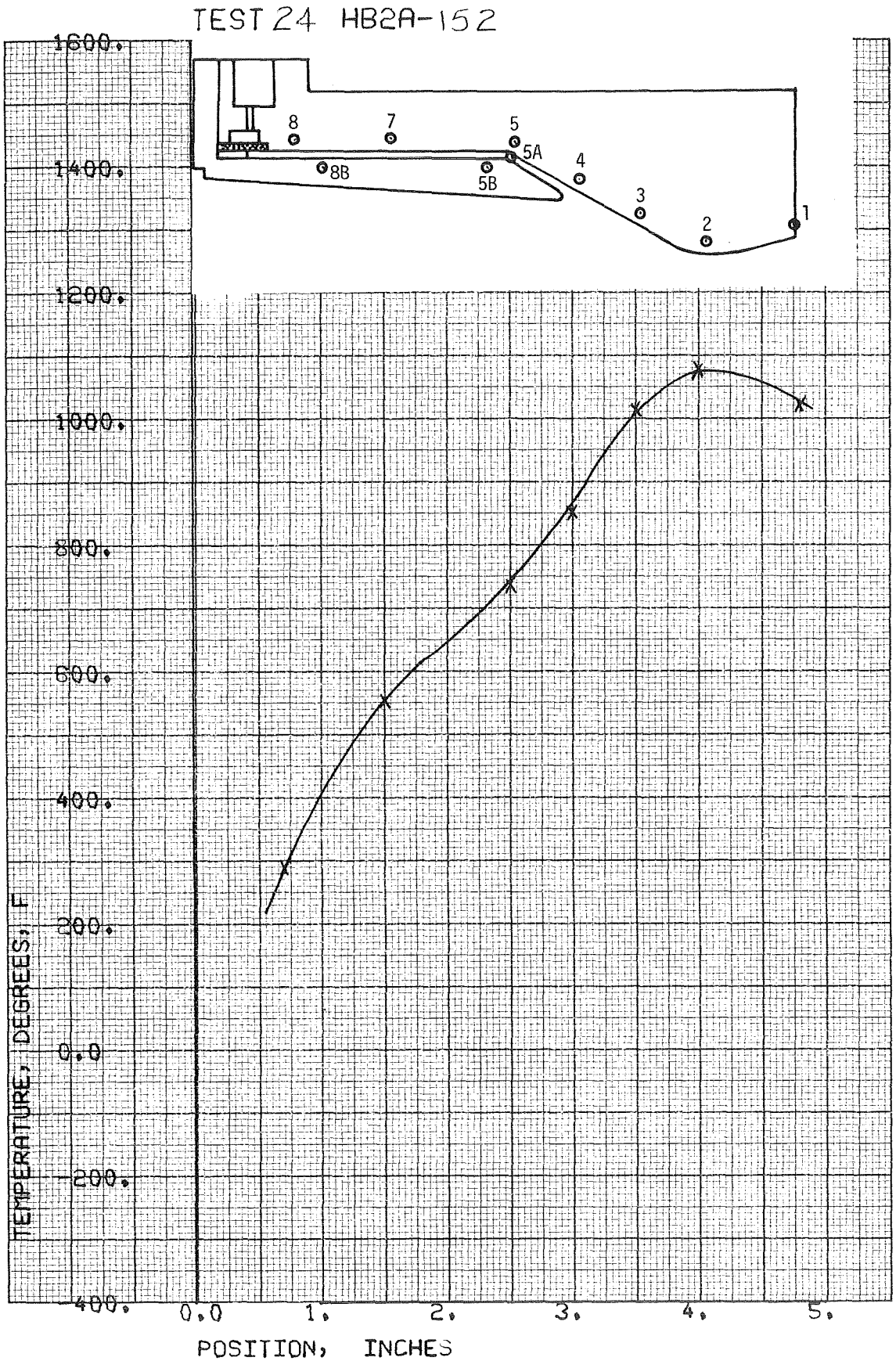

Figure 5-17. Axial Temperature Distribution for the Distributed Duct Chamber (Test 24)

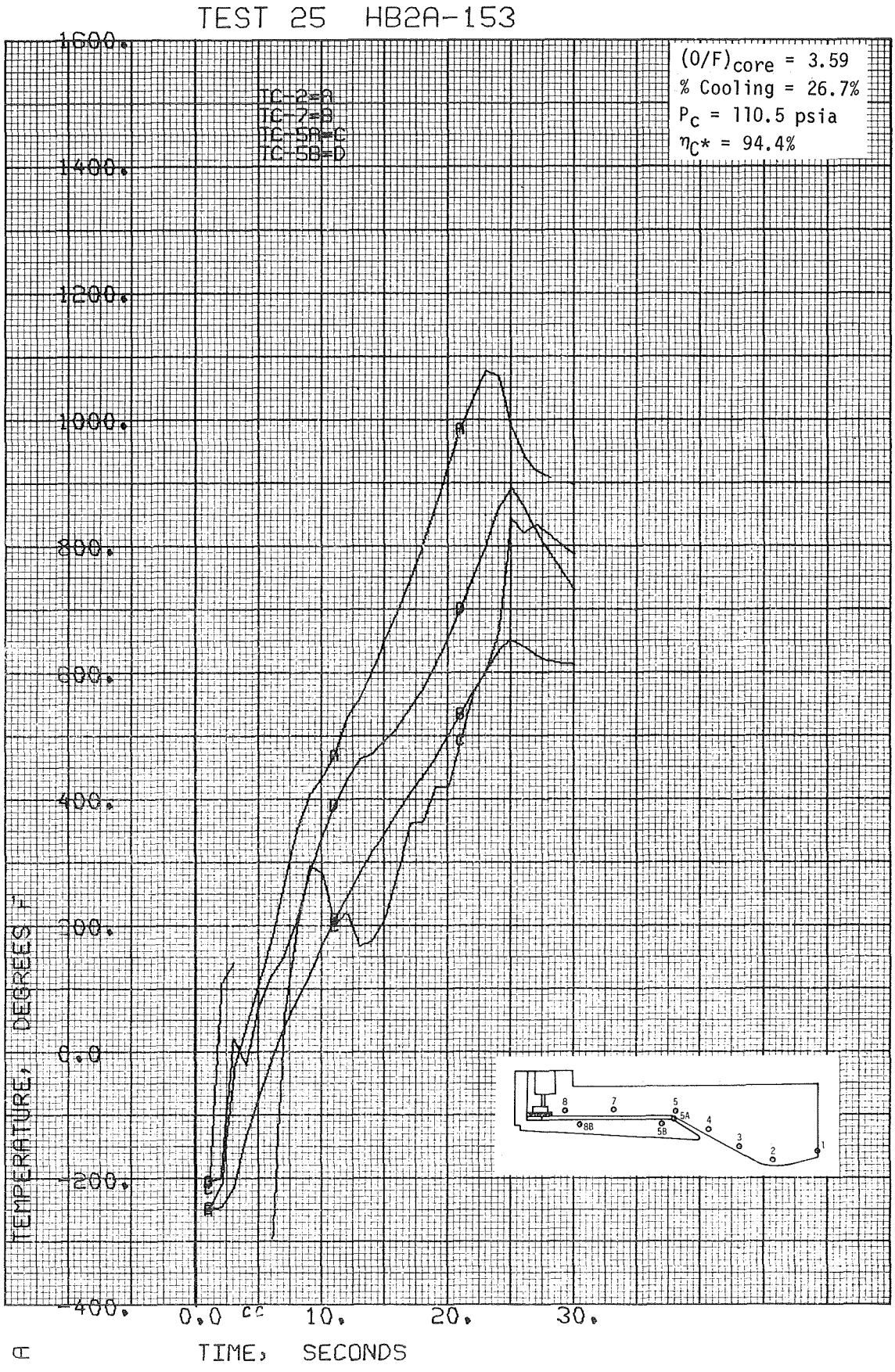

Figure 5-18. Transient Thermal Data for the Distributed Duct Chamber (Test 25)

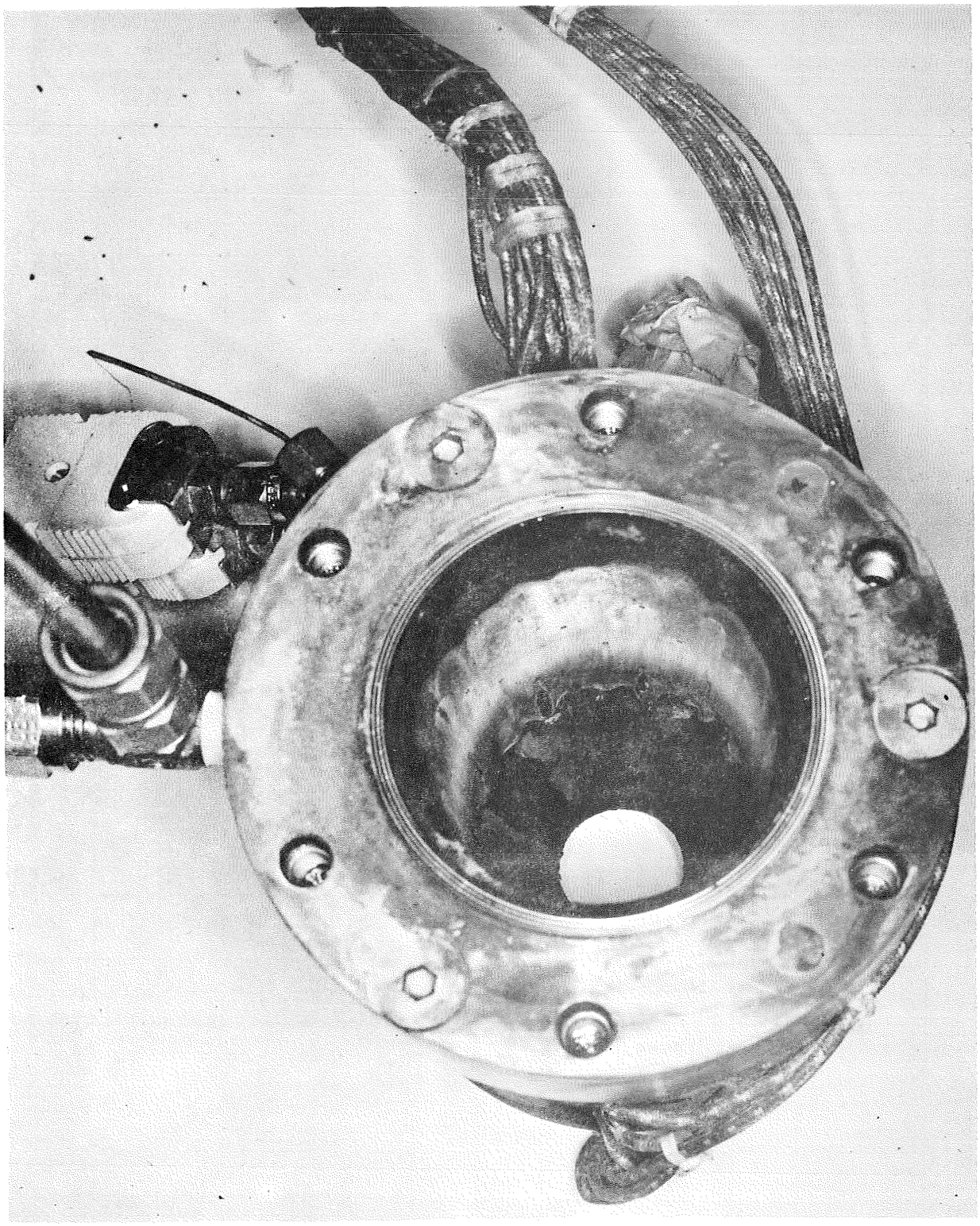

Figure 5-19. View of Distributed Duct Following Three Tests

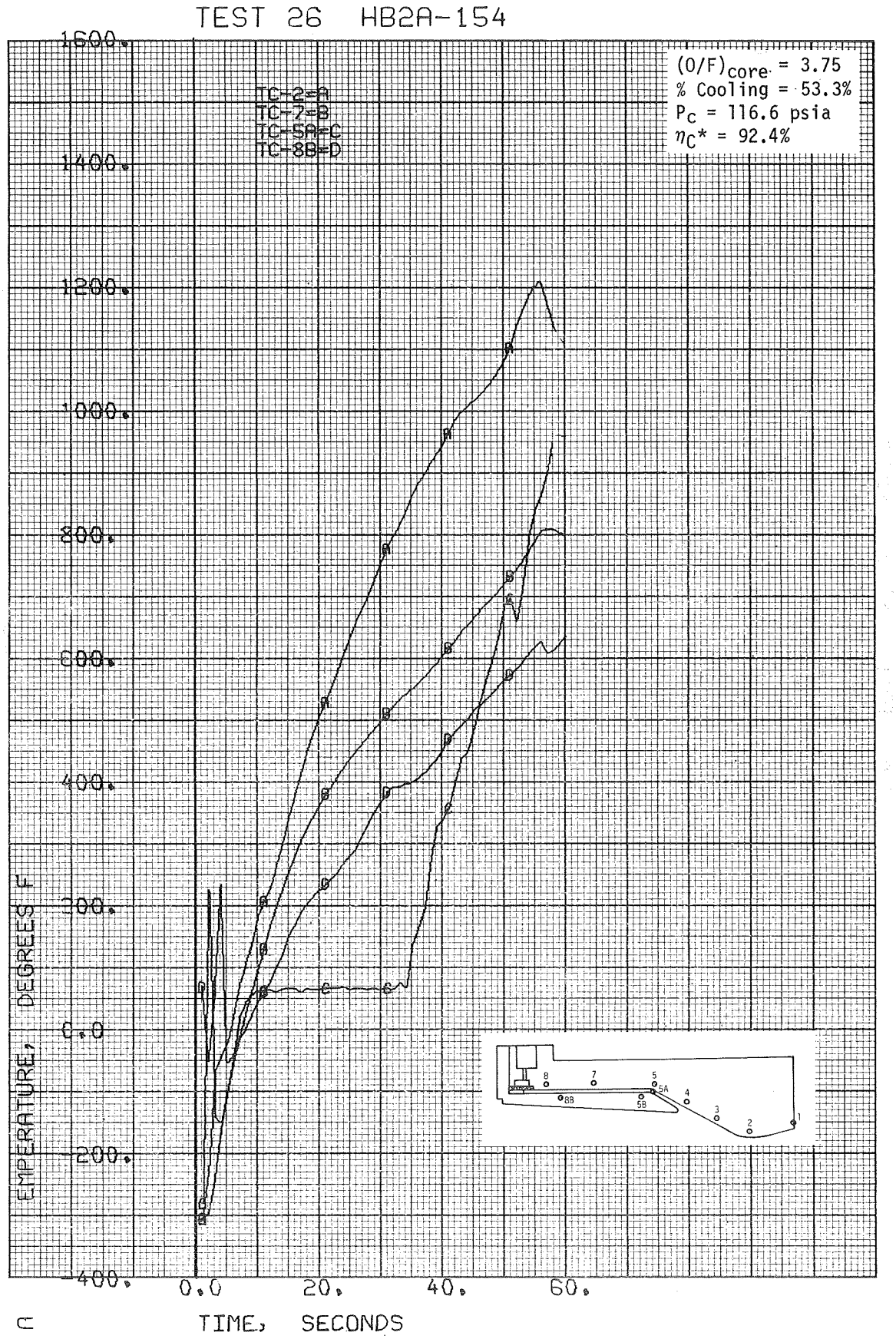

Figure 5-20. Transient Thermal Data for the Total Duct Chamber (Test 26)

nozzle heat load and allowed the duct coolant to remain as saturated vapor and liquid, however, the coolant was still not sufficient to adequately protect the throat region as noted in Figure 5-21. The final test with this total duct design used a lower "core" mixture and hence more coolant even though the coolant fraction remained the same. As can be seen from the transient thermal data (Figure 5-22), successful steady-state inter-regen operation was achieved with a run duration of 90 seconds. This test represents the first unqualified successful inter-regen thrust chamber operation using space storable propellants. Figure 5-23 shows the axial temperature distribution for this test while Figure 5-38 illustrates the isotherms and conduction paths within the thrust chamber. A photograph of the total duct thrust chamber following these tests appears in Figure 5-24. As noted, this duct sleeve was also eroded. The thermal data indicates that this occurred in test 26 when the duct coolant flow rate was low. The nature of the erosion led to the conclusion that the duct wall thickness was too large at the exit, a factor that was corrected in the design of the next series of ducts. The greatly increased carbon deposition seen in both Figures 5-19 and 5-24 illustrates the increased coolant protection afforded by the duct wall. Combustion performance with the total duct was only marginally lower than with the distributed duct and as good as with the conventional film cooled chamber indicating that the performance losses predicted for high duct coolant flow rates was not experienced.

Following a preliminary data evaluation of these ducts, it was decided to perform further duct tests to determine their limits with a goal to conduct a test with run duration of 300 seconds. As described in Section 4.2.1, a slightly modified ducted chamber design was made which had provisions to extend the duct further into the convergent nozzle region.

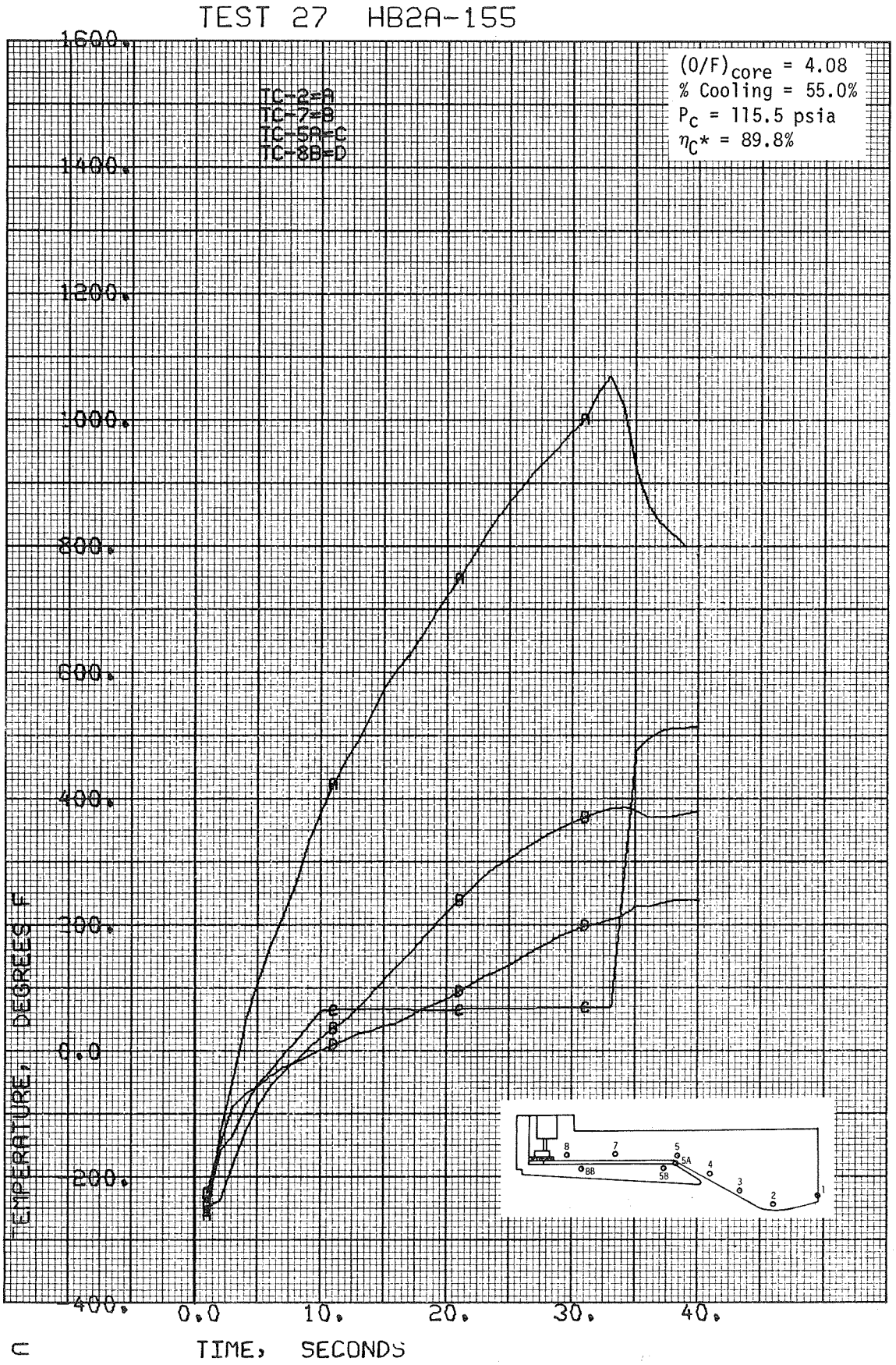

Figure 5-21. Transient Thermal Data for the Total Duct Chamber (Test 27)

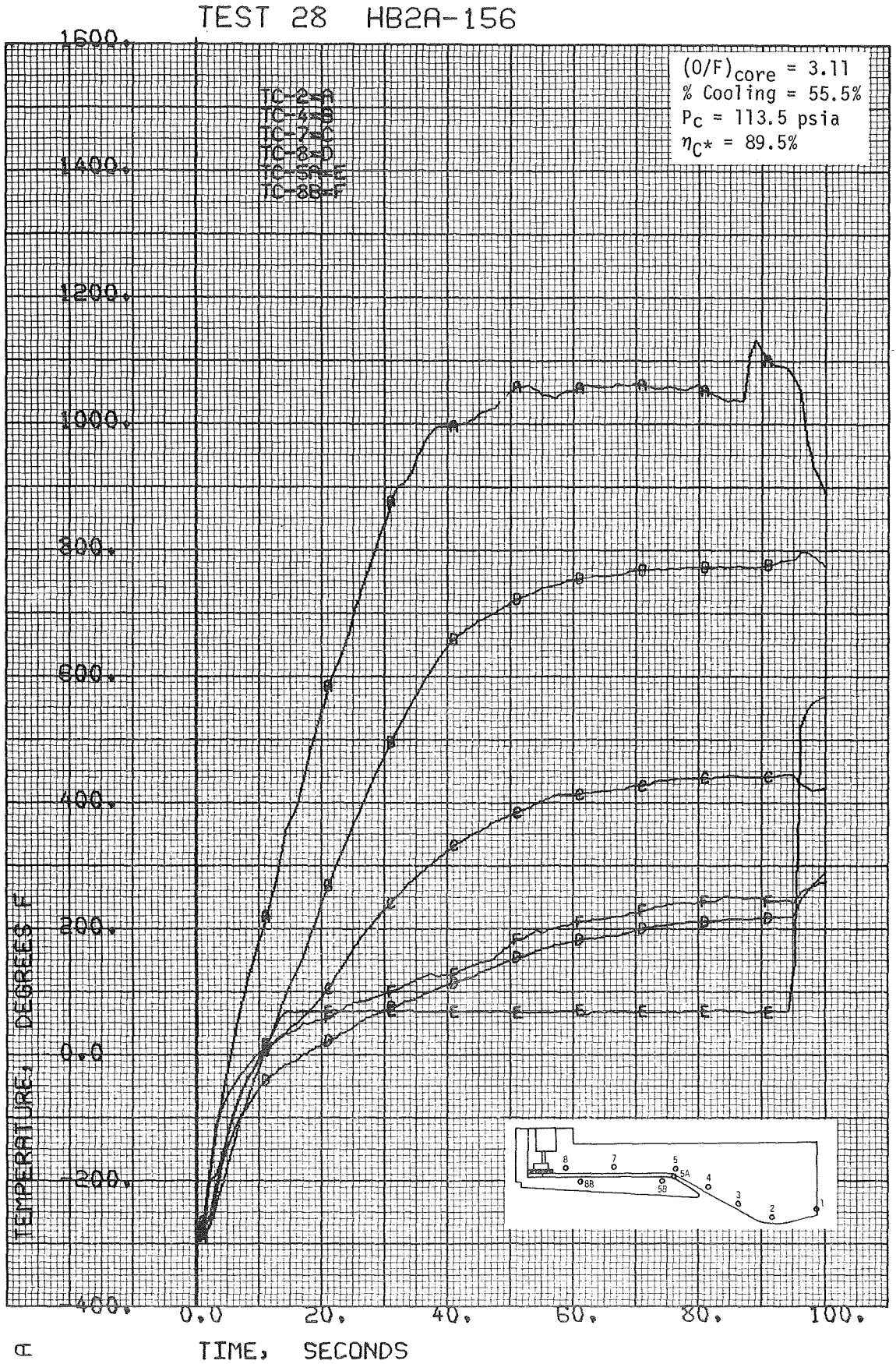

Figure 5-22. Transient Thermal Data for the Total Duct Chamber (Test 28)

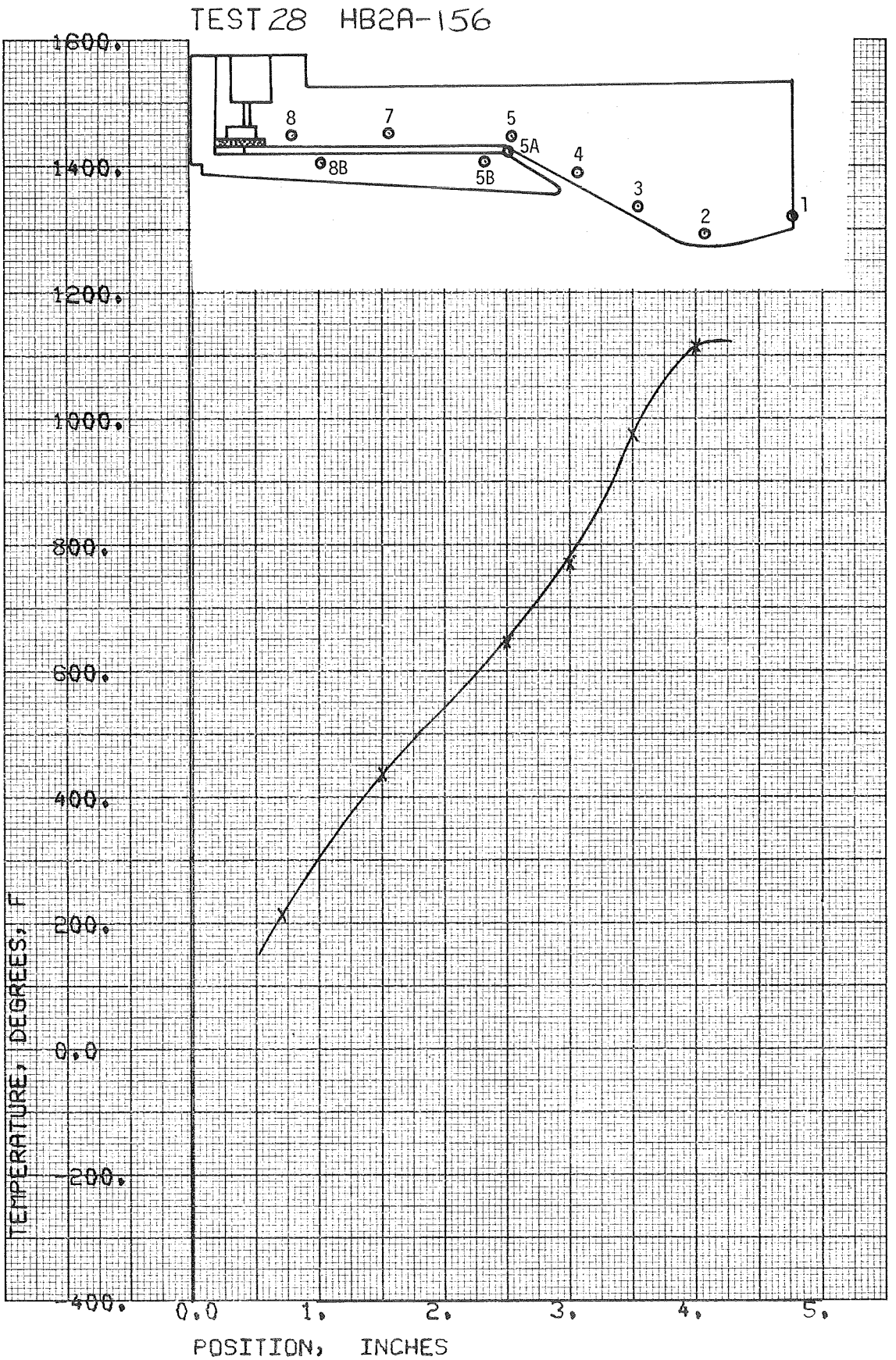

Figure 5-23. Axial Temperature Distribution for the Total Duct Chamber (Test 28)

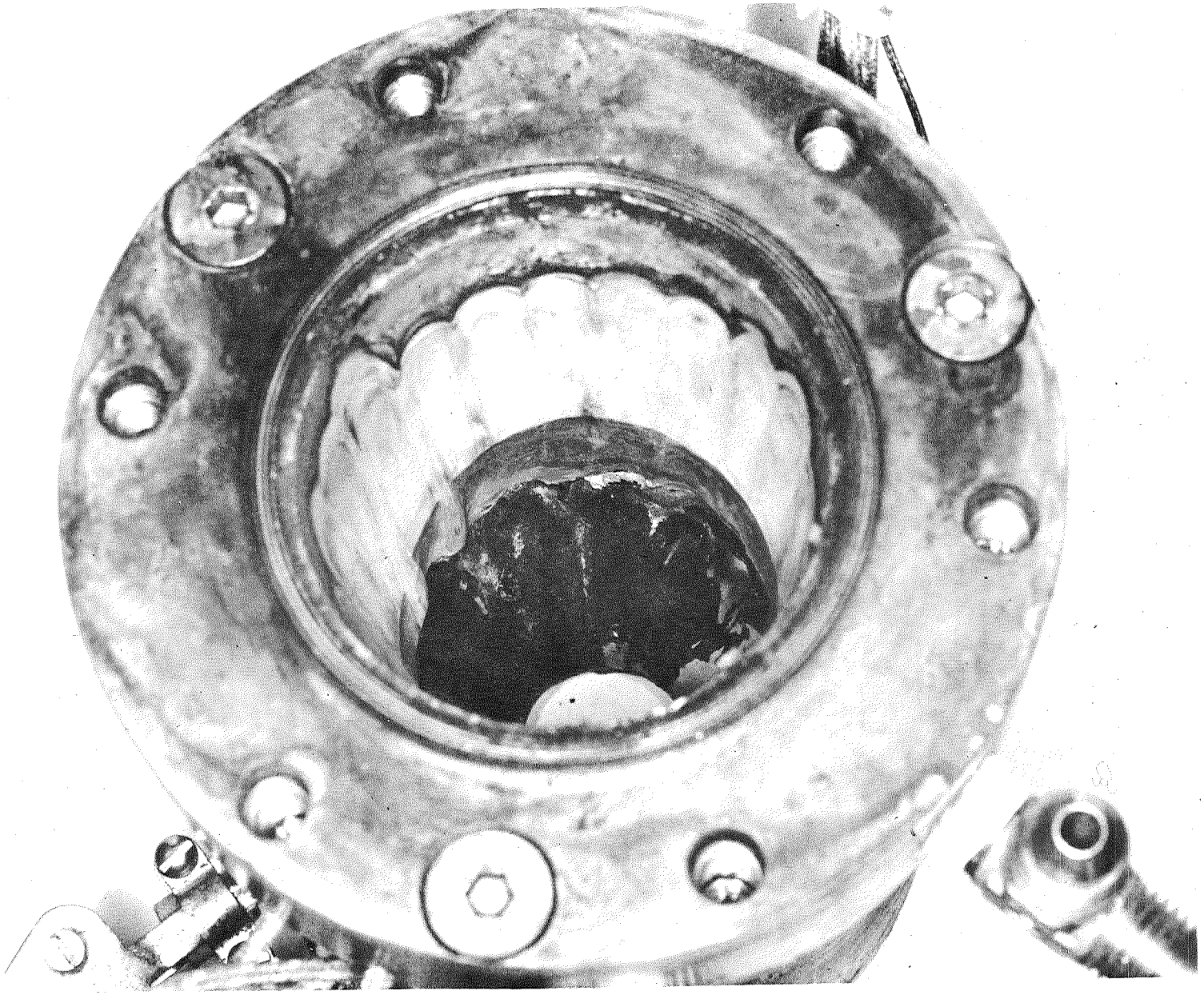

Figure 5-24. View of Total Duct Following Three Tests

Tests (29-30): These tests were of short duration with no meaningful thermal data available. Test number 30 had an unintentional fuel lead which resulted in a hard start.

Test (31): The distributed duct with no extension was tested with optimum "core" mixture and a high coolant flow rate, however, steady-state operation was not achieved. Figure 5-25 shows the transient thermal data for this test. The photographs appearing in Figures 5-26 and 5-27 show the condition of the chamber and the duct, respectively. As can be seen, severe throat erosion occurred for the first time. This has been attributed to the abrupt duct exit configuration which acted to produce a turbulent region that decreased the effectiveness of the coolant to protect the throat. As seen in Figure 5-27, the duct itself was unharmed indicating sufficient coolant flow rate.

Test (32): Using a backup chamber with the same distributed duct and adding the duct extension, a run was conducted to evaluate the duct extension. A poor fuel split between the film coolant and the core resulted in a very high "core" mixture ratio and poor performance. The transient thermal data is shown in Figure 5-28 and reveals that steady operation was not achieved.

Test (33): This test was the final duct cooled test on the program and used the total duct design with extension with a high "core" mixture ratio and film coolant flow rate. The transient thermal data shown in Figure 5-29 shows the results, 310 seconds of operation under steady conditions with high combustion efficiency. The oscillation in the temperature data are caused by carbon flaking from the throat and then redepositing. Figure 5-30 shows the axial temperature profile. Photographs of the post-test hardware are shown in Figure 5-31 and 5-32. These show the carbon buildup in the throat and nozzle with no throat erosion.

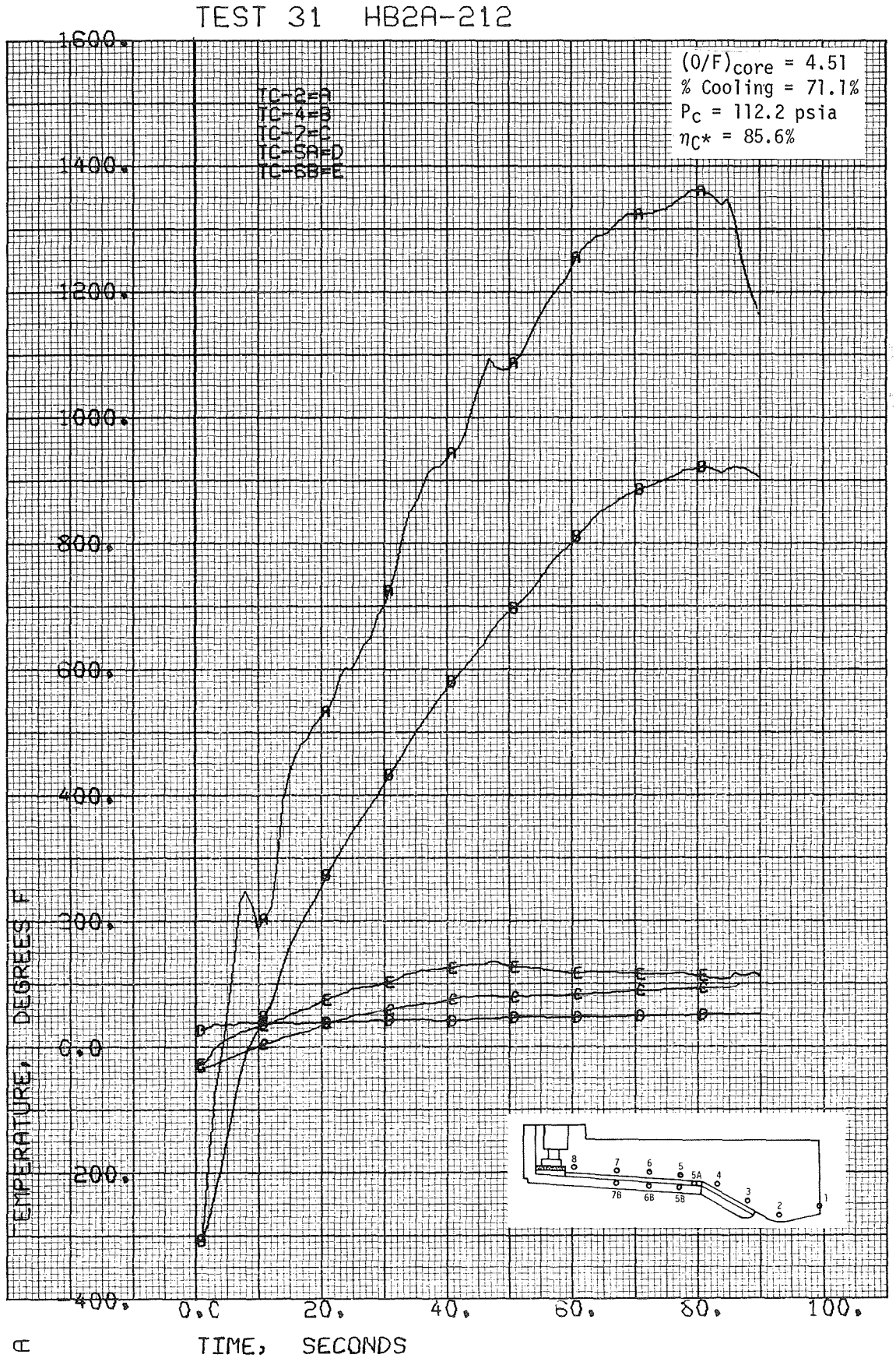

Figure 5-25. Transient Thermal Data for the Modified Distributed Duct Chamber (Test 31)

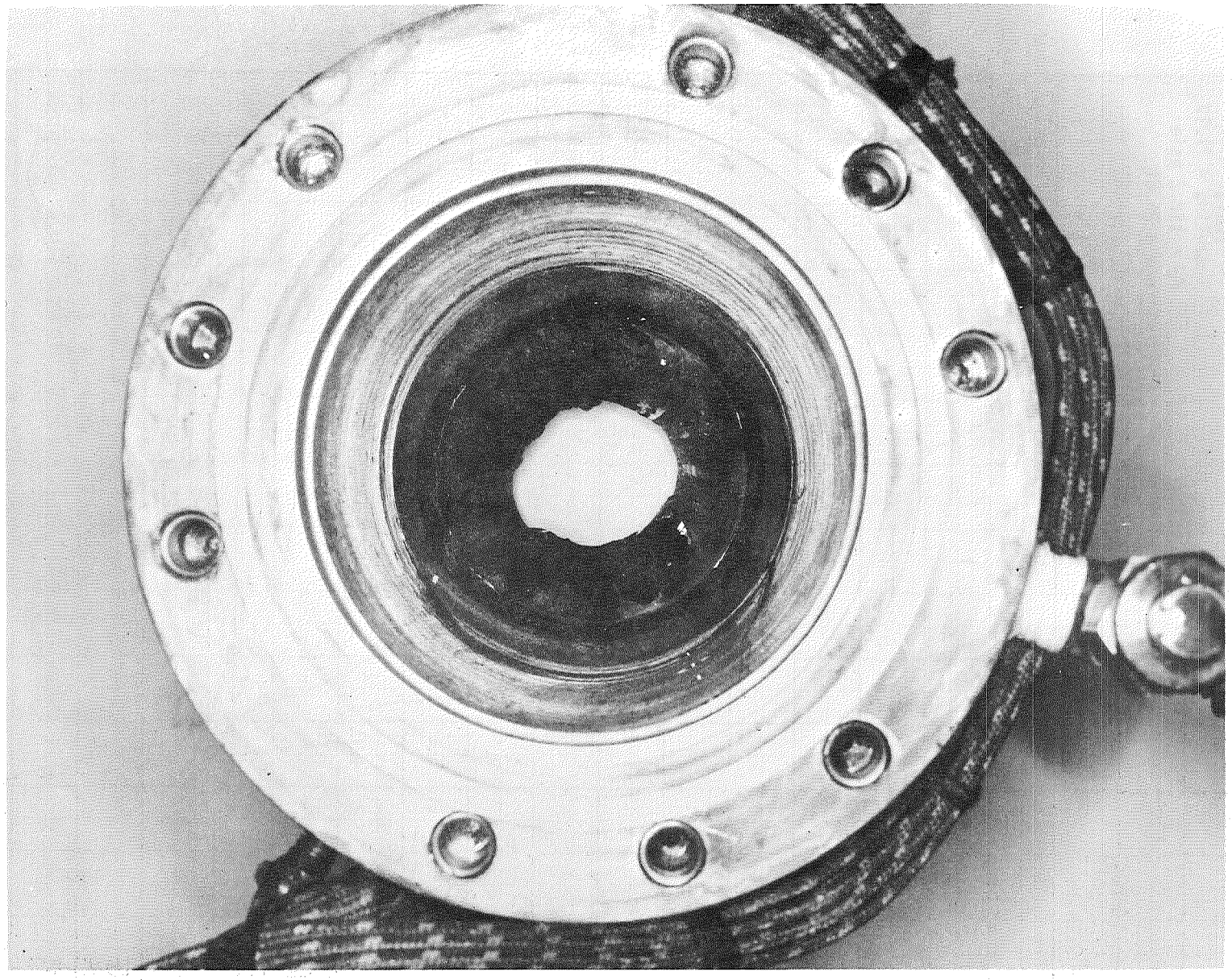

Figure 5-26. Post-Test View of Distributed Duct Chamber Without Extension Showing Throat Erosion Due to Short Duct Length

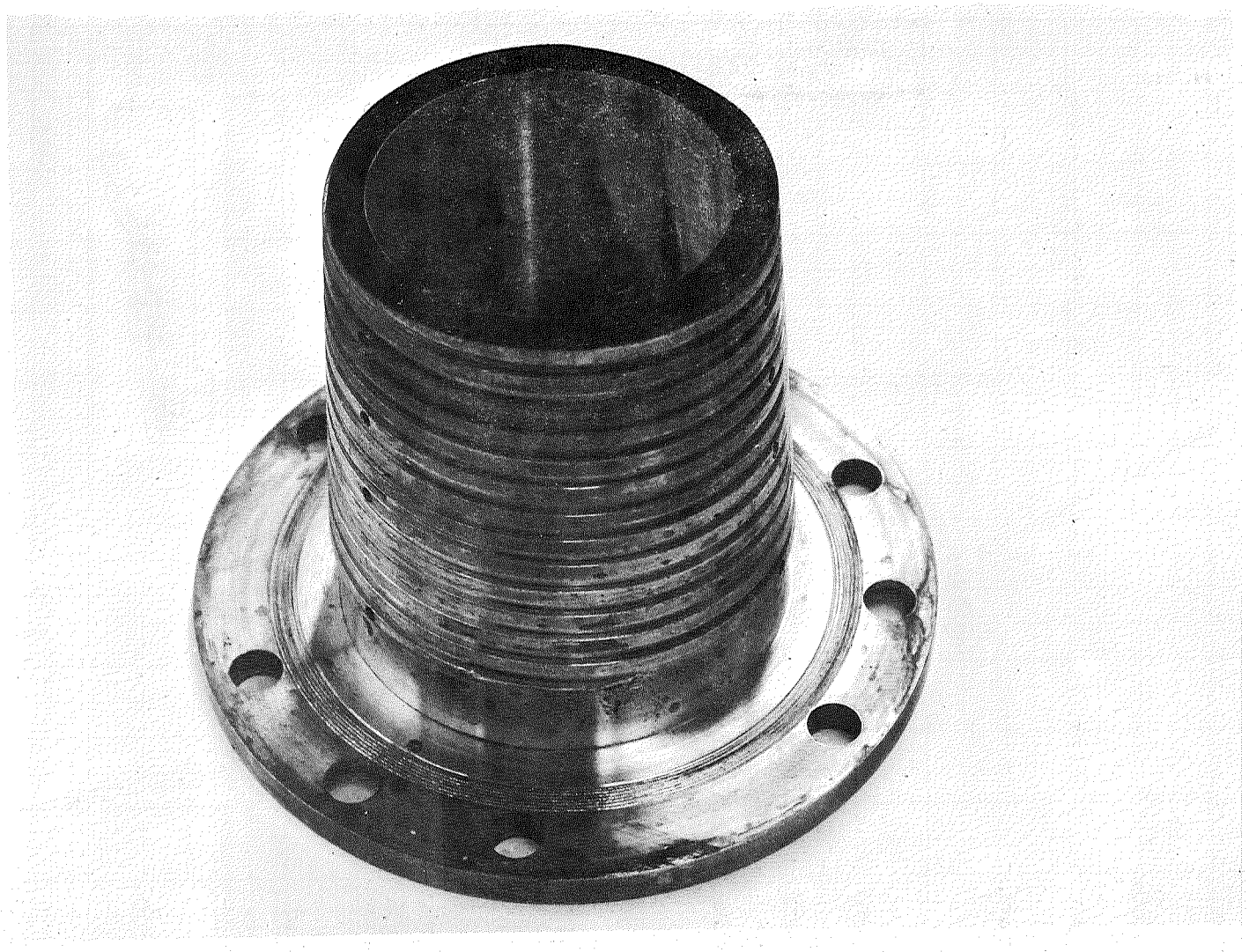

Figure 5-27. Post-Test View of Distributed Duct

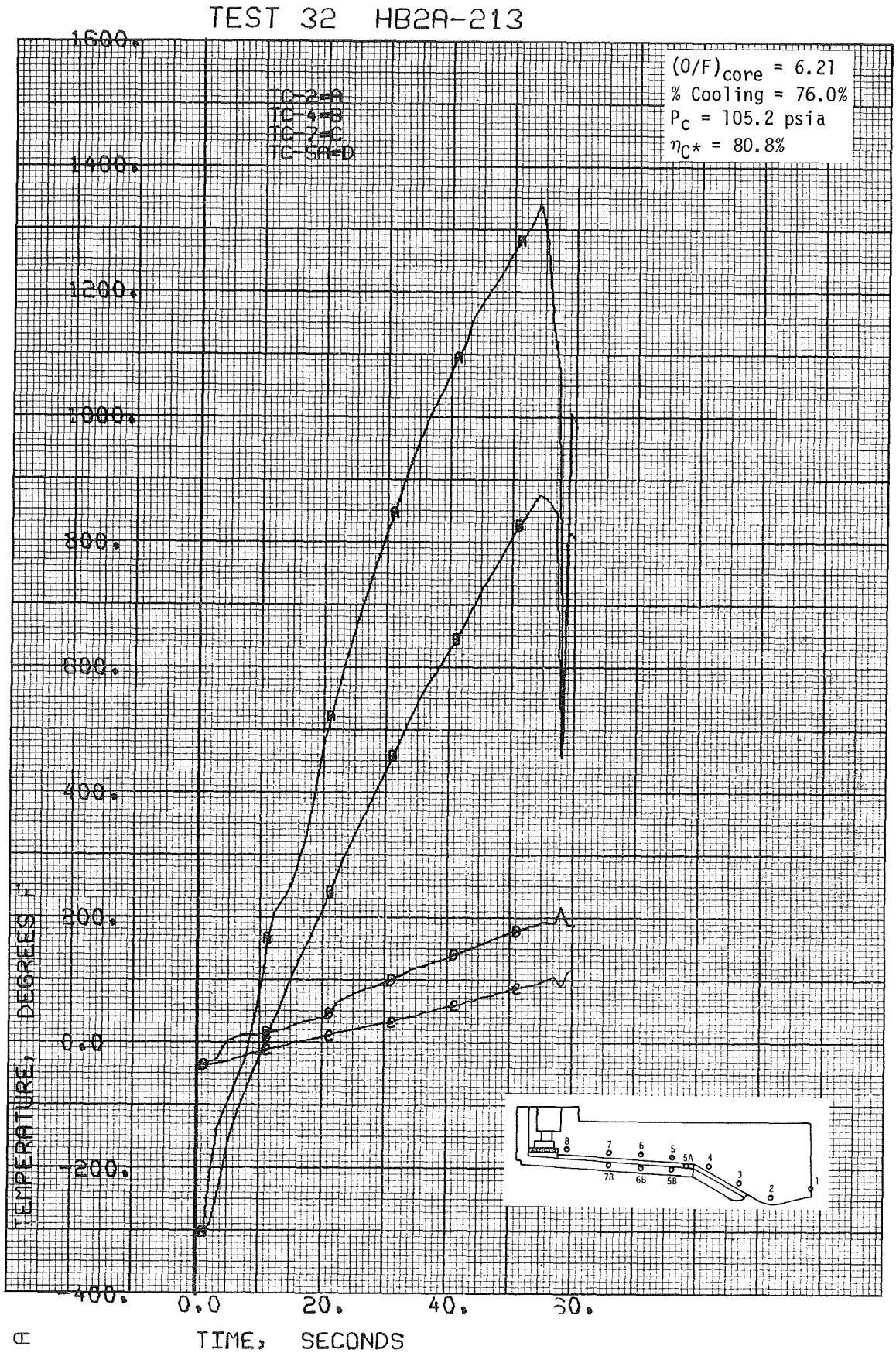

Figure 5-28. Transient Thermal Data for the Modified Distributed Duct Chamber (Test 32)

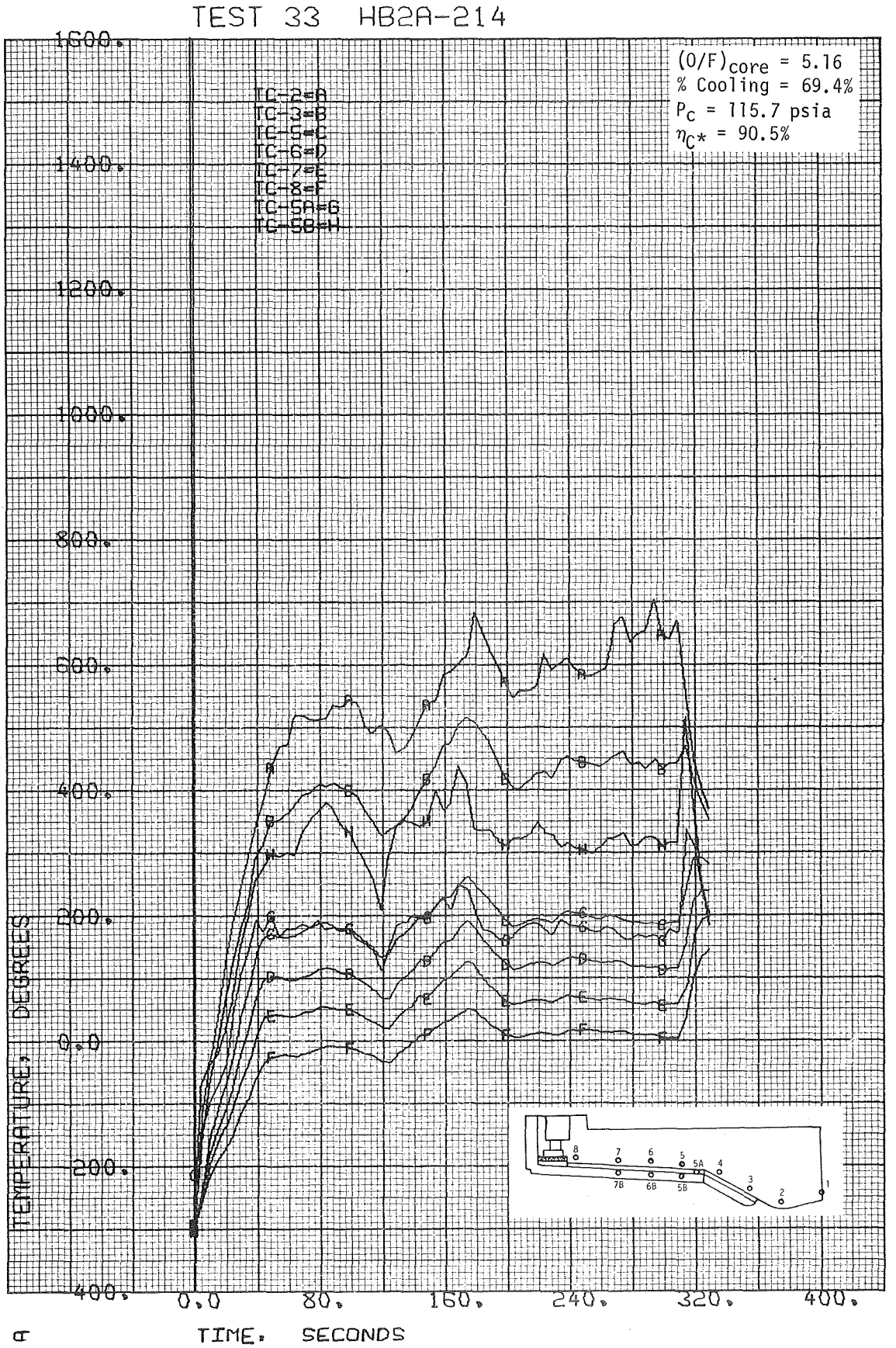

Figure 5-29. Transient Thermal Data for the Modified Total Duct Chamber (Test 33)

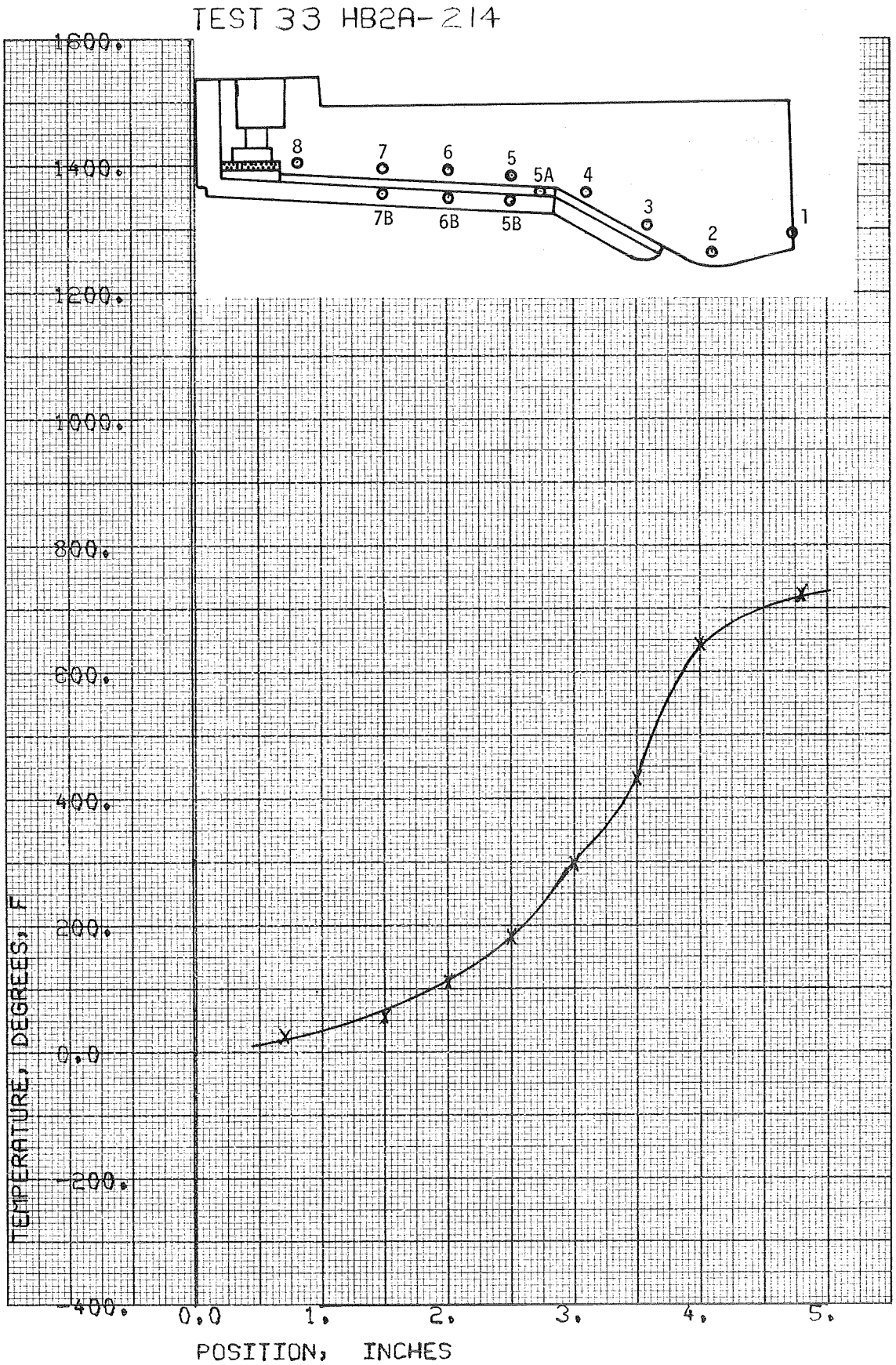

Figure 5-30. Axial Temperature Distribution for the Modified Total Duct Chamber (Test 33)

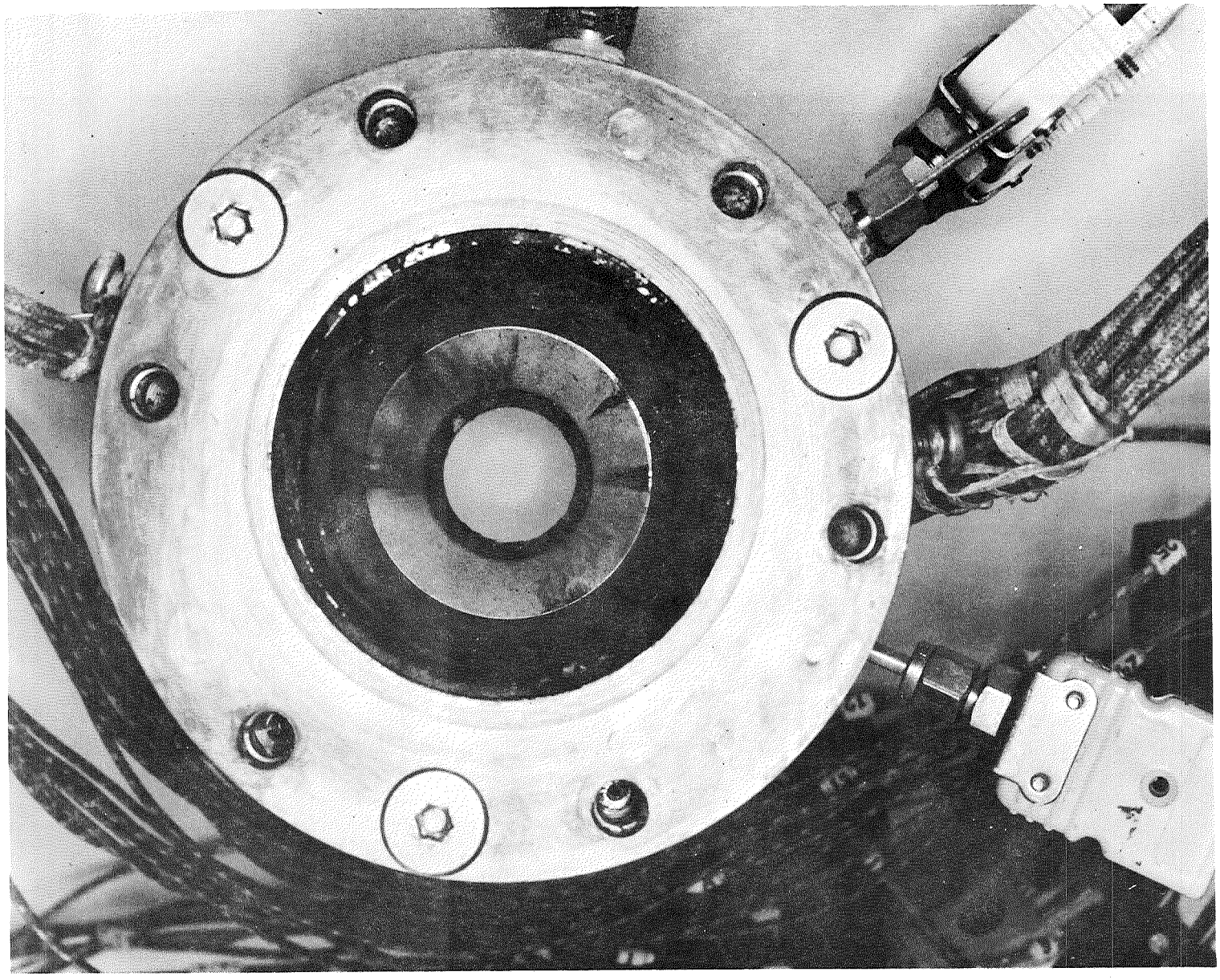

Figure 5-31. Post-Test View of Extended Duct Chamber Following 310 second Test

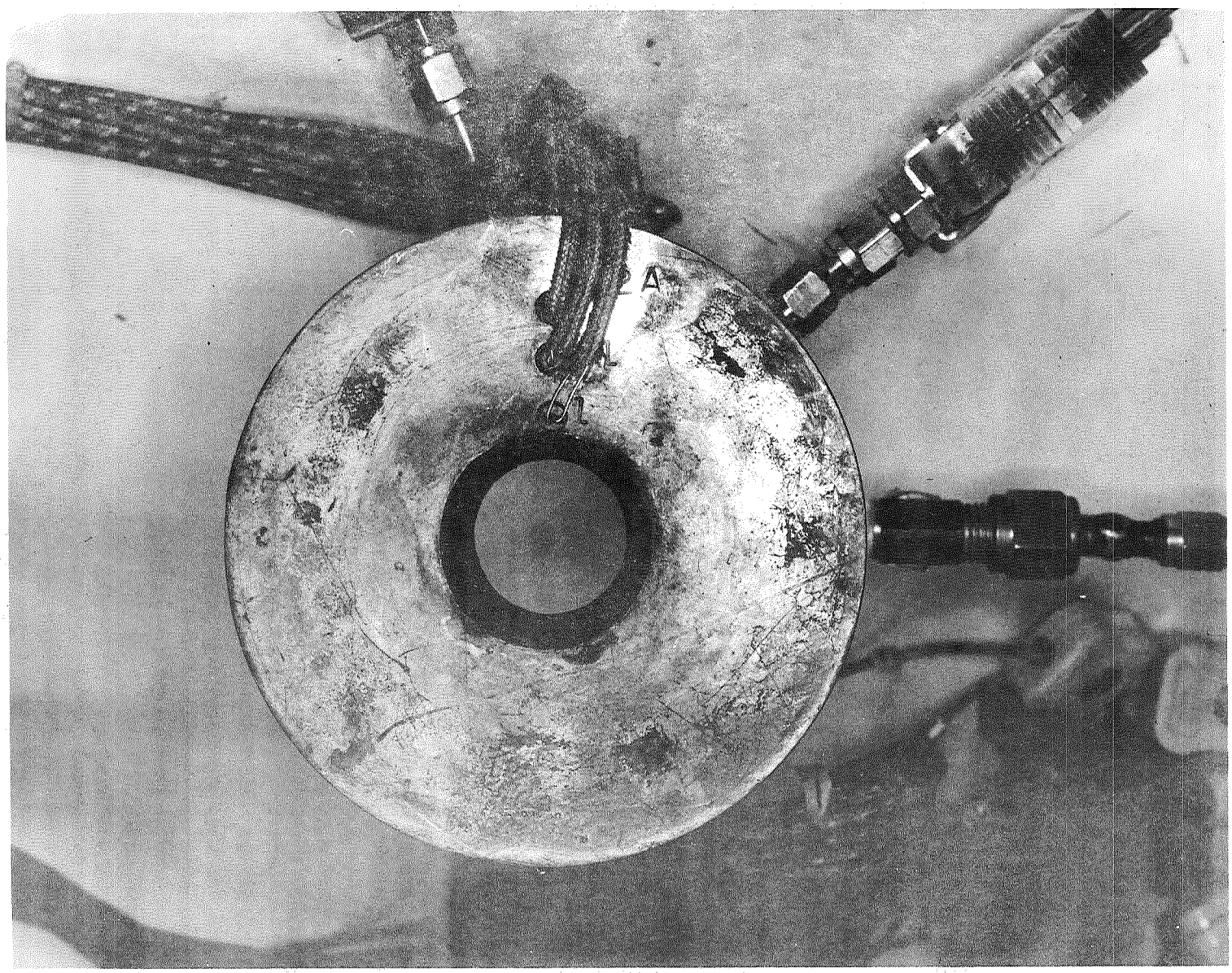

Figure 5-32. Post-Test Exit View of Extended Duct Chamber Noting Throat Carbon Deposition Following 310 second Test

Figure 5-31 shows the inside of the chamber and the extremely good condition of the duct and its extension. Figure 5-33 shows a post-test view of the injector with deposits of carbon and various fluorides coated on its face. It should be noted that even with these deposits surrounding the pintle and fuel sheet combustion performance remained high. Further thermal analyses of this test is found in Section 5.3.2.

5.2 GRAPHITIC CHAMBER TESTING

A single test was performed using an insulated graphitic material thrust chamber with conventional film cooling. This chamber internal contour was geometrically similar to the copper inter-regen thrust chamber. The test objective was to determine the throat erosion and carbon deposition characteristics with a hot inner wall chamber. The results of test number 34 are pictured in Figure 5-34. In a run duration of about 40 seconds the chamber burned through in the head end region about 1-2 inches (.0254-.0508 m) below the injector. The burn-through appeared to be aligned with the oxidizer s streams for the injector. The throat exhibited very little erosion or carbon deposition.

5.3 DATA EVALUATION

Following the test program, a complete evaluation of all data was made and is reported in the following sections with emphasis on the specific objectives of each program task. Table 5-3 summarizes all of the test data. Since the primary parameters were those required for thermal analysis the combustion performance was uncorrected for the effects of friction, nozzle entrance effects, heat transfer, etc. In the worst case, this correction would only amount to about 3%. Appendix A gives a complete compilation of the

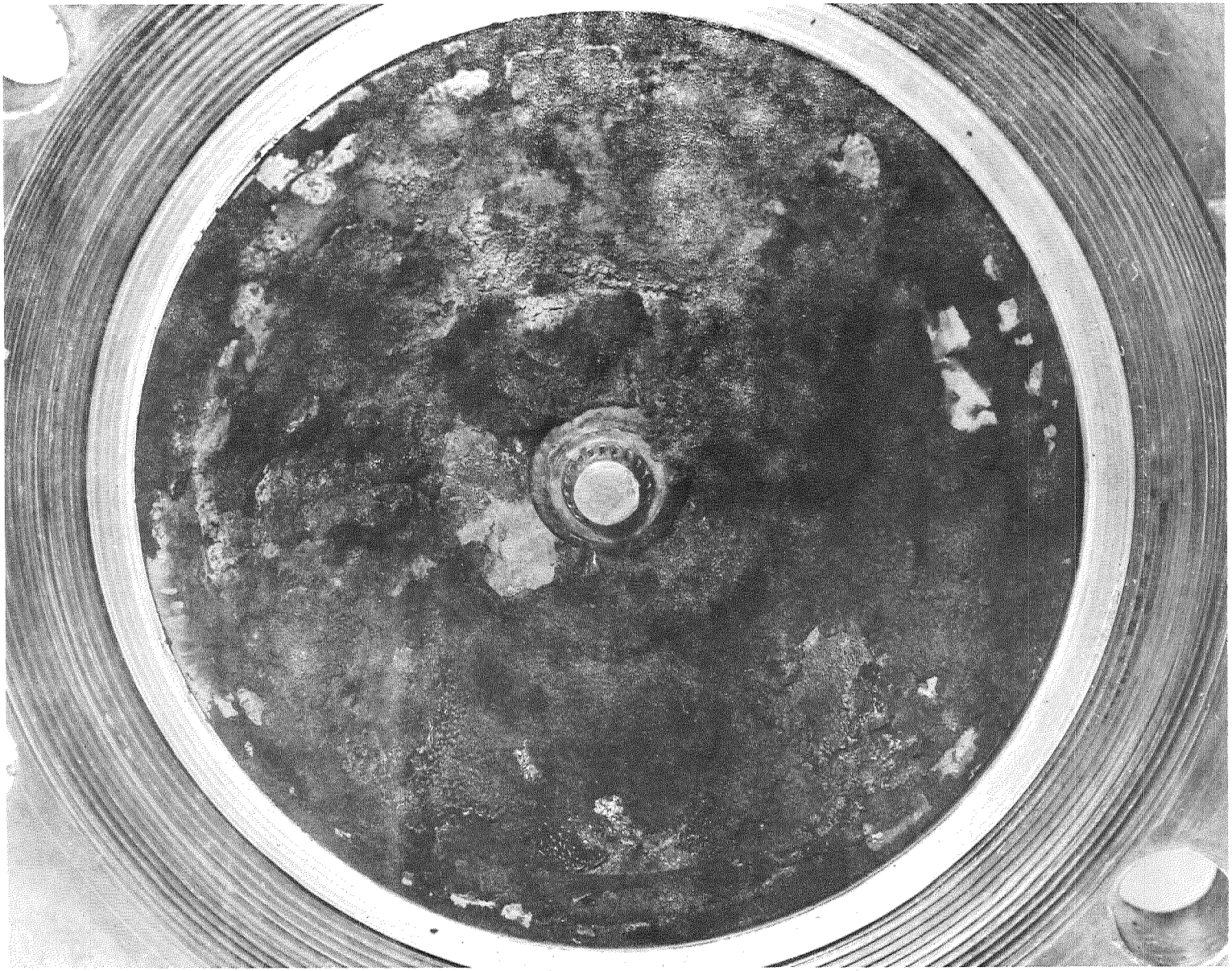

Figure 5-33. Post-Test View of Injector Face Following 310 second Test

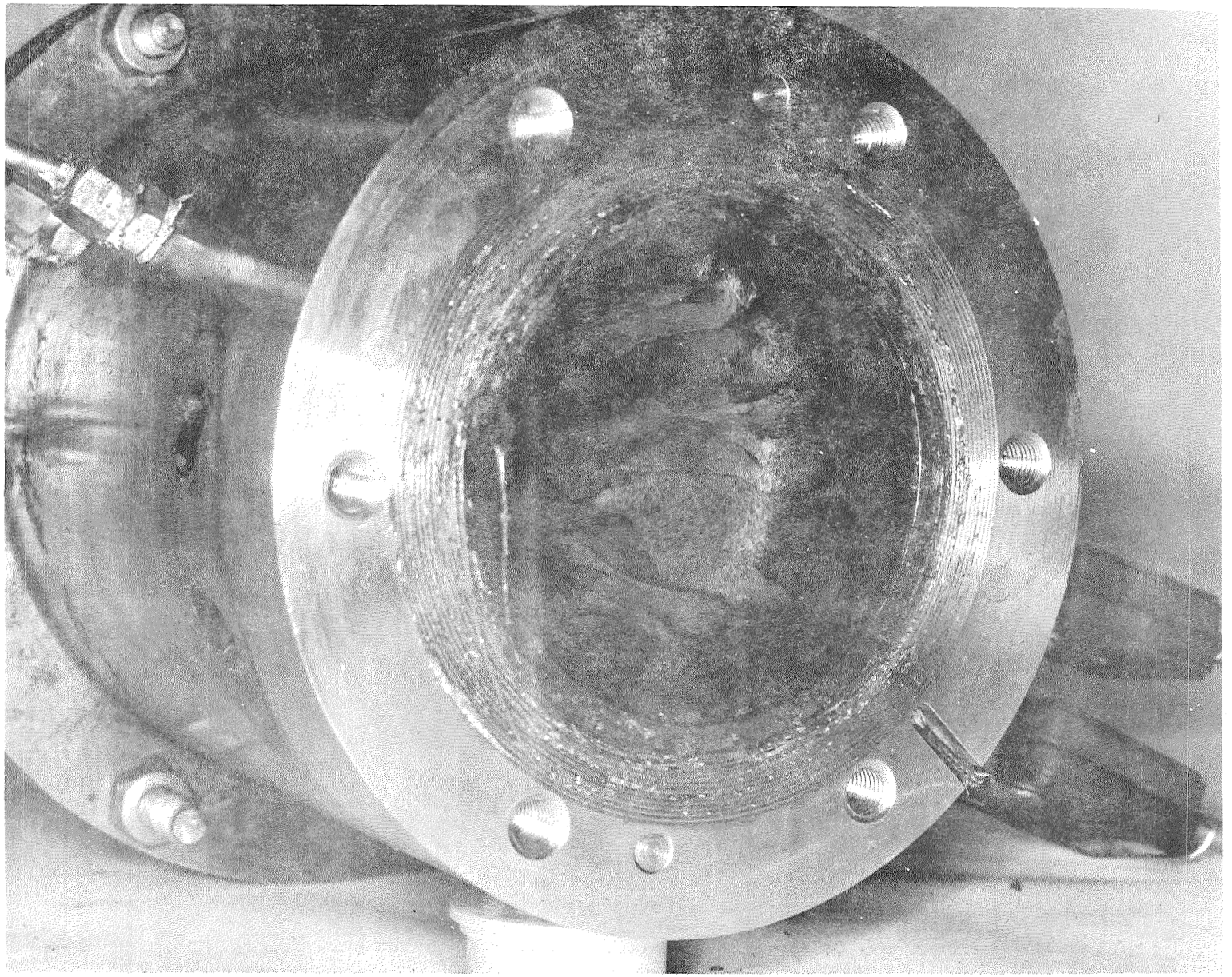

Figure 5-34. Post-Test View of Insulated Graphitic Thrust Chamber Showing Injector Induced Erosion

Table 5-3. Test Data Summary

Test No.	Duration (sec)	$(O/F)_{overall}$	$(O/F)_{core}$	$\dot{\omega}_T$ (lbm/sec)	$\dot{\omega}_T$ (Kg/sec)	% Cool	P_o (lbf/in²)	P_o (nt/m²) x10⁻⁵	C^*_p (ft/sec)	C^*_p (m/sec)	ηC^*_p (uncorr)	$F_{(corr)}$ (lbf)	$F_{(corr)}$ (nt)	C^*_F (ft/sec)	C^*_F (m/sec)	ηC^*_F (uncorr.)	Remarks
Task I																	
1	9.5			DIGITAL DATA NOT AVAILABLE													
2	10.75	4.44	5.89	.3096	.1404	24.6	92.6	6.4	5627	1715	82.6	94.1	418.6	5584	1702	82.0	
3	14	4.45	5.93	.3147	.1427	25.0	93.3	6.4	5577	1700	81.9	78.4	348.7	5565	1696	81.7	
4	26	3.28	3.79	.3386	.1536	13.5	96.1	6.6	5342	1628	80.9	86.7	385.7	5703	1738	86.4	
5	20	2.57	4.12	.3308	.1500	37.6	99.8	6.9	5679	1731	88.2	85.0	378.1	5701	1738	88.6	
6	32	2.33	4.52	.3720	.1687	48.4	102.4	7.1	5181	1579	81.5	92.4	411.0	5552	1692	87.4	Baseline Injector
7	43			DIGITAL DATA NOT AVAILABLE													
8	46	1.99	4.77	.3942	.1788	58.3	103.4	7.1	4939	1505	79.2	86.4	384.3	4955	1510	79.4	
9	48	1.82	4.30	.4042	.1833	57.6	102.9	7.1	4792	1461	78.4	85.9	382.1	4777	1456	78.1	Chamber-Injector Leak
10	84	1.42	3.32	.4180	.1896	57.3	95.7	6.6	4308	1313	74.4	76.7	341.2	4227	1288	73.0	
11	26	3.24	3.51	.3378	.1532	7.5	101.7	7.0	5667	1727	85.8	79.5	353.6	5483	1671	83.0	
12	24	2.76	3.28	.3482	.1579	16.2	105.6	7.3	5710	1740	87.8	86.3	383.9	5675	1730	87.3	
13	28	3.87	5.78	.3272	.1484	33.0	99.1	6.8	5700	1737	84.7	81.3	361.6	5695	1736	84.6	
14	24	3.45	4.85	.3290	.1492	28.9	100.2	6.9	5734	1748	86.5	92.1	409.7	6278	1914	94.9	
15	22	2.89	5.02	.3465	.1572	42.5	106.6	7.4	5789	1764	88.4	87.2	387.9	5650	1722	86.3	
16	21	2.37	4.76	.3661	.1661	50.2	111.5	7.7	5732	1747	89.8	96.2	427.9	5888	1795	92.2	30° Canted Injector
17	40	1.34	4.38	.4344	.1970	69.4	114.0	7.9	5080	1548	88.8	95.1	423.0	5256	1692	91.9	
18	40	2.10	5.81	.3782	.1715	63.9	115.0	7.9	5884	1793	93.5	97.7	434.6	5800	1768	92.2	
19	24	1.84	5.25	.3882	.1761	65.0	112.2	7.7	5597	1706	91.2	96.1	427.5	5560	1695	90.6	
20	42	1.38	3.82	.4070	.1846	63.8	104.9	7.2	4990	1521	86.7	91.8	408.3	5061	1543	88.0	
Task II																	
21	--			HARD START													
22	--			FUEL FROZE													30° Canted Injector
23	58	1.73	4.64	.3884	.1762	62.6	119.4	8.2	5788	1764	95.3	103.4	459.9	5978	1822	98.4	
24	90	1.38	3.66	.4101	.1860	62.3	113.2	7.8	5199	1585	90.2	97.2	432.4	5322	1622	92.3	Distributed Duct Chamber
25	20	2.63	3.59	.3466	.1572	26.7	110.5	7.6	6004	1830	92.9	95.6	425.2	6192	1887	95.8	
26	52	1.76	3.75	.3884	.1762	53.3	116.6	8.0	5653	1723	92.8	96.8	430.6	5596	1706	91.9	
27	30	1.84	4.08	.3970	.1801	55.0	115.5	8.0	5480	1670	89.2	98.2	436.8	5554	1693	90.4	Total Duct Chamber
28	90	1.38	3.11	.4071	.1847	55.5	113.5	7.8	5250	1600	91.0	92.0	409.2	5074	1547	88.0	
29	5			DIGITAL DATA NOT AVAILABLE													
30	--			HARD START													
31	82	1.31	4.51	.4377	.1985	71.1	112.2	7.7	4864	1483	85.6	--	--	--	--	--	Distributed Duct Chamber
32	50	1.49	6.21	.4255	.1930	76.0	105.2	7.3	4752	1448	80.8	--	--	--	--	--	" " "
33	310	1.60	5.16	.4116	.1867	69.4	115.7	8.0	5408	1667	90.5	--	--	--	--	--	Total Duct Chamber
34	40	1.39	4.33	.4392	.1992	68.1	123.6	8.5	5302	1616	91.4	99.0	440.4	5061	1543	87.2	Graphite Chamber

thermal data obtained during the program including both temperature-time and temperature-position plots.

5.3.1 Film Cooled Tests

The principal result of these tests was that propane was shown to have no advantage as a conventional film coolant over the methane/ethane fuel blend previously investigated. Liquid propane could not be made to persist over more than about the first 0.5 inch (.00127 m) of the copper thrust chamber wall. This was attributed to both the physical properties of propane and to the shear interaction with the primary injection element. It is important to note that a test using MMH as the film coolant (Reference 1) resulted in the coolant remaining on the wall and thus indicating that the physical properties of the coolants determine its film coolant stability and that injector interactions are of secondary importance. However, differences in the axial temperature profiles for the two different injector pintles did indicate that mixing between the primary propellants and the film coolant was occurring. The baseline pintle gave maximum temperatures in the head end region of the chamber indicating a high degree of interaction and resultant high mixture ratios in the region, while the 30 canted pintle yielded the more conventional thermal profiles with the maximum temperature near the throat region. In addition, it was found that the use of propane as the film coolant did not result in any increase in carbon deposition in the nozzle as had been expected. This could perhaps be due to some unexpected kinetic effects in the decomposition of the propane.

5.3.2 Duct Cooled Tests

The major portion of data analysis was expended on the duct cooled tests. The results of tests 24, 28 and 33 were analyzed using the thermal model previously described (Figure 3-16). Using the measured thermal data from the thermocouples as the program input the heat loads and heat fluxes were determined for each of these tests. The selection of these tests for analysis was based upon their successful operation in an inter-regen mode. The analysis will be used to determine the effects of the different duct geometries on the chamber thermal operating characteristics.

5.3.2.1 Test Number 24

This test used the distributed duct and ran for 90 seconds. True steady-s operation was not achieved but the test was sufficiently close to thermal equil to warrant further analysis. Figure 5-35 shows the thermal distribution within the chamber. The isotherms and heat conduction paths are noted on the figure. The thermal analysis indicated a total inter-regen heat load of 5.2 Btu/sec (54 This is somewhat higher than desired if the throat temperature is to remain below the material limits. Figure 5-36 shows the accumulated heat load and heat flux variation with axial position. As can be seen the heat input to the nozzle is conducted by the total length of the chamber with the major portion of it being absorbed by the duct coolant in the initial region of the duct. Figure 5-37 shows the axial temperature distribution on the chamber side of the duct. Three distinct regions can be noted. These are regions in which the coolant changes its film coefficient. The initial region is associated with heat transfer to turbulent liquid flow and/or to a nucleate boiling liquid.

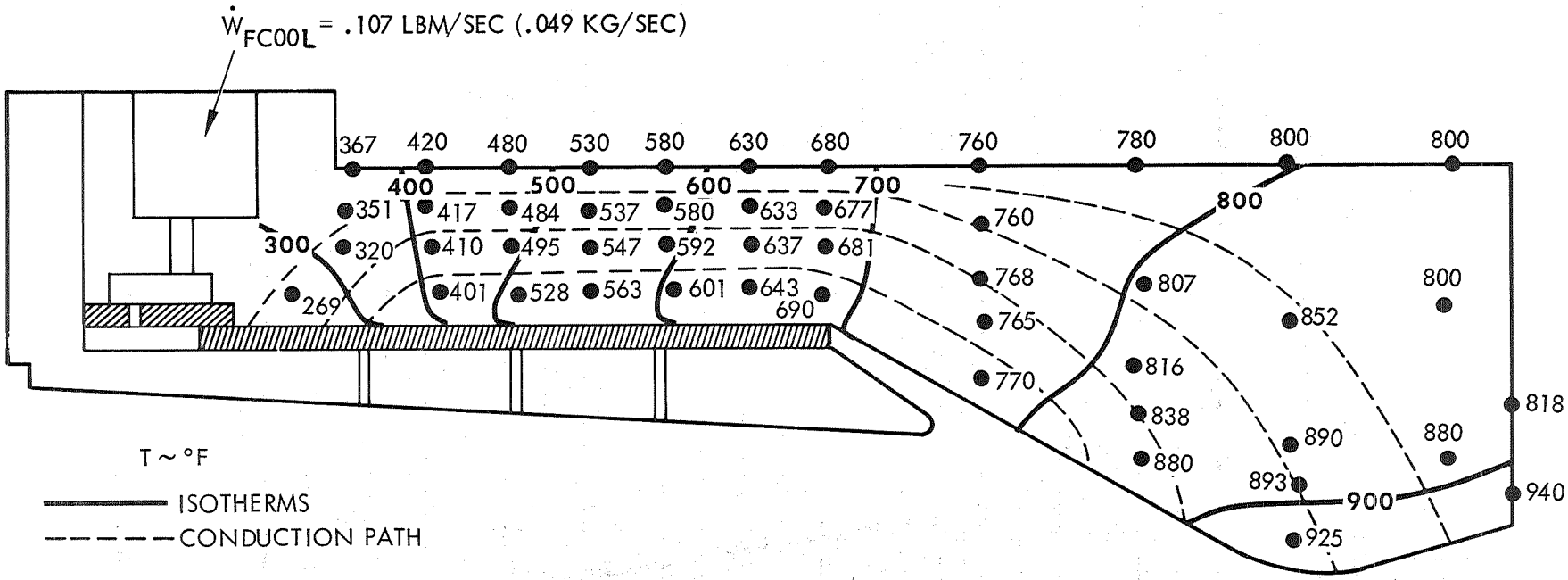

Figure 5-35. Temperature Distribution for Duct Test 24

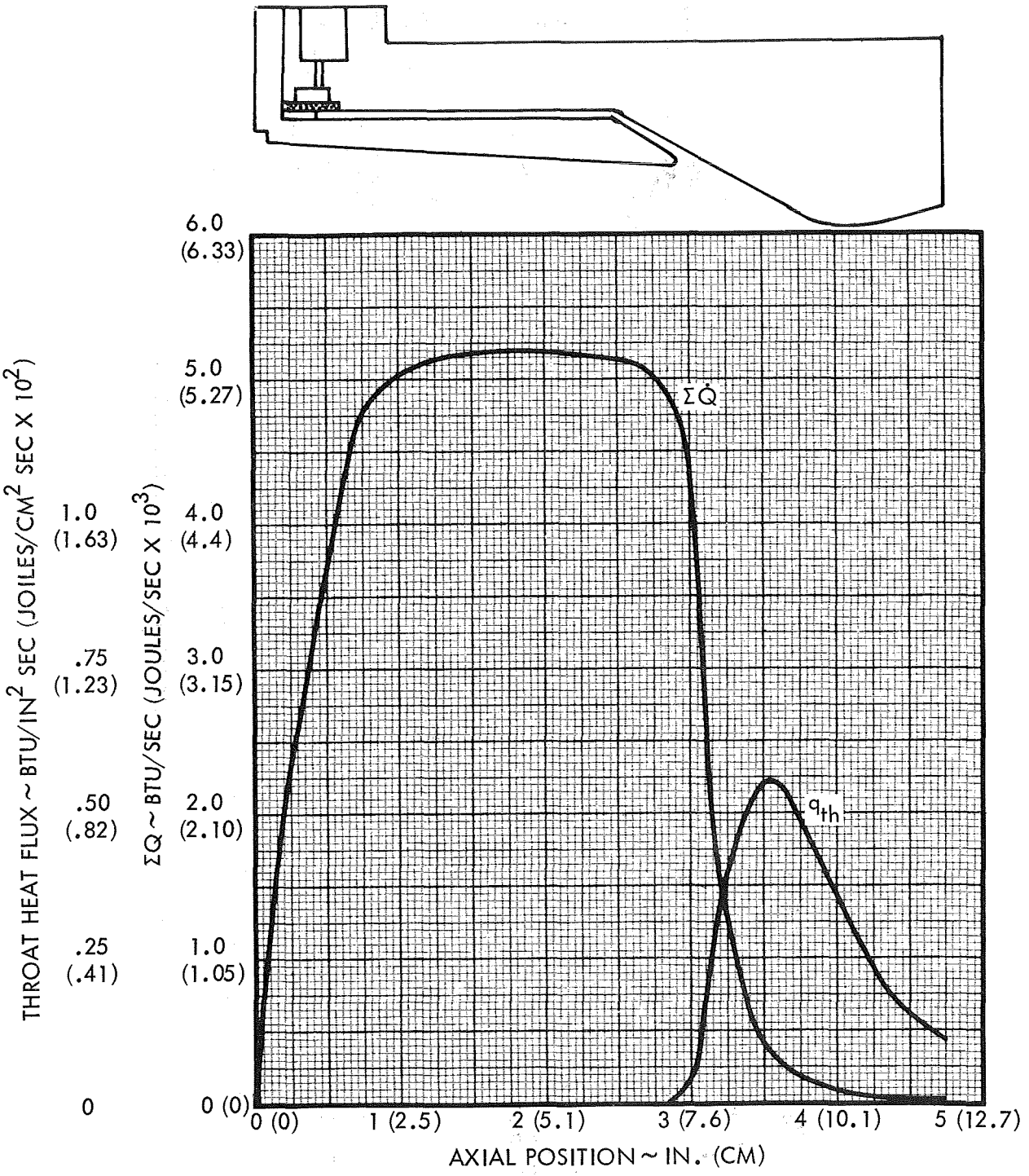

Figure 5-36. Axial Heat Load and Heat Flux for Duct Test 24

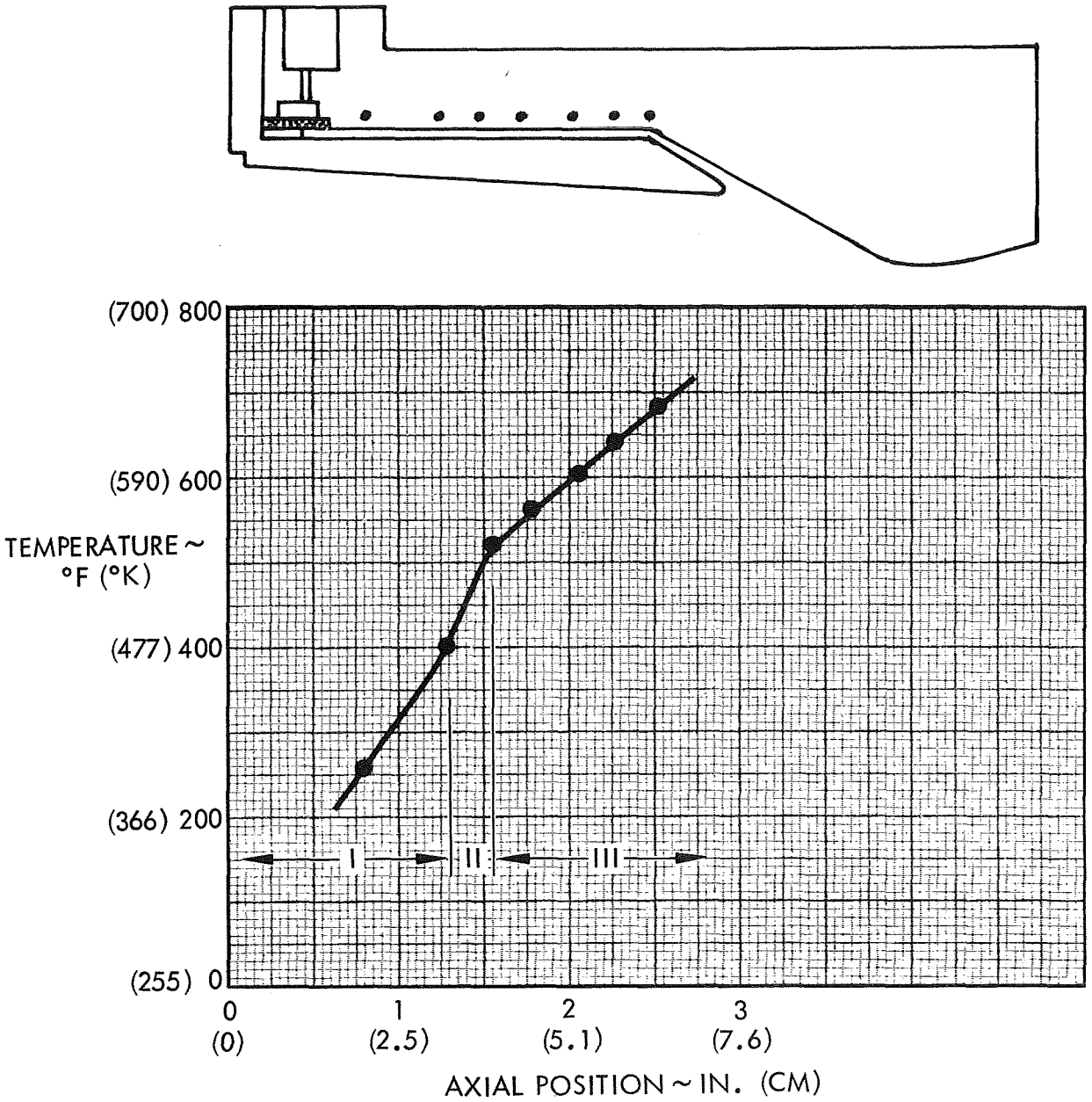

Figure 5-37. Axial Duct Temperature Distribution for Duct Test 24

Region II corresponds to a film bound region with a large increase in temperature while region III corresponds to heat transfer to the two-phase coolant fluid.

5.3.2.2 Test Number 28

The total duct was used for this test and resulted in a steady-state run of 90 seconds duration. Figure 5-38 shows the thermal distribution within the chamber with isotherms and heat conduction paths noted. Thermal analysis gave the inter-regen heat load as 4.45 Btu/sec. (4690 watts). This is low enough to allow the throat to operate at temperatures well below the material limits. The reduced heat loads indicate that the total duct acts more effectively than the distributed duct to protect the nozzle from the combustion gas. This was expected since the actual coolant flow rate exiting the total duct was greater than the distributed duct. Figure 5-39 shows the accumulated heat load and heat flux axial variation. Again, most of the conducted heat is absorbed by the coolant in the initial duct region. The duct coolant heat transfer characteristics noted on test number 24 are also noted on this test as seen in Figure 5-40. This is to be expected from the similar geometries and heat loads involved.

5.3.2.3 Test Number 33

A test duration of 310 seconds was accomplished using the modified total duct design. The success of this test was principally the result of moving the duct exit to just upstream of the throat. Previous tests with the modified ducts cut off at the beginning of the convergent region were very unsuccessful due to the formation of a very turbulent region following the end of the duct. Figure 5-41 shows the temperature distribution, isotherms and heat conduct paths for this test. An inter-regen heat load of 3.83 Btu/sec. (4035 watts) was determined from the thermal model. This is appreciably lower than for the other ducted chambers

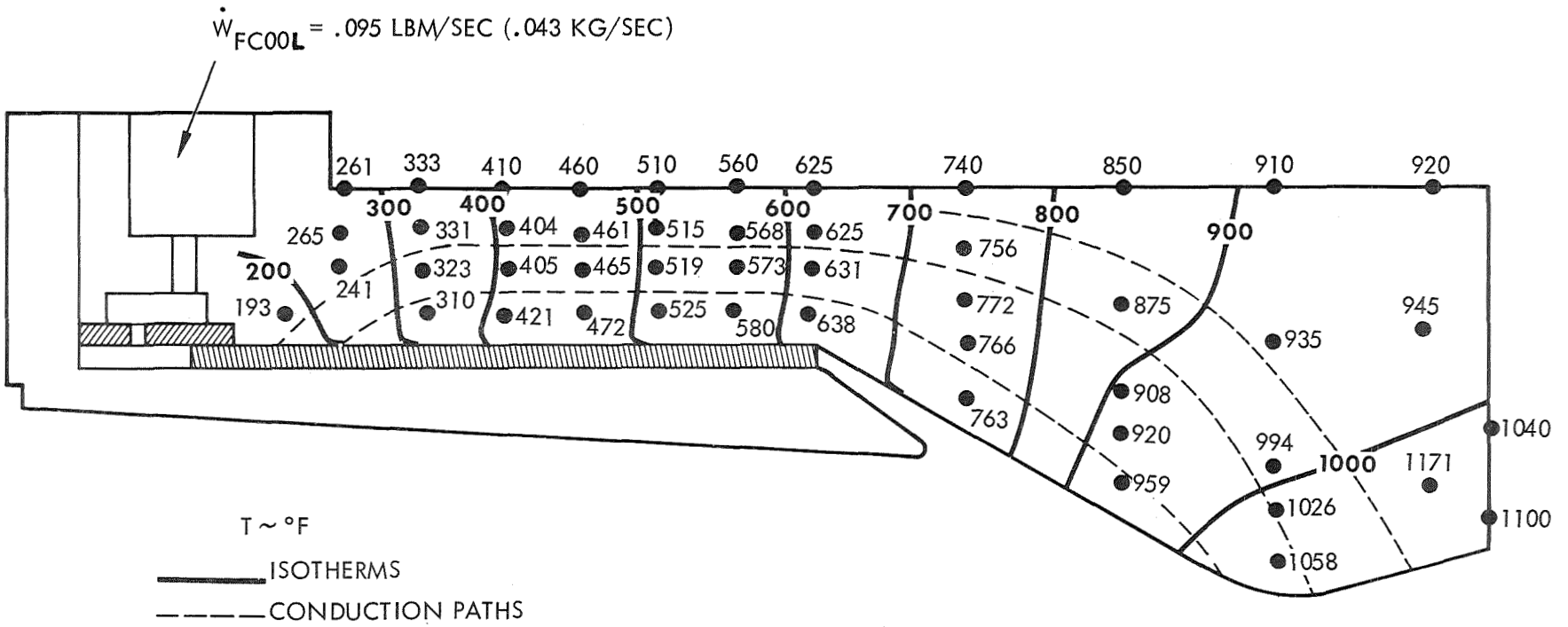

Figure 5-38. Temperature Distribution for Duct Test 28

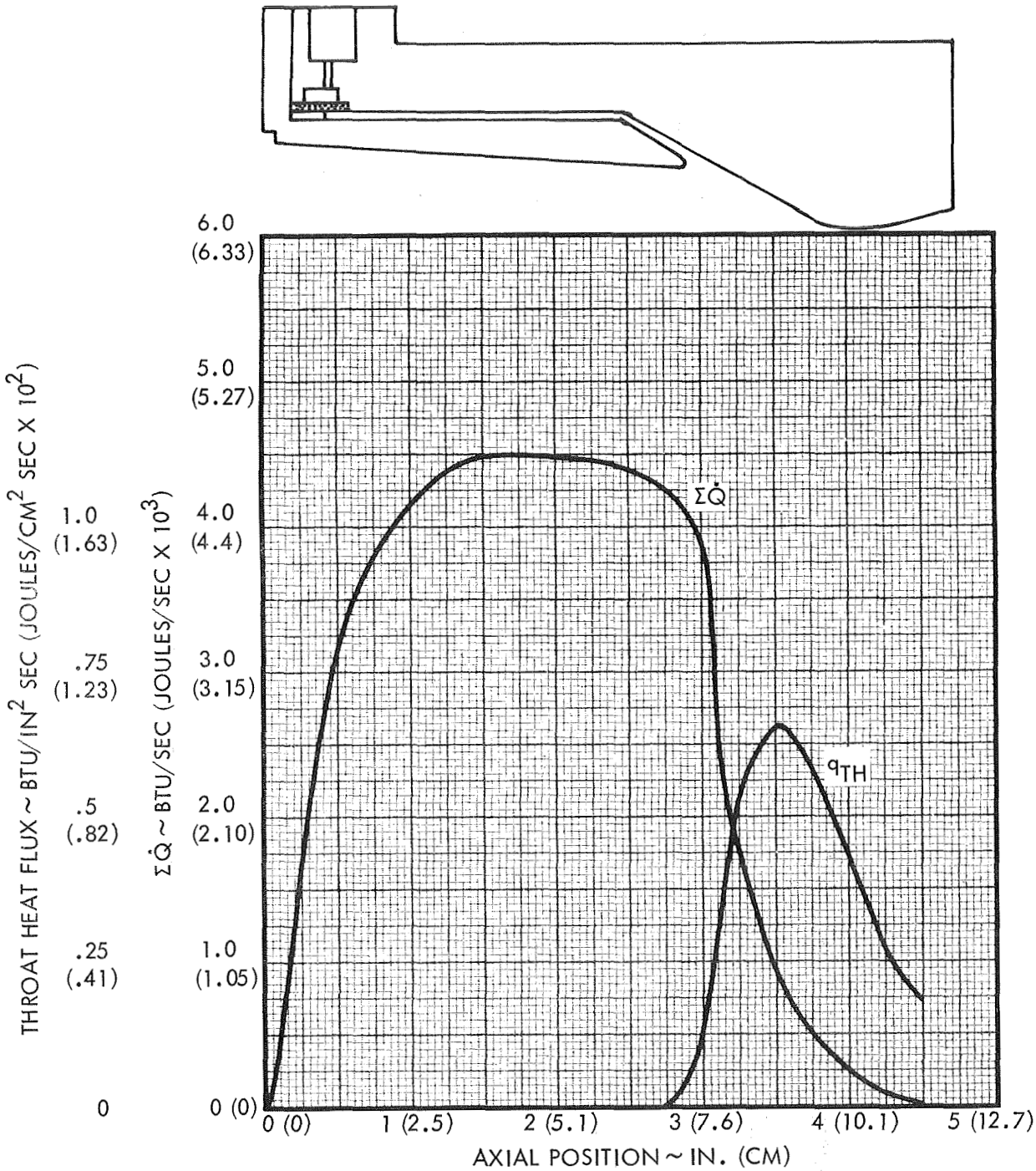

Figure 5-39. Axial Heat Load and Heat Flux for Duct Test 28

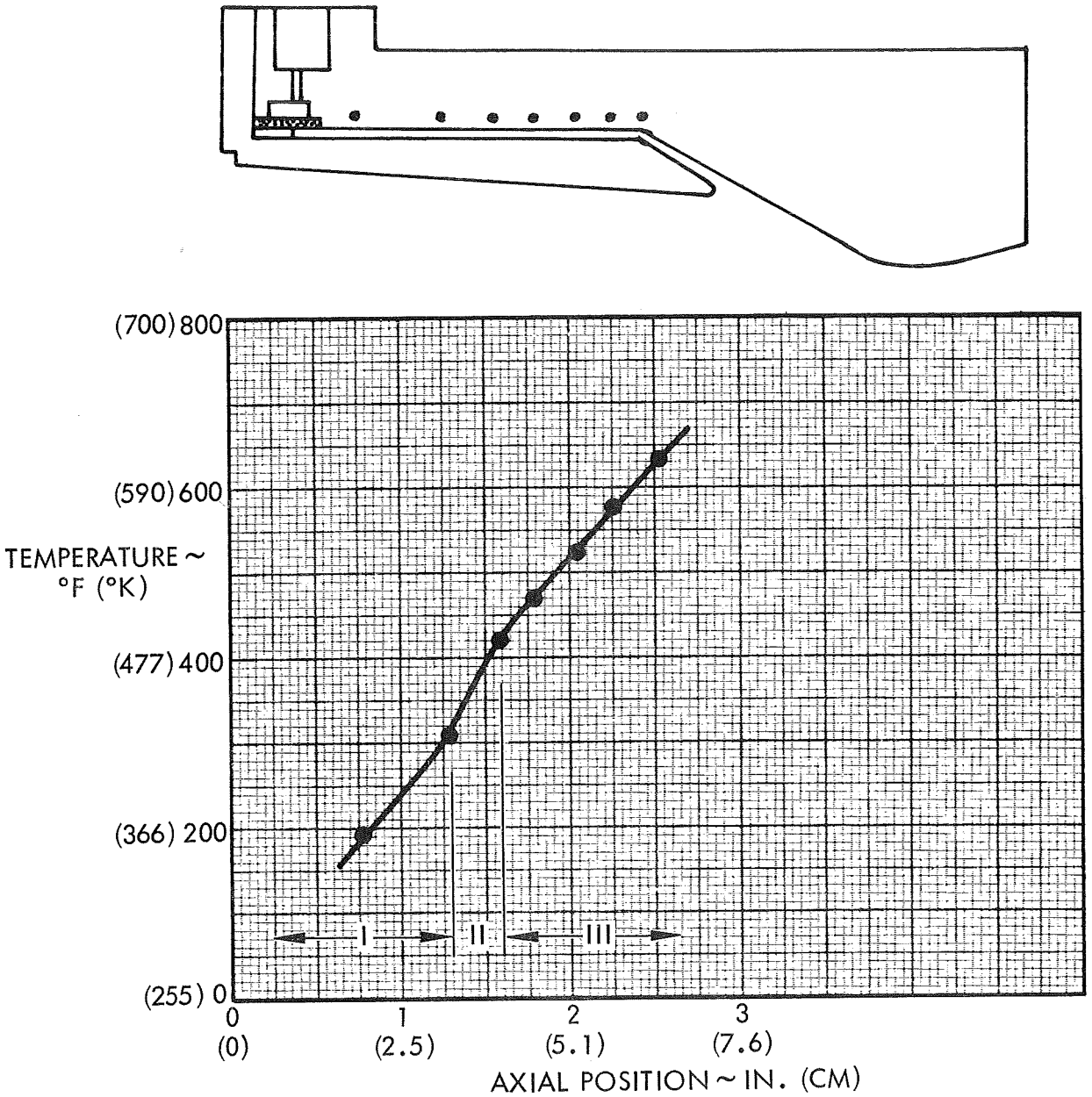

Figure 5-40. Axial Duct Temperature Distribution for Duct Test 28

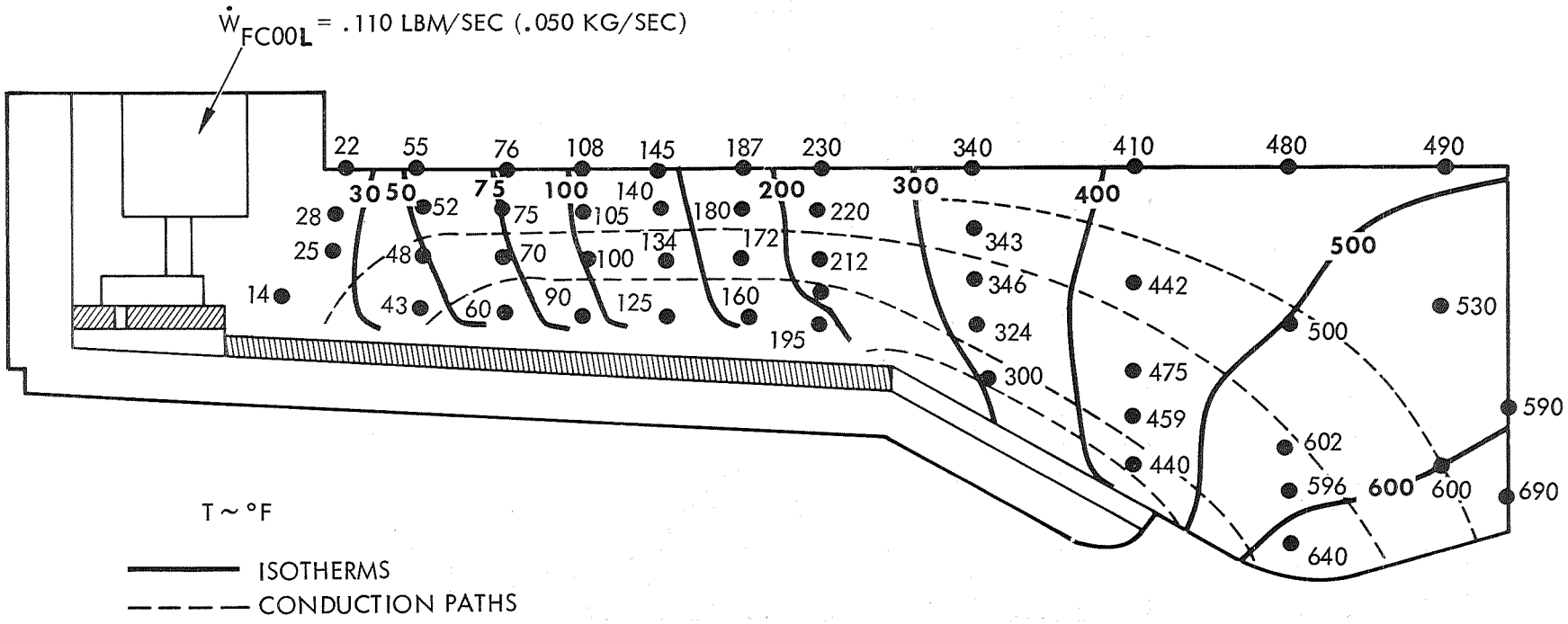

Figure 5-41. Temperature Distribution for Duct Test 33

as indicated by the lower throat temperature. Figure 5-42 shows the accumulated heat load and heat flux axial variation for this test and reveals a greatly different coolant heat input distribution. The heat input to the coolant is much more distributed than in the previous tests. Another indication of this is revealed in the axial temperature on the chamber side of the duct (Figure 5-43). Apparently, the reduced heat loads and higher duct coolant pressure of this test have eliminated the film bound region (region II) previously observed.

5.3.2.4 Final Duct Inter-Regen Thermal Model

Based on the data evaluation of the three successful inter-regen tests previously discussed, a duct cooled inter-regen thermal model was formulated. This appears in Figure 5-44. Duct design should account for the various flow regions that were experimentally found; however, different propellants or duct configurations may eliminate some of the regions. At present, it is very difficult to accurately estimate the carbon resistance in the nozzle since many complex mechanisms are involved in this process.

5.3.3 Graphitic Chamber Test

The insulated graphitic thrust chamber test resulted in a burn through in the head end chamber region after 40 seconds of operation. The burnout appeared to be directly in line with the primary oxidizer streams with burnout being caused by a combination of high local temperature from the mixing of the oxidizer and film coolant and the oxygen present in the fluorinated oxidizer. Unfortunately, this was the only chamber available so that no tests with a ducted graphitic thrust chamber could be made.

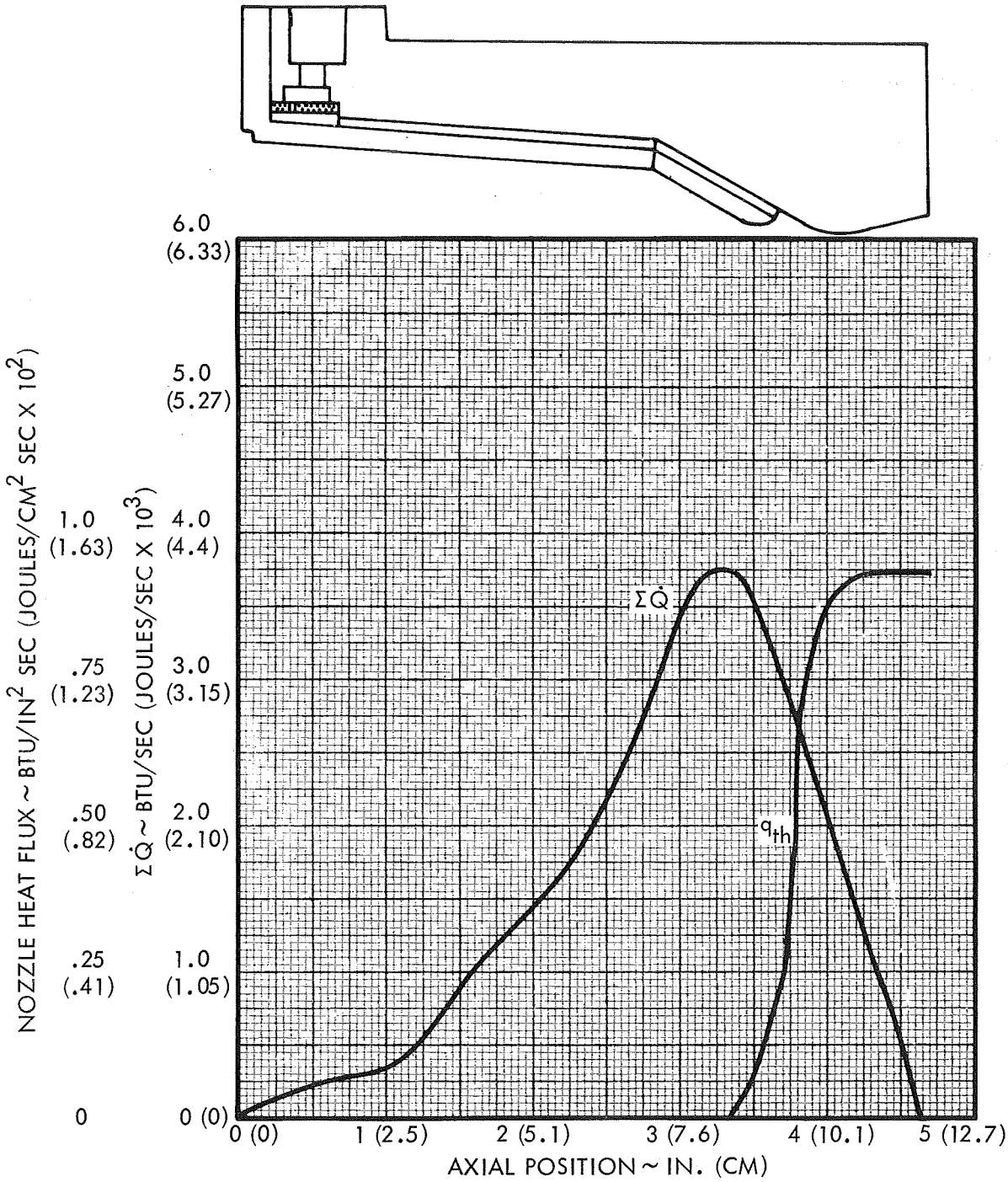

Figure 5-42. Axial Heat Load and Heat Flux for Duct Test 33

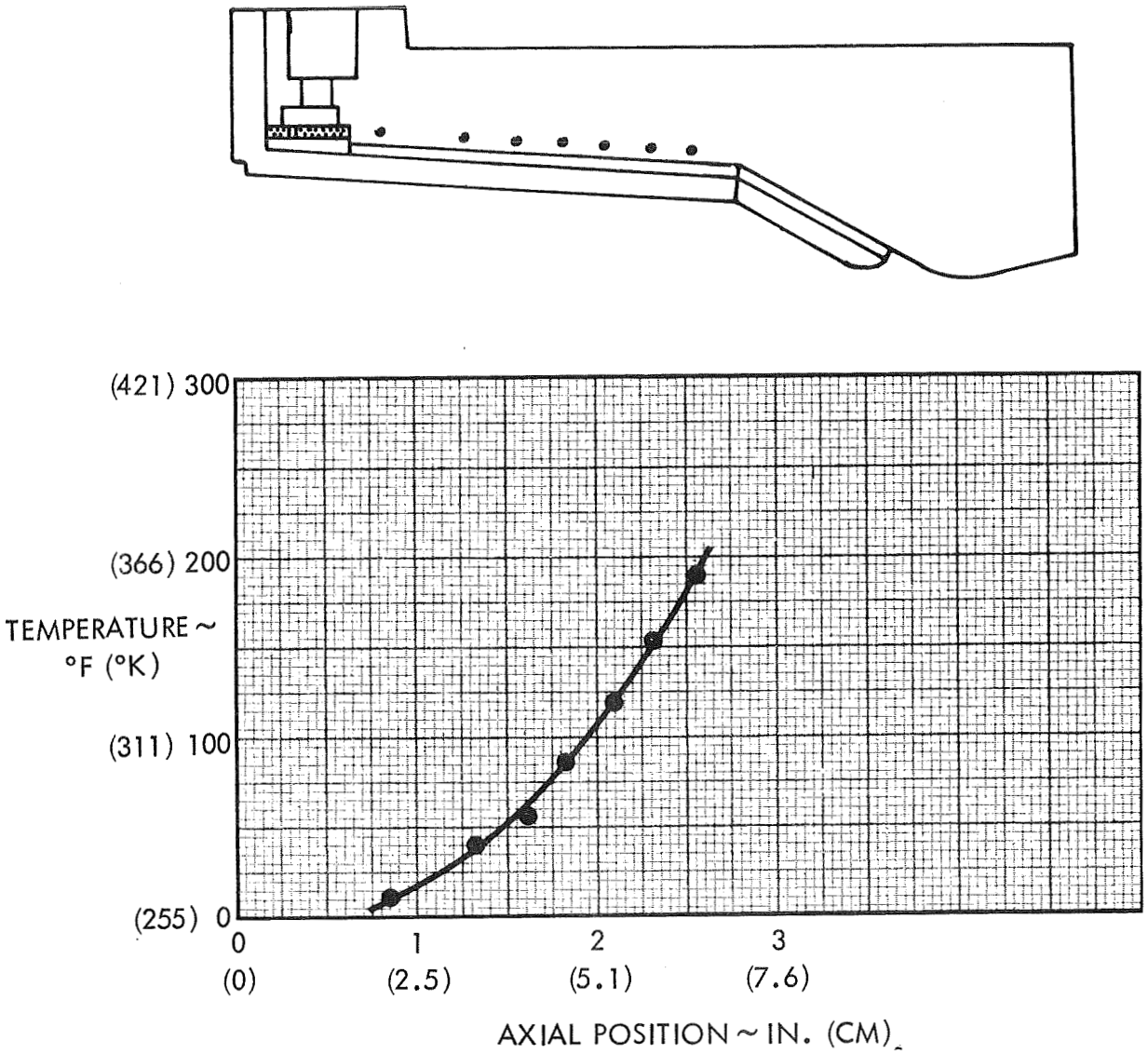

Figure 5-43. Axial Duct Temperature Distribution for Duct Test 33

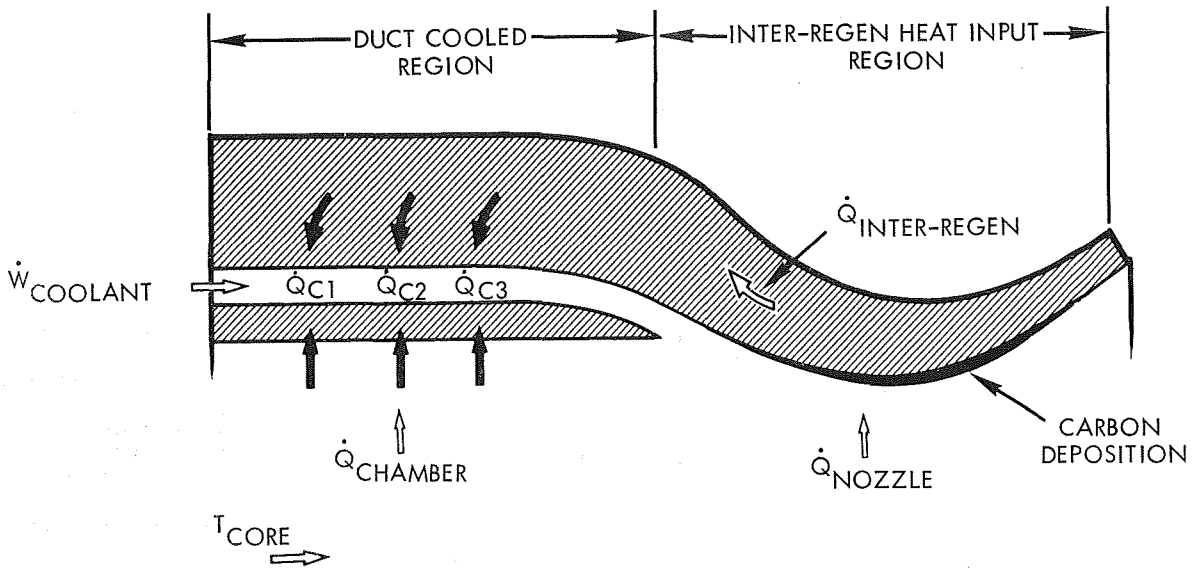

$\dot{Q}_{CHAMBER} = h_g (X) A_{CH} (T_{CORE} - T_{WC} (X))$; h_g = GAS FILM COEFFICIENT (BARTZ)

$\dot{Q}_{NOZZLE} = \overline{h_g} (X) A_N (T_{CORE} - T_{WN} (X))$; $\overline{h_g} = \dfrac{1}{\dfrac{1}{h_g} + R_{CARBON}}$

$\dot{Q}_{C1} = \eta_{C1}\dot{Q}_{CH} + \eta_{N1}\dot{Q}_N = h_1 A_1 (T_W (X) - T_{COOL})$; h_1 = TURBULENT FLOW FILM COEFFICIENT

$\dot{Q}_{C2} = \eta_{C2}\dot{Q}_{CH} + \eta_{N2}\dot{Q}_N = h_2 A_2 (T_W (X) - T_{SAT})$; h_2 = NUCLEATE BOILING FILM COEFFICIENT

$\dot{Q}_{C3} = \eta_{C3}\dot{Q}_{CH} + \eta_{N3}\dot{Q}_N = h_3 A_3 (T_W (X) - T_{SAT})$; h_3 = TWO-PHASE FILM BOILING FILM COEFFICIENT

$\Sigma \eta_{C1} + \eta_{C2} + \eta_{C3} = 1.0$

$\Sigma \eta_{N1} + \eta_{N2} + \eta_{N3} = 1.0$

$\dot{Q}_{NOZZLE} = \dot{Q}_{INTER-REGEN}$

Figure 5-44. Duct Cooled Inter-Regen Thermal Model

6. DISCUSSION AND CONCLUDING REMARKS

This section discusses the basic results of the experimental studies and data evaluation. Also given are some basic recommendations concerning the design of inter-regen thrust chambers employing the space storable propellants.

6.1 EXPERIMENTAL RESULTS AND DATA EVALUATION

The principal objective of this program as previously stated was to obtain a better understanding of the mechanisms and factors affecting inter-regen operation of a thrust chamber using the space storable propellants. Specific objectives were: 1) to investigate propane as a coolant and compare it to methane/ethane, 2) to determine the effect of coaxial injector pintle variations on inter-regen operation, 3) to determine the limits and operational characteristics of a ducted inter-regen chamber and 4) to experimentally test a graphitic material chamber with the film cooled coaxial injector to determine carbon deposition and erosion characteristics. Each of these objectives are discussed below.

6.1.1 Propellant Effects

The principal effect of changing to propane as the coolant fluid is associated with the differences in physical properties of various LPG propellants. A secondary effect is the change in the optimum mixture ratio. Propellants with a lower optimum mixture ratio allow the use of more fuel as a coolant and consequently if the coolant capabilities of the lower mixture ratio fuel are the same, better inter-regen operation should be achieved. The primary

reason for the selection of propane as the fuel for this program was to examine the effect that a higher saturation temperature and hence wider liquid range would have on the coolants effectiveness. In addition, propane should have better carbon deposition characteristics due to its higher carbon to hydrogen ratio than the methane/ethane fuel blend. However, the experimental results of the Task I testing did not reveal any increase in the effectiveness of propane as a coolant with the test conditions and hardware used. Thermal data did not indicate the presence of liquid propane for more than about 0.5 inch of the chamber. This result was analytically substantiated by the analysis of Section 3.1.3. It is difficult to make a comparison of fuels for the duct test since methane/ethane was never used with the duct configuration. Reference 1 reported heavy uniform carbon deposits in the nozzle using 60% film cooling with methane/ethane; however, the Task I tests did not result in nearly as good carbon deposition. A precise explanation of this effect is unknown at this time but perhaps it is due to certain kinetic effects. Another possibility is a temperature difference in the boundary layer of the two coolants. Reference 4 found a very strong temperature influence on carbon deposition. It is thus the conclusion of this program that propane was no better and in some respects worse than methane/ethane as a conventional film coolant.

6.1.2 Coaxial Injector Effects

The results of Reference 1 indicated that perhaps the combustion zone produced by the coaxial injector was interacting with the film coolant and decreasing its effectiveness. This result was partially discounted following a test reported in Reference 1 where MMH was used as the film coolant while maintaining the FLOX/methane/ethane core. This test showed liquid MMH along the entire length of the chamber and hence indicated that the primary propellants interaction with the film coolant was small. However, any interaction

is apparently amplified with the use of volatile, low viscosity propellants as film coolants. This program investigated the interaction effect by using two pintle variations. One was the same as was used with the methane/ethane coolant with the primary propellant resultant momentum vector canted only 8° downstream while the other canted the resultant momentum vector another 30° downstream. The baseline pintle element tests resulted in hot spots in the head end portion of the chamber indicating interaction between the primary propellants and the film coolant with subsequent combustion adjacent to the chamber wall. The 30° canted element did not reduce the heat loads sufficiently to allow steady-state inter-regen operation, but it did reverse the axial thermal gradients to the more conventional trends which allowed conduction from the throat toward the injector. This indicated much less interaction with the film coolant.

6.1.3 Duct Cooled Chamber Effects

Bearing in mind the analysis of Section 3.1.3 and the experimental results of Task I the obvious solution is to protect the coolant from the primary combustion gases. This can be accomplished with the use of a duct. The coolant is then used to keep both the duct wall cool by a regenerative-type operation and the throat cool by inter-regenerative operation. This allows the coolant to be decoupled from any injector effects providing performance losses can be minimized or eliminated. The ducted chambers tested in Task II used both distributed and total duct cooling with the ducts extending to various axial positions and with various duct exit configurations. The results indicated that inter-regen operation was possible providing the coolant leaving the duct was allowed to persist through the throat and hence protect the throat region.

This was possible only if no large turbulent region was created after the end of the duct. Two tests resulted in steady-state operation for 90 and 310 seconds and a third in nearly steady operation for 90 seconds. Indications were that the distributed duct was inferior to the total duct for protecting the throat region, but that performance was higher. Surprisingly, performance on both types of ducts was higher than with conventional film cooling. Thermal analysis of the successful inter-regen tests showed that propane did not remain a liquid during its residence within the duct passages, but that two-phase flow was exiting from the duct. This is what was predicted from the analysis of Section 3.1.4. Actually, several heat transfer regions are present within the duct as depicted in the duct inter-regen thermal model shown in Figure 5-44.

6.1.4 Graphite Chamber Effects

The graphite chamber test was aimed at determining the effects of carbon deposition and throat erosion using the film cooled coaxial injector. The test resulted in severe head end chamber erosion caused by the high mixture ratio at the wall. A combination of high gas temperatures and the presence of oxygen at the wall is the most feasible explanation for this result.

6.2 RECOMMENDATIONS

The results of this program have provided considerable additional data on the application of the space storable propellants to inter-regeneratively cooled thrust chambers. The experimental activities have demonstrated successful inter-regen operation for long duration with high performance and excellent chamber and injector durability.

These efforts have resulted in the basic recommendation that for inter-regen operation using the space storable propellants the coolant should be decoupled from the injection processes. This might be possible with conventional film cooling if great enough control can be obtained over the chamber mixture ratio variations and provided interactions between the film coolant and the primary combustion gases can be minimized. However, a greater certainty that the coolant and injection processes have been decoupled can be obtained with the use of the ducted chamber. Additional investigations are required to further develop and refine the use of ducted chambers from both a cooling effectiveness and overall thruster performance standpoint. Although combustion performance was not found to be degraded by high duct coolant flow rates the specific impulse performance should be determined under simulated altitude conditions to investigate possible effects of duct cooling on the nozzle altitude thrust coefficient. It is also recommended that the duct cooled chamber testing not be limited to metallic thrust chambers. The graphitic materials still offer great promise and should permit lower coolant flow rate requirements.

APPENDIX A

THERMAL DATA COMPILATION

A complete compilation of the thermal data from each test is included in this appendix, including the temperature-time history and the chamber axial temperature distributions. Specific operating conditions for each test firing can be found in Section 5 (Table 5-3).

TEST 2 HB2A-100

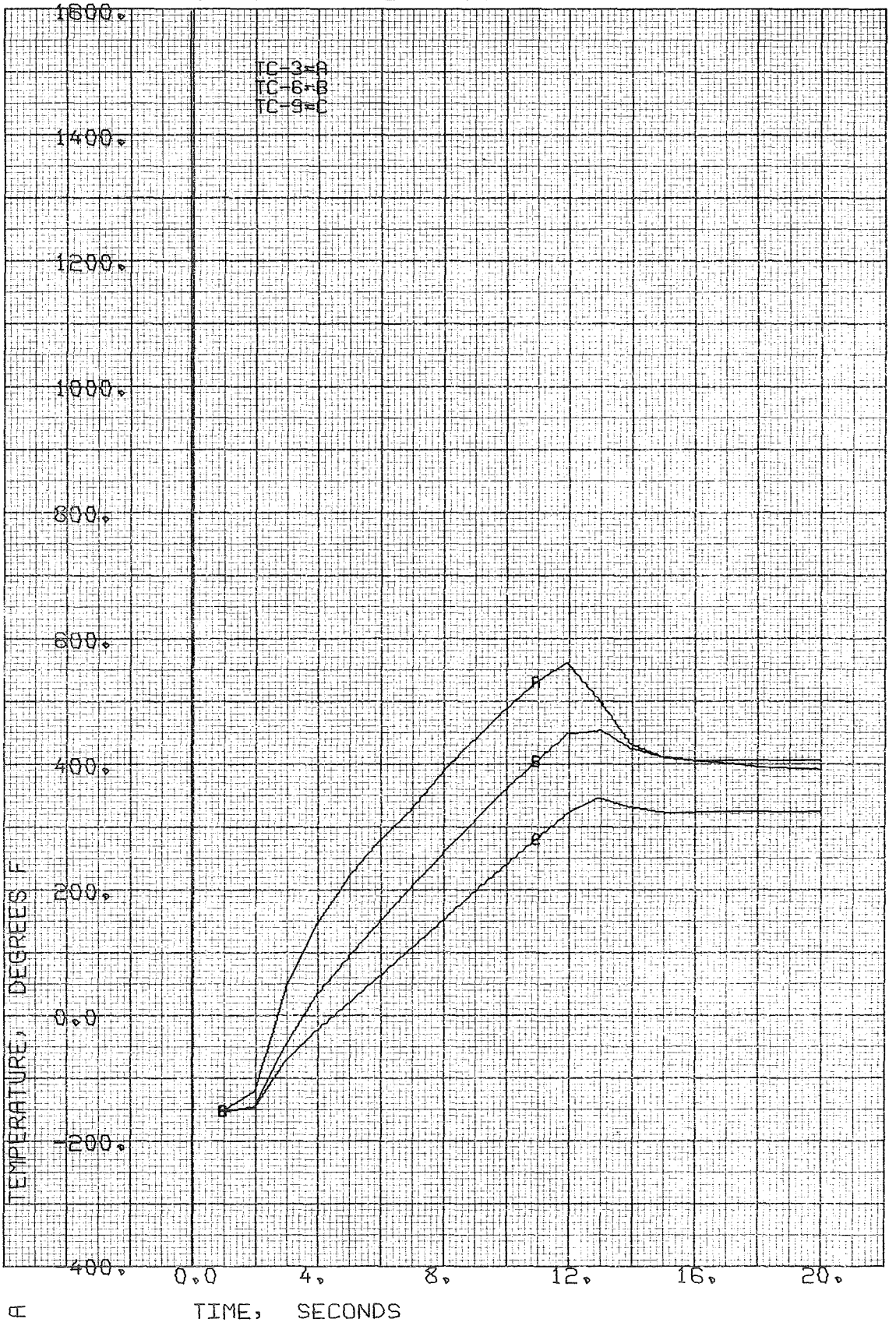

TEST 2 HB2A-100

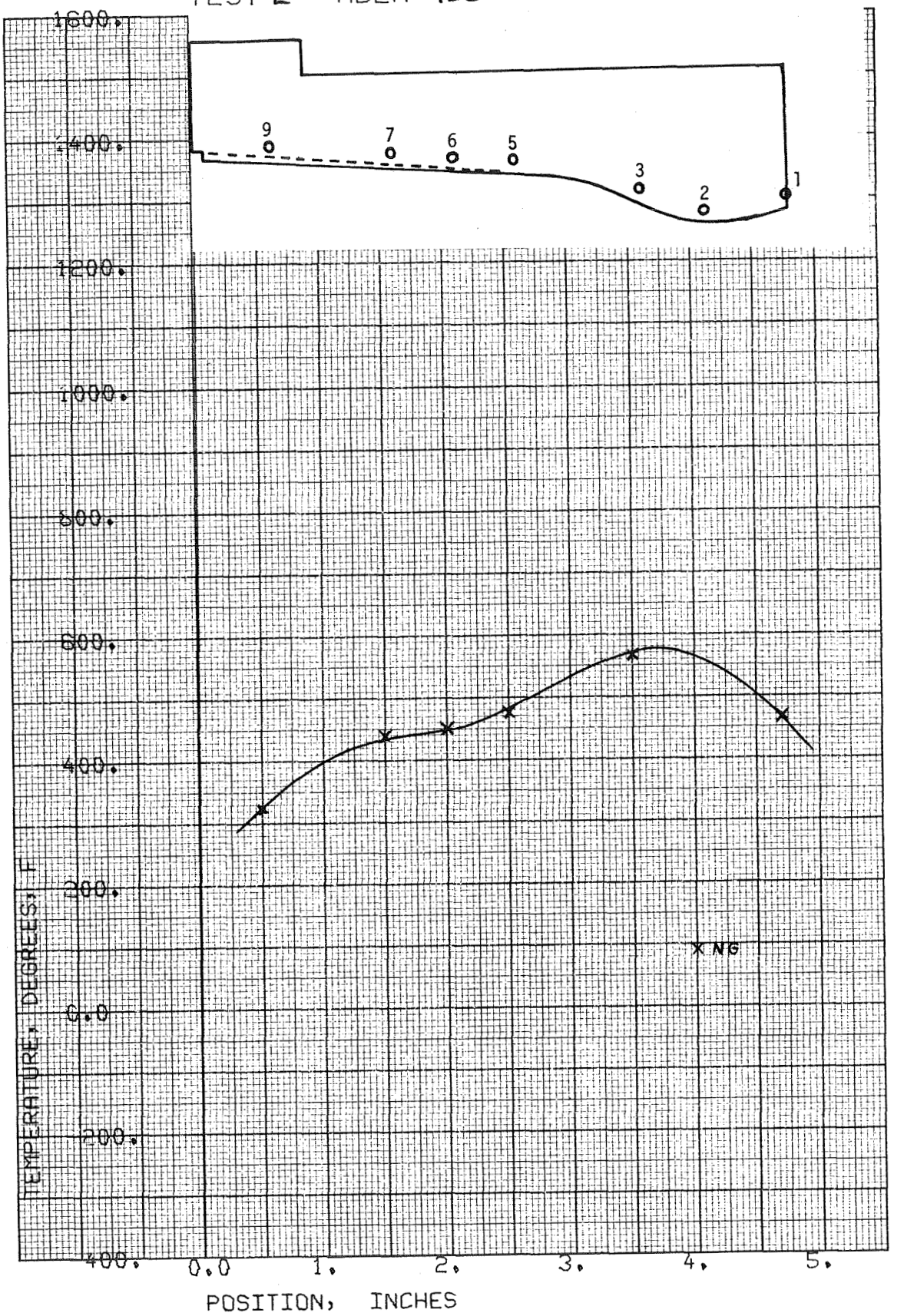

TEST 3 HB2A-101

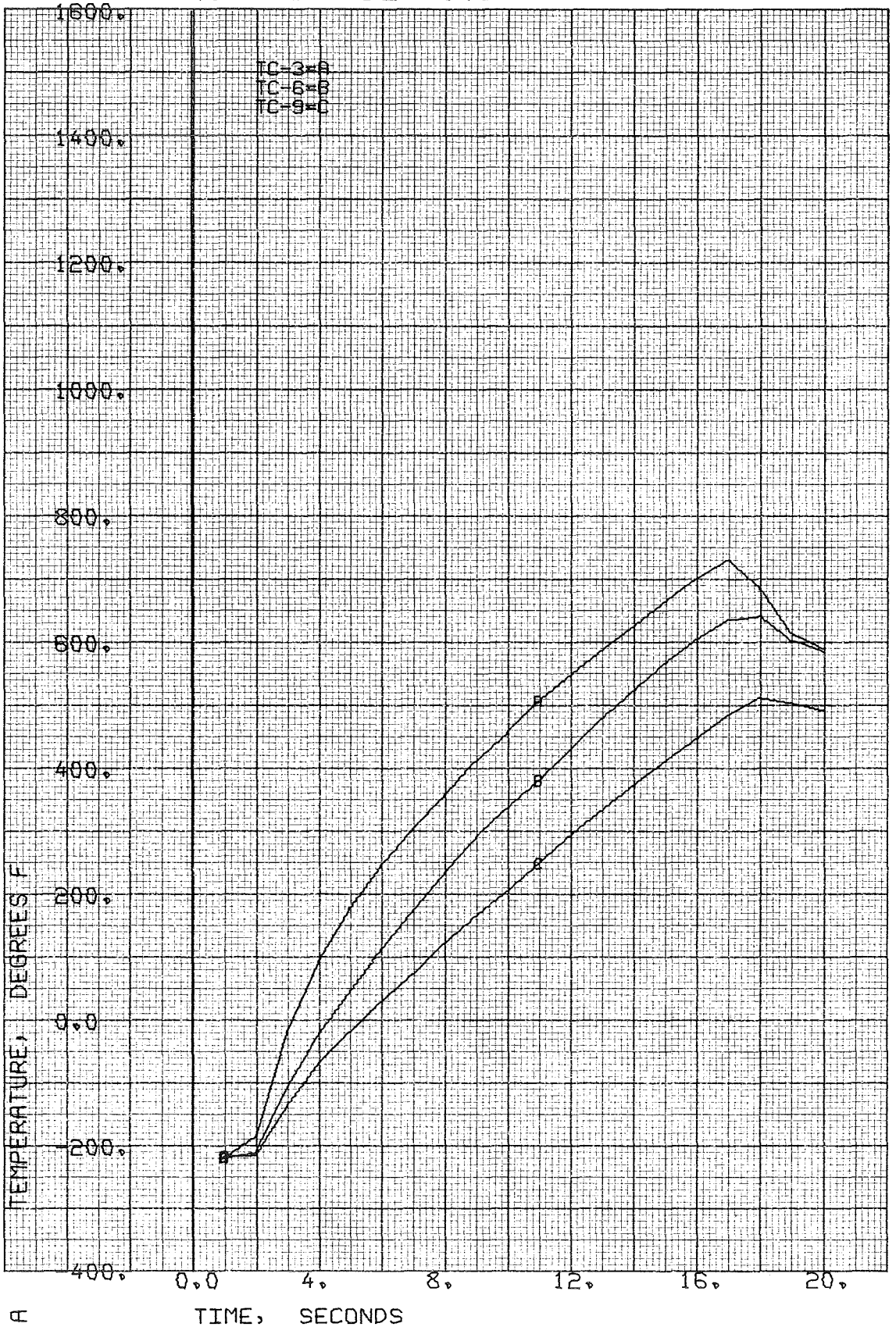

TEST 3 HB2A-101

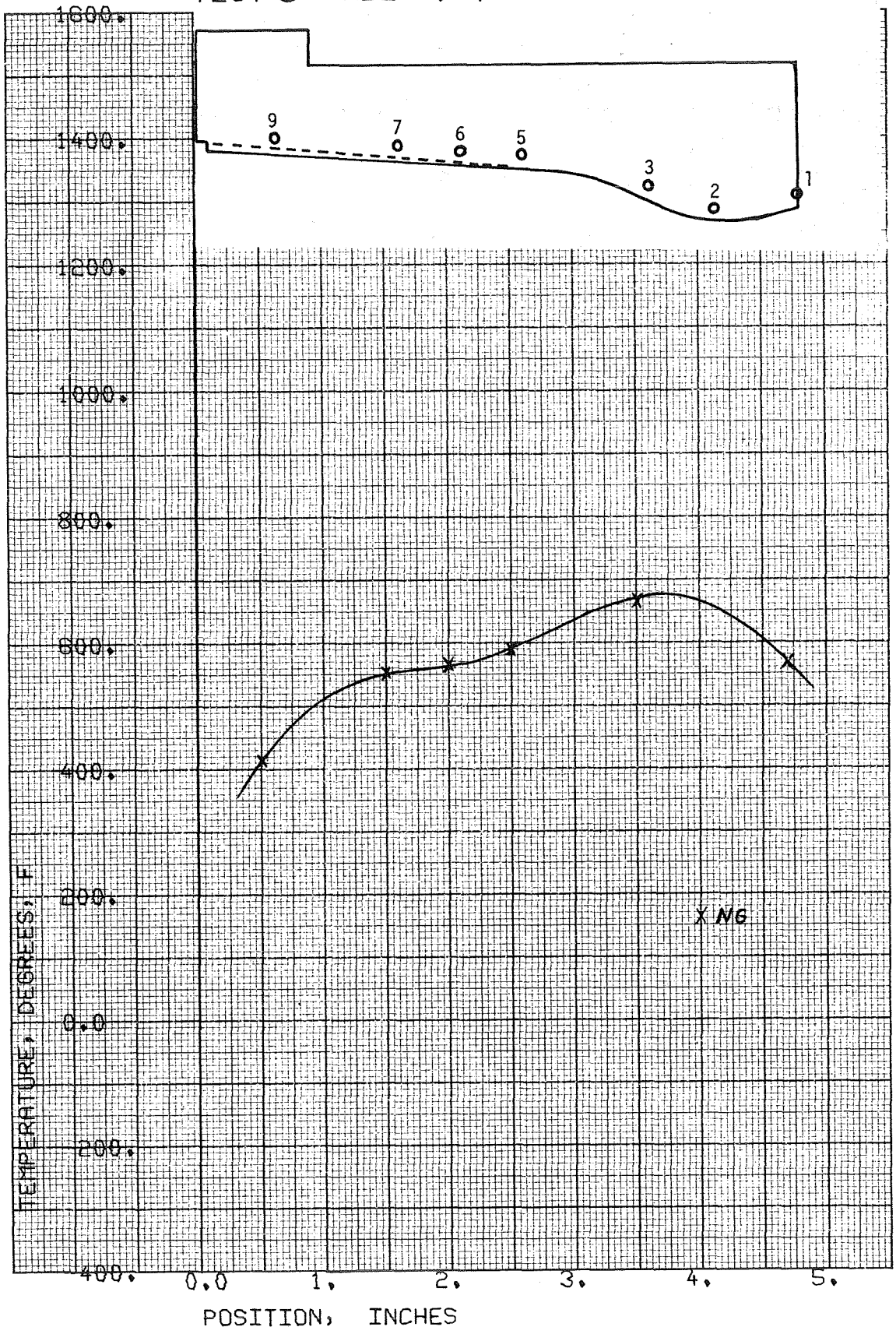

TEST 4 HB2A-102

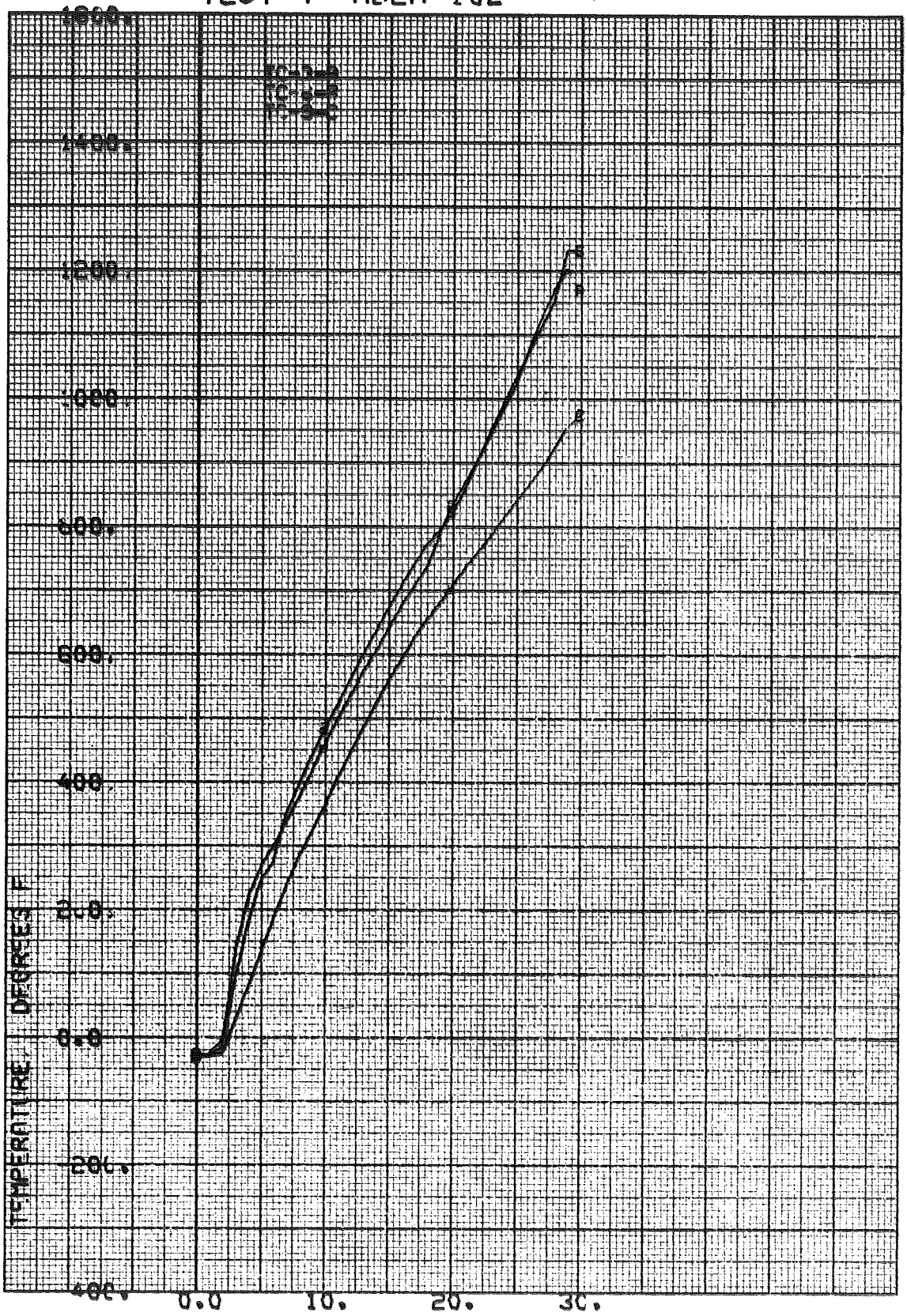

TEST 4 HB2A-102

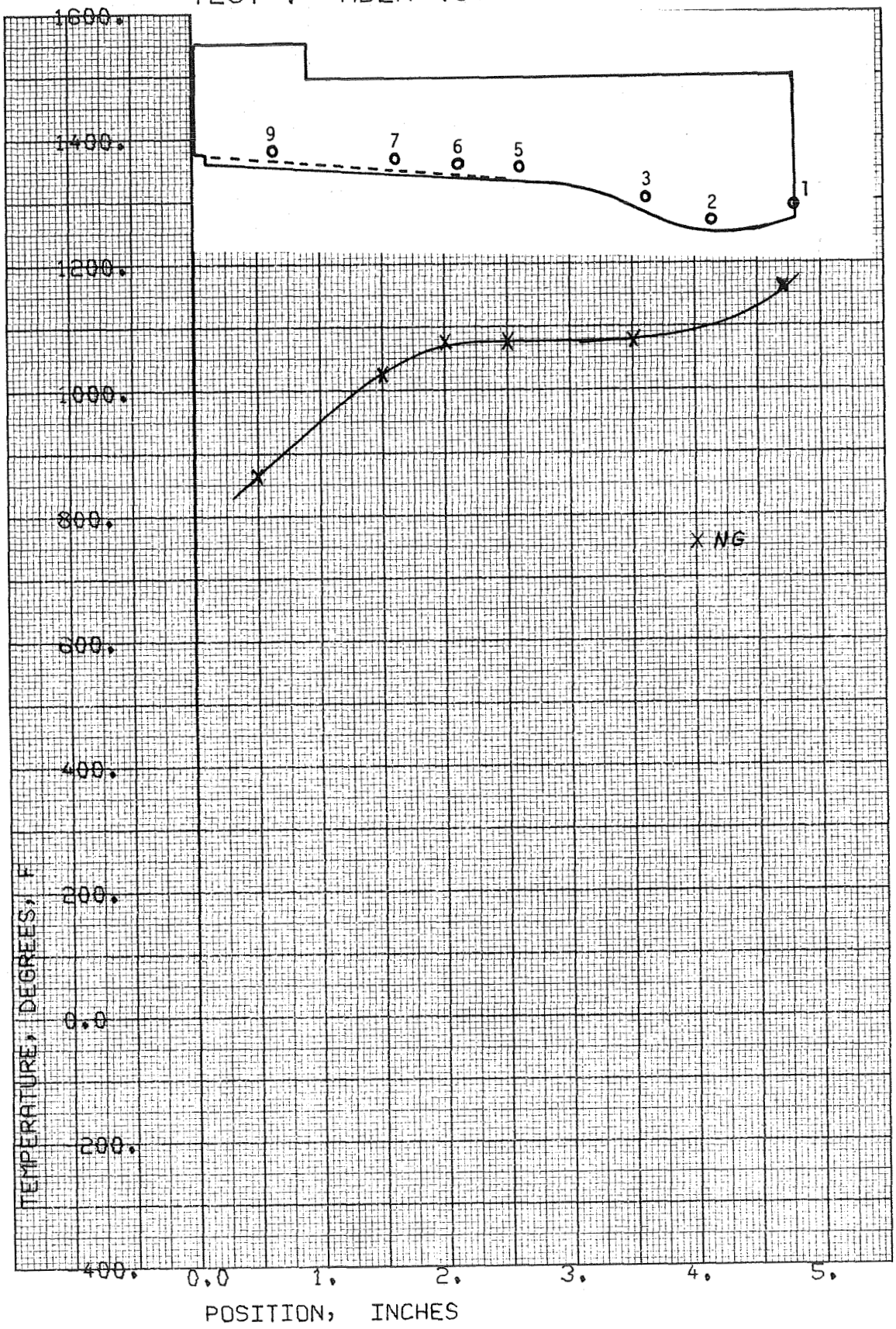

3

TEST 5 HB2A-103

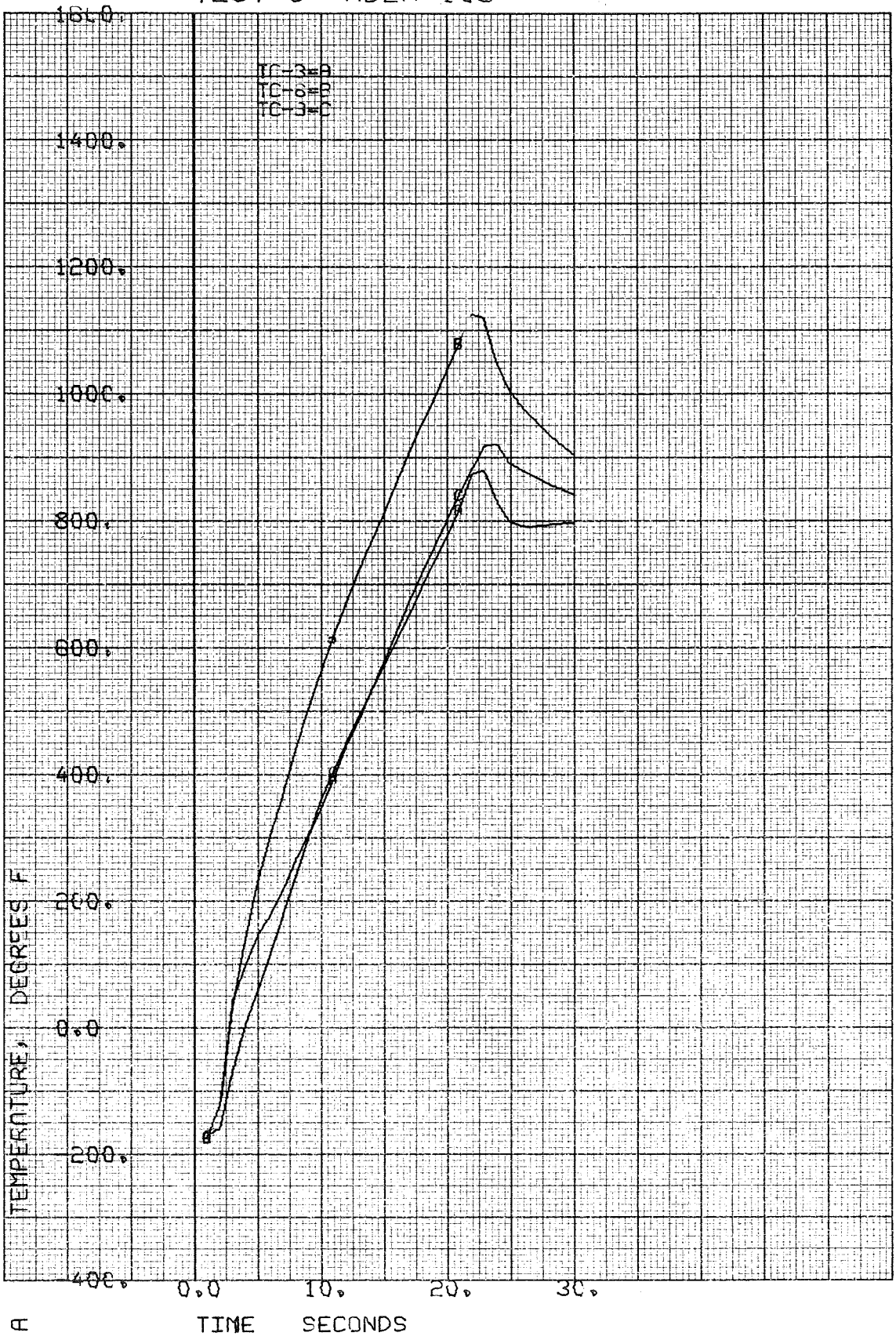

TEST 5 HB2A-103

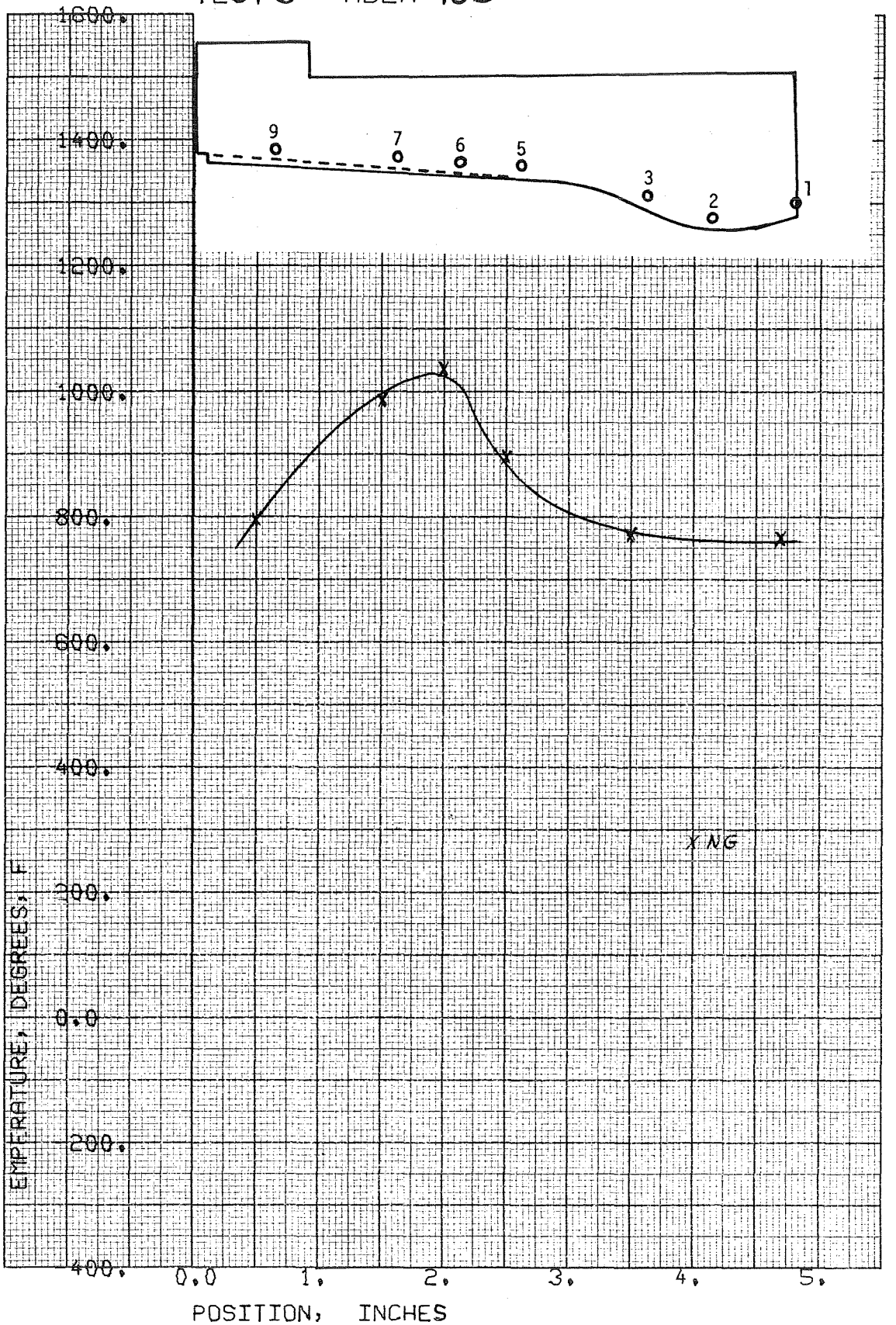

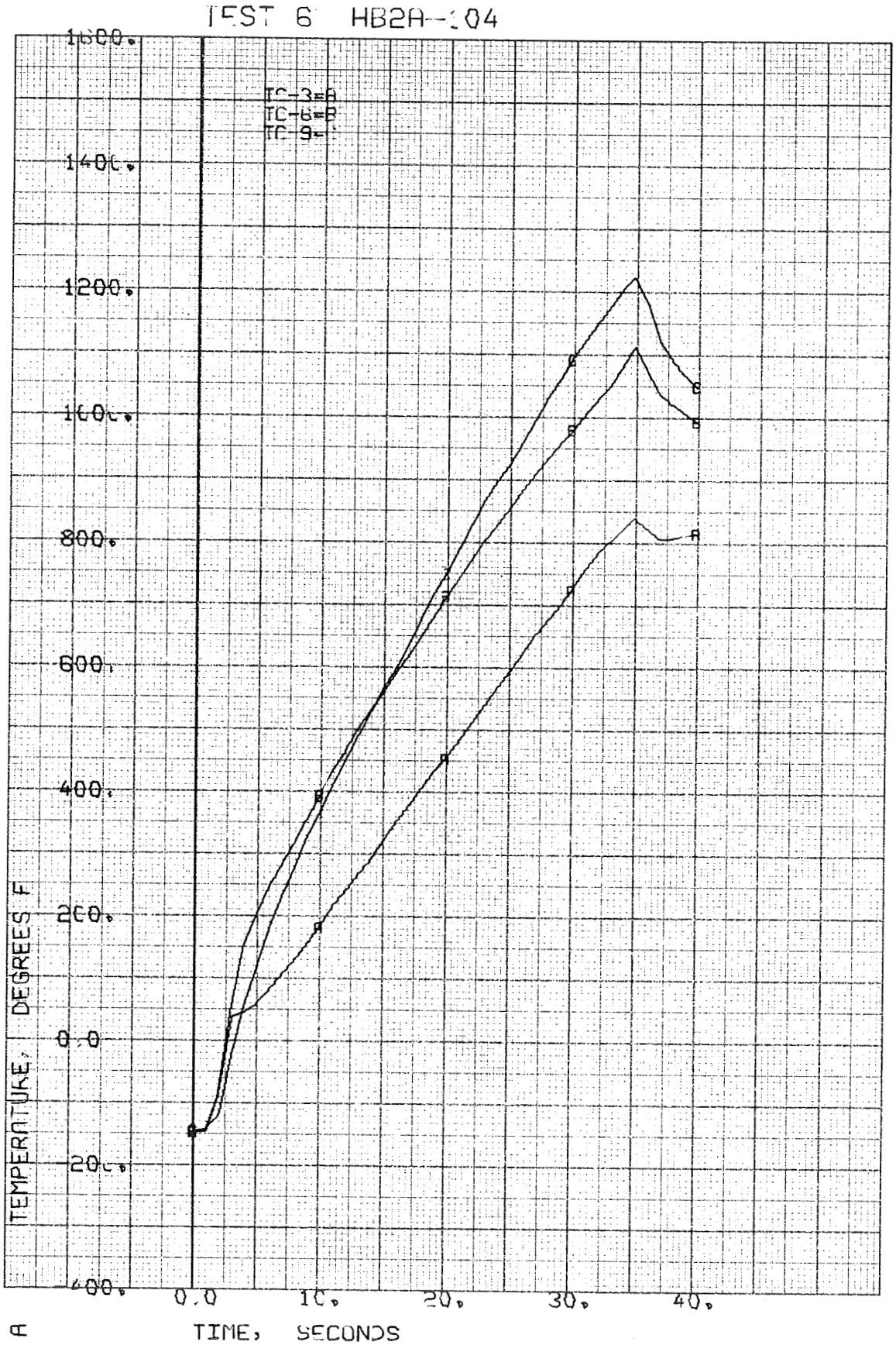
TEST 6 HB2A-104
TC-3=A
TC-6=B
TC-9=C
1600.
1400.
1200.
1000.
800.
600.
400.
200.
0.0
-200.
-400.
0.0
10.
20.
30.
40.
TEMPERATURE, DEGREES F
TIME, SECONDS

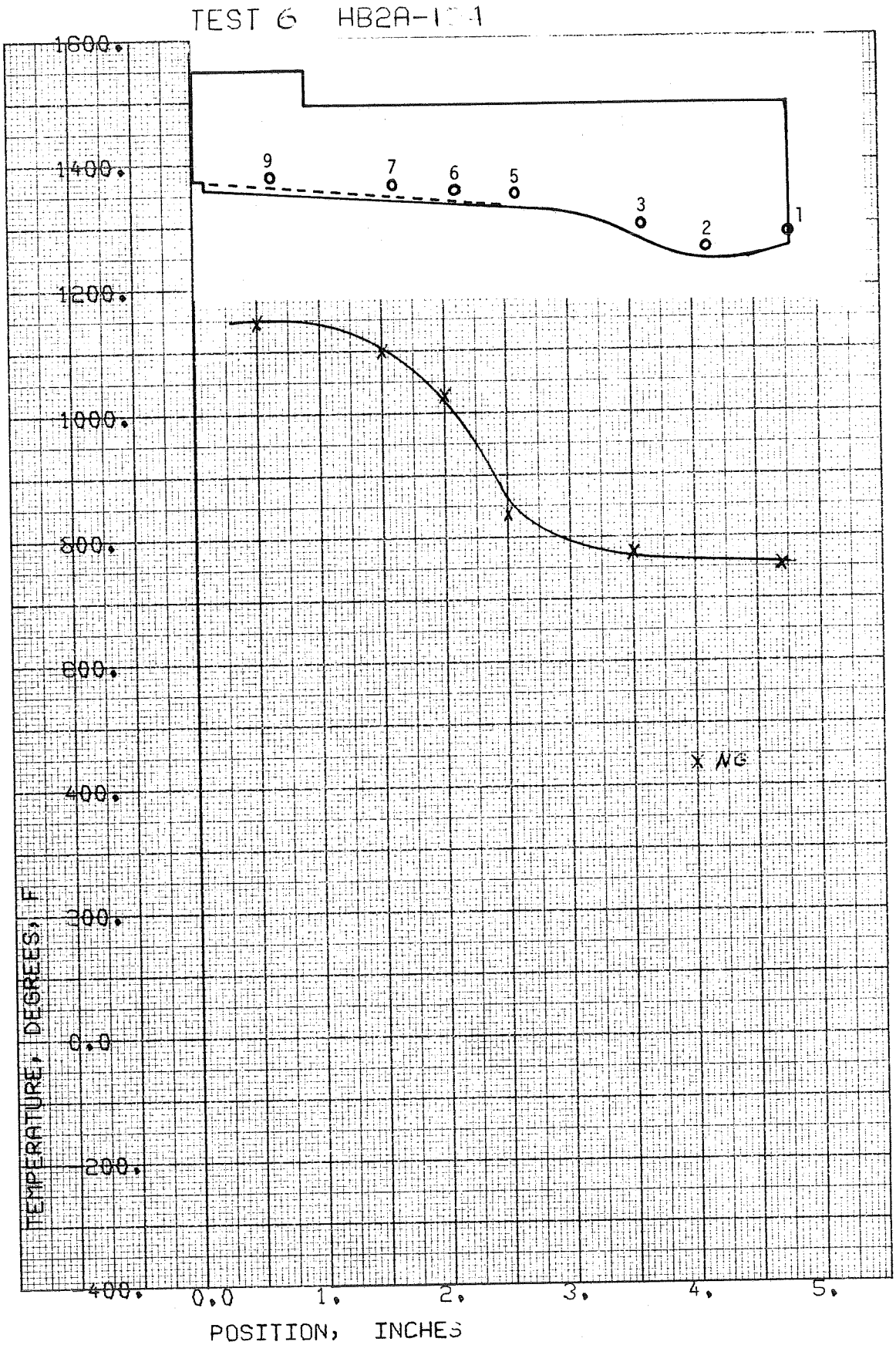
TEST 6 HB2A-1
1600.
1400.
1200.
1000.
800.
600.
400.
300.
0.0
-200.
-400.
TEMPERATURE, DEGREES, F
0.0
1.
2.
3.
4.
5.
POSITION, INCHES
9
7
6
5
3
2
1
X NG

TEST 8 HB2A-106

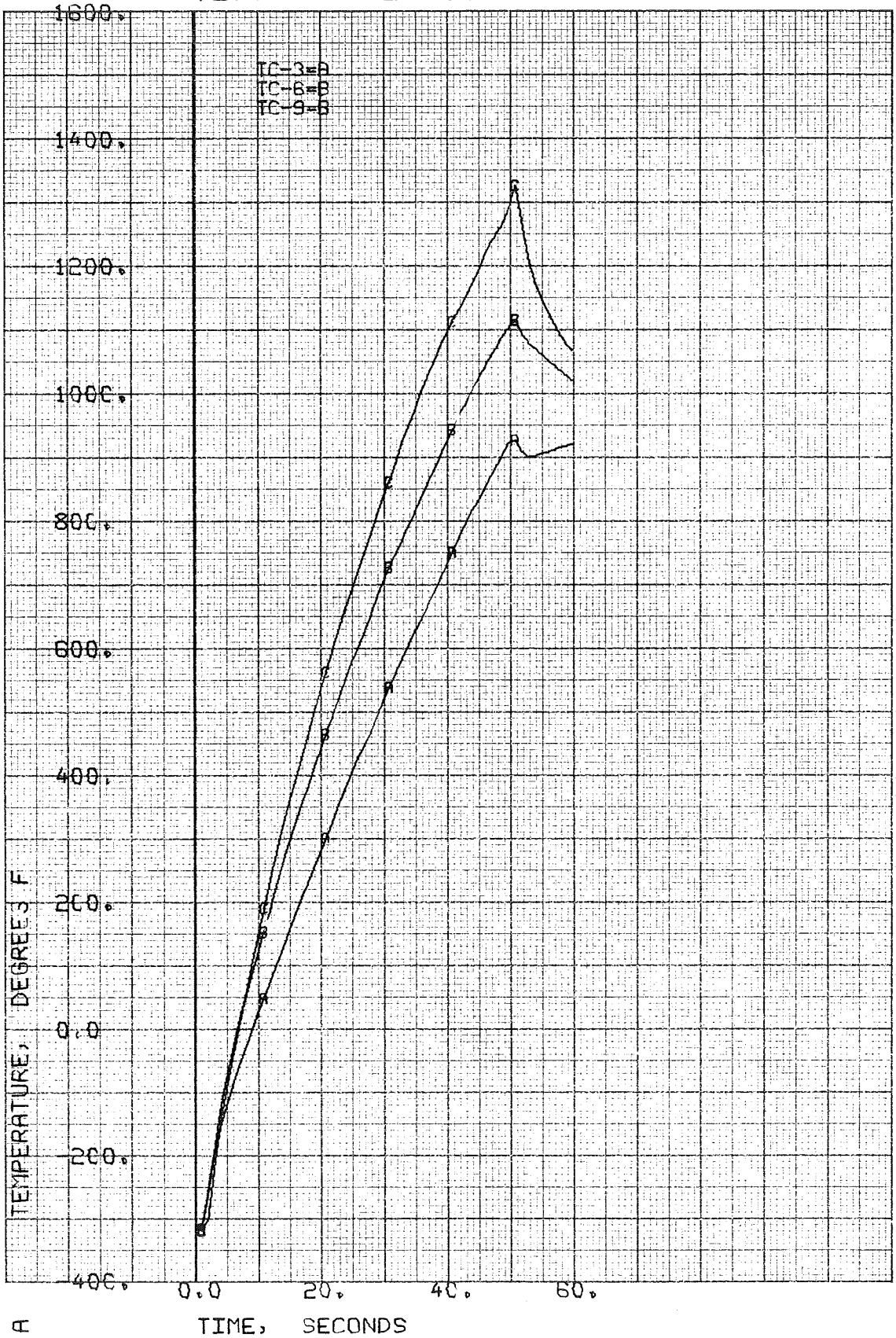

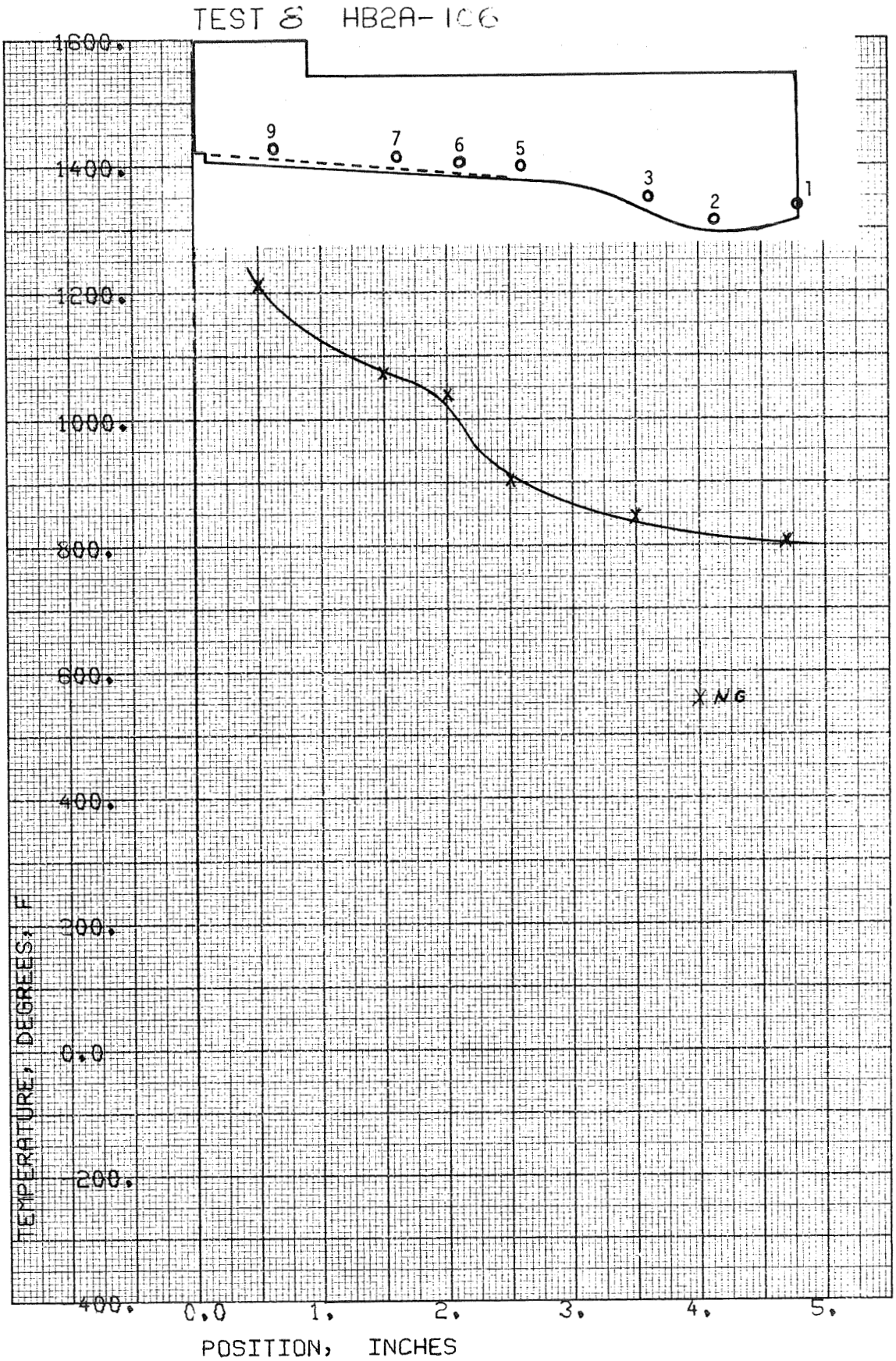
TEST 8 HB2A-106
1600.
1400.
1200.
1000.
800.
600.
400.
200.
0.0
-200.
-400.
TEMPERATURE, DEGREES, F
9
7
6
5
3
2
1
NG
0.0
1.
2.
3.
4.
5.
POSITION, INCHES

TEST 9 HB2A-107

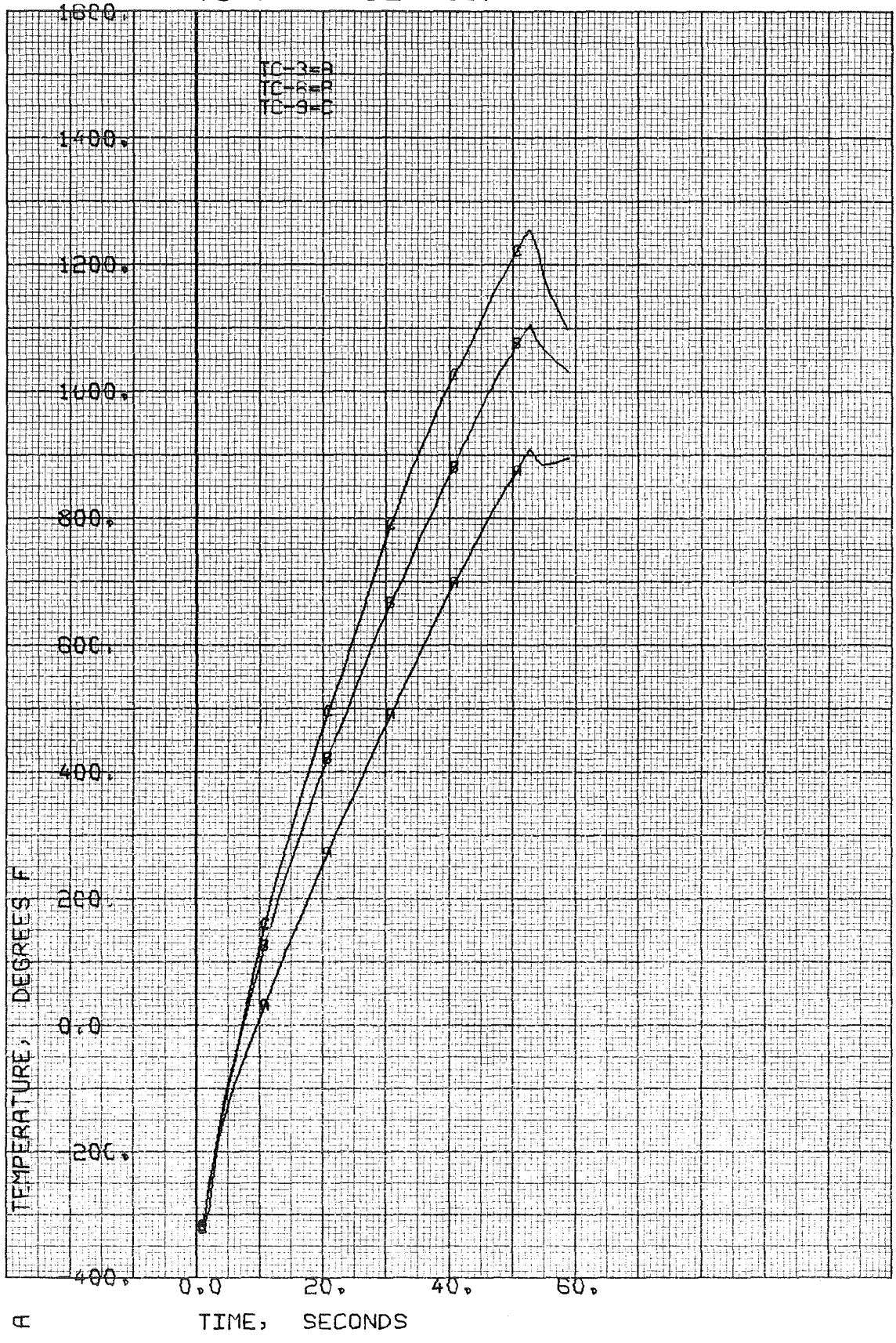

TEST 9 HB2A-107

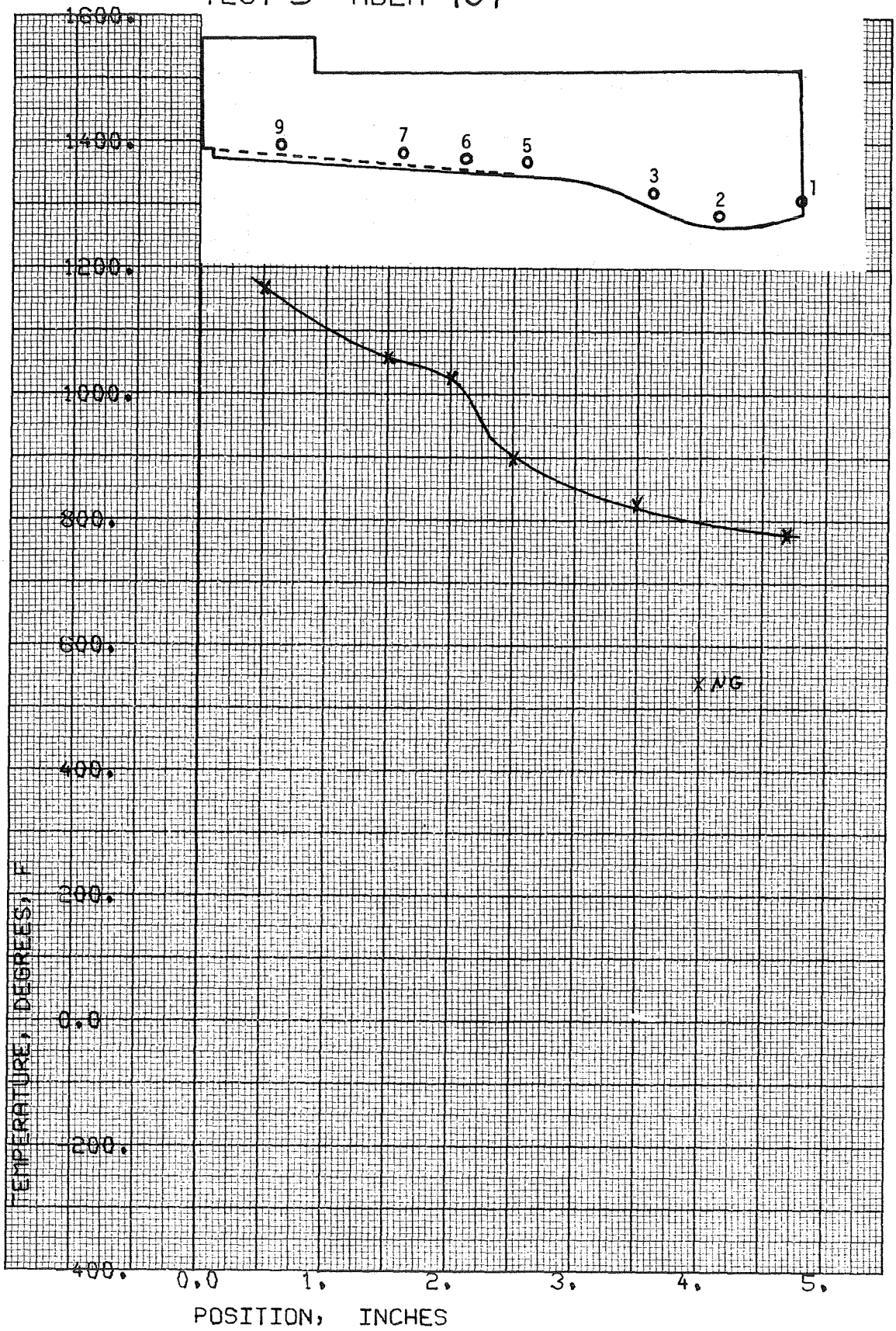

TEST 10 HB2A-108

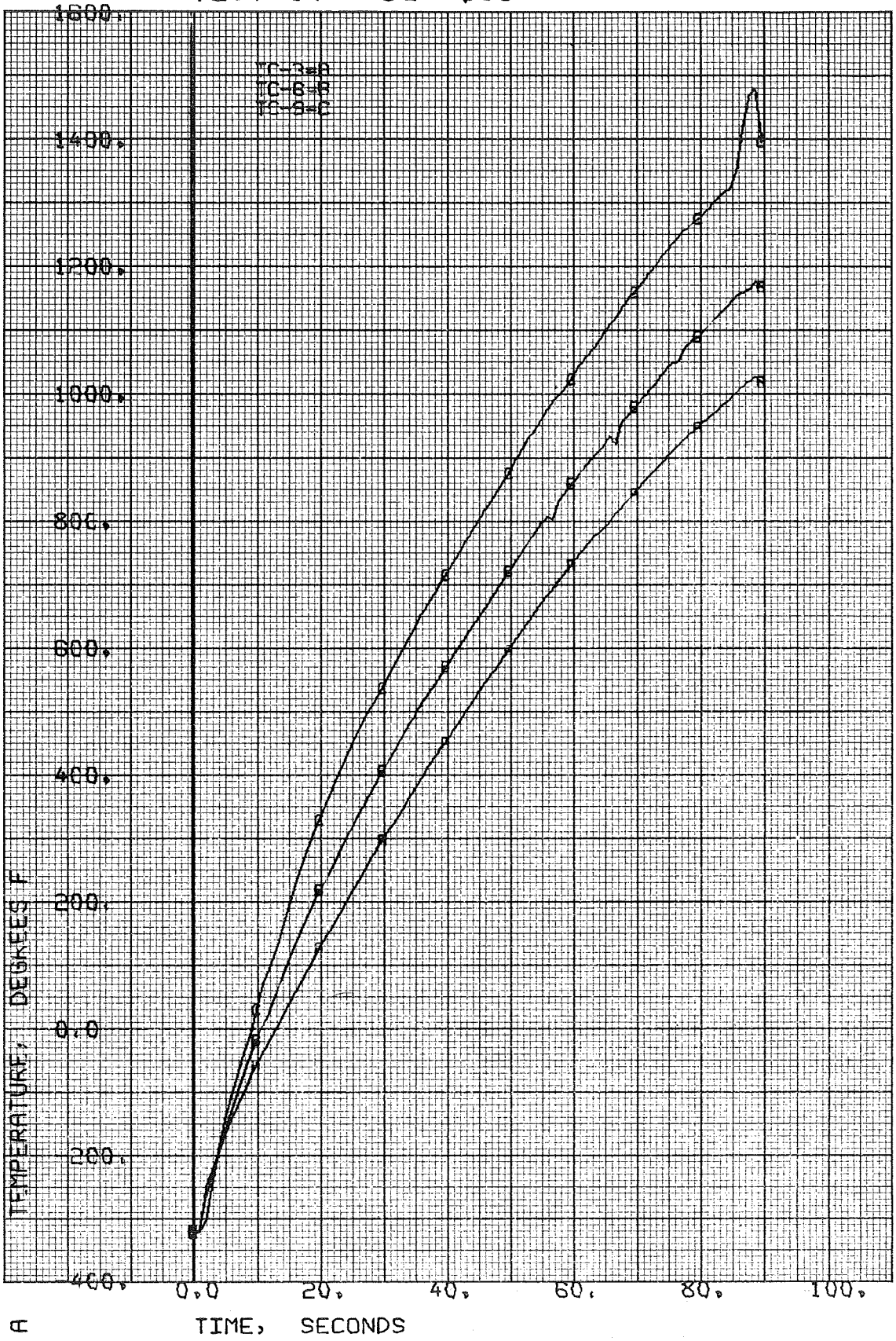

TEST 10 HB2A-108

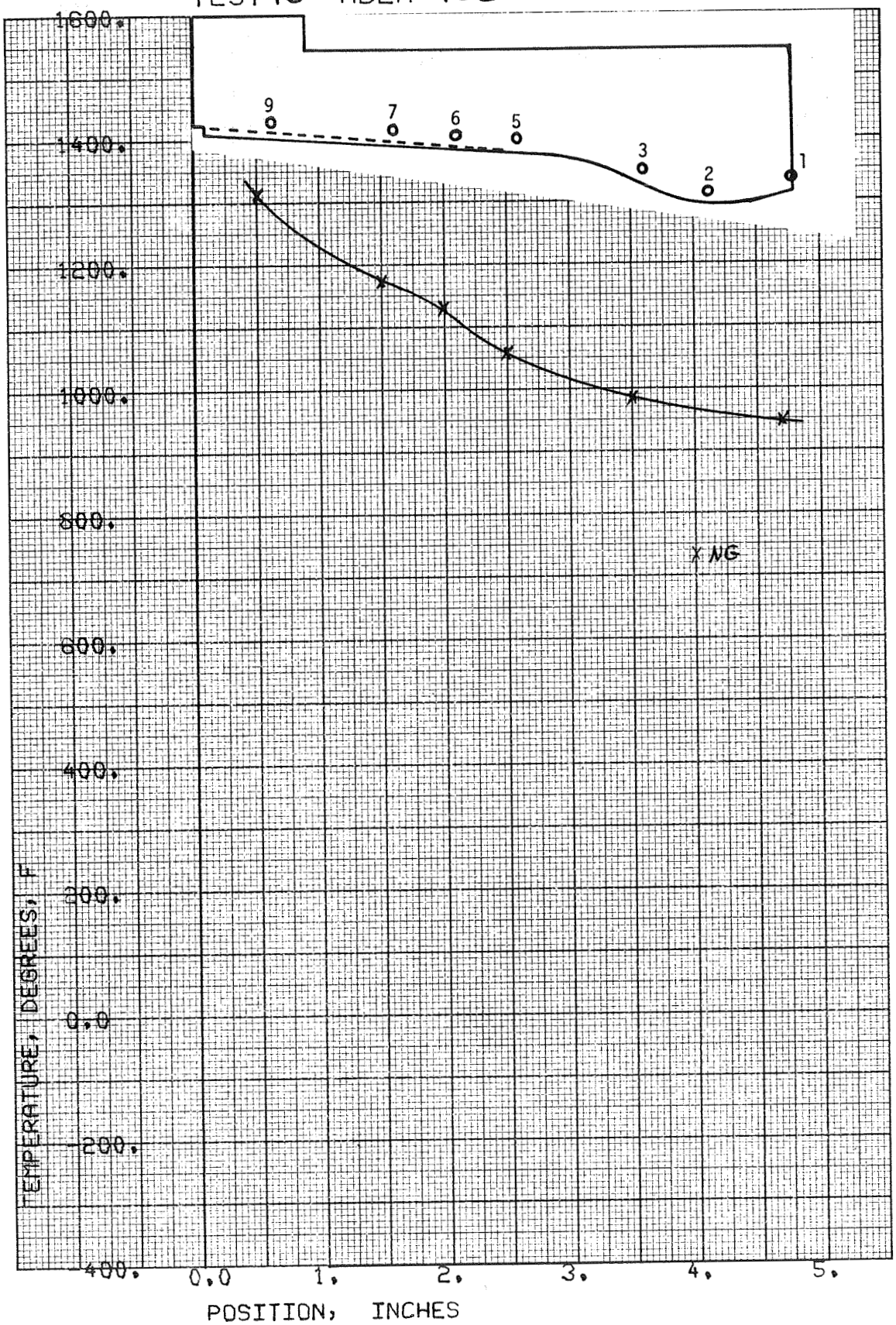

TEST 11 HB2A-109

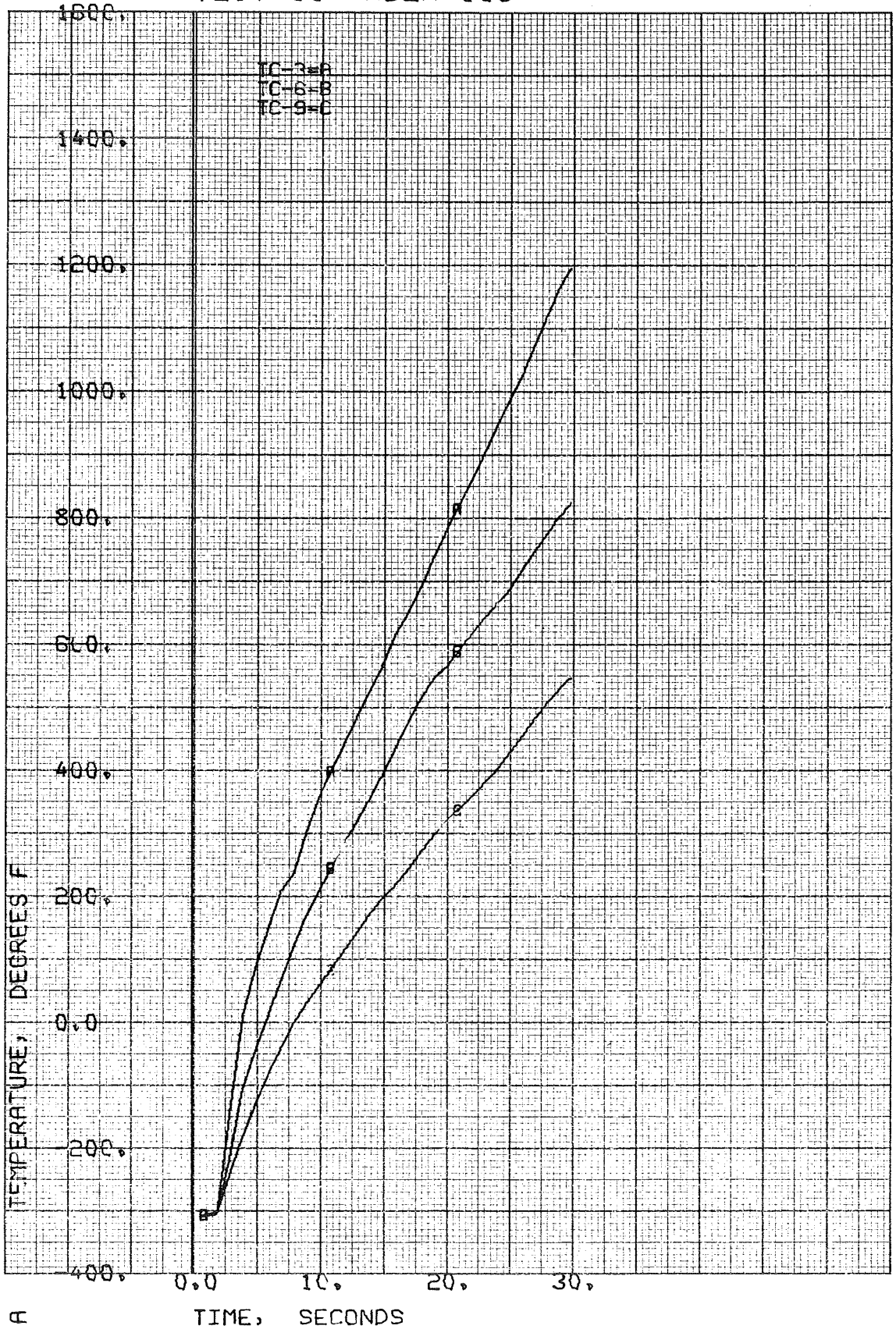

TEST 11 HB2A-109

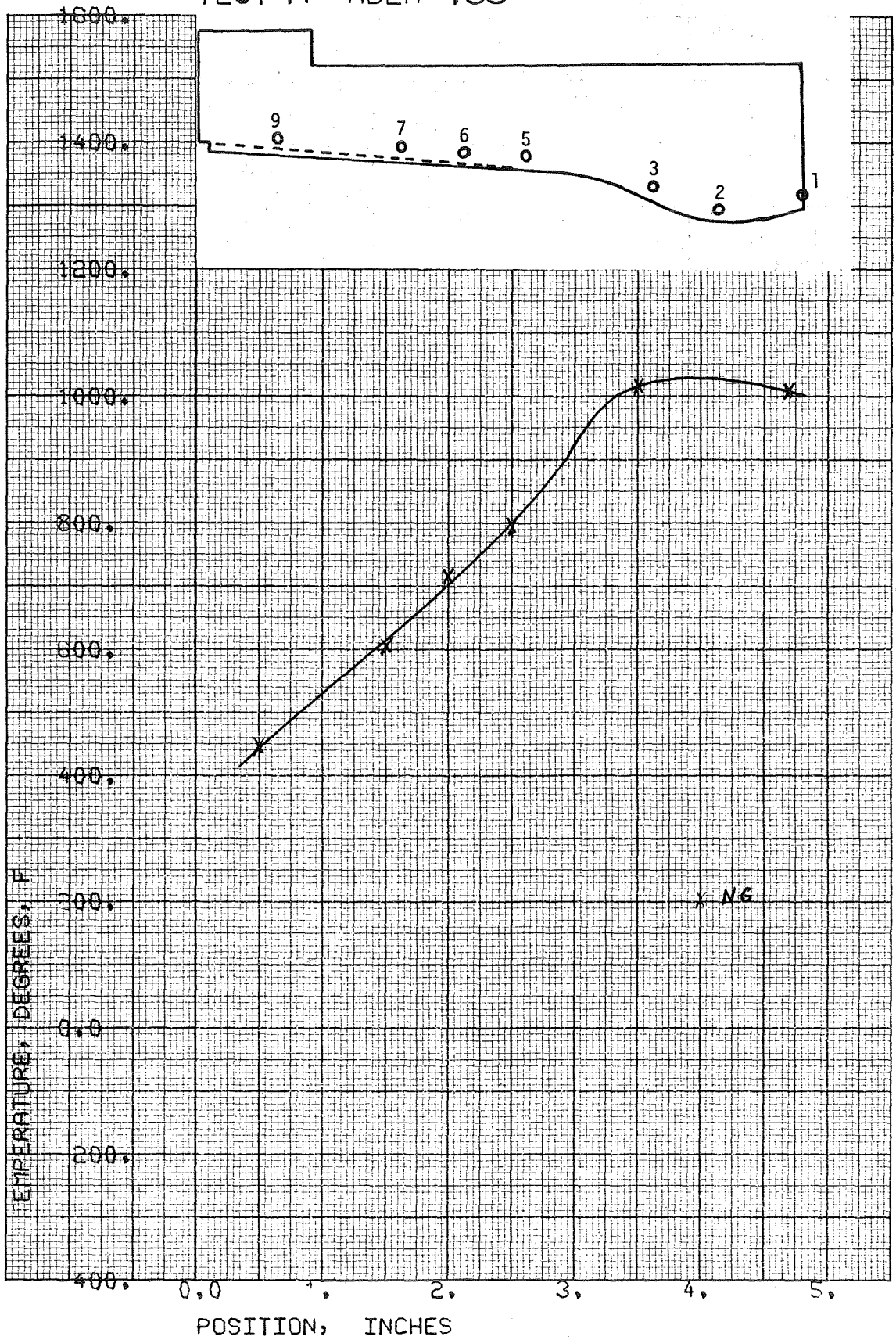

TEST 12 HB2A-110

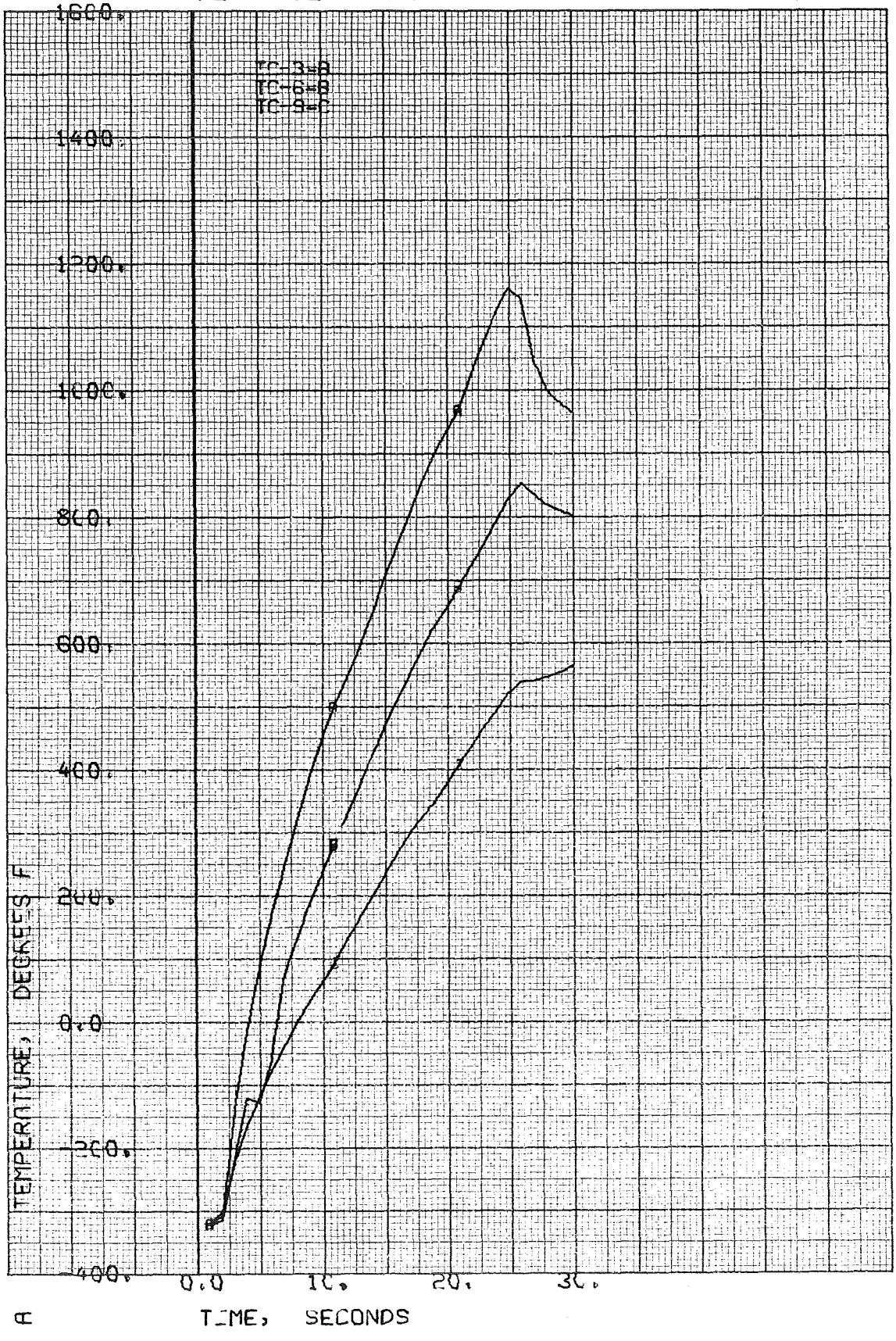

TEST 12 HB2A-110

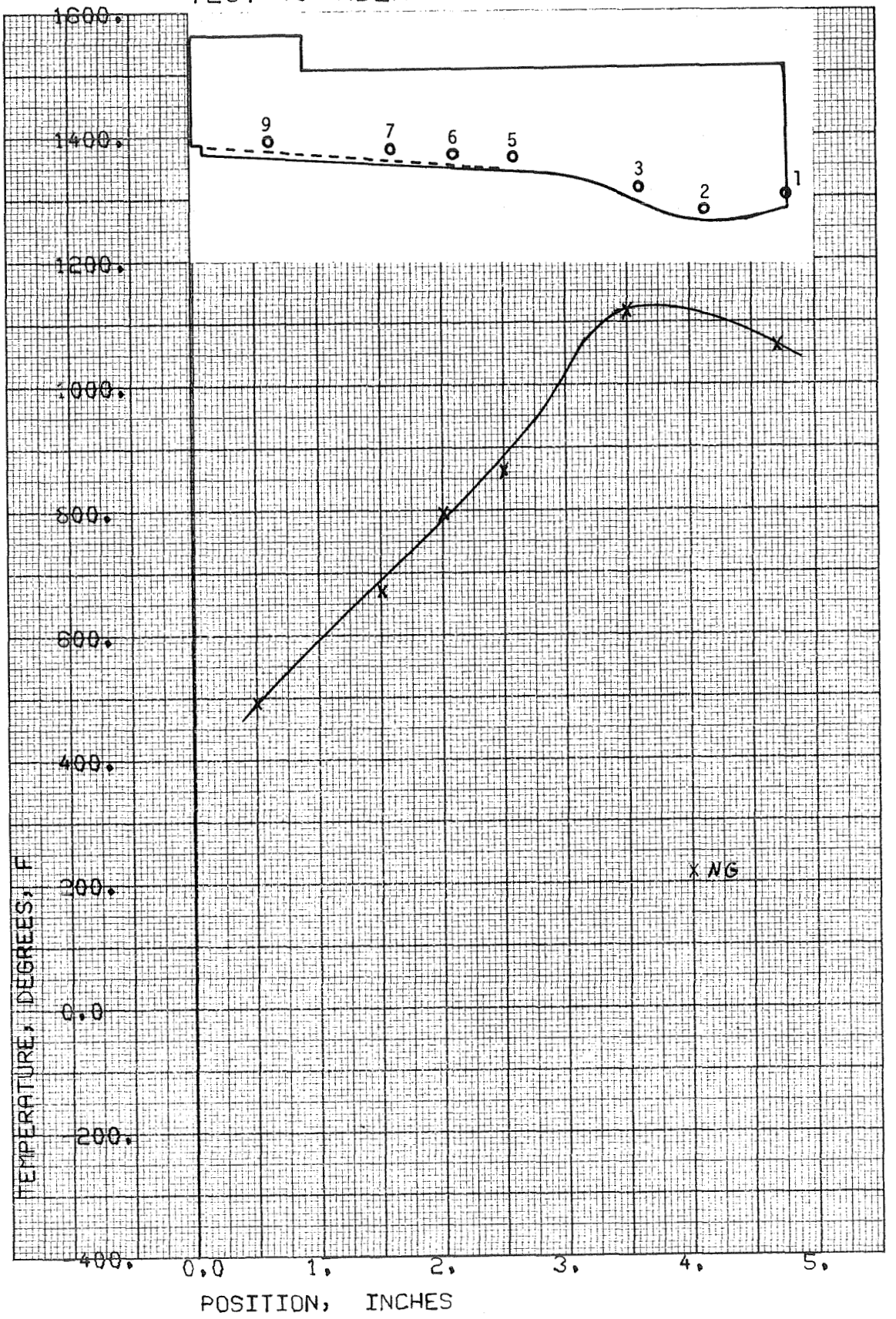

TEST 13 HR2A-111

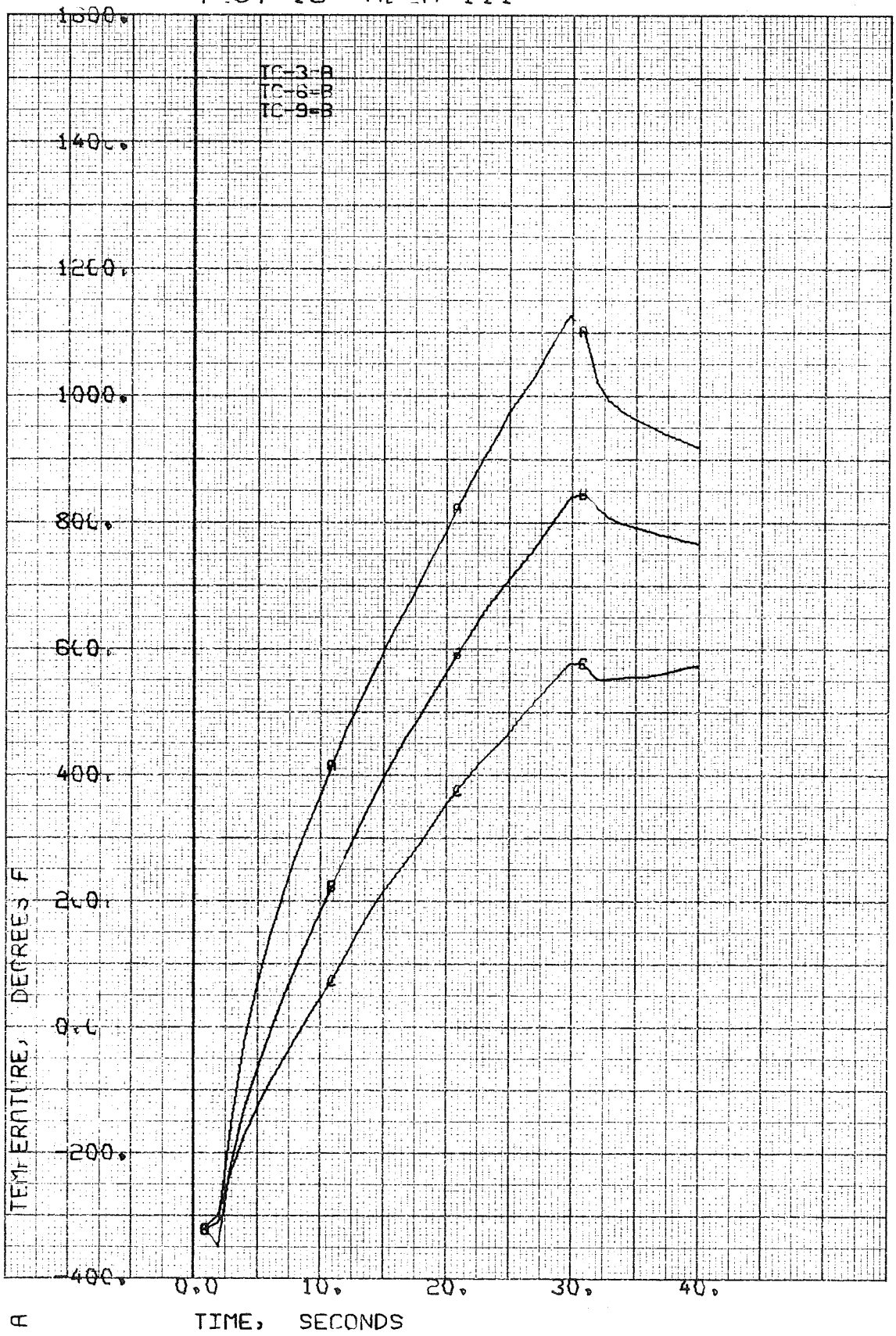

TEST 13 HB2A-111

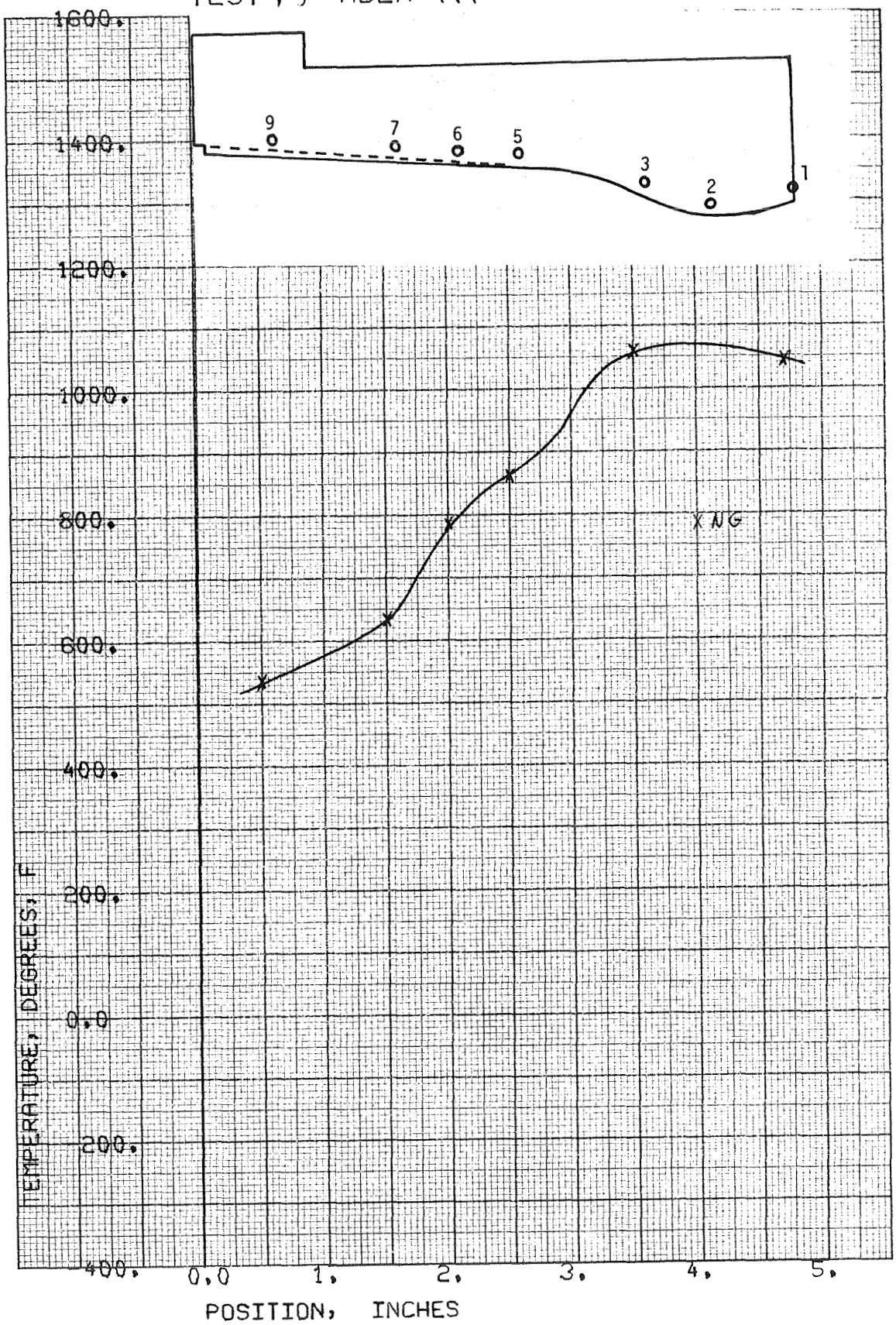

TEST 14 HB2A-112

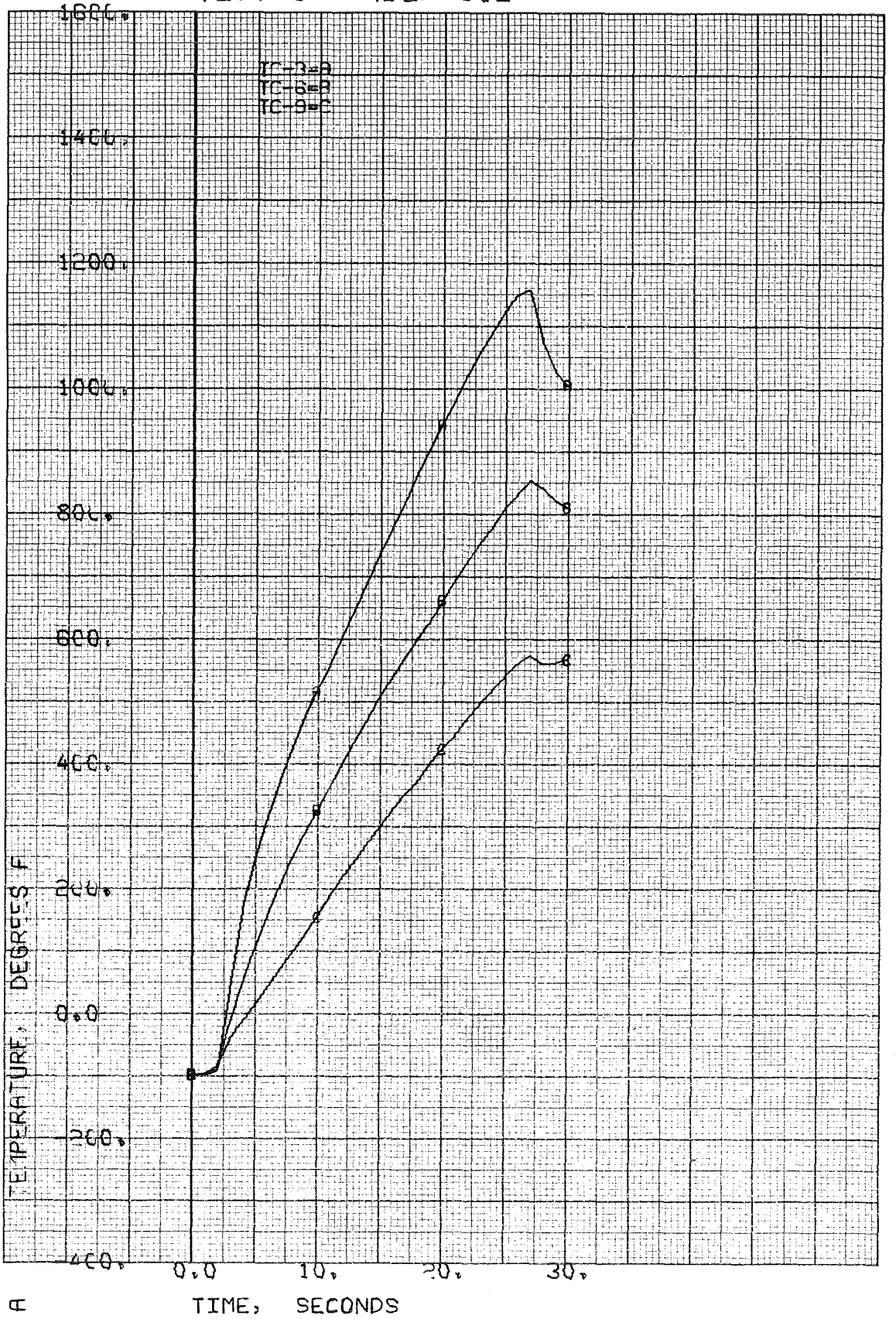

TEST 14 HB2A-112

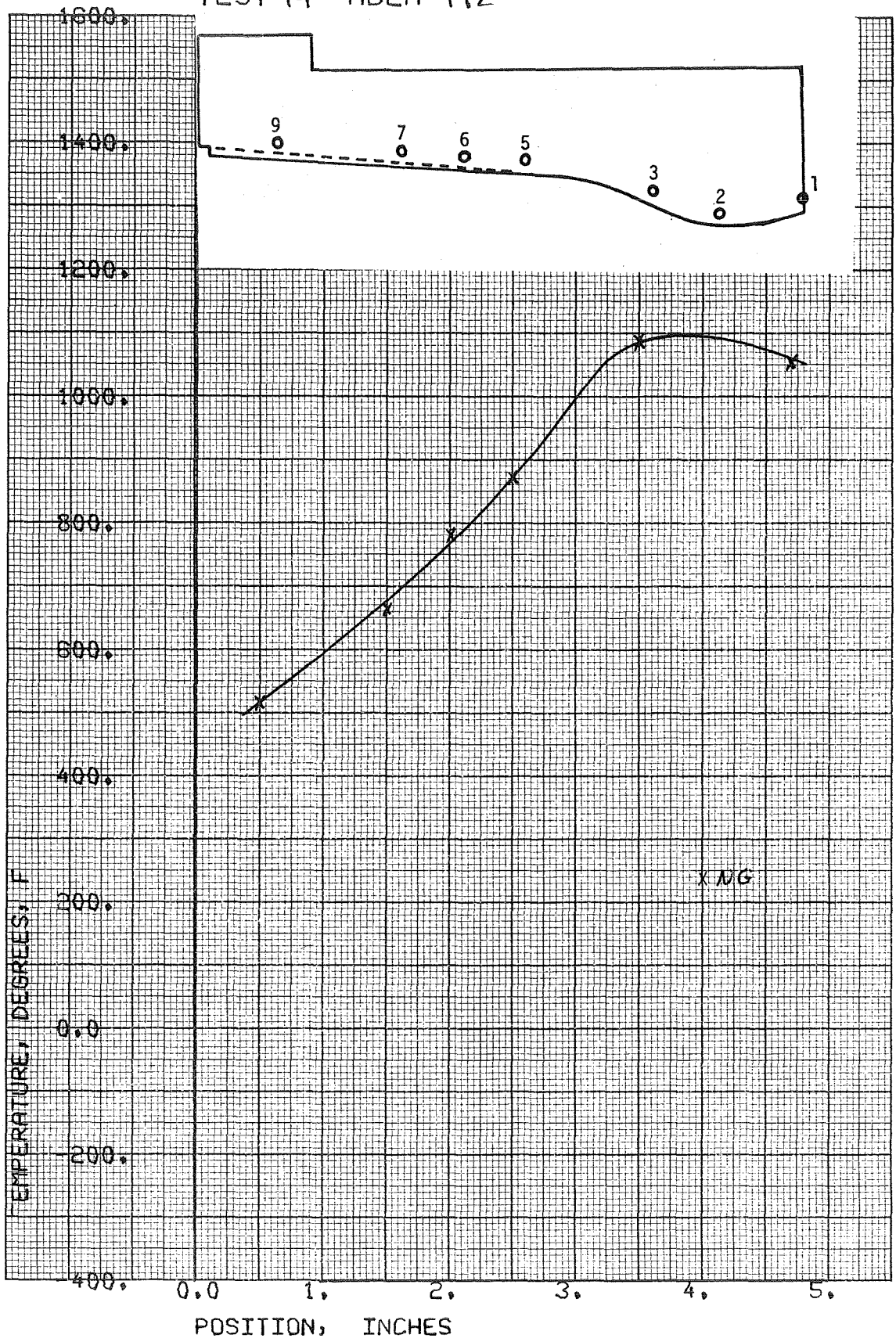

TEST 15 HB2A-113

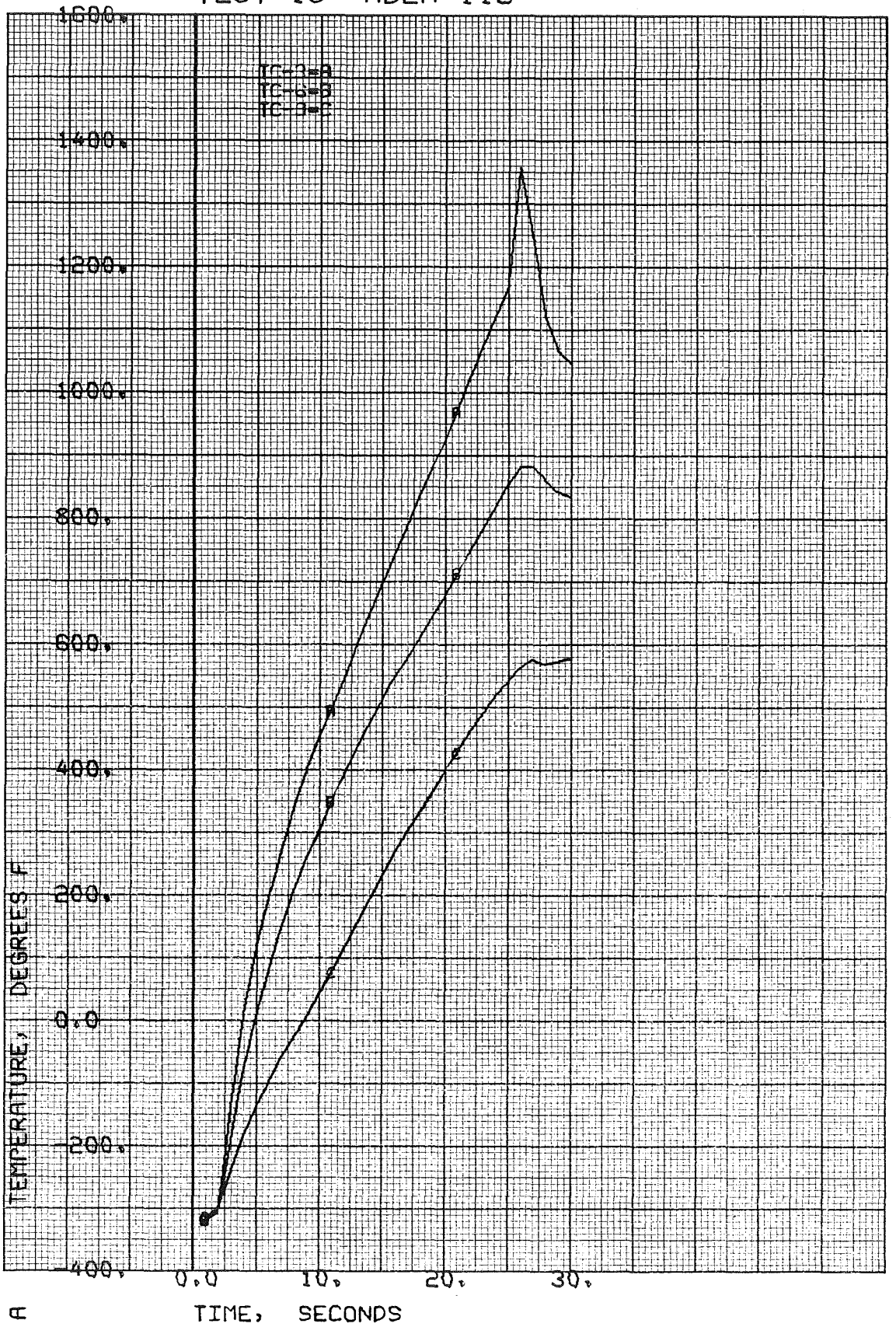

A

TEST 15 HB2A-113

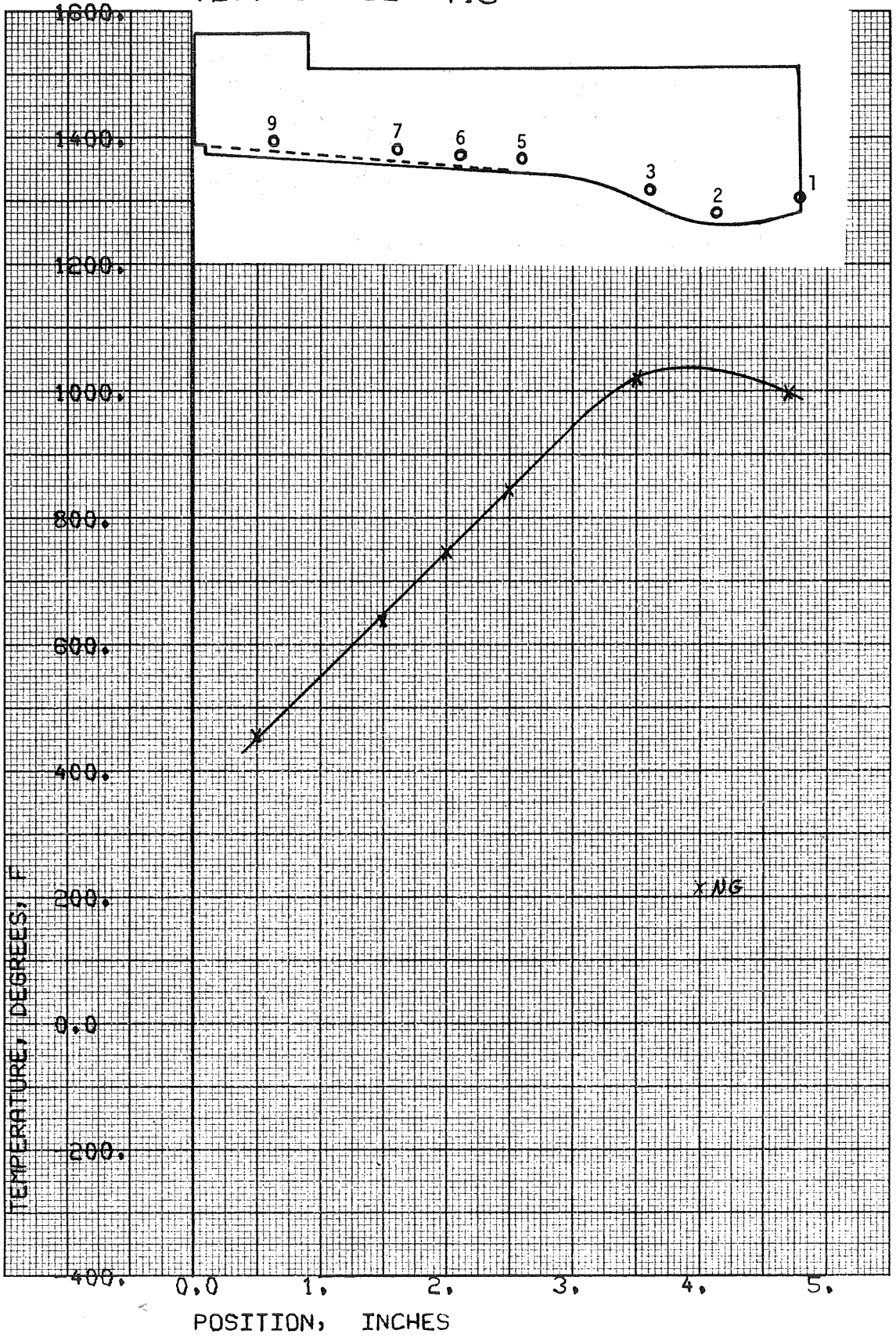

TEST 16 HB2A-114

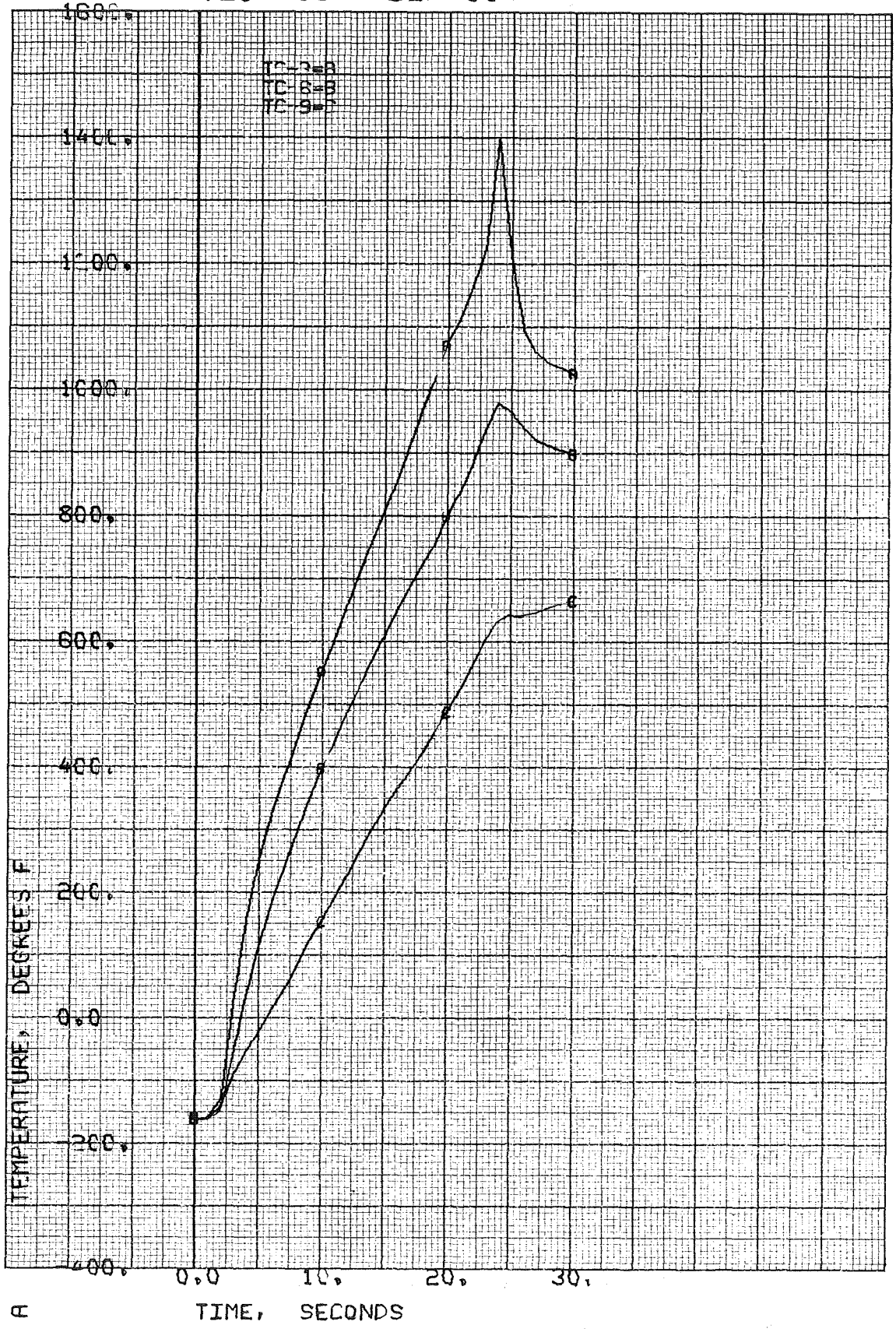

TEST 16 HB2A-114

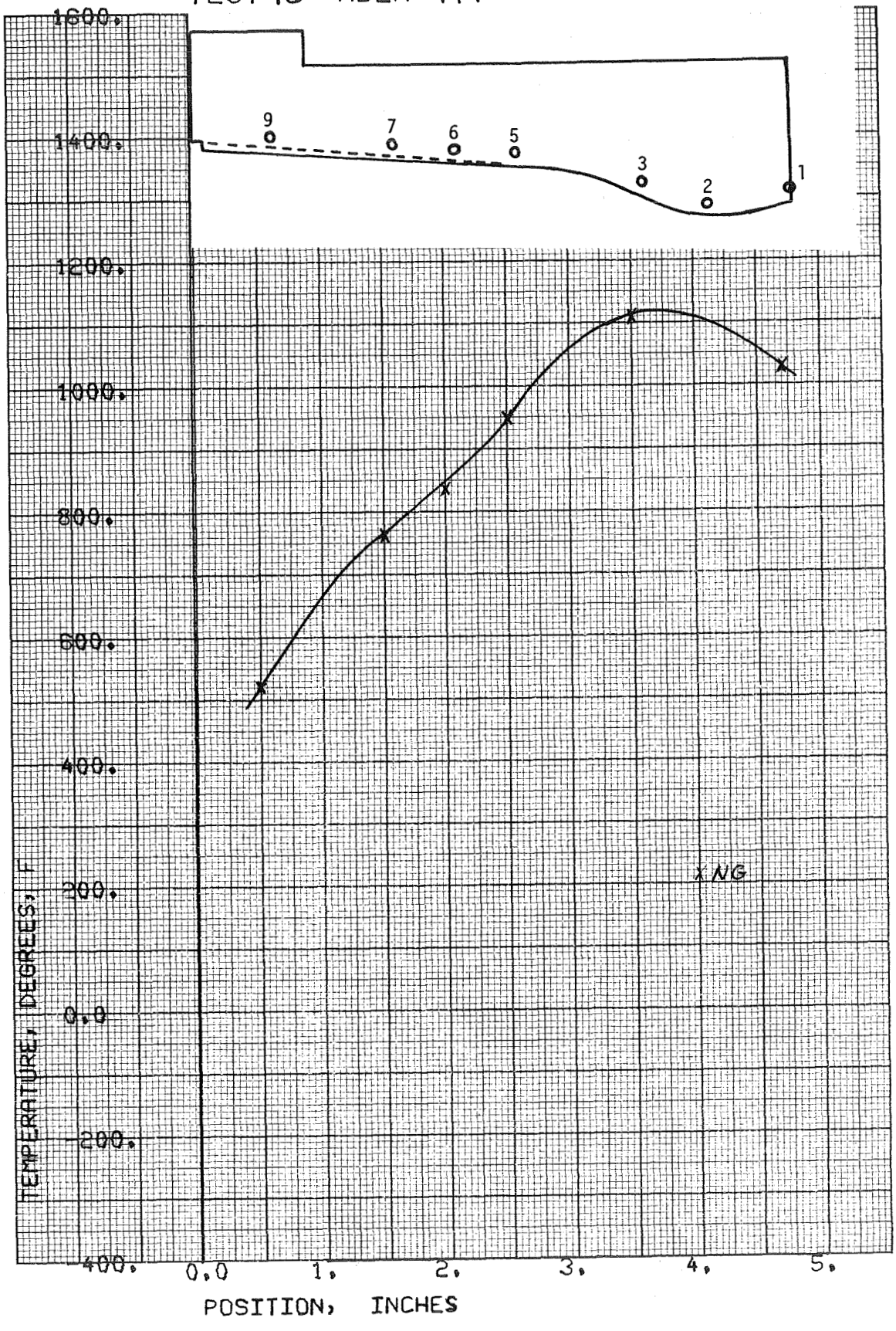

TEST 17 HB2A-157

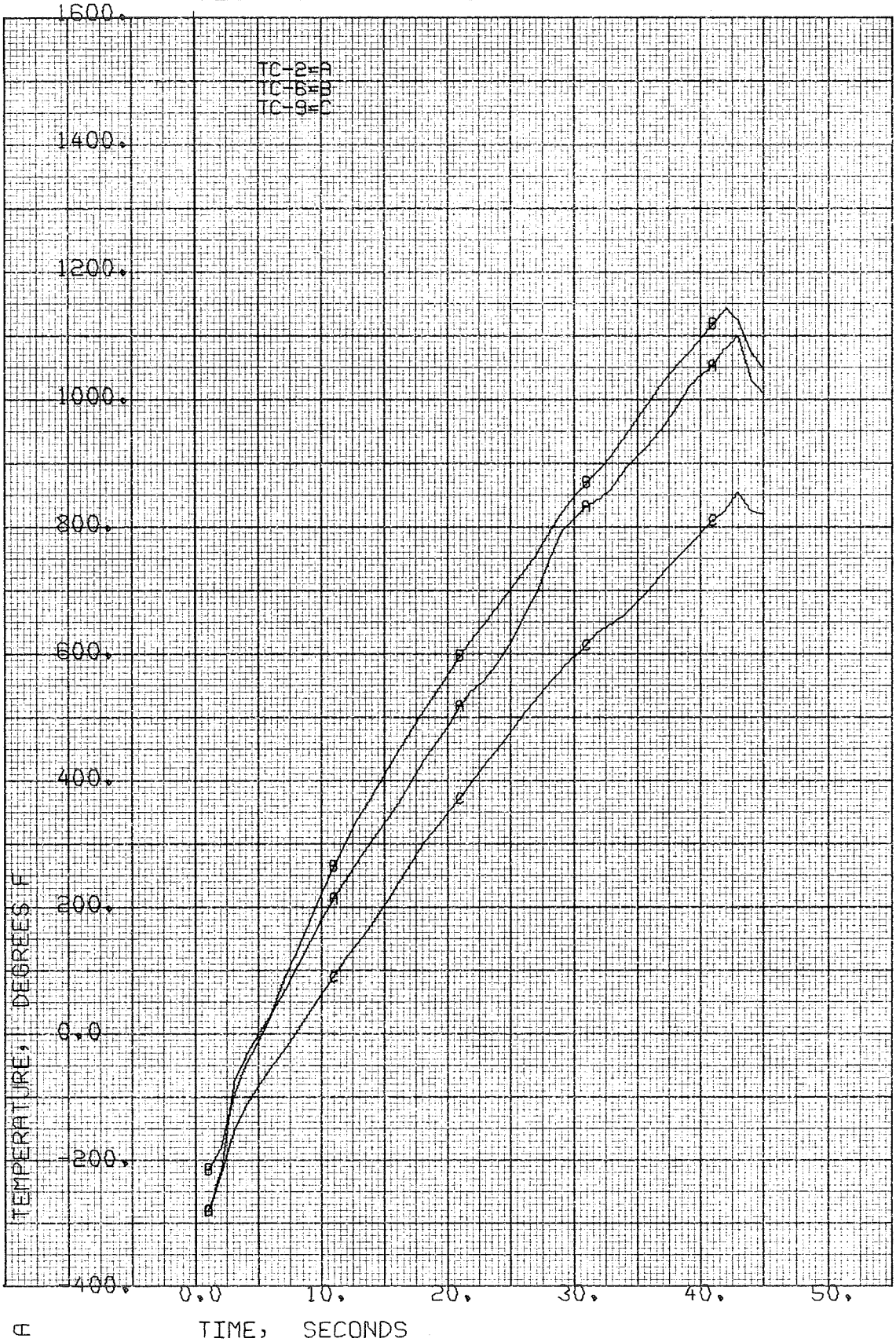

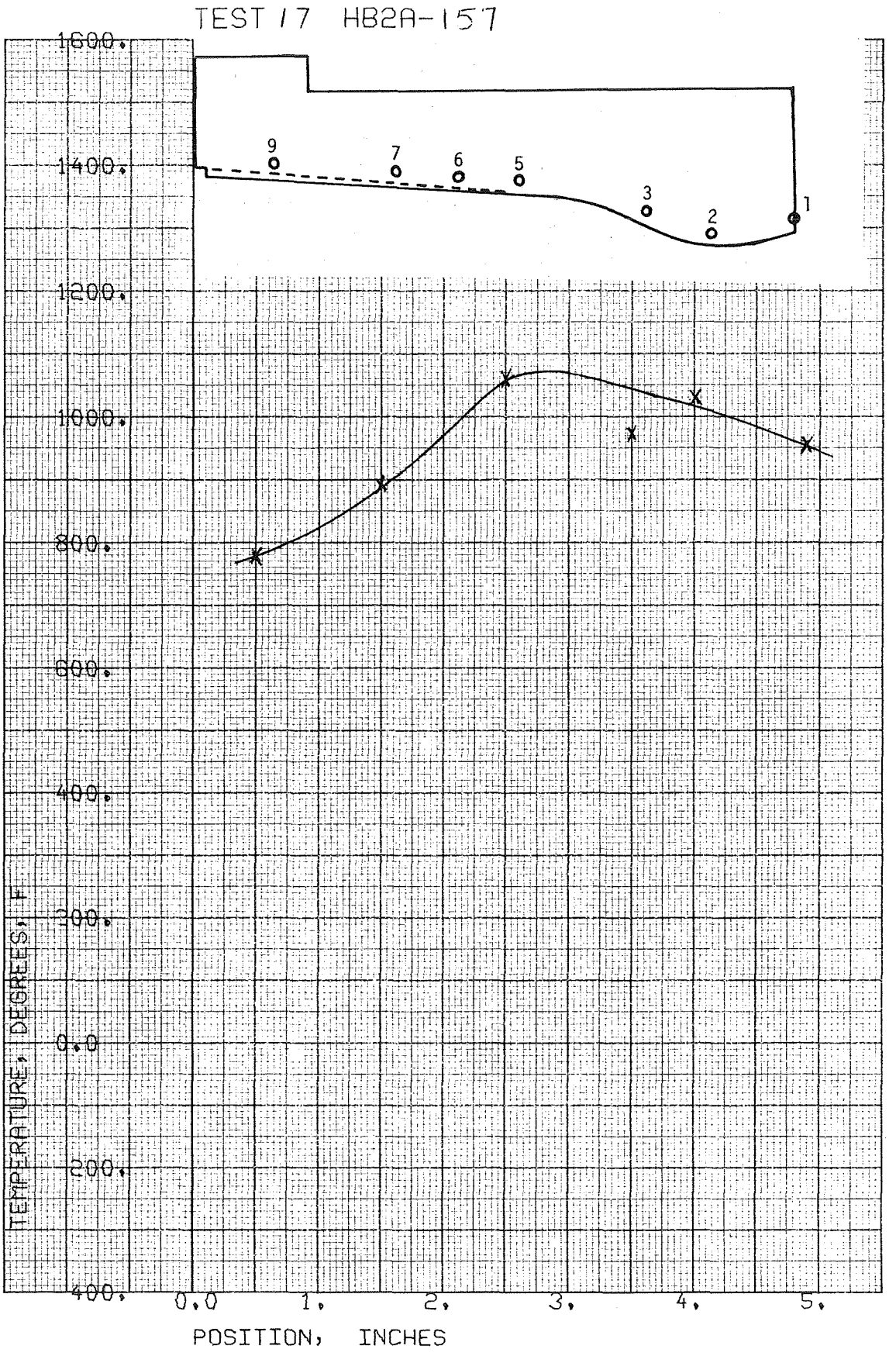
TEST 17 HB2A-157
1600.
1400.
1200.
1000.
800.
600.
400.
300.
0.0
200.
400.
TEMPERATURE, DEGREES, F
0.0
1.
2.
3.
4.
5.
POSITION, INCHES
9
7
6
5
3
2
1

TEST 18 HB2A-158

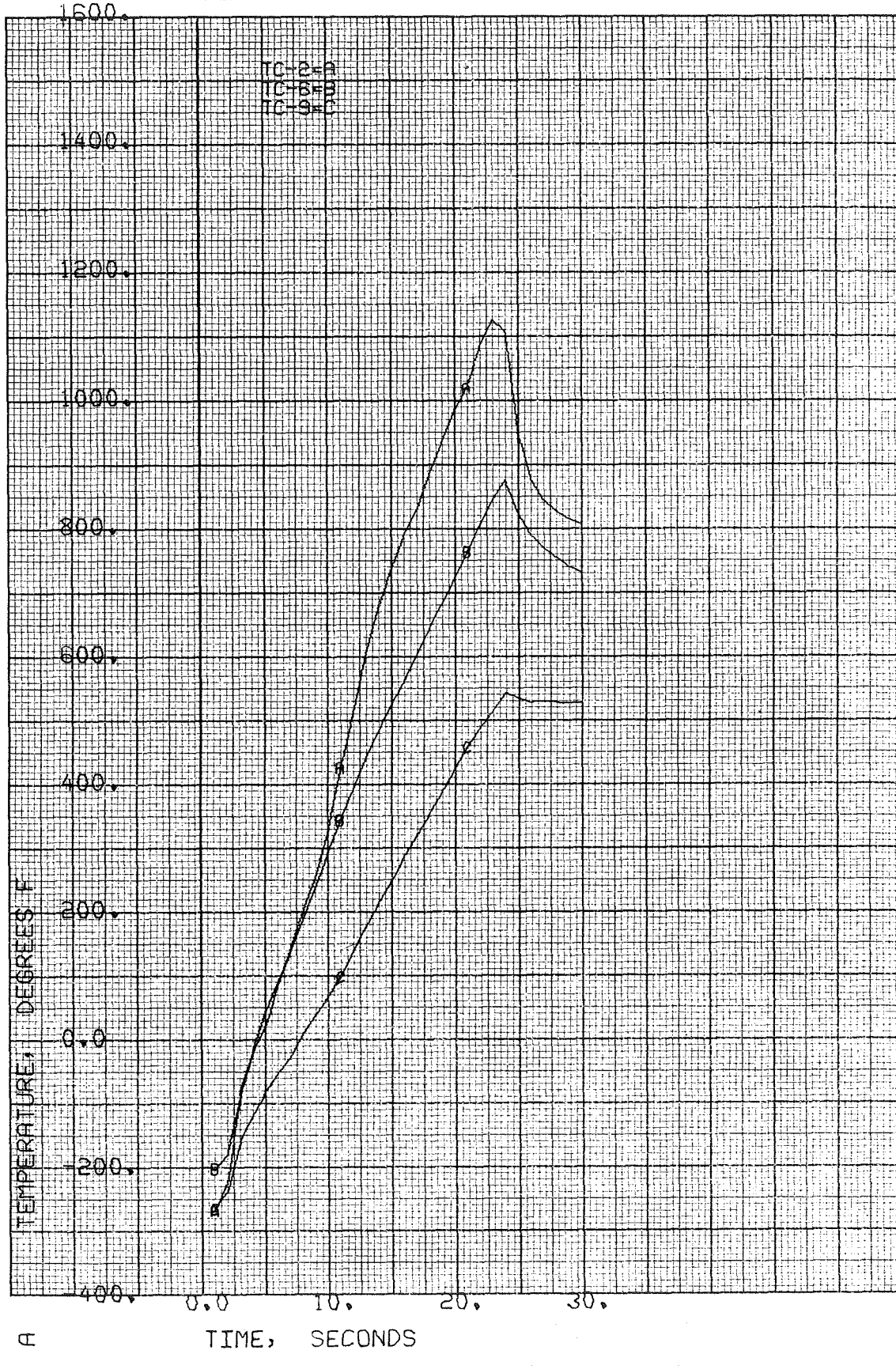

TEST 18 HB2A-158

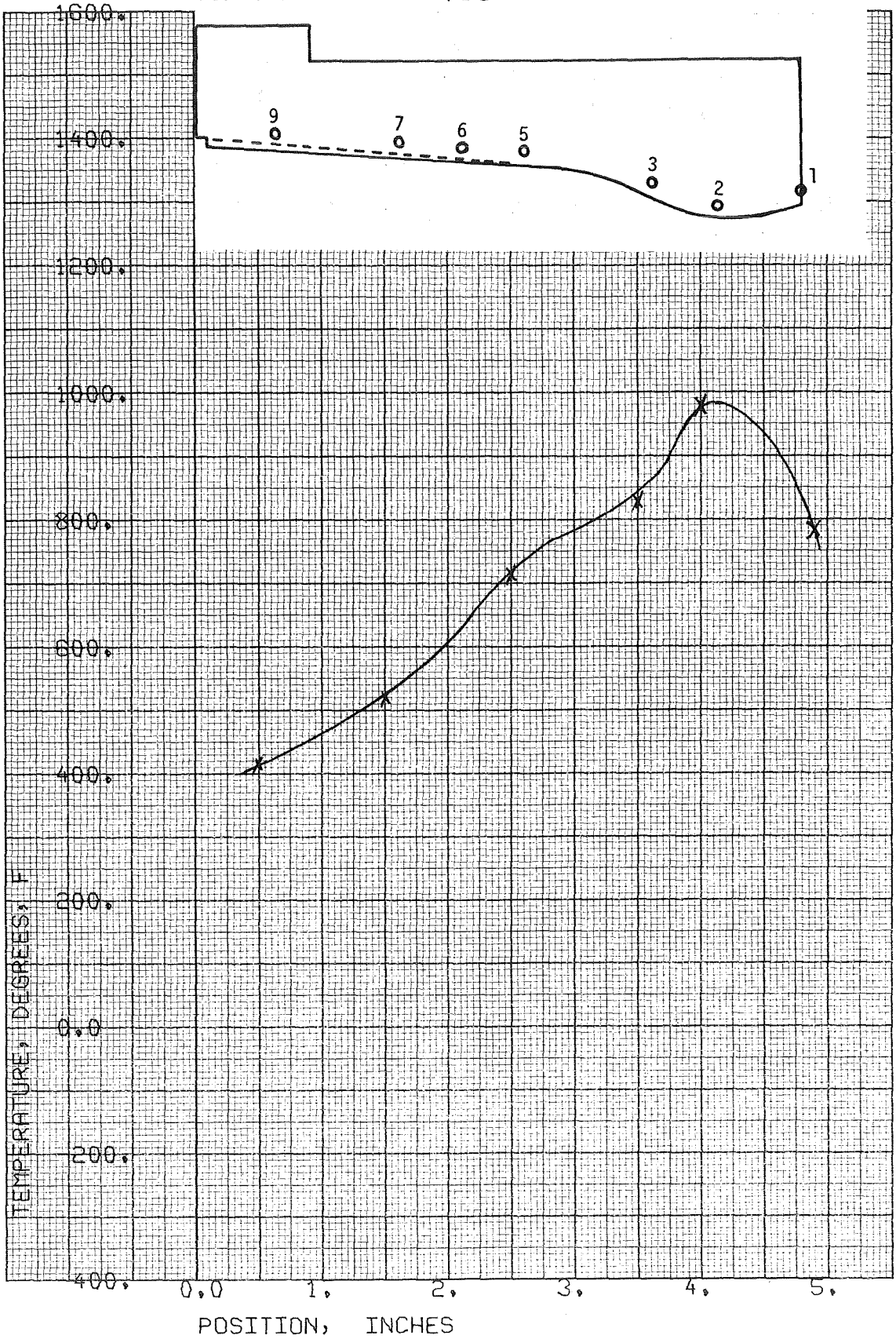

TEST 19 HB2A-159

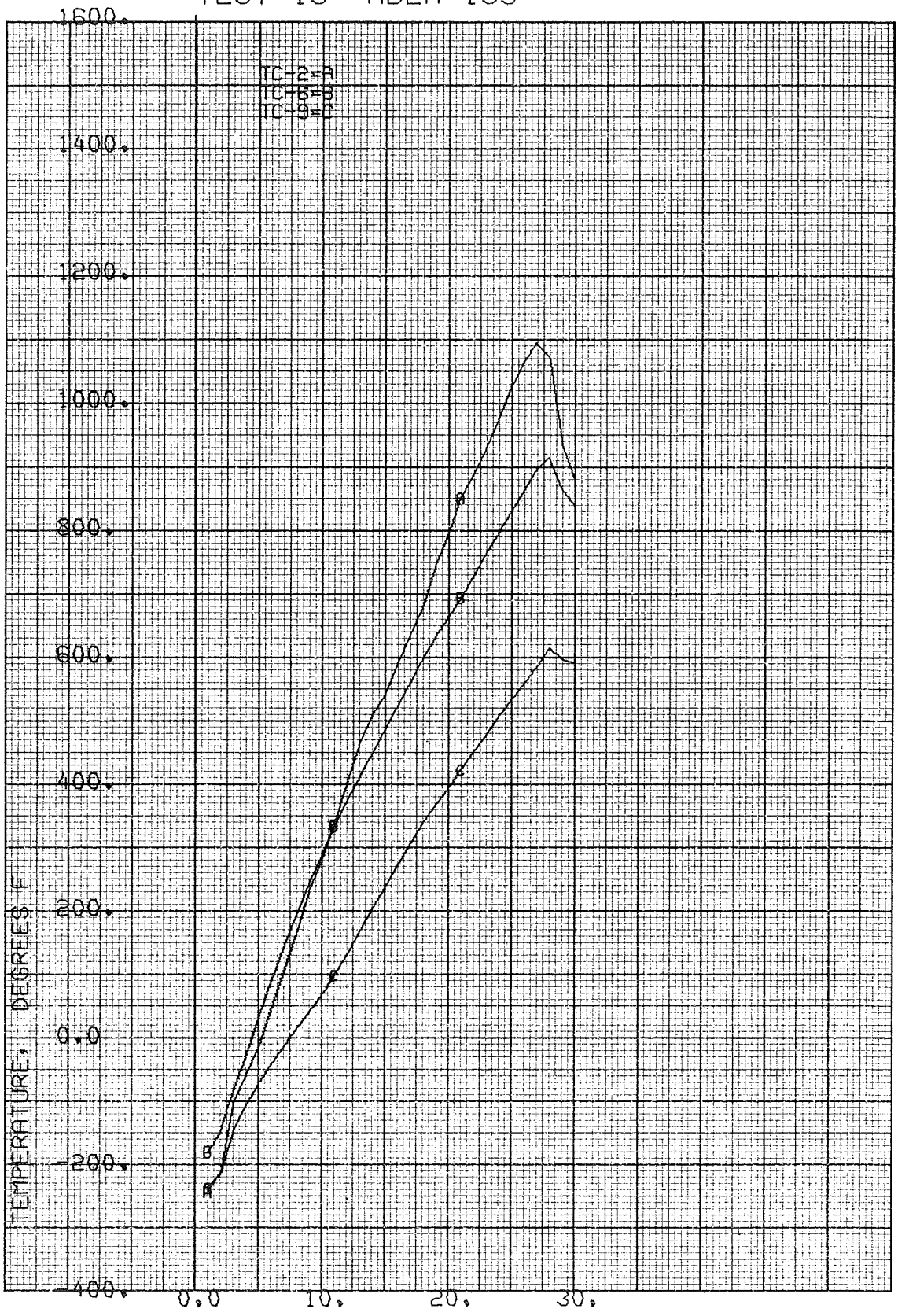

TEST 19 HB2A-159

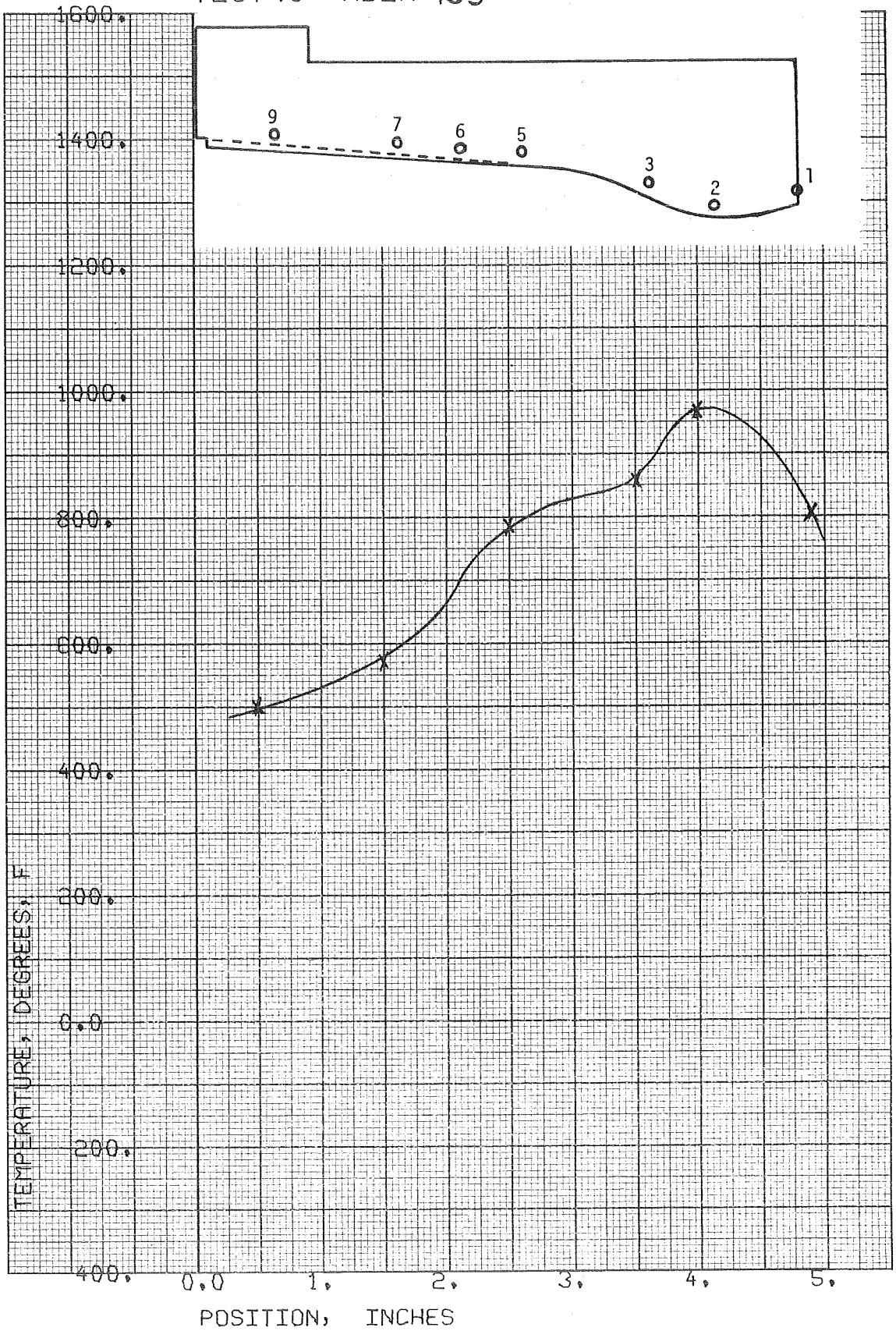

TEST 20 HB2A-160

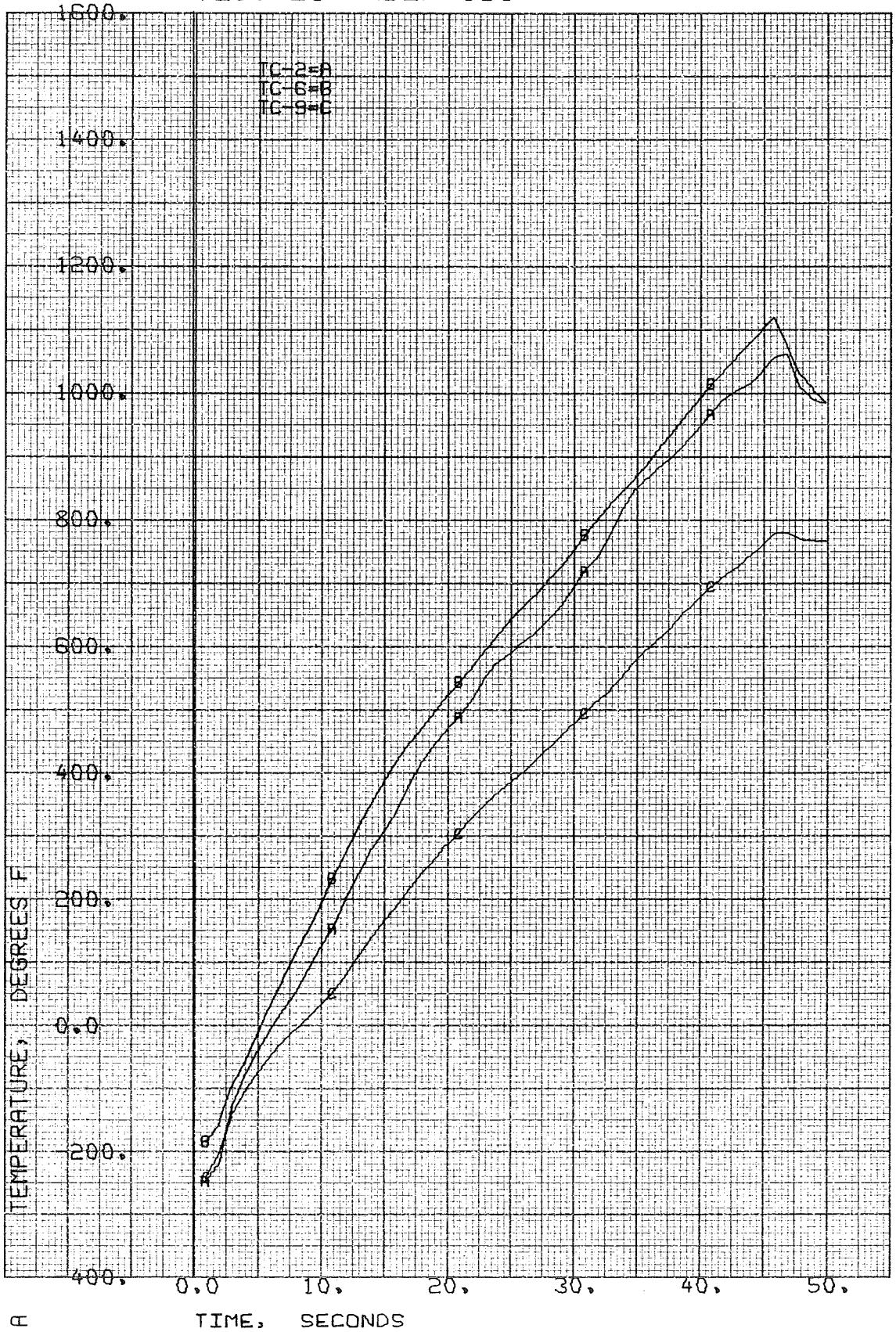

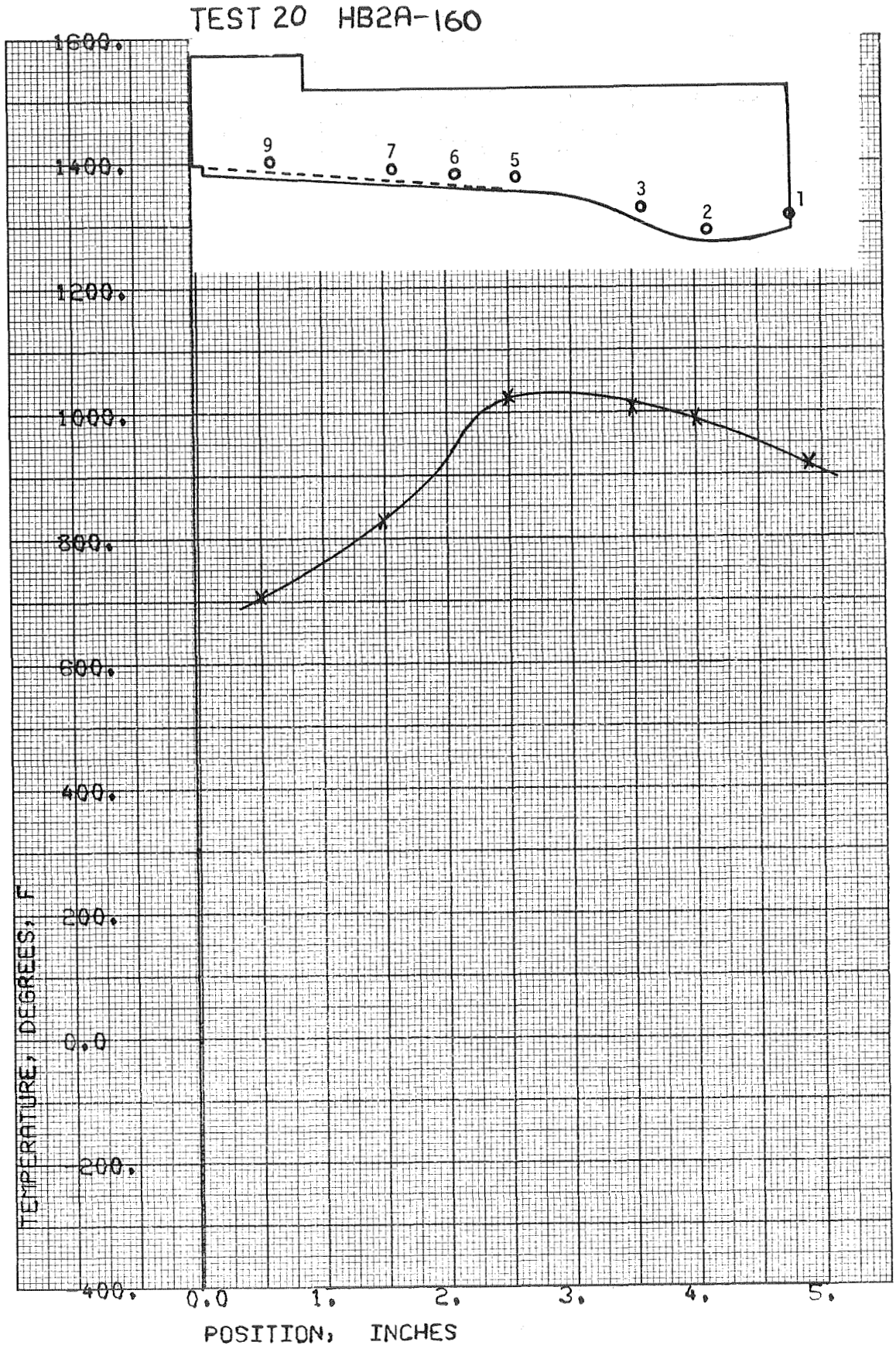
TEST 20 HB2A-160
9
7
6
5
3
2
1
1600.
1400.
1200.
1000.
800.
600.
400.
200.
0.0
-200.
-400.
TEMPERATURE, DEGREES, F
0.0
1.
2.
3.
4.
5.
POSITION, INCHES

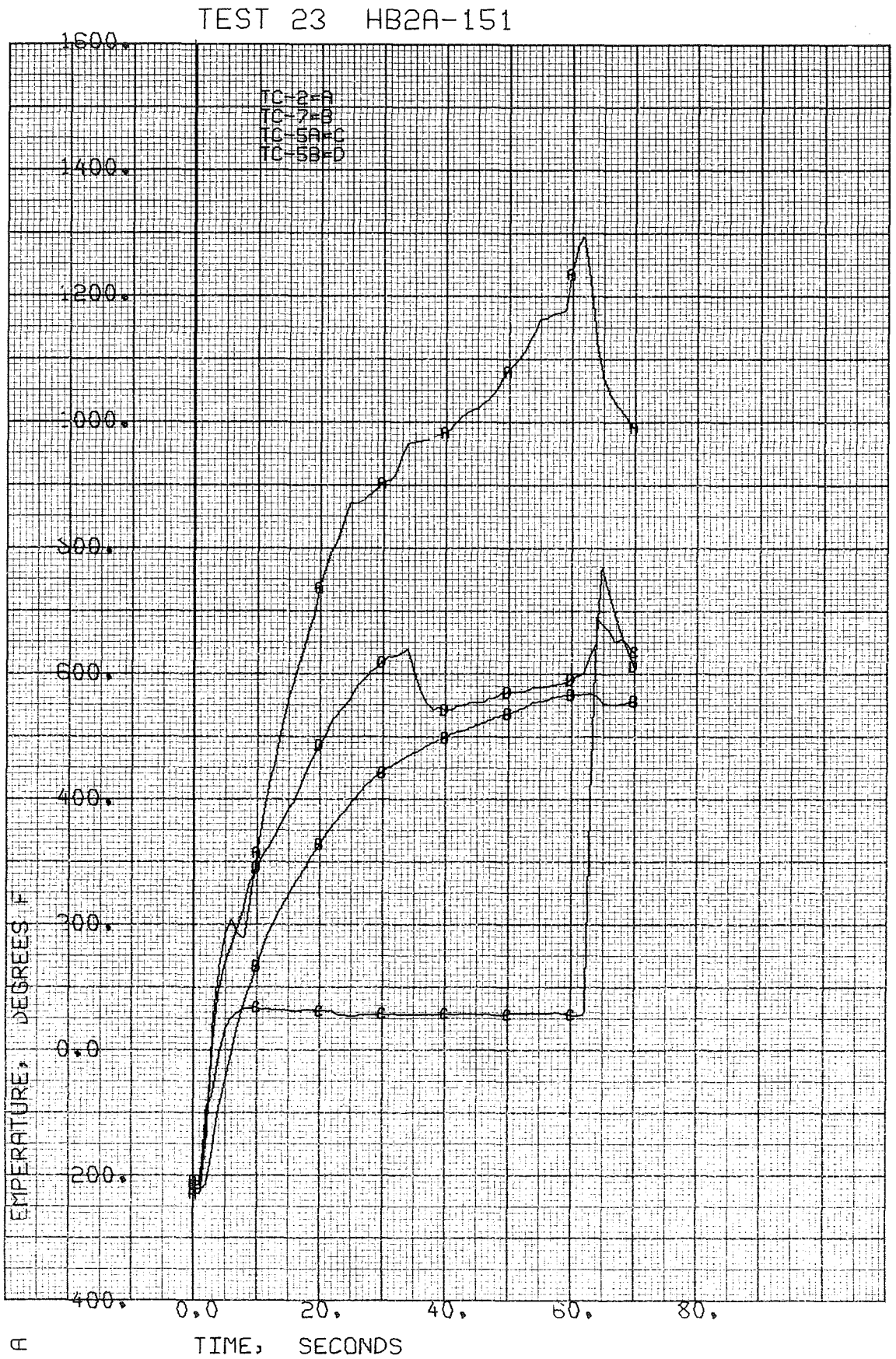
TEST 23 HB2A-151
TC-2=A
TC-7=B
TC-5A=C
TC-5B=D
1600.
1400.
1200.
1000.
800.
600.
400.
200.
0.0
-200.
-400.
EMPERATURE, DEGREES F
0.0
20.
40.
60.
80.
TIME, SECONDS

TEST 23 HB2A-151

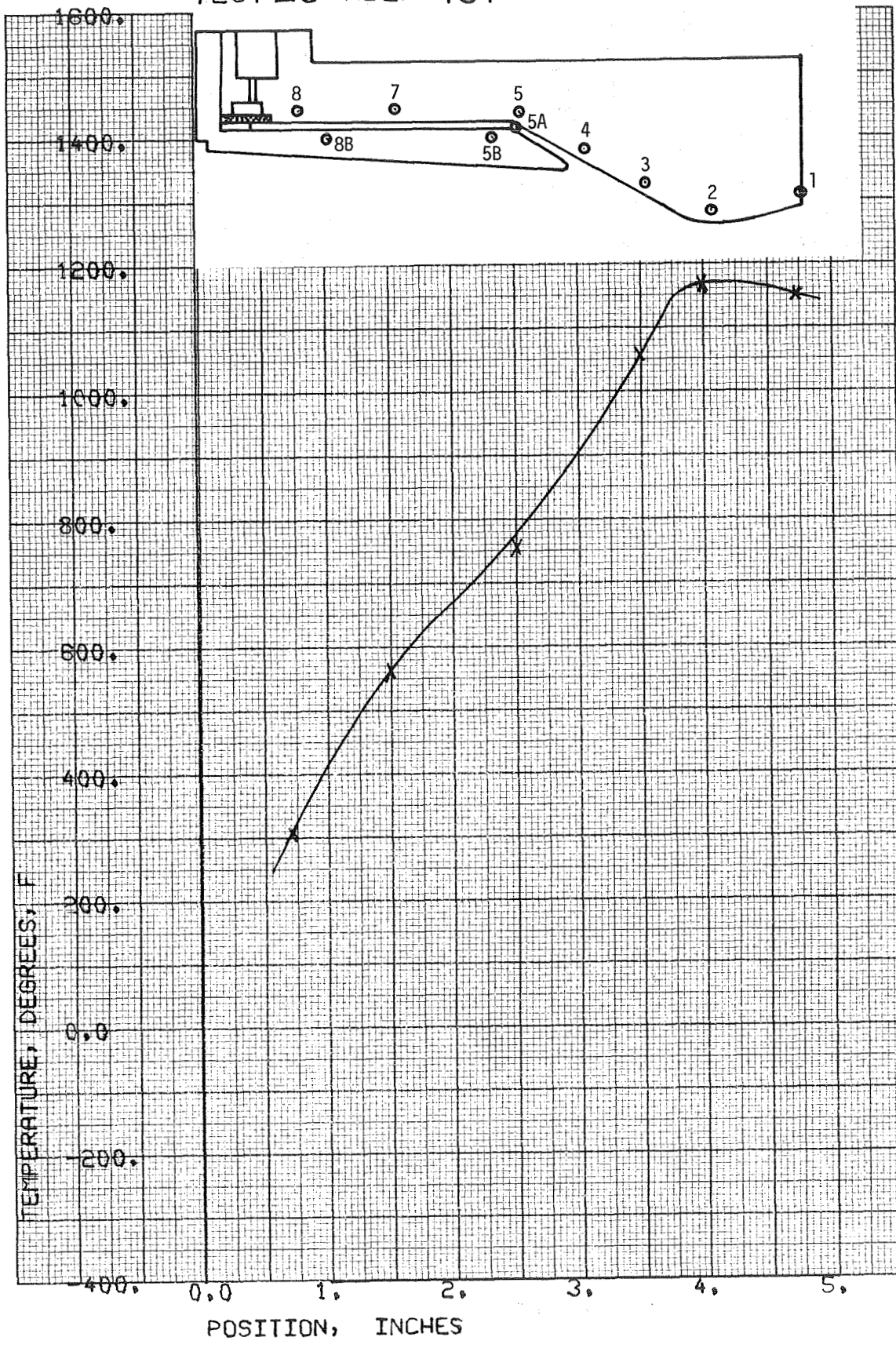

TEST 24 HB2A-152

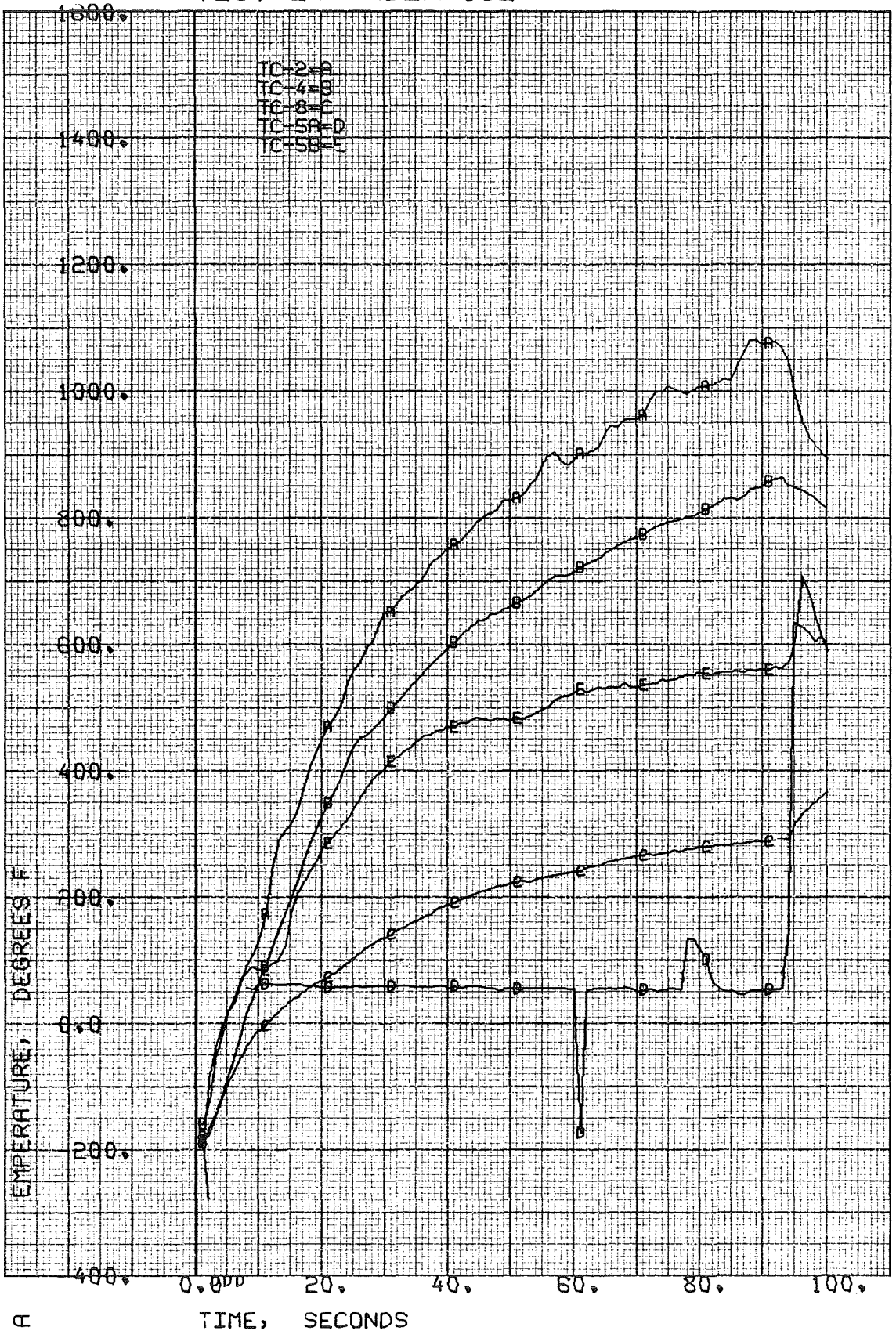

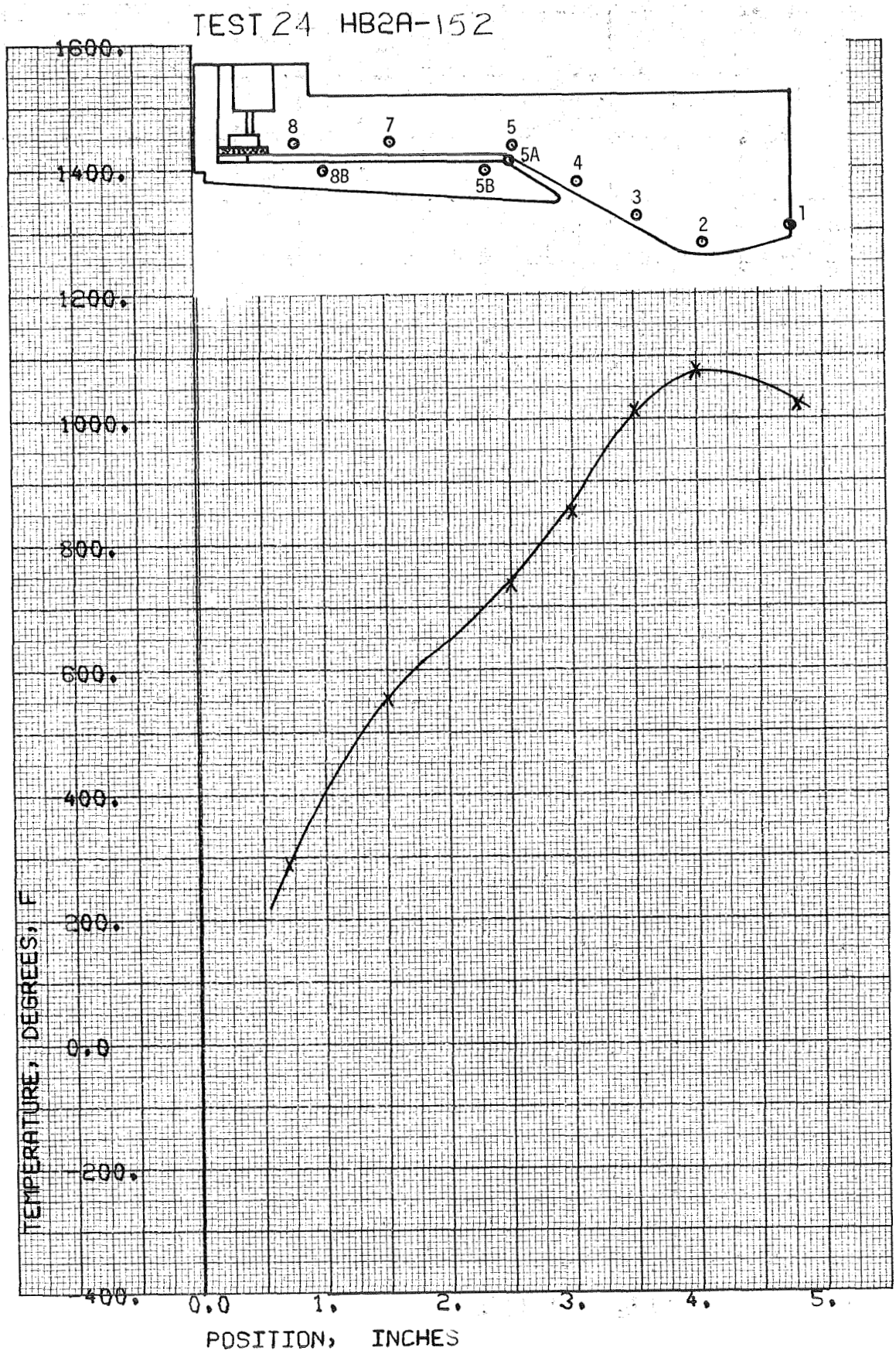
TEST 24 HB2A-152
8
7
5
5A
4
8B
5B
3
2
1
1600.
1400.
1200.
1000.
800.
600.
400.
200.
0.0
-200.
-400.
TEMPERATURE, DEGREES, F
0.0
1.
2.
3.
4.
5.
POSITION, INCHES

TEST 25 HB2A-153

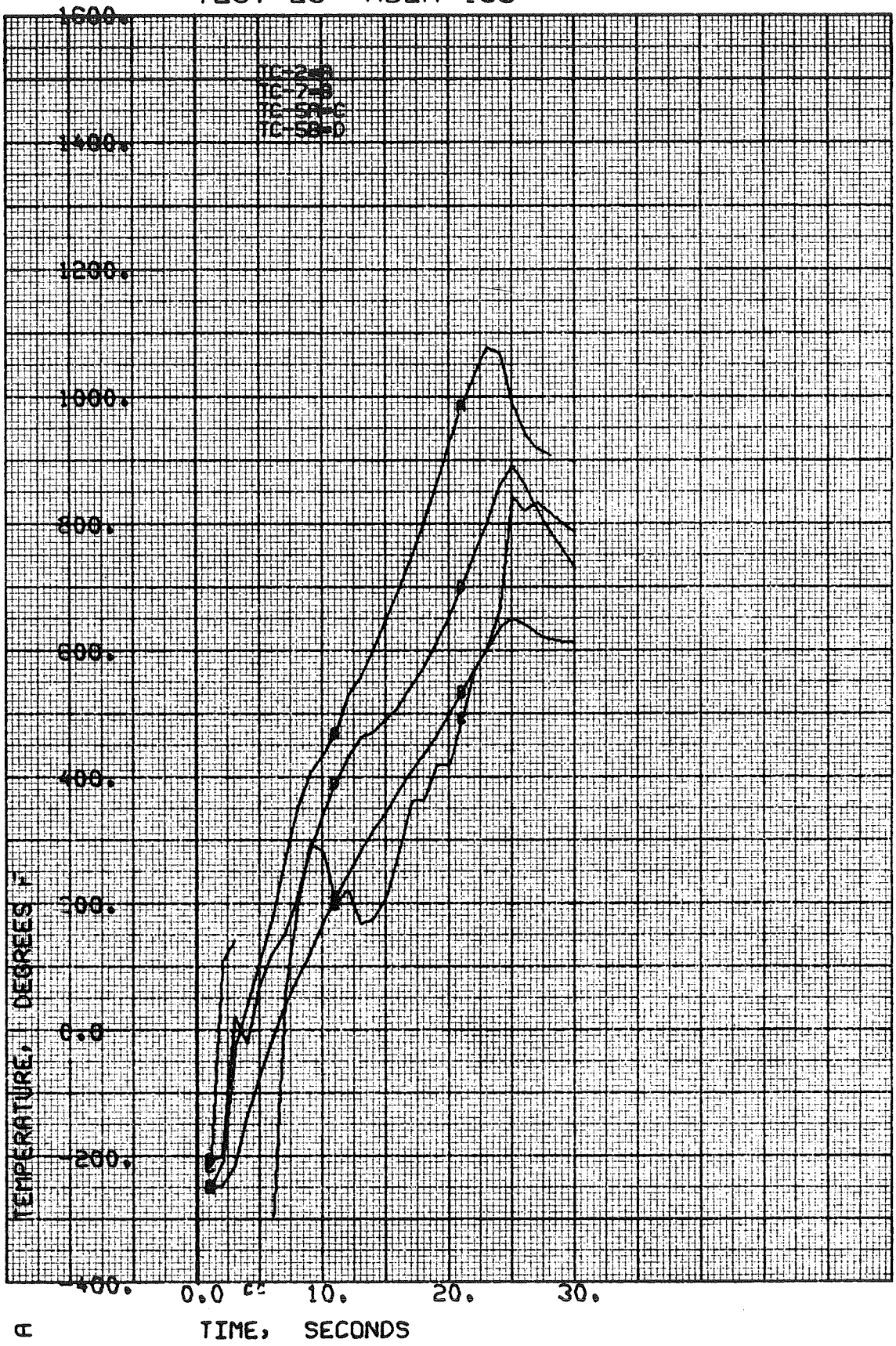

TEST 25 HB2A-153

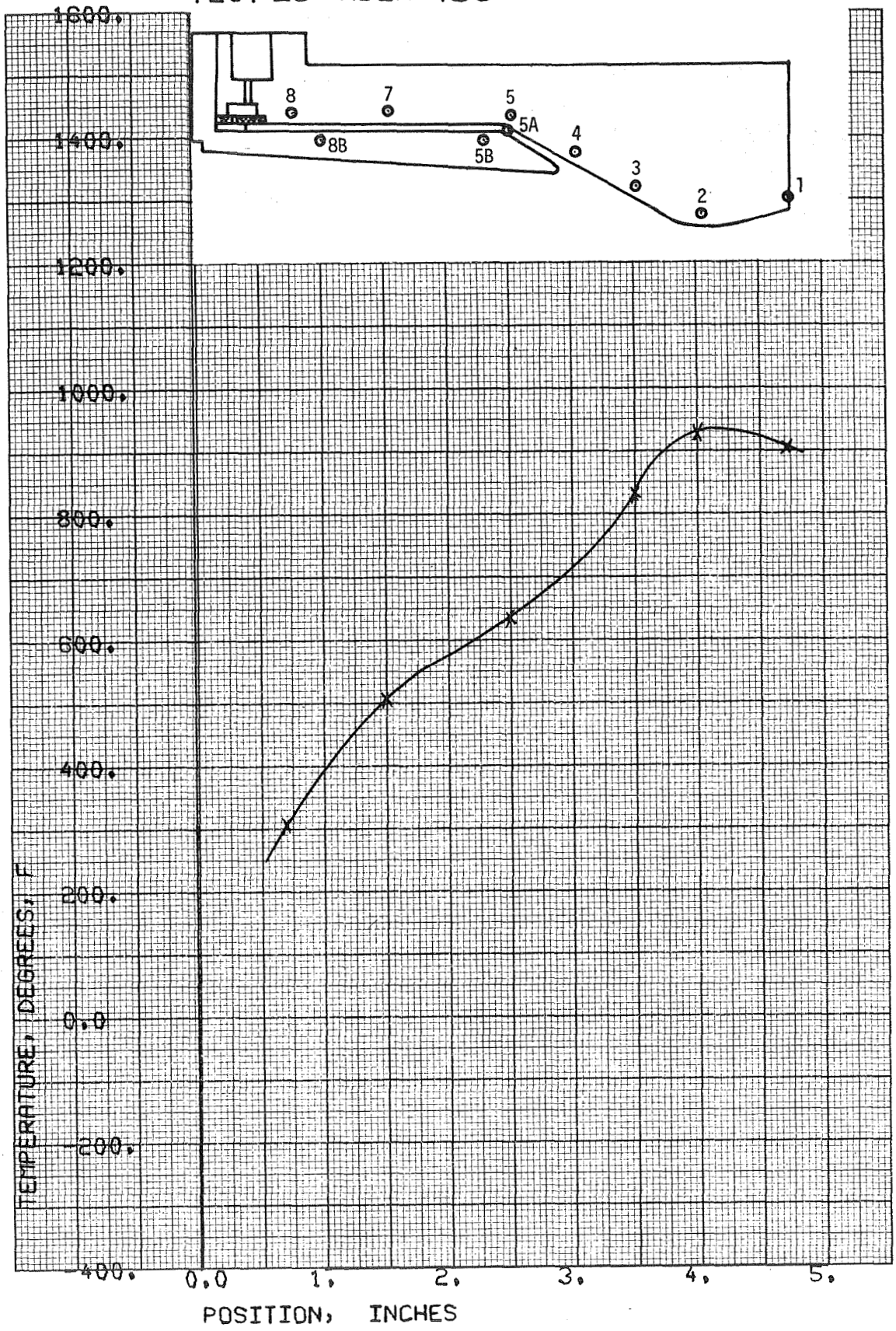

TEST 26 HB2A-154

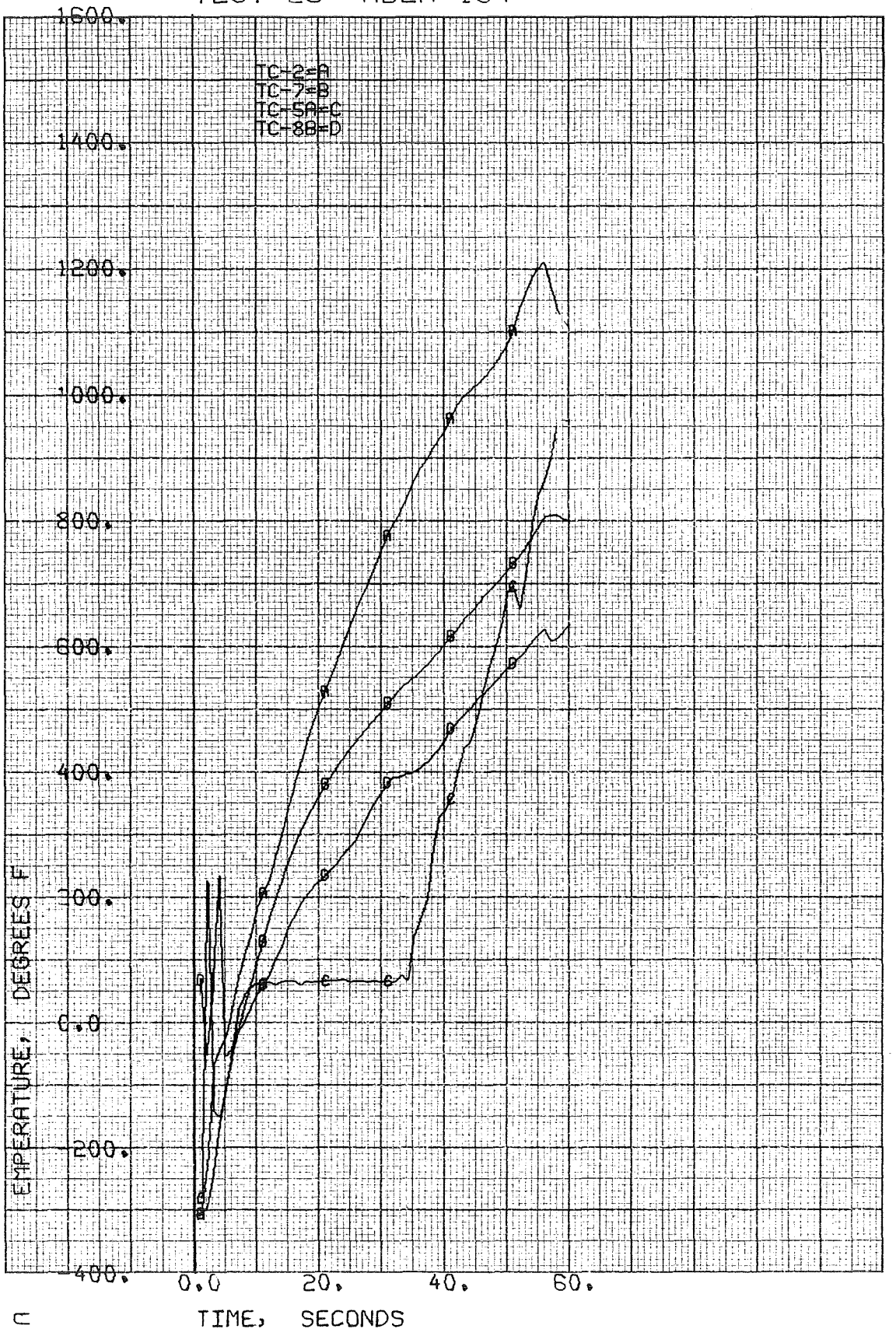

TEST 26 HB2A-154

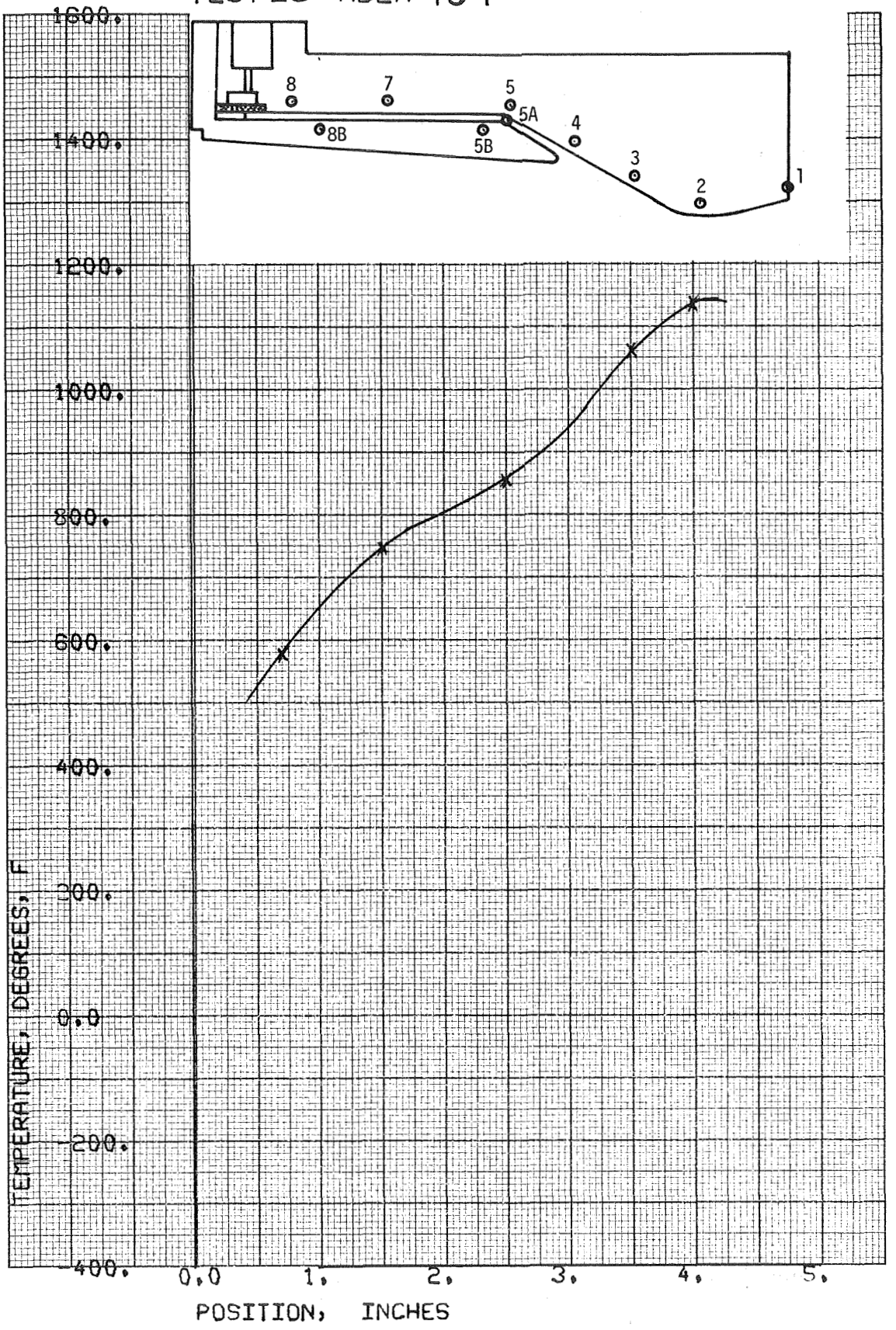

TEST 27 HB2A-155

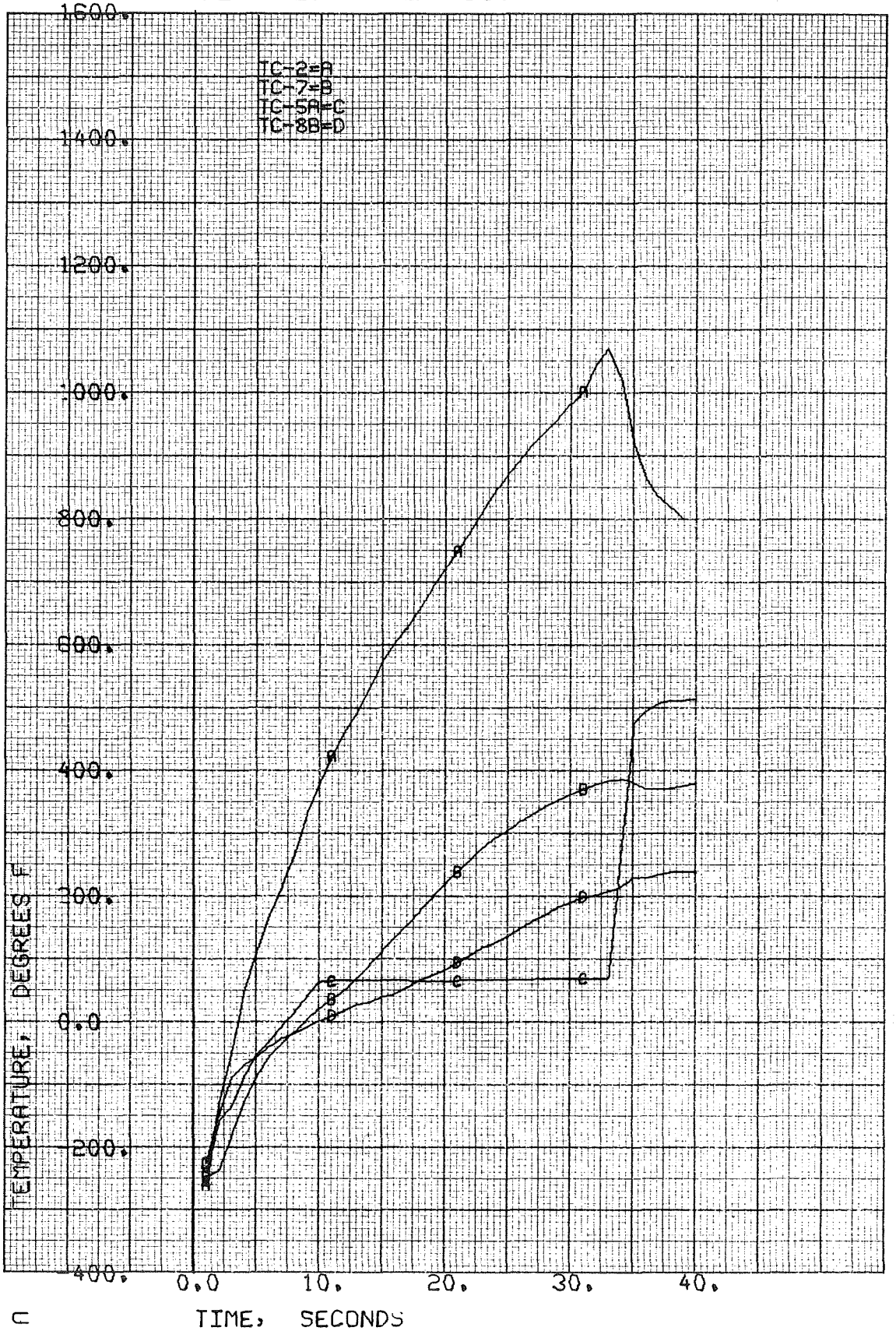

TEST 27 HB2A-155

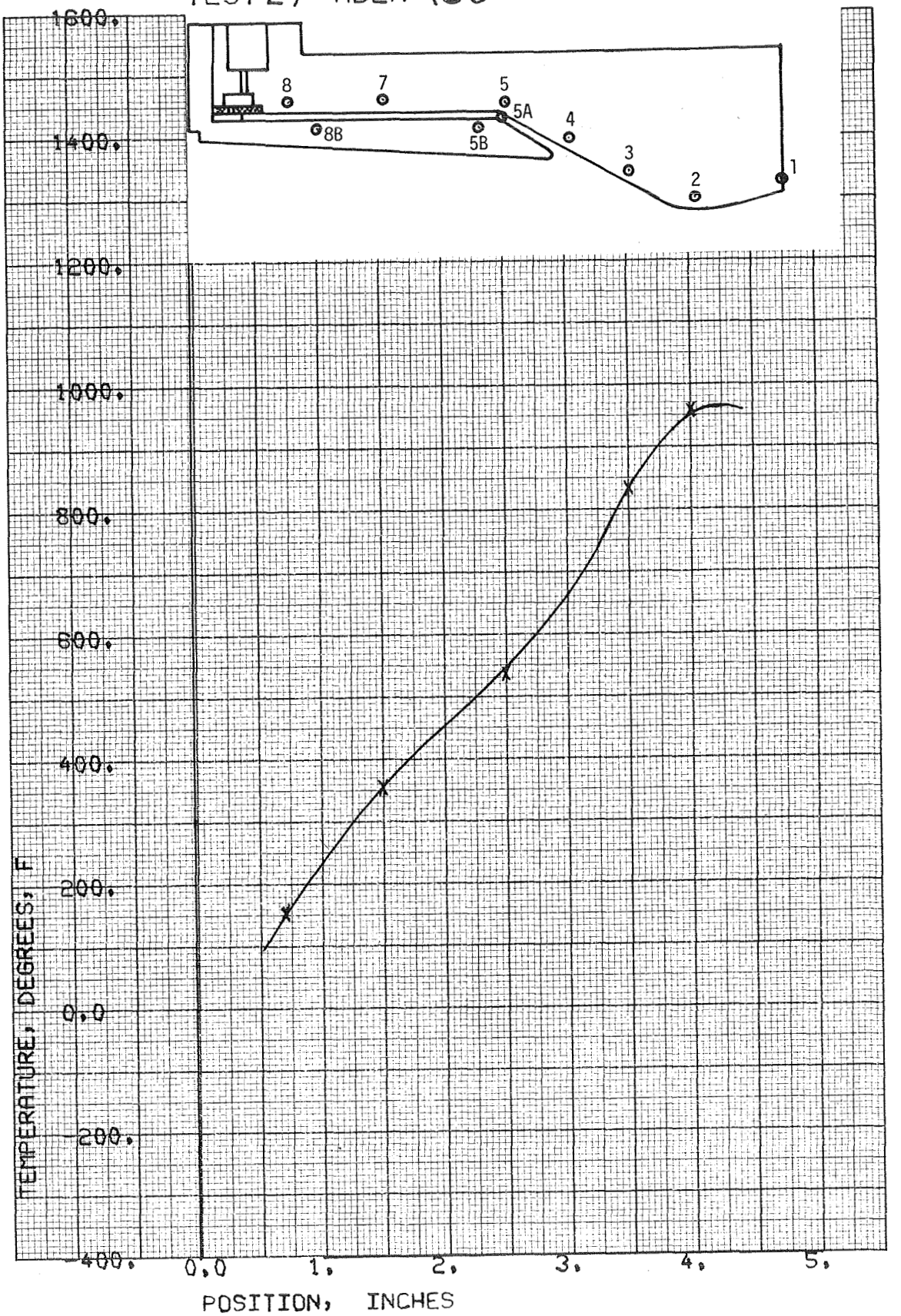

TEST 28 HB2A-156

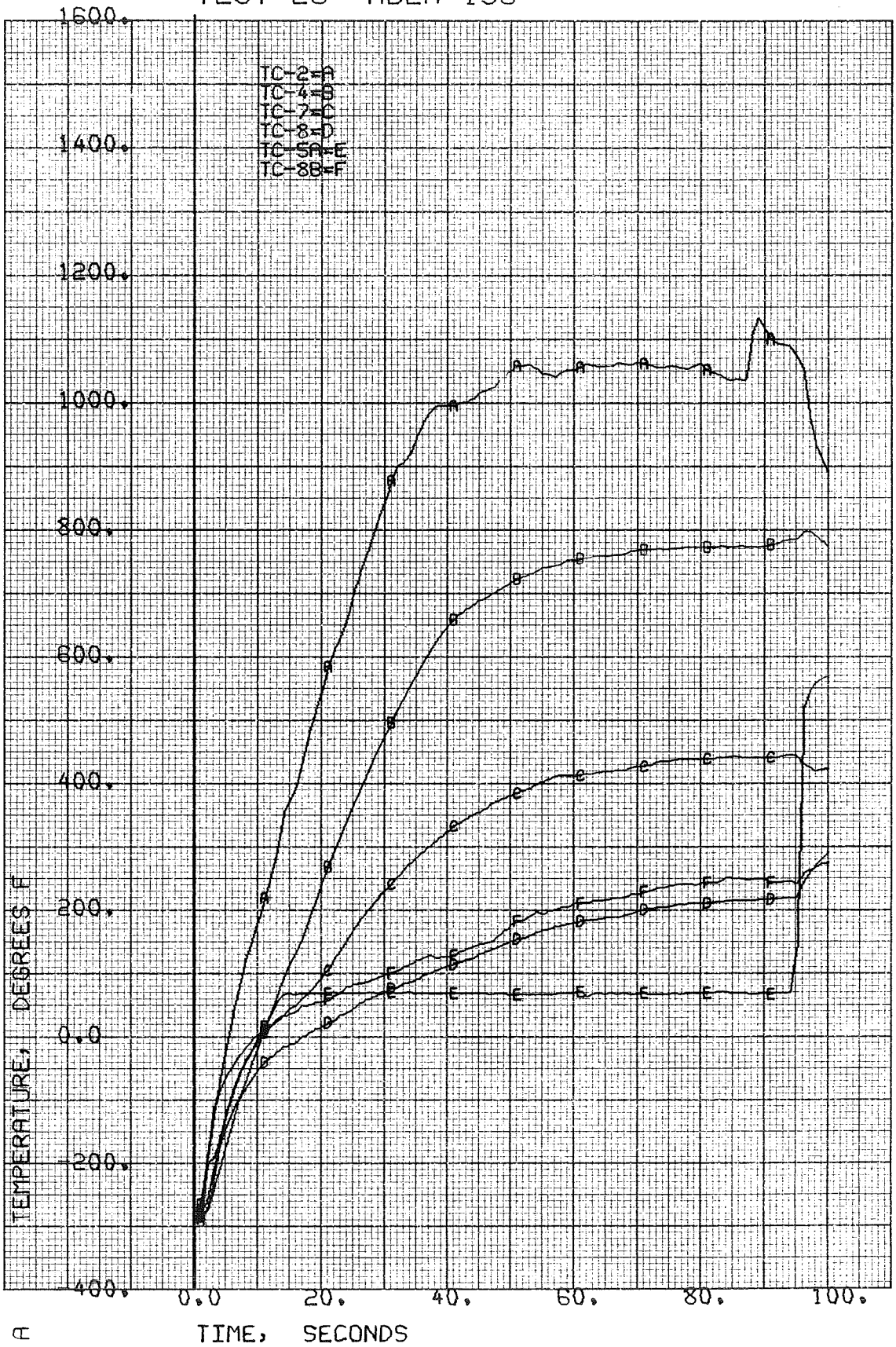

TEST 28 HB2A-156

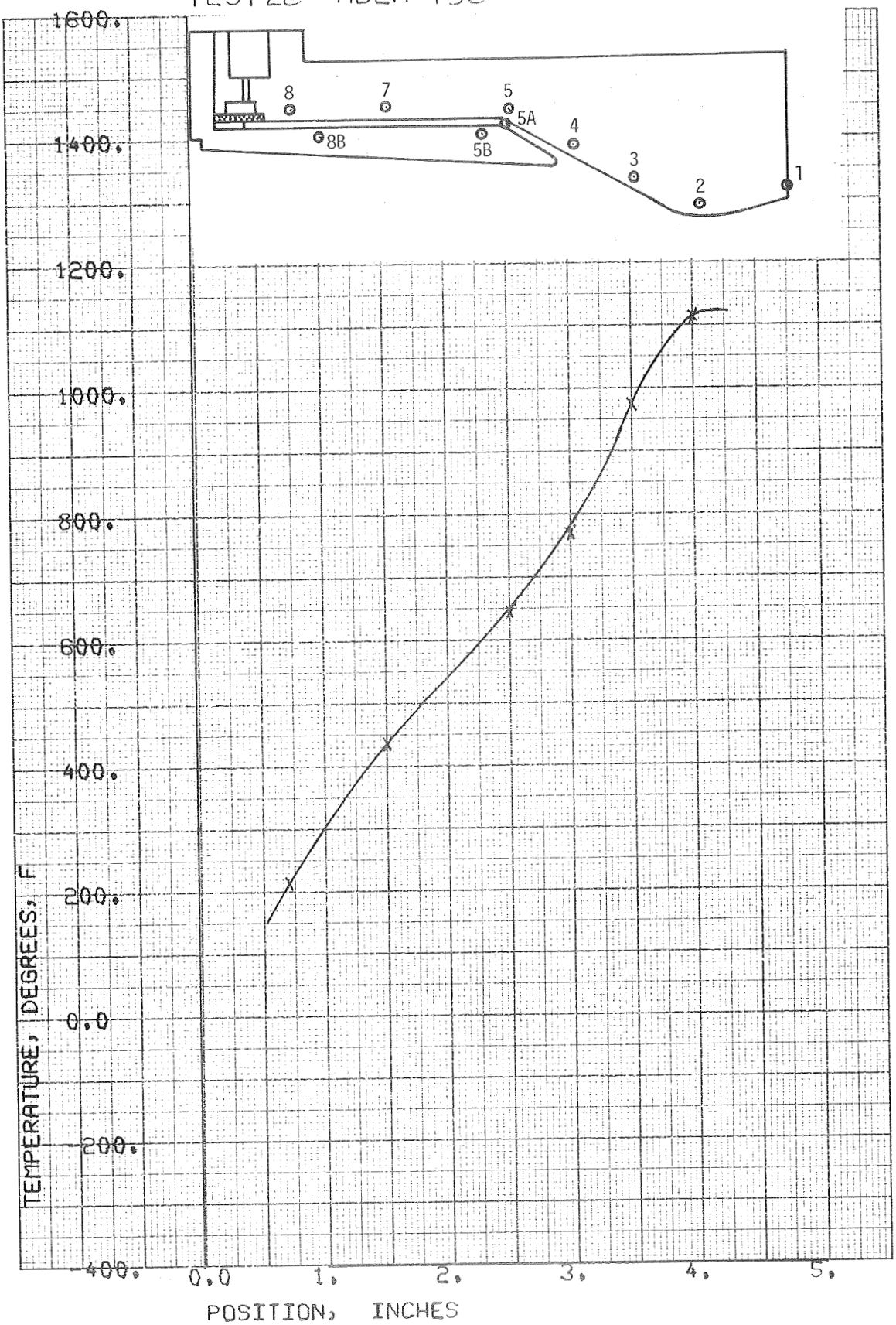

TEST 31 HB2A-212

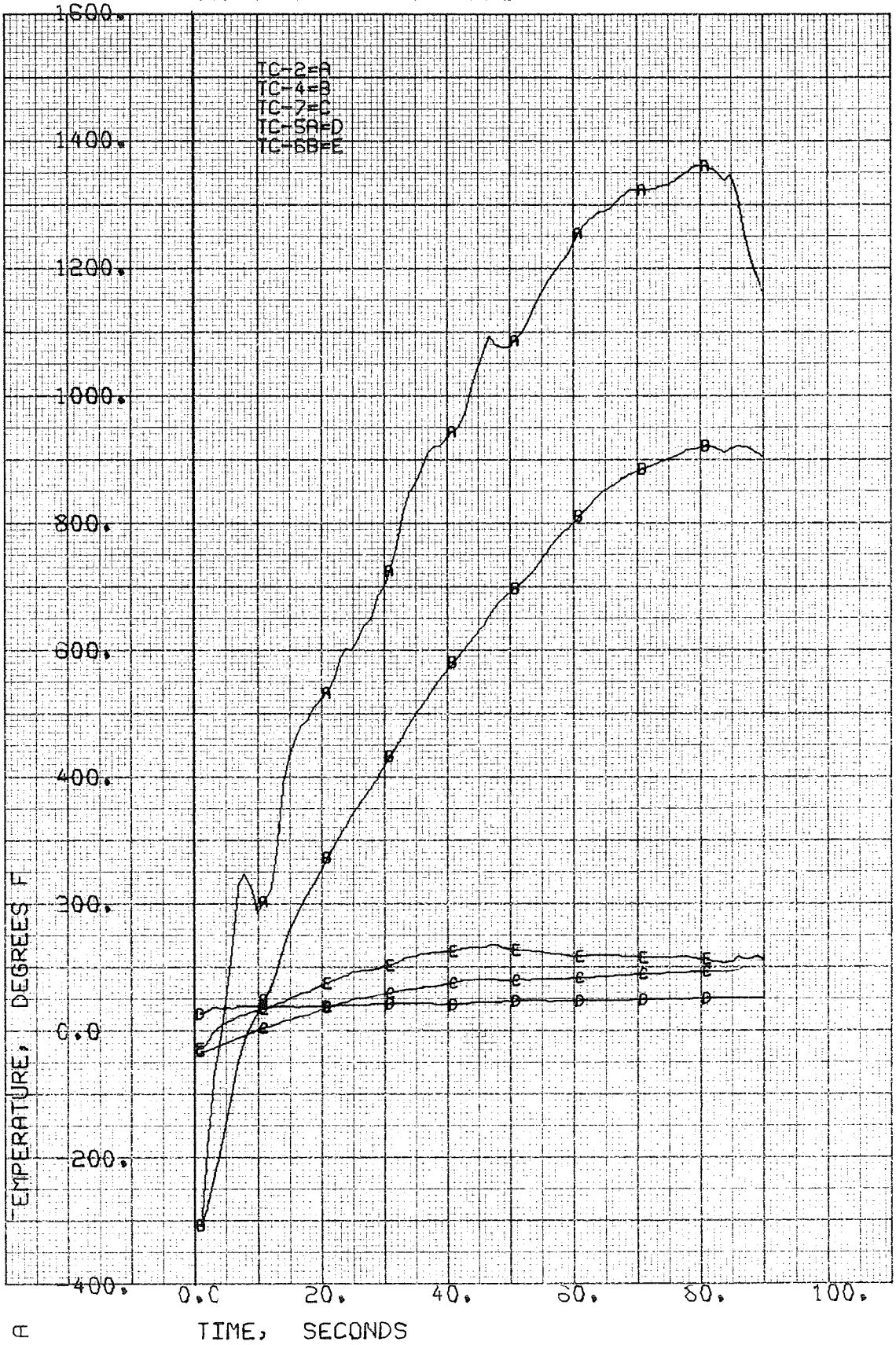

TEST 31 HB2A-212

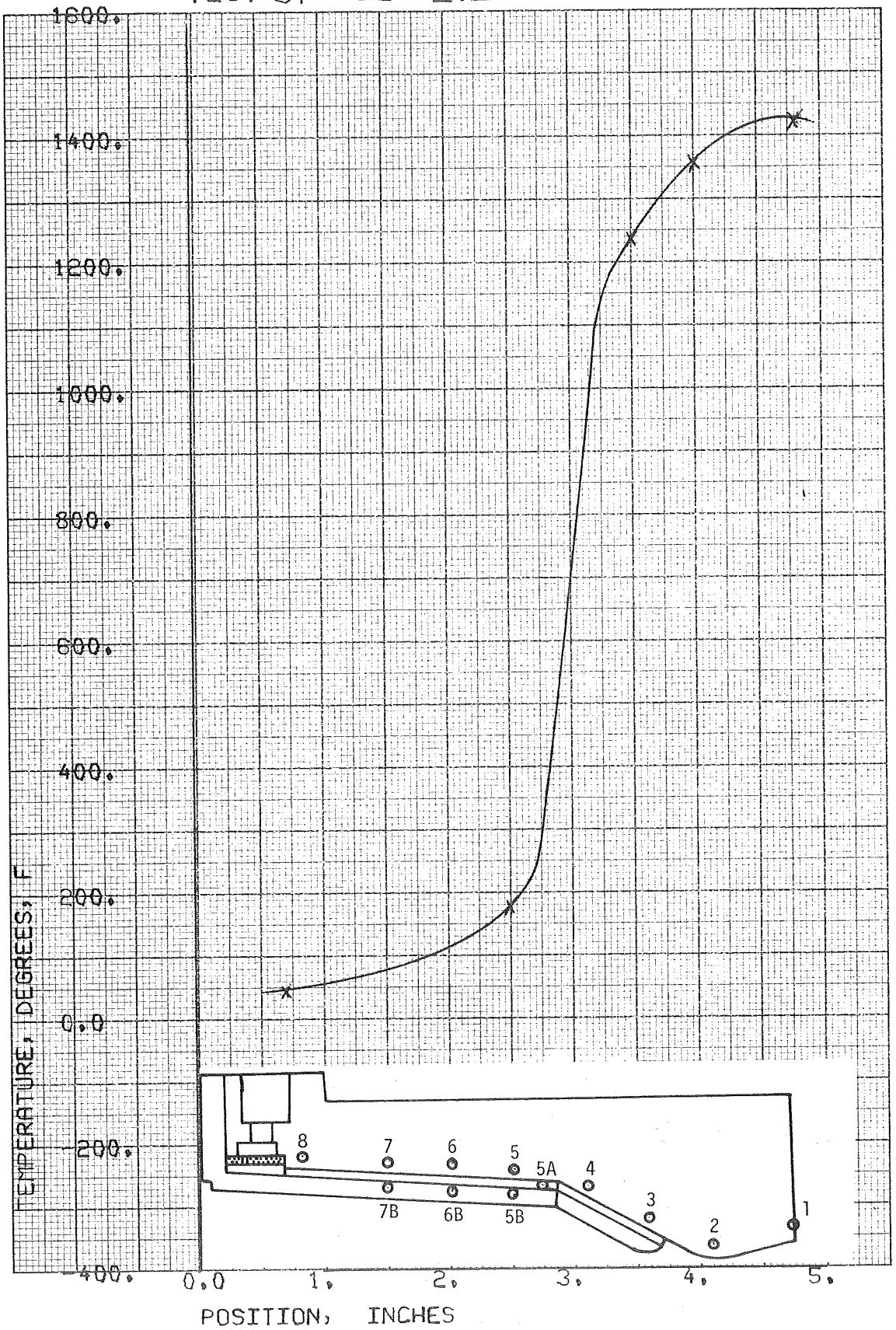

TEST 32 HB2A-213

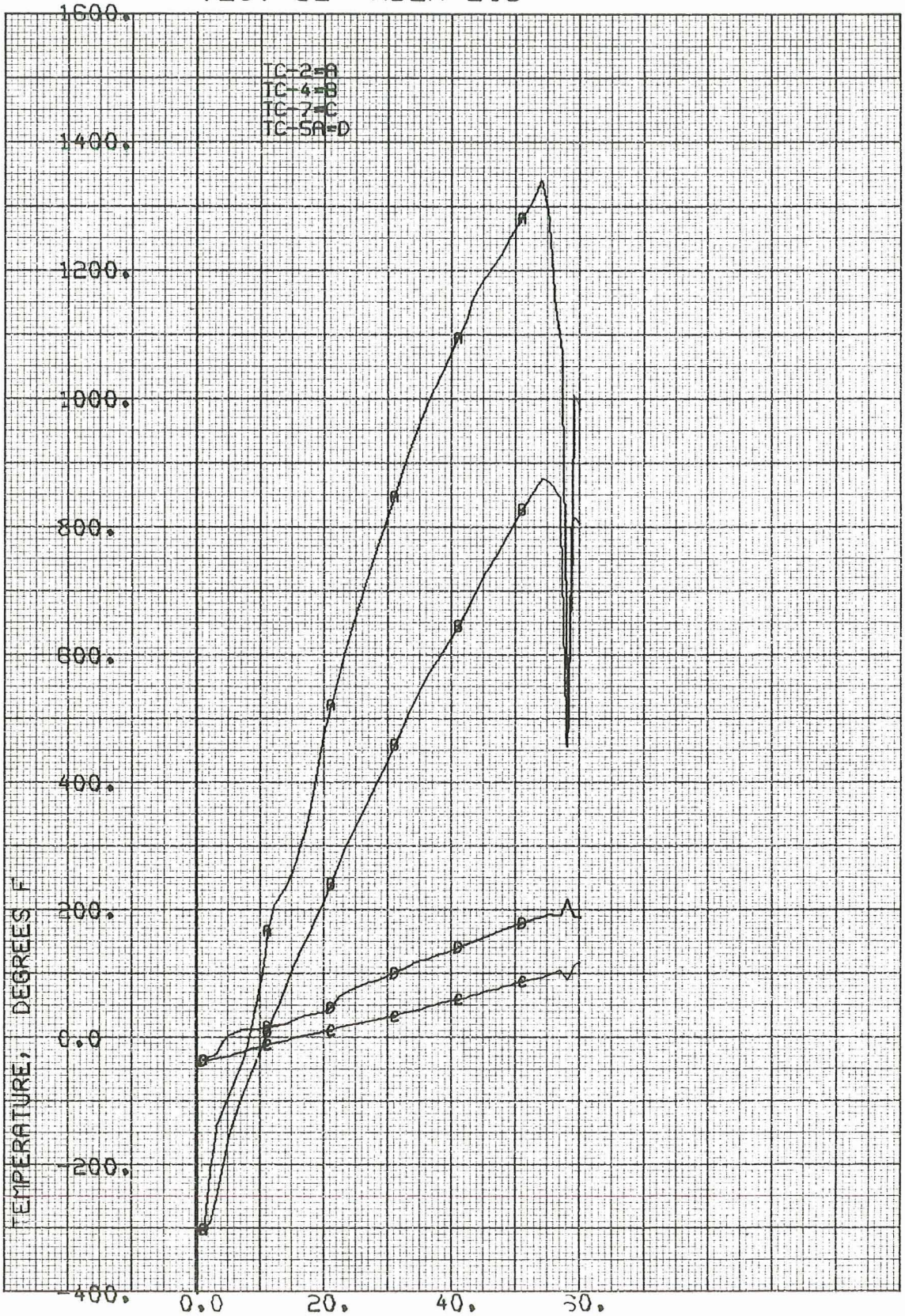

TEST 32 HB2A-213

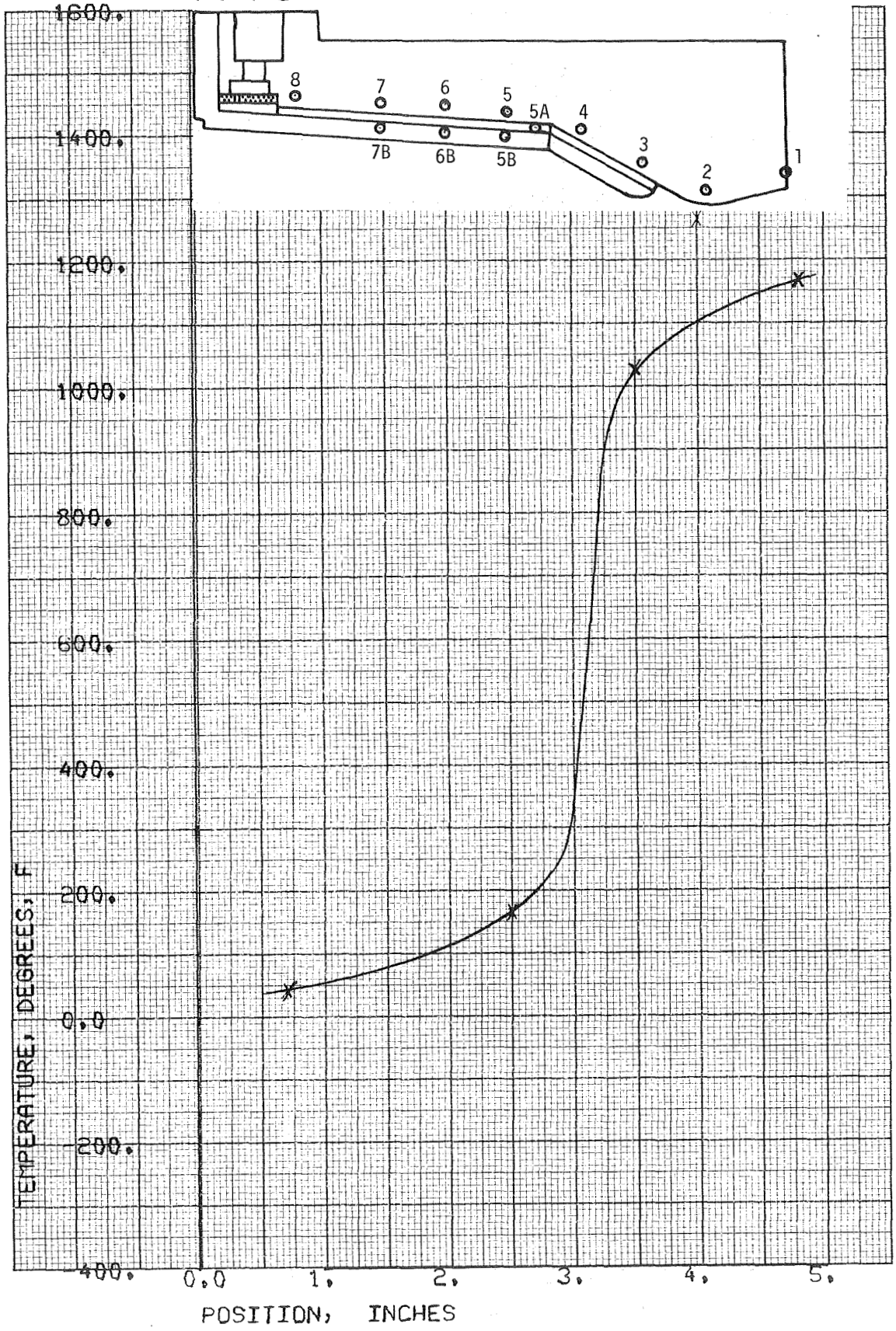

TEST 33 HB2A-214

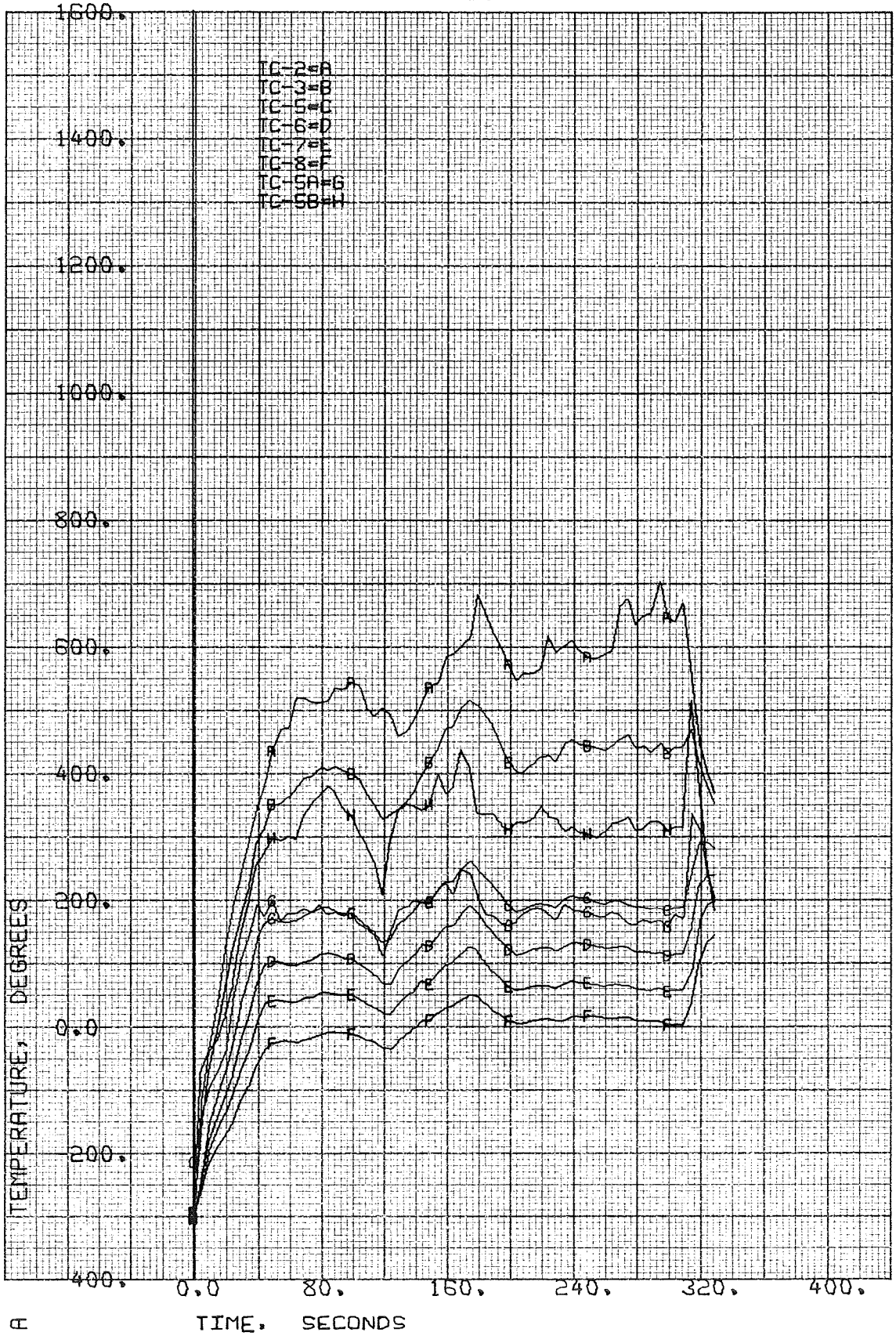

TEST 33 HB2A-214

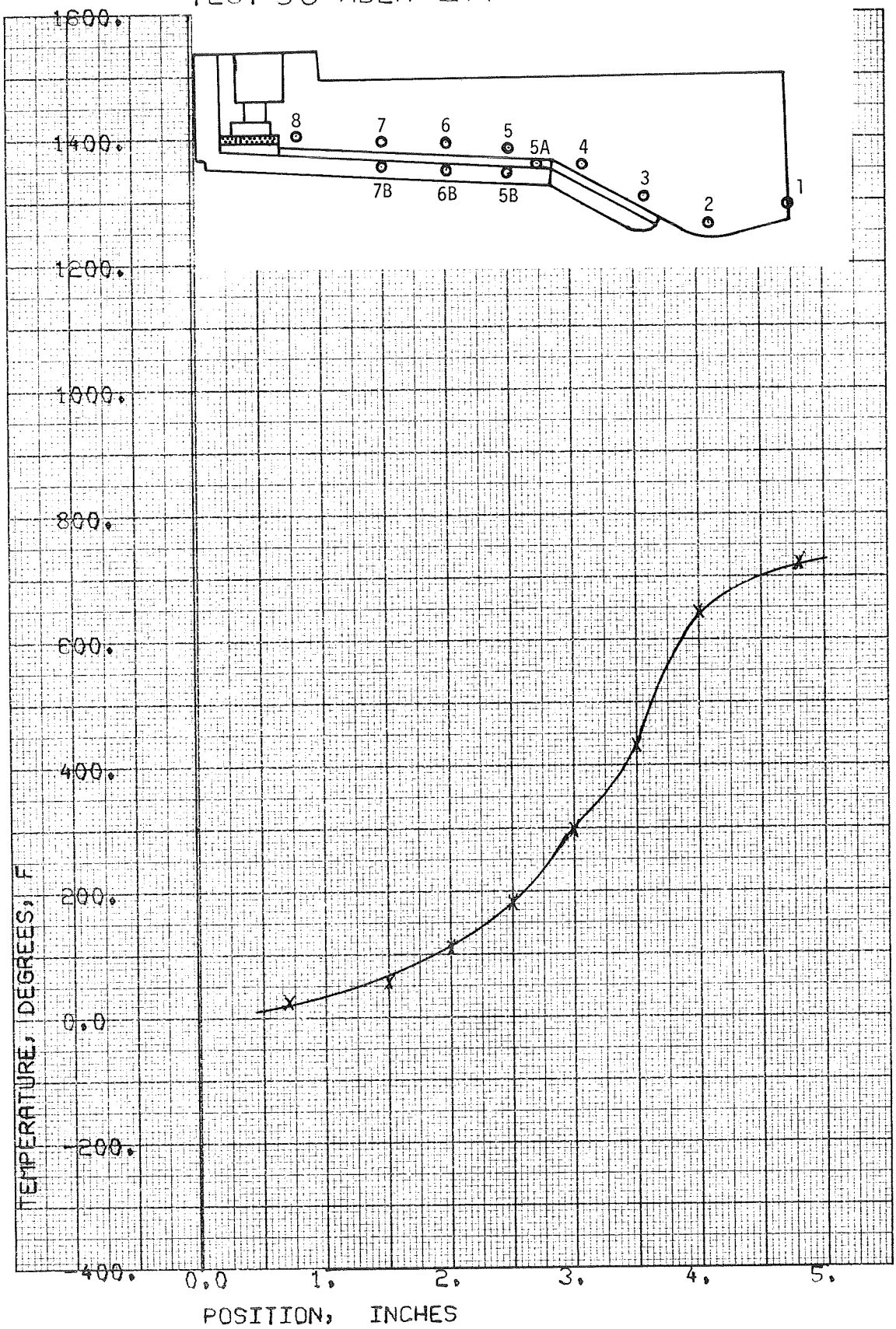

APPENDIX B

DISTRIBUTION LIST

REPORT COPIES R	D	RECIPIENT	DESIGNEE
		National Aeronautics & Space Administration Lewis Research Center 21000 Brookpark Road Cleveland, Ohio 44135	
1		Attn: Contracting Officer, MS 500-313	
5		Liquid Rocket Technology Branch, MS 500-209	
1		Technical Report Control Office, MS 5-5	
1		Technology Utilization Office, MS 3-16	
2		AFSC Liaison Office, MS 4-1	
2		Library	
1		Office of Reliability & Quality Assurance, MS 500-111	
1		D. L. Nored, Chief, LRTB, MS 500-209	
3		Paul N. Herr, Project Manager, MS 500-209	
1		E. W. Conrad, MS 500-204	
2		Chief, Liquid Experimental Engineering, RPX Office of Advanced Research & Technology NASA Headquarters Washington, D.C. 20546	
2		Chief, Liquid Propulsion Technology, RPL Office of Advanced Research & Technology NASA Headquarters Washington, D.C. 20546	
1		Director, Launch Vehicles & Propulsion, SV Office of Space Science & Applications NASA Headquarters Washington, D.C. 20546	
1		Chief, Environmental Factors & Aerodynamics Code RV-1 Office of Advanced Research & Technology NASA Headquarters Washington, D.C. 20546	
1		Chief, Space Vehicles Structures Office of Advanced Research & Technology NASA Headquarters Washington, D.C. 20546	
1		Director, Advanced Manned Missions, MT Office of Manned Space Flight NASA Headquarters Washington, D.C. 20546	

REPORT COPIES R D	RECIPIENT	DESIGNEE
6	NASA Scientific & Technical Information Facility P.O. Box 33 College Park, Maryland 20740	
1	Director, Technology Utilization Division Office of Technology Utilization NASA Headquarters Washington, D.C. 20546	
1	National Aeronautics & Space Adminstration Ames Research Center Moffett Field, California 94035 Attn: Library	Hans M. Mark Mission Analysis Division
1	National Aeronautics & Space Adminstration Flight Research Center P.O. Box 273 Edwards, California 93523 Attn: Library	
1	National Aeronautics & Space Administration Goddard Space Flight Center Greenbelt, Maryland 20771 Attn: Library	Merland L. Moseson, Code 620
1	National Aeronautics & Space Administration John F. Kennedy Space Center Cocoa Beach, Florida, 32931 Attn: Library	Dr. Kurt H. Debus
1	National Aeronautics & Space Administration Langley Research Center Langley Station Hampton, Virgina 23365 Attn: Library	Ed Cortwright, Director
1	National Aeronautics & Space Administration Manned Spacecraft Center Houston, Texas 77001 Attn: Library	J. G. Thiobodaux, Jr. Chief, Propulsion & Power Division
1	National Aeronautics & Space Administration George C. Marshall Space Flight Center Huntsville, Alabama 35812 Attn: Library	Keith Chandler Hans G. Paul James Thomas
1	Jet Propulsion Laboratory 4800 Oak Grove Drive Pasadena, California 91103 Attn: Library	Henry Burlage, Jr. Duane Dipprey

REPORT COPIES R	D	RECIPIENT	DESIGNEE
1		Defense Documentation Center Cameron Station Building 5 5010 Duke Street Alexandria, Virginia 22314 Attn: TISIA	
1		Office of the Director of Defense Research & Engineering Washington, D.C. 20301 Attn: Office of Asst. Dir. (Chem. Technology)	
1		Arnold Engineering Development Center Air Force Systems Command Tullahoma, Tennessee 37389 Attn: Library	Dr. H. K. Doetsch
1		Aeronautical Systems Division Air Force Systems Command Wright-Patterson Air Force Base, Dayton, Ohio Attn: Library	D. L. Schmidt Code ARSCNC-2
1		Air Force Rocket Propulsion Laboratory (RPR) Edwards, California 93523 Attn: Library	
1		Air Force Rocket Propulsion Laboratory (RPM) Edwards, California 93523 Attn: Library	
1		Air Force FTC (FTAT-2) Edwards Air Force Base, California 93523 Attn: Library	Donald Ross
1		Air Force Office of Scientific Research Washington, D.C. 20333 Attn: Library	SAEP, Dr. J. F. Masl
1		Space & Missile Systems Organization Air Force Unit Post Office Los Angeles, California 90045 Attn: Technical Data Center	
1		Commanding Officer U.S: Army Research Office (Durham) Box CH, Duke Station Durham, North Carolina 27706 Attn: Library	

REPORT COPIES R D	RECIPIENT	DESIGNEE
1	U.S. Army Missile Command Redstone Scientific Information Center Redstone Arsenal, Alabama 35808 Attn: Document Section	Dr. W. Wharton
1	Bureau of Naval Weapons Department of the Navy Washington, D.C. Attn: Library	J. Kay, Code RTMS-41
1	Commander U.S. Naval Weapons Center China Lake, California 93557 Attn: Library	W. F. Thorm Code 4562
1	Picatinny Arsenal Dover, New Jersey 07801 Attn: Library	I. Forsten
1	Air Force Aero Propulsion Laboratory Research & Technology Division Air Force Systems Command United States Air Force Wright-Patterson AFB, Ohio 45433 Attn: APRP (Library)	R. Quigley C. M. Donaldson
1	Propulsion Division Aerojet-General Corporation P.O. Box 15847 Sacramento, California 95803 Attn: Technical Library 2484-2015A	R. Stiff
1	Aeronutronic Division of Philco Ford Corp. Ford Road Newport Beach, California 92663 Attn: Technical Information Department	Dr. L. H. Linder
1	Aerospace Corporation 2400 E. El Segundo Blvd. Los Angeles, California 90045 Attn: Library-Documents	J. G. Wilder
1	ARO, Incorporated Arnold Engineering Development Center Arnold AF Station, Tennessee 37389 Attn: Library	
1	Susquehanna Corporation Atlantic Research Division Shirley Highway & Edsall Road Alexandria, Virginia 22314 Attn: Library	Dr. Ray Friedman

REPORT COPIES R D	RECIPIENT	DESIGNEE
1	Battelle Memorial Institute 505 King Avenue Columbus, Ohio 43201 Attn: Report Library, Room 6A	
1	Beech Aircraft Corporation Boulder Facility Box 631 Boulder, Colorado Attn: Library	Douglas Pope
1	Bell Aerosystems, Inc. Box 1 Buffalo, New York 14205 Attn: Library	T. Reinhardt W. M. Smith
1	Bendix Systems Division Bendix Corporation 3300 Plymouth Street Ann Arbor, Michigan Attn: Library	John M. Brueger
1	Bellcomm 955 L'Eufant Plaza, S.W. Washington, D.C. Attn: Library	H. S. London
1	Boeing Company Space Division P.O. Box 868 Seattle, Washington 98124 Attn: Library	J. D. Alexander C. F. Tiffany
1	Chemical Propulsion Information Agency Applied Physics Laboratory 8621 Georgia Avenue Silver Spring, Maryland 20910	Tom Reedy
1	Chrysler Corporation Missile Division P.O. Box 2628 Detroit, Michigan Attn: Library	
1	Chrysler Corporation Space Division New Orleans, Louisiana Attn: Libranian	
1	Grumman Aircraft Engineering Corporation Bethpage, Long Island, New York Attn: Library	Joseph Gavin

REPORT COPIES R D	RECIPIENT	DESIGNEE
1	Grumman Aircraft Engineering Corporation Bethpage, Long Island, New York Attn: Library	Joseph Gavin
1	Honeywell Inc. Aerospace Division 2600 Ridgeway Road Minneapolis, Minnesota Attn: Library	Gordon Harris
1	Kidde Aerospace Division Walter Kidde & Company, Inc. 567 Main Street	R. J. Hanville
1	Ling-Temco-Vought Corporation P.O. Box 5907 Dallas, Texas 75222 Attn: Library	
1	Lockheed Missiles and Space Company P.O. Box 504 Sunnyvale, California 94087 Attn: Library	
1	Lockheed Propulsion Company P.O. Box 111 Redlands, California 92374 Attn: Library, Thackwell	H. L. Thackwell
1	Marquardt Corporation 16555 Saticoy Street Box 2013 - South A-nex Van Nuys, California 91409	L. R. Bell, Jr.
1	Denver Division Martin-Marietta Corporation P.O. Box 179 Denver, Colorado 80201 Attn: Library	Dr. Morganthaler F. R. Schwartzberg
1	Western Division McDonnell Douglas Aircraft Company, Inc. 3000 Ocean Park Blvd. Santa Monica, California 90406 Attn: Library	R. W. Hallet G. W. Burke
1	McDonnell Douglas Aircraft Corporation P.O. Box 516 Lambert Field, Missouri 63166 Attn: Library	R. A. Herzmark

REPORT COPIES R D	RECIPIENT	DESIGNEE
1	Rocketdyne Division North American Rockwell Inc. 6633 Canoga Avenue Canoga Park, California 90134 Attn: Library	Dr. R. J. Thompson S. F. Iacobellis
1	Northrop Space Laboratories 3401 West Broadway Hawthorne, California Attn: Library	Dr. William Howard
1	Radio Corporation of America Astro-Electronics Products Princeton, New Jersey Attn: Library	
1	Rocket Research Corporation Sillow Road at 116th Street Redmond, Washington 98052 Attn: Library	F. McCullough, Jr.
1	TRW Incorporated TAPCO Division 23555 Euclid Avenue Cleveland, Ohio 44117	P. T. Angell
1	United Aircraft Corporation Corporation Library 400 Main Street East Hartford, Connecticut 06108 Attn: Library	Dr. David Rix Frank Owen
1	United Aircraft Corporation Pratt & Whitney Division Florida Research & Development Center P.O. Box 2691 West Palm Beach, Florida 33402 Attn: Library	R. J. Coar Dr. Schmitko
1	Curtiss-Wright Corporation Wright Aeronautical Division Woodridge, New Jersey Attn: Library	G. Kelley
1	Fairchild Stratos Corporation Aircraft Missiles Division Hagerstown, Maryland Attention: Library	
1	Research Center Fairchild Hiller Corporation Germantown, Maryland Attn: Library	Ralph Hall

REPORT COPIES R	D	RECIPIENT	DESIGNEE
1		Republic Aviation Fairchild Hiller Corporation Farmington, Long Island New York	
1		General Dynamics/Convair P.O. Box 1128 San Diego, California 92112 Attn: Library	Frank Dore
1		Missiles and Space Systems Center General Electric Company Valley Forge Space Technology Center P.O. Box 855 Philadelphia, Pa. 19010 Attn: Library	A. Cohen F. Schultz
1		General Electric Company Flight Propulsion Lab. Department Cincinnati, Ohio Attn: Library	D. Slchu Leroy Smith
1		United Aircraft Corporation United Technology Center P.O. Box 358 Sunnyvale, California 94038 Attn: Library	Dr. David Altman
1		Vickers Incorporated Box 307 Troy, Michigan	
1		Vought Astronautics Box 5907 Dallas, Texas Attn: Library	

SYMBOLS

A	-	area
C_p	-	specific heat at constant pressure
C^*	-	characteristic exhaust velocity
c	-	wave speed
d	-	diameter
F	-	thrust
h	-	wave height
	-	film coefficient
h_{fg}	-	heat of vaporization
H	-	enthalpy
H	-	channel depth
I_{sp}	-	specific impulse
k	-	thermal conductivity
L	-	channel spacing
P	-	pressure
Pr	-	Prandtl Number
q	-	heat flux
$\dot{Q}$	-	heat load
Re	-	Reynolds Number
T	-	temperature
V	-	velocity
$\dot{w}$	-	flow rate
W	-	channel width
ϵ	-	area ratio
η	-	efficiency
ρ	-	density
σ	-	surface tension
μ	-	viscosity
λ	-	wave length

Subscripts

ox	-	oxidizer	o	-	stagnation
f	-	fuel	g,G	-	gaseous
fcore	-	fuel core	ℓ	-	liquid
fcool, fc	-	fuel coolant	C	-	chamber
ftot	-	total fuel	N	-	nozzle

REFERENCES

1. R. M. Williams and F. E. Arndt, "Space Storable Thruster Investigation," NASA CR-72495, August 1, 1969.

2. H. Lamb, Hydrodynamics, Dover Pub. Inc., N. Y. 1932, 6th Ed.

3. L. M. Milne-Thomson, Theoretical Hydrodynamics, The MacMillan Co. N. Y., 1955.

4. C. D. Coulbert and R. J. FioRito, "Space Storable Thruster Investigation," NASA CR-72526, June 11, 1969.